New Time Series Models for Spatial Extremes in Solar Flare Detection

by

Jili Wang

A dissertation submitted in partial fulfillment of

the requirements for the degree of

Doctor of Philosophy

(Statistics)

at the

UNIVERSITY OF WISCONSIN–MADISON

2020

Date of final oral examination: 06/18/2020

The dissertation is approved by the following members of the Final Oral Committee:

Zhengjun Zhang, Professor, Statistics

Peter Chien, Professor, Statistics

Bret Larget, Professor, Botany and Statistics

Brian S. Yandell, Professor, Statistics

Chunming Zhang, Professor, Statistics

© Copyright by Jili Wang 2020

All Rights Reserved

Acknowledgments

First and foremost, I would like to express my sincere gratitude to my advisor Professor Zhengjun Zhang for being a tremendous mentor for me. He introduced new knowledge area such as extreme value theory to me and also supported me to investigate research problem I am interested in. I am the first one in our research group who had motivation in galaxy clustering. Professor Zhang taught me how to face a new problem, how to do the preliminary analysis, and how to solve it step by step. This is my precious experience which guides me do data analysis and investigate problems in the future. As everyone knows, Ph.D. students always have a tough time because we are trying to enter in unknown areas with less experience. But I am never alone because Professor Zhang is always by my side. His encouragement and enthusiasm supported me to continue my research no matter what difficulty we were facing. It is my honor to be his Ph.D. student.

I would also like to thank my dissertation committee: Professor Peter Chien, Professor Bret Larget, Professor Brian S. Yandell, and Professor Chunming Zhang for their helpful guidance and invaluable ideas to improve my dissertation work.

Moreover, I would like to thank all the professors and faculty members who taught me knowledge and advised me during these five years. Professor Grace Wahba who is my first academic advisor provided much help to me when I started my Ph.D. life. Professor Chunming Zhang, Dr. Derek Bean, Professor Jun Shao, and Professor Yazhen Wang taught me the foundation of mathematical statistics. Professor Richard J. Chappell and Professor Murray Clayton showed me the world of statistical methods and applications. Professor

Kam-Wah Tsui, Professor Zhengjun Zhang, Professor Anru Zhang, Professor Menggang Yu, and Professor Chunming Zhang taught me different subareas of statistics, which opened my eyes and inspired me to do my own research. Professor Brian Yandell guided me to solve real world problems which gave me application experience. My dissertation topic came from one of my project in his class. Besides them, I would like to thank all other faculty and staff members in our department for their help and support.

In addition, I would like to acknowledge my academic siblings in Professor Zhang's research group. I want to especially express my thanks to Zifeng Zhao, who is an Assistant Professor in University of Notre Dame, and Yuqing Xu who not only provided support for my research but also helped me in my common life. I also want to thank all my friends in Madison and all over the world. Their encouragement and sharing of happiness made my Ph.D. life more enjoyable and memorable.

Finally, I want to express my sincere thanks to my family. I would like to thank my parents Qiang Wang and Li Xie for their emotional and financial support from the first moment to the last in this five years. They always gave me the best they had. I want to thank my girlfriend Ningchen Zou. She always stays with me no matter how hard life is.

Contents

Abstract **x**

1 Introduction **1**

1.1 Spatial Extreme 1

1.2 Modeling Time Series of Maxima 2

1.3 Solar flare detection 5

2 Preliminary Analysis of Solar Flare Data Frame **8**

2.1 Data Characteristics and Preprocessing 8

2.2 Preliminary Analysis Using Extreme Value Sampling 9

3 Model specification **15**

3.1 Autoregressive conditional Fréchet Model with Logarithm Functions 15

3.2 Parameter Estimation 17

3.3 Simulation 20

3.4 Empirical Application 22

3.5 AcFL model with $k = 2$ 29

3.5.1 Extended Version of AcFL Model 29

3.5.2 Theoretical Properties 30

3.5.3 Simulation 31

3.5.4 Solar flare detection 33

4 Models with Spatial Correlations **38**

4.1 Spatial Correlations 38

4.2 Parameter Estimations 40

4.3 Simulation 41

4.4 Empirical Application 46

5 Discussion **53**

6 Appendix A **55**

6.1 Proofs for AcFL model 55

6.1.1 Proof of stationarity and ergodicity 55

6.1.2 Proof of consistency and asymptotic normality 59

6.2 Proofs for AcFL model with spatial correlations 71

6.2.1 Proof of stationarity and ergodicity 71

6.2.2 Proof of consistency and asymptotic normality 74

6.3 First and second order partial derivative of $l_t(\theta)$ 81

7 Appendix B **83**

7.1 AcFL model 84

7.2 AcFL model with $k = 2$ 110

7.3 AcFL model with spatial correlation 136

List of Tables

2.1 Descriptive statistics of extreme values in part 1, part 34, and part 45. . . . 13

3.1 The performance of MLE with the sample size of 1000 (S1) and 5000 (S2) using the parameters from analysis in part 1, 12, 33, 34, 44, and 45. Mean and Std. Dev. are the sample mean and standard deviation of the MLE's obtained from 500 simulations. 21

3.2 Estimated parameter values of standard AcFL model. 23

3.3 Solar Flare Detection Time Comparison. 28

3.4 The performance of MLE with the sample size of 1000 (S1) and 5000 (S2) using the parameters from extended version of AcFL models. Mean and Std. Dev. are the sample mean and standard deviation of the MLE's obtained from 500 simulations. 32

3.5 Estimated parameter values of AcFL model with $k = 2$ 34

4.1 The performance of MLE with the sample size of 1000 (S1) and 5000 (S2) using the parameters from analysis in part 1, 12, 33, 34, 44, and 45. Mean and Std. Dev. are the sample mean and standard deviation of the MLE's obtained from 500 simulations. 46

4.2 Estimated parameter values of AcFL model with spatial correlation 48

List of Figures

2.1 First solar flare snapshots of original data (a, b, c) and data after differencing(d, e, f) where the top panels are with color and the bottom panels are with grey scale: a/d is at frame t = 186/185, the moment right before the first solar flare starts; b/e is at frame t = 198/197, when the first solar flare is brightest; c/f at frame t = 202/201, when the first solar flare is nearly over. 10

2.2 Second solar flare snapshots of original data (a, b, c) and data after differencing(d, e, f) where the top panels are with color and the bottom panels are with grey scale: a/d is at frame t = 215/214, the moment right before the second solar flare starts; b/e is at frame t = 230/229, when the second solar flare is brightest; c/f at frame t = 268/267, when the second solar flare is nearly over. 11

2.3 Line graphs of the extreme values in part 1, part 12, part 33, part 34, part 44, and part 45. It is noted that part 33 and 34 cover the first solar flare, while part 44 and 45 cover the second one. 12

2.4 Left plot shows the moving window graph of parameter ξ in part 45; right plot shows the moving window graph of parameter σ in part 45; dashed lines indicate the fitted values using the static GEV with whole data set. 14

3.1 Histogram plots of simulated data (orange) and real data (blue) in part 1 (top), part 34 (middle), and part 45 (bottom) 22

3.2 Estimated α_t (left) and σ_t(right) in part 1 (top), part 34 (middle), and part 45 (bottem) using standard AcFL model. For the plots of α_t, the horizontal lines indicate the smallest α_t in $t = 1 \sim 185$ (α_{small}). The first vertical line in each plot displays the first time when the α_t is smaller than α_{small}. And the second vertical line shows the the last α_t which is smaller α_{small} after α_t goes beyond the smallest value.The σ_t is shown in the same way with opposite direction. 25

3.3 Estimated α_t (left) and σ_t(right) in part 12 (top), part 33 (middle), and part 44 (bottem) using AcFL model. For the plots of α_t, the horizontal lines indicate the smallest α_t in $t = 1 \sim 185$ (α_{small}). The first vertical line in each plot displays the first time when the α_t is smaller than α_{small}. And the second vertical line shows the the last α_t which is smaller α_{small} after α_t goes beyond the smallest value.The σ_t is shown in the same way with opposite direction. . 26

3.4 Estimated α_t (left) and σ_t(right) in part 22 (top) and part 99 (bottem) using AcFL model after removing large value in the beginning. 27

3.5 Histogram plots of simulated data (orange) and real data (blue) in part 1 (top), part 34 (middle), and part 45 (bottom) 33

3.6 Estimated α_t (left) and σ_t(right) in part 1 (top), part 34 (middle), and part 45 (bottem) using Acf model with log function and $k = 2$. For the plots of α_t, the horizontal lines indicate the smallest α_t in $t = 1 \sim 185$ (α_{small}). The first vertical line in each plot displays the first time when the α_t is smaller than α_{small}. And the second vertical line shows the the last α_t which is smaller α_{small} after α_t goes beyond the smallest value.The σ_t is shown in the same way with opposite direction. 35

3.7 Estimated α_t (left) and σ_t(right) in part 12 (top), part 33 (middle), and part 44 (bottem) using Acf model with log function and $k = 2$. For the plots of α_t, the horizontal lines indicate the smallest α_t in $t = 1 \sim 185$ (α_{small}). The first vertical line in each plot displays the first time when the α_t is smaller than α_{small}. And the second vertical line shows the the last α_t which is smaller α_{small} after α_t goes beyond the smallest value.The σ_t is shown in the same way with opposite direction. 36

4.1 The scatter plots of original data in part 33 (first solar flare), part 34 (first solar flare), part 43 (without solar flare), and part 44 (second solar flare). . . 39

4.2 Histogram plots of simulated data (orange) and real data (blue) in part 1 (top), part 34 (middle), and part 45 (bottom) 42

4.3 Histogram plots of simulated data (orange) and real data (blue) in part 33 (top), and part 44 (bottom) for AcFL model (left) and spatial ACFL model (right) 43

4.4 Estimated α_t (left) and σ_t(right) in part 1 (top), part 34 (middle), and part 45 (bottem) using spatial AcFL model. For the plots of α_t, the horizontal lines indicate the smallest α_t in $t = 1 \sim 185$ (α_{small}). The first vertical line in each plot displays the first time when the α_t is smaller than α_{small}. And the second vertical line shows the the last α_t which is smaller α_{small} after α_t goes beyond the smallest value.The σ_t is shown in the same way with opposite direction. . 50

4.5 Estimated α_t (left) and σ_t(right) in part 12 (top), part 33 (middle), and part 44 (bottem) using saptial AcFL model. For the plots of α_t, the horizontal lines indicate the smallest α_t in $t = 1 \sim 185$ (α_{small}). The first vertical line in each plot displays the first time when the α_t is smaller than α_{small}. And the second vertical line shows the the last α_t which is smaller α_{small} after α_t goes beyond the smallest value.The σ_t is shown in the same way with opposite direction. 51

4.6 Top plot shows the original data in part 33 (blue) and part 34 (orange); bottom plot shows original data in part 44 (blue) and part 45 (orange) . . . 52

Abstract

Motivated by solar flare detection problem, we propose a new autoregressive conditional Fréchet model with logarithm functions (AcFL) of time-verying parameters for spatial extremes. We describe a novel and direct method similar to max-stable process to remove the background information and extract maximum features to analyze rare events in big data streams. This method reduces the dimension of data frames and obtains the characteristics of original data without assumptions. Our AcFL model can be used to detect, even predict solar activity. With this dynamic extreme value modeling, we can detect the occurrence and climax of solar activity earlier than existing algorithms. The empirical study shows that our model outperforms the existing detection algorithms with sampling strategies. In addition, the stationarity and ergodicity of tail and scale indices are proved. We also study the theoretical properties of irregular MLE such as the consistency and asymptotic normality of estimators for parameters.

Moreover, we generalize standard AcFL to a model with spatial correlation. The standard AcFL model is a specific case of spatial model. We also apply spatial AcFL model on solar flare data and compare the prediction results with the standard one. In real data analysis, the spatial AcFL model has better prediction performance than the standard AcFL in some subareas. The simulation data for spatial models in those parts are more similar to real data than standard model which is consistent with empirical study.

Chapter 1

Introduction

1.1 Spatial Extreme

Extreme value theory (EVT) and methods find wide application in many areas such as finance (e.g. Dahan and Mendelson 2001; Laurini and Tawn, 2009; Zhao et al. 2018), environmental science (e.g. Thompson et al. 2001; Kharin and Zwiers 2005; Buishand, de Haan, and Zhou 2008; Deng and Zhang 2018, 2020), aeronautics (e.g. Chiapino et al. 2019). Under EVT frame work, there are two common approaches to analyze and characterise the behavior of maxima: Maxima-generalized extreme value distribution (GEV) methodology and peak-over-threshold (POT) methodology based on generalized Pareto distribution (GPD).

Big data with complex spatial (or spatial temporal) structure motivated the development of statistical methods and tools in extreme value studies. Cooley, Nychka, and Naveau (2007) proposed Bayesian hierarchical models in which they assumed the extreme value at each location followed a univariate generalized Pareto distribution (GPD). In order to capture spatial dependence, the parameters of the GPD follow a separate spatial model. Sang and Gelfand (2009) followed their ideas by assuming that the observations follow generalized extreme value (GEV) distributions. The dependence is captured using multivariate Markov random field models. Jalbert et al. (2017) used an intrinsic Gaussian Markov random fields (IGMRF)

model to estimate spatially varying location and scale parameters. Reich and Shaby (2019) proposed a spatial Markov model for climate areal extremes. They used latent clustering of neighboring regions to capture spatial dependence. Huser and Wadsworth (2019) proposed a class of spatial processes which makes a smooth transition between asymptotic dependence and asymptotic independence by composing two random variables.

There are also many models for spatial extremes based on max-stable processes (Schlather 2002; Kabluchko, Schlather, and de Haan 2009; Padoan et al. 2010; Reich and Shaby 2019), generalized Pareto processes (Ferreira and de Haan 2014; Thibaud and Opitz 2015; de Fondeville and Davison 2018), and latent mixing variables (Reich and Shaby 2012; Morris et al.2017). Max-stable processes are a widely used approach in spatial extremes analysis because they are natural analogues of the GEV distribution with its elegant mathematical properties. More precisely, let $\{Y_i(t) : t \in T\}, i = 1, \ldots, n$, be n independent and identically distributed replications of a continuous stochastic process $\{Y(t) : t \in T\}$. If there exist sequences of continuous functions $a_n(t) > 0$ and $b_n(t) \in \mathbb{R}$ such that

$$M(t) \stackrel{\mathrm{d}}{=} \max_{1 \le i \le n} \frac{Y_i(t) - b_n(t)}{a_n(t)}$$

has nondegenerate marginals, the limiting process $M(t)$ is a max-stable process (de Haan 1984; de Haan and Ferreira 2006).

Similar to max-stable process, we obtain the maximum value in a particular region at one time point and treat the sequence of those maxima as time series.

1.2 Modeling Time Series of Maxima

Time series modeling for maxima and extreme observations is one common subject in modern extreme value studies. Max-stable process was applied in modeling univariate stationary time series, for examples, maxima of moving maxima (M3) processes (Deheuvels 1983; Hall et al. 2002) and max-autoregressive moving average model (Davis and Resnick 1989, 1993; Naveau

et al. 2011). Multivariate maxima of moving maxima (M4) process which is a generalized framework from M3 process (Smith and Weissman 1996) has been applied to returns in multivariate financial time series in order to predict extreme co-movements (Zhang and Smith 2010). Tang et al.(2013) proposed a sparse M4 random coeffcient model (SM4R) which contains a much smaller set of parameters than M4 process but can capture the main characteristics in financial time series. Zhang and Zhu (2016) considered a class of copula structured M4 (CSM4) processes which increase the estimation efficiency, the flexibility of models, and can be used in empirical application directly.

The behavior of time series for maxima may change over time, for examples, structure changes and large variation clustering in finance, climate, and environmental fields. Therefore, researchers consider dynamic modeling to detect and analyze extreme events in time series. Bayesian technology has been investigated to update the time-varying GPD parameters (Smith and Goodman 2000; Chavez-Demoulin et al. 2014). Kelly (2014) and Kelly and Jiang (2014) used POT-GPD approach to propose a model with dynamic tail for panel data. Massacci (2016) and Zhang and Schwaab (2017) followed the observation-driven approach to propose dynamic POT-GPD model with time-varying tail index. Zhao (2020) built a dynamic bivariate PoT model to investigate time-varying behavior of joint tail risk in financial markets.

Besides POT-GPD approach, there are also some studies on Maxima-GEV approach. Bali and Weinbaum (2007) built a time-varying GEV model to estimate the realized volatility in empirical application of financial time series. Zhao et al. (2018) created an autoregressive conditional Fréchet (AcF) model which updates the parameters of Fréchet distribution with autoregressive models. Mao and Zhang (2018) is closely related to AcF, but specified as a state-space model. Still, researches on dynamic GEV model are much less than POT-GPD.

In the dissertation, we focus on modeling time series of cross-sectional maxima $\{Q_t\}$, where $\{Q_t\}$ is a univariate time series of maximum values obtained from a set of time series $\{X_{it}\}_{i=1}^{p}$, that is $Q_t = \max_{1\leq i\leq p} X_{it}$. Hence "maxima" and "extreme event" are different.

It should be noticed that "maxima" is the maximum value of a set of observations while "extreme event" is rare observations over a high threshold. "Maxima" is not equivalent to "extreme event". $\{Q_t\}$ which is a time series of maxima can be observed at every t but extreme event cannot. It may happen at one time point or occurs several times within a time period. We propose new time series models for spatial extremes to detect rare events in big data with complex structures.

One application about time series for spatial extremes is solar flare detection. Solar flare is a rare event which suddenly happens in some regions of Sun's surface and then disappears. Classical detection methods face difficulties when dealing with this type of high-dimensional image data. One can find more details about solar flare detection in Section 1.3. This natural science problem motivated us to propose new models in the dissertation.

Our new time series model for spatial extremes can be used to investigate solar activity in short term and analyze solar flare without assumptions. We extract maximum values as features to reduce dimensions and detect solar flare with dynamic conditional modeling. Solar flare data set used in this study is the same as that in Xie et al. (2013), Liu et al. (2015), and Wang et al. (2018).

In Chapter 2, we discuss the data preprocessing and conduct a preliminary analysis on solar flare data frames. Since original data is captured from solar image, there are lots of noises which will influence the analysis of solar flare. In the previous literature, researchers used a simple way to remove the noise but it needs a strong assumption about the data. Here we introduce a new method for noise cancellation without any data assumptions. Moreover, we talk about a different sampling method to reduce the dimension of original data set.

Chapter 3 contains the details of autoregressive conditional Fréchet model with logarithm functions (AcFL) and an extended version of AcFL model. We also investigate probabilistic properties of AcFL model and statistical properties of maximum likelihood estimators (MLE) used for estimation in Section 3.2. In Section 3.3, we conduct simulation studies to evaluate the performance of MLE in finite sample sizes. Section 3.4 offers empirical applications on

solar flare data set. In section 3.5, we use the same real data set on extended AcFL model and compare its results with the standard one.

Chapter 4 is organized as following. We discuss potential spatial relationship between sampling subareas and introduce an AcFL model including spatial correlations in Section 4. The AcFL model in Chapter 3 is a special case on AcFL model in Chapter 4. We provide theoretical properties in Section 4.2. Additionally, we use the same method to simulate the data in order to evaluate the performance of MLE in our model in Section 4.3. Section 4.4 provides real data applications on the same data set. We also compare this model which includes both temporal and spatial relationships with models in Chapter 3.

In Chapter 5, we provide discussion about the modeling results and further extention of AcFL models. The proofs of theorems are all in Chapter 6. The parameter results and plots of real data set can be found in Chapter 7.

1.3 Solar flare detection

A solar flare is defined as a sudden, rapid, and intense variation in brightness on Sun's surface (Auguesto et al. 2011). It is created by huge energy which is suddenly released due to the change of magnetic fields. In the report of NASA (2009), it was pointed out that the power of solar flare burst is approximately equal to a billion atomic bombs. Although Sun is far away from Earth, solar flare can damage the human society easily because the modern daily life relies on a network of interconnected high-tech systems. For example, solar flare can disable satellites and destroy radio communications (NASA 2009). As a result, GPS navigation and air travel can be severely affected. Therefore, detecting solar flares as soon as possible is scientifically desirable to reduce the damage of solar activity.

NASA (2009) mentioned that every day 1.5 TB of high-resolution solar images data were captured by satellites for detection use. To deal with big data set, many machine-learning algorithms are developed previously to detect the solar flare. Colak and Qahwaji (2009) in-

troduced an automated solar flare prediction model based on neural network. They analyzed years of solar flare image data and created a system to detect this solar activity, group and classify the sunspots by using McIntosh classification. They mentioned that the performance of their system was related with sample size. A larger training set would provide a better prediction performance. After this research, an advanced feature selection algorithm developed by Ahmed et al. (2013) improved the performance of solar flare detection compared with neural network. In the study, they not only used original data but also analyzed other data like soft X-ray flux. The authors tried to extract features for example mean, median, max value and min value to catch the characteristics of solar flare. Nishizuka et al. (2018) introduced a new deep learning model which could calculate the probability of solar flare in the following 24 hours in the selected regions. They indicated that the prediction process of common DNN model was a black box but their Deep Flare Net could be used to analyze the importance of selected features.

Besides neural network, there are many other machine learning methods used in solar flare detection. Li et al. (2008), Huang et al. (2013), Winter et al. (2015), and Nishizuka et al. (2017) developed different learning methods based on k-nearest neighbor algorithm to deal with detection problem. Qahwaji and Colak (2007) pioneered the use of support vector machine for solar activity detection. Bobra and Couvidat (2015), Boucheron et al. (2015) and Raboonik et al. (2017) followed their idea to investigate other support vector machine. Other approach for example decision tree (Yu et al. 2009, 2010), regression model (Lee et al. 2007; Song et al. 2009), SVM regression (Boucheron et al. 2015) have also been investigated in solar flare detection problem.

Although these machine-learning algorithms can deal with large data set directly, there are three major problems. First, the performance of machine-learning algorithms above is not stable. In other words, they depend on the splitting of data set (Nishizuka et al. 2017). Different training and testing set have an impact on the prediction accuracy of the models. Second, the computation efficiency of machine-learning algorithms is a big problem. It should

be noticed that many algorithms not only use one kind of image data such as line-of-sight magnetogram, but also use other big data like the light curves of the soft X-ray emission and vector magnetogram to extract useful features (Leka and Barnes 2003; Welsch et al. 2009; Kusano et al. 2012).

In addition, researchers tried to obtain more and more features from original data, for example, the gradient of the magnetic field (Yuet al. 2009; Steward et al. 2011), the effective magnetic field (Georgoulis and Rust 2007; Papaioannou et al. 2015), the unsigned magnetic flux, and the magnetic neutral lines (Steward et al. 2011; Falconer et al. 2011). Even though these features make the prediction more accurate than before, the huge data set makes online monitoring become a big problem due to less computation efficiency and resources constraints for data transmission (Liu et al. 2015; Wang et al. 2018).

In order to improve computation efficiency, Liu et al. (2015) developed a sampling strategy, called top-r based adaptive sampling (TRAS) to reduce the dimention of solar flare data. This method uses the sum of top-r local CUSUM statistics to detect possible mean shifts in all directions which can be applied to solar activity detections. In their paper, only 3% of solar flare data will be used but the detection times are closed to true solar flare time. Moreover, Wang et al. (2018) proposed a new procedure named spatial adaptive sampling and monitoring (SASAM) which includes spatial information for change detection. Same as TRAS, SASAM is an approach to detect mean shift in data streams. When sample size is smaller, the performance of SASAM is better than TRAS. However, both TRAS and SASAM use residual data obtained from MOUSSE algorithm (Xie et al. 2013) and assume the residuals follow normal distribution. Instead of mean shift, we decide to detect extreme event in solar brightness variation, which is consistent with the definition of solar flare.

Chapter 2

Preliminary Analysis of Solar Flare Data Frame

2.1 Data Characteristics and Preprocessing

The data is from the Solar Dynamics Observatory AIA 193 Angstrom sensor, recorded in a video format, and publicly available online[1]. There are in total 300 frames, which are measured every 12 seconds, in the video. Each data frame includes a size of $232 \times 292 = 67744$ dimensional data, which can be treated as a matrix with 232 rows and 292 columns. The elements of matrix represent the brightness of pixels in the video. There are at least two transient flares which happen at frames $t = 187 \sim 202$ (weak) and $t = 216 \sim 268$ (strong), respectively.

In the literatures (Liu et al. 2015; Wang et al. 2018), the background information is removed by the MOUSSE algorithm (Xie et al. 2013) and the residuals are assumed to be normally distributed. Here we use a more simple way. We calculate the difference between consecutive data frames to get rid of the background noise. It is reasonable since the definition of solar flare is related with variation in the brightness as mentioned in the introduction.

[1]The video can be found at https://voices.uchicago.edu/willett/research/software/mousse/

Figure 2.1 and Figure 2.2 show snapshots of original data and data after differencing. It is noted that there are 299 frames in data after differencing, therefore detecting a solar flare at $t = 186$ with data of difference means we find solar flare happens at $t = 187$ in original data. According to Figure 2.1 and Figure 2.2, taking difference is a good way to remove the background noise and catch the variation in brightness when a solar flare occurs. The first solar flare occurs at $t = 186$ and it is brightest at $t = 197$. The second one appears at $t = 215$ and the brightest time is $t = 229$. It is easy to see that the second solar flare is brighter than first one.

2.2 Preliminary Analysis Using Extreme Value Sampling

High dimensional solar flare data set causes two important issues. First, it is very hard to do modeling with full data stream which has nearly 70 thousand dimensions and the data set actually only includes a small region of Sun's surface. Second, as mentioned in Liu et al. (2015) and Wang et al. (2018), traditional methods using full data set overstep the limit of transmission and processing capabilities in real time. They are not able to detect solar flare online. Therefore, dimension reduction is necessary before we model the data frames.

Due to the characteristics of solar flare being rare events, we consider extreme value sampling through the following steps: 1) Split the data frame into 120 parts with equal size, 2) Extract the maximum value in each subarea. As a result, we finally have 299 vectors with 120 dimensions. There are more than 500 pixels in each subarea. As a result, time series of maximum in 120 parts are locally stationary. If we split the data frame into more than 120 parts, we cannot guarantee the stationarity of the maximum value time series. It need to be noted that unlike Liu et al. (2015) and Wang et al. (2018), we treat solar flare as rare event in stationary process. Hence we detect the abnormal changes in maximum value which is different from detecting mean structure change or variation change in whole process. There

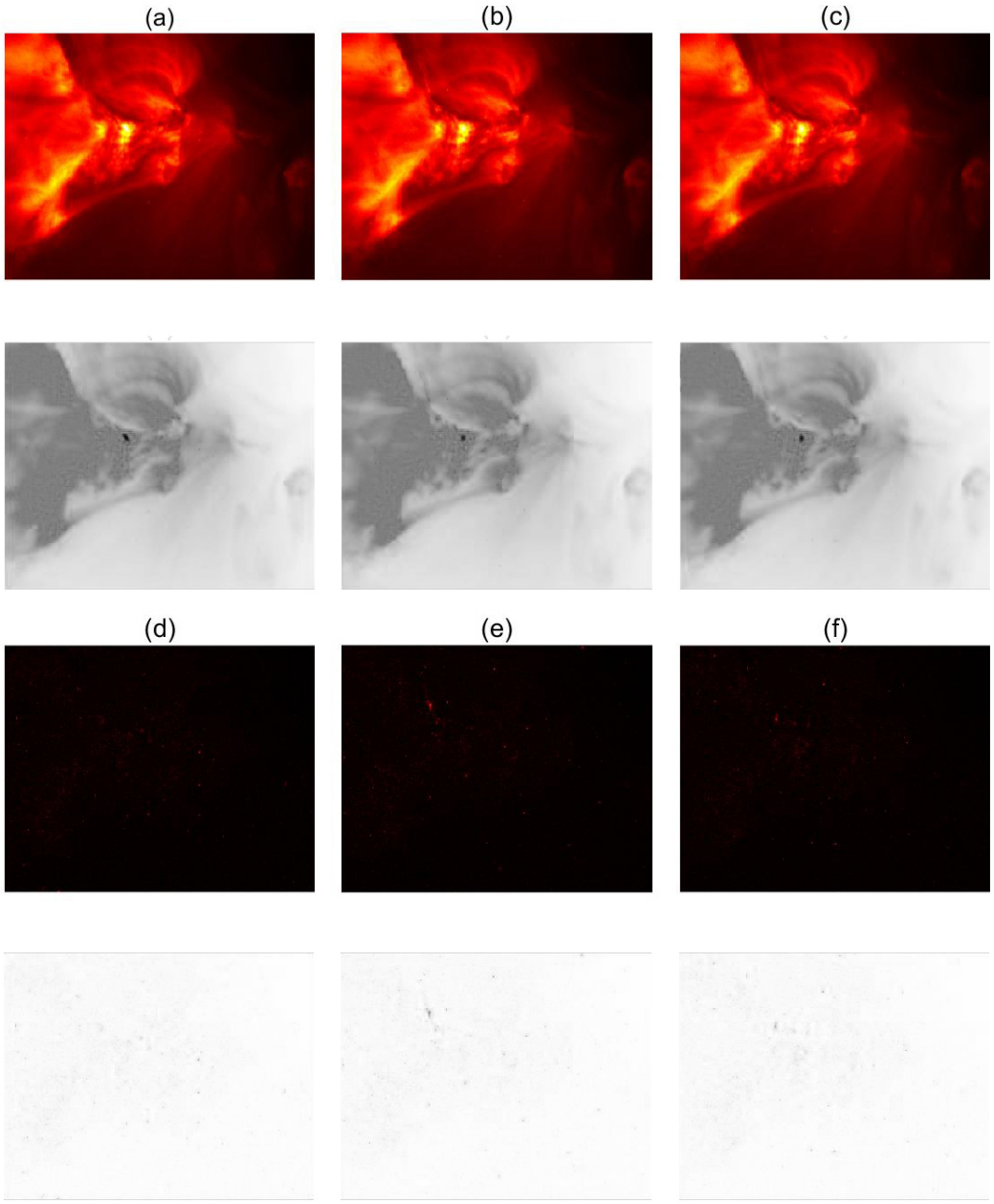

Figure 2.1: First solar flare snapshots of original data (a, b, c) and data after differencing(d, e, f) where the top panels are with color and the bottom panels are with grey scale: a/d is at frame t = 186/185, the moment right before the first solar flare starts; b/e is at frame t = 198/197, when the first solar flare is brightest; c/f at frame t = 202/201, when the first solar flare is nearly over.

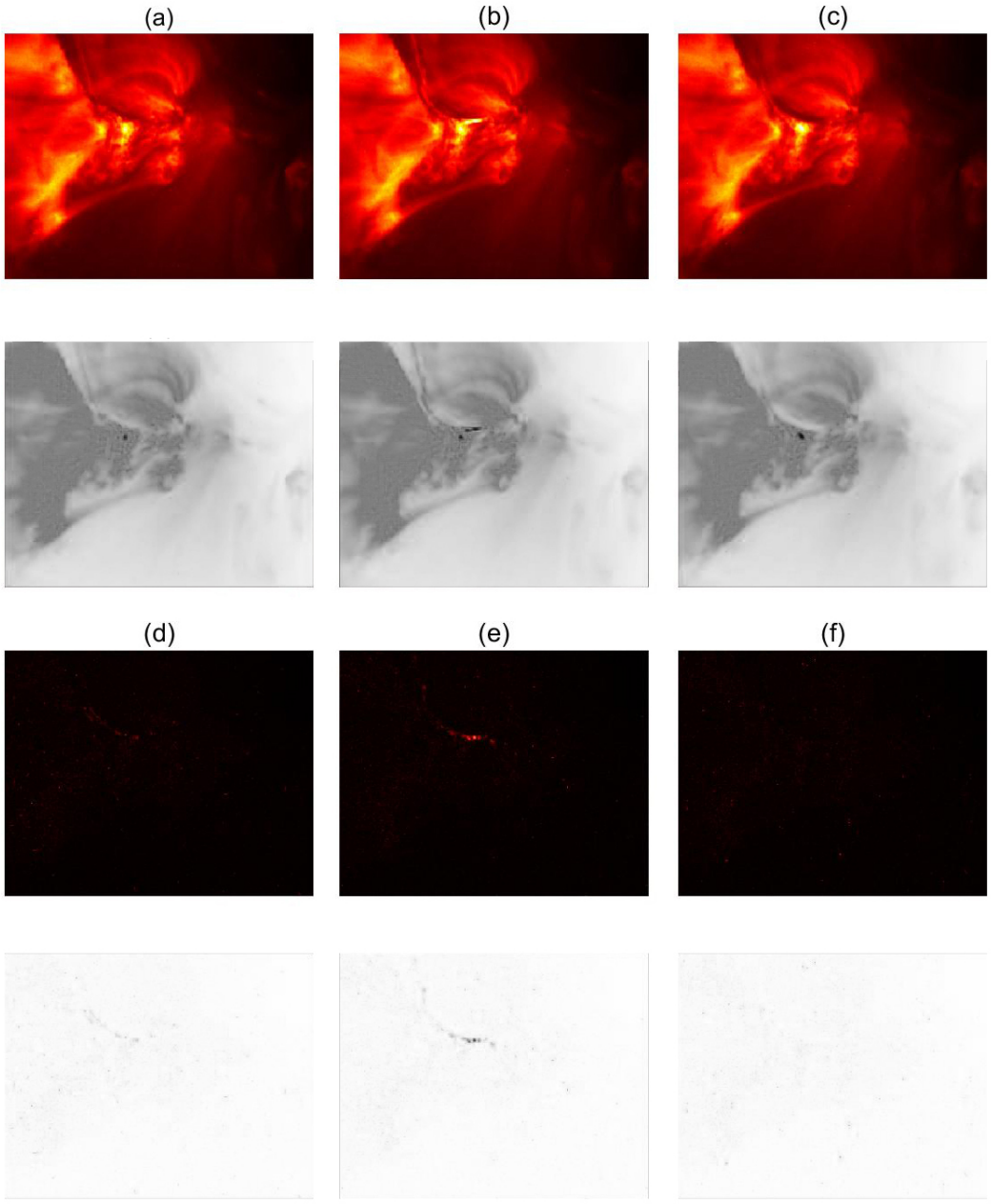

Figure 2.2: Second solar flare snapshots of original data (a, b, c) and data after differencing(d, e, f) where the top panels are with color and the bottom panels are with grey scale: a/d is at frame t = 215/214, the moment right before the second solar flare starts; b/e is at frame t = 230/229, when the second solar flare is brightest; c/f at frame t = 268/267, when the second solar flare is nearly over.

are two advantages of using maximum to detect solar flare. First, maximum value includes the information in the whole parts, not only the information of some points. Second, the analysis of maximum value can also imply the changes in variation or mean through scale and location parameters in extreme value distributions.

In these 120 subareas, part 33 and part 34 cover the field where the first solar flare happens, while part 44 and part 45 cover the area where the second flare occurs. Figure 2.3 shows the maximum value in six subareas (part 1, part 12, part 33, part 34, part 44, part 45). The maximum value plot of all 120 subareas can be found in Appendix B.

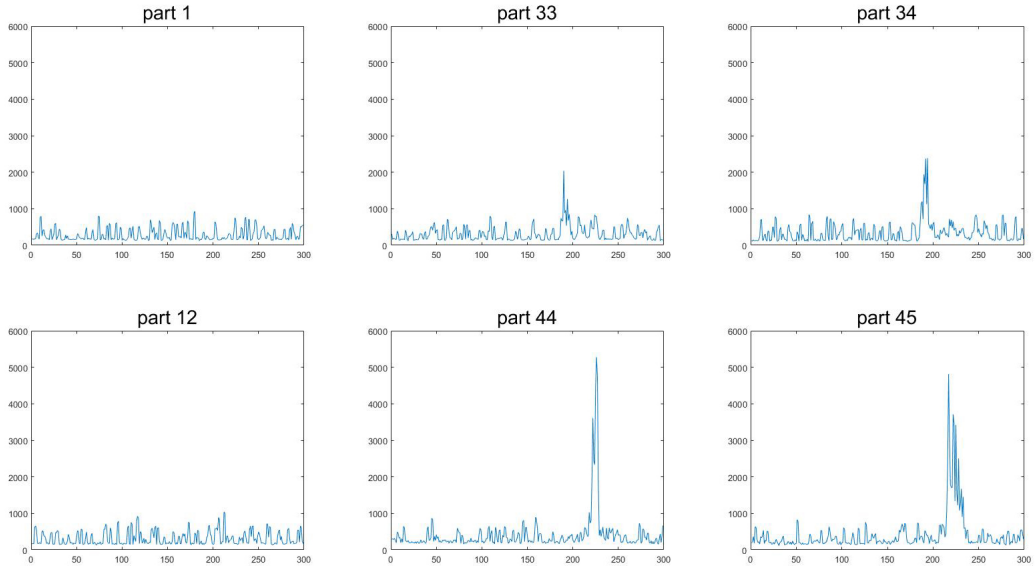

Figure 2.3: Line graphs of the extreme values in part 1, part 12, part 33, part 34, part 44, and part 45. It is noted that part 33 and 34 cover the first solar flare, while part 44 and 45 cover the second one.

From Figure 2.3, it is obvious that when first solar flare happens, $t = 187 \sim 202$, the extreme values in part 33 and part 34 suddenly jump to high values and decrease slowly. Moreover, the increase is much higher in parts 44 and 45 during the occurrence of the second flare. This is coincident with the phenomena in original video, thus we think the extreme values of difference is a good feature which can be used to detect the solar flare. We analyzed all 120 parts. For illustrative purpose, in the following parts, we will only use part 1 (without

solar flare), part 12 (without solar flare), part 33 (first solar flare), part 34 (first solar flare), part 44 (second solar flare), and part 45 (second solar flare) as examples. Table 2.1 shows the descriptive statistics of these three subareas. The median and minimum values in six subareas are similar, but the maximum values are quite different because of the solar flare. The mean and standard deviation are influenced by the maximum values.

	Part 1	Part 12	Part 33	Part 34	Part 44	Part 45
Mean	291.0435	320.2508	314.6321	345.4582	412.7559	413.8294
Median	199	213	230	240	271	237
Maximum	931	1039	2037	2388	5277	4812
Minimum	124	134	122	104	157	118
Std. Dev.	178.9819	195.3419	213.622	299.1839	551.8888	540.7012

Table 2.1: Descriptive statistics of extreme values in part 1, part 34, and part 45.

Suppose X_{tij} is the value of brightness variation of jth pixel at time t in subarea i. Define,

$$Q_{ti} = \max_j X_{tij} \quad \text{for} \quad i = 1, \ldots, 120. \tag{2.1}$$

Under certain conditions in extreme value theory, e.g., Smith (1985), Q_t can be modeled by a generalized extreme value (GEV) distribution as following:

$$F\left(x; \mu_t, \sigma_t, \xi_t\right) = \exp\left\{ -\left[1 + \xi_t \left(\frac{x - \mu_t}{\sigma_t}\right)\right]_+^{-1/\xi_t} \right\} \tag{2.2}$$

where μ_t and σ_t are location-scale parameters and ξ_t is the shape parameter (tail index) at time t.

We first fit a static GEV distribution in order to get the basic image of our real data set. In other words, we treat $\{Q_t\}$ as i.i.d. variable in each subarea and use the whole data set to do the fitting. Then we perform a 200 data moving window GEV fitting on $\{Q_k\}_{k=t}^{k+199}$, for $1 \leq t \leq 100$. The estimated shape parameters and scale parameters in part 45 are displayed in Figure 2.4 where horizontal dashed lines indicate the static parameters obtained from the whole data set in part 45. It is obvious that the estimated values of shape and scale

parameters dynamically vary during observation period. Therefore, we need a dynamic model to fit the solar flare data set. Additionally, one can see that the estimated shape parameters are positive in Figure 2.4, which lead us to consider about Fréchet distribution. When we split the data frame into less than 120 parts, moving window approach indicates the large range of shape parameters from negative value to positive value, which leads to uncertainty in extreme value analysis. In the next section, we will discuss the model combining the dynamic modelling and Fréchet distribution together.

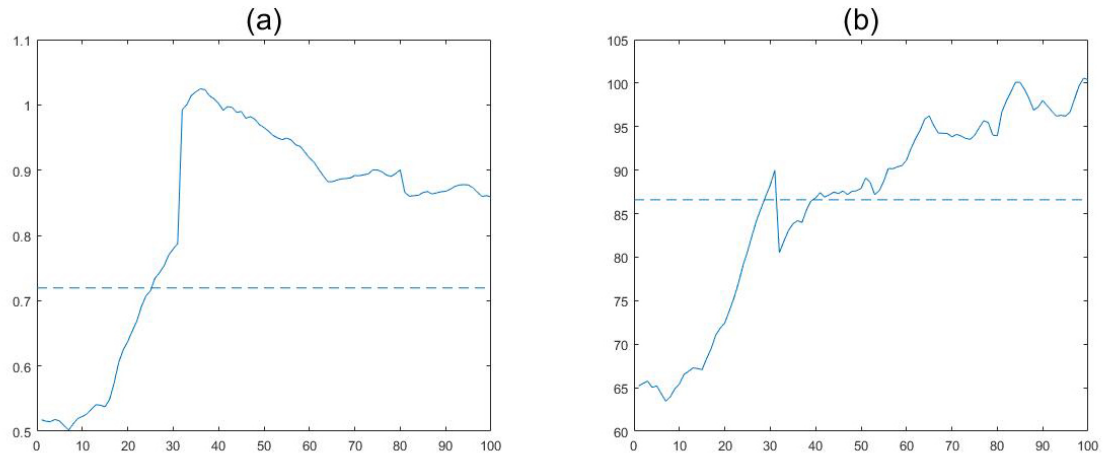

Figure 2.4: Left plot shows the moving window graph of parameter ξ in part 45; right plot shows the moving window graph of parameter σ in part 45; dashed lines indicate the fitted values using the static GEV with whole data set.

Chapter 3

Model specification

3.1 Autoregressive conditional Fréchet Model with Logarithm Functions

Autoregressive conditional Fréchet (AcF) Model, introduced by Zhao et al.(2018), models a time series of maxima $\{Q_t\}$ conditionally by a Fréchet distribution with dynamic parameters $(\mu_t, \sigma_t, \alpha_t)$ where μ_t and σ_t are location-scale parameters and $\alpha_t = 1/\xi_t$ is the shape parameter (tail index) of Fréchet distribution:

$$Q_t = \mu_t + \sigma_t Y_t^{1/\alpha_t} \tag{3.1}$$

where $\{Y_t\}$ is a sequence of i.i.d. unit Fréchet random variables with the distribution function $F(x) = e^{-\frac{1}{x}}, x > 0$ and $(\mu_t, \sigma_t, \alpha_t) \in \mathcal{F}_{t-1} = \sigma\left(Q_{t-1}, Q_{t-2}, \ldots\right)$. Note that $Q_t > \mu_t$. Moreover, AcF model assumes $\mu_t = \mu$ i.e., time invariant and the following dynamic equations for σ_t and α_t:

$$\log \sigma_t = \beta_0 + \beta_1 \log \sigma_{t-1} + \eta_1 \left(Q_{t-1}\right), \tag{3.2}$$

$$\log \alpha_t = \gamma_0 + \gamma_1 \log \alpha_{t-1} + \eta_2 \left(Q_{t-1}\right), \tag{3.3}$$

where $\beta_1, \gamma_1 \geq 0$. $\eta_1(\cdot)$ and $\eta_2(\cdot)$ are the observation-driven factors of $\{\log \sigma_t\}$ and $\{\log \alpha_t\}$. AcF model assumes that $\eta_1(\cdot)$ is a continuous increasing function while $\eta_2(\cdot)$ is a continuous decreasing function of Q_{t-1}. The autoregressive structure used in σ_t and α_t can be found in the literatures (Bollerslev 1986; Hansen 1994; Engle and Russell 1998).

There is a wide selection of $\eta_1(\cdot)$ and $\eta_2(\cdot)$ provided that they satisfy some conditions to guarantee the stationarity and ergodicity of dynamic processes. Zhao et al.(2018) considered exponential functions due to its monotonicity, differentiability, boundedness and generally used in the literature. Here we decide to use logarithm function in order to increase the effects of extremely large number in brightness change on dynamic parameters because of the large range of solar flare data. $\{\sigma_t, \alpha_t\}$ will be used as indices for solar flare detection in empirical study.

Therefore, we consider the following model:

$$Q_t = \mu + \sigma_t Y_t^{1/\alpha_t}, \tag{3.4}$$

$$\log \sigma_t = \beta_0 + \beta_1 \log \sigma_{t-1} - \beta_2 / \log \left(\beta_3 Q_{t-1}\right), \tag{3.5}$$

$$\log \alpha_t = \gamma_0 + \gamma_1 \log \alpha_{t-1} + \gamma_2 / \log \left(\gamma_3 Q_{t-1}\right), \tag{3.6}$$

where $\{Y_t\}$ is a sequence of i.i.d. unit Fréchet random variables, $\mu < \min(Q_t)$, $0 \leq \beta_1, \gamma_1 < 1$, $\beta_2 > 0$, $\beta_3 > e/\min(Q_t)$, $\gamma_2 > 0$, $\gamma_3 > e/\min(Q_t)$, and e is the base of the natural logarithm. The restriction of β_3 and γ_3 makes sure the boundedness of logarithm functions. To distinguish (3.4) - (3.6) from AcF, we call the new model as AcFL.

We further rewrite the model (3.5) and (3.6) as:

$$\log \sigma_t = \beta_0 + \beta_1 \log \sigma_{t-1} - \beta_2 / \log \left(\beta_3 \left(\mu + \sigma_{t-1} Y_{t-1}^{1/\alpha_{t-1}}\right)\right), \tag{3.7}$$

$$\log \alpha_t = \gamma_0 + \gamma_1 \log \alpha_{t-1} + \gamma_2 / \log \left(\gamma_3 \left(\mu + \sigma_{t-1} Y_{t-1}^{1/\alpha_{t-1}}\right)\right). \tag{3.8}$$

Here $\{\sigma_t, \alpha_t\}$ form a homogeneous Markov chain in $\mathbb{R}^2$. We note that in the time series

literature, a functional change in the model often leads to a very different performance and very different technical justifications, which happen in our new model. The technical arguments in Zhao et al. (2018) cannot be used in the AcFL model. We will mainly apply Harris Chain framework in the proof. The following theorem provides a sufficient condition under which the sequence $\{\sigma_t, \alpha_t\}$ is stationary and ergodic.

Theorem 1 *(Stationarity and ergodicity) For an AcFL model with* $\beta_0, \gamma_0 \in \mathbb{R}$ *and* $0 \leq \beta_1, \gamma_1 < 1$, $\beta_2, \gamma_2 > 0$,$\beta_3, \gamma_3 > e/min(Q_t), \mu < min(Q_t)$, *e is the base of the natural logarithm, the latent process* $\{\sigma_t, \alpha_t\}$ *is stationary and geometrically ergodic.*

The proof can be found in Appendix A. Hence $\{Q_t\}$ is also stationary and ergodic since it is a coupled process of $\{\sigma_t, \alpha_t\}$ through (3.4).

3.2 Parameter Estimation

We denote arbitrary parameters by $\theta = (\beta_0, \beta_1, \beta_2, \beta_3, \gamma_0, \gamma_1, \gamma_2, \gamma_3, \mu)$ and denote $\Theta_s = \{\theta | \beta_0, \gamma_0 \in \mathbb{R}, 0 \leq \beta_1, \gamma_1 < 1, \beta_2, \gamma_2 > 0, \beta_3, \gamma_3 > e/\min(Q_t), \mu < \min(Q_t)\}$. We assume that all allowable parameters are in Θ_s, including the true parameters $\theta_0 = (\beta_0^0, \beta_1^0, \beta_2^0, \beta_3^0, \gamma_0^0, \gamma_1^0, \gamma_2^0, \gamma_3^0, \mu_0)$. We also denote the true value of (σ_1, α_1) as (σ_1^0, α_1^0). It is evident that one cannot know (σ_1^0, α_1^0) because of the hidden processes of (σ_t, α_t). But the effects of initial value (σ_1, α_1) reduce exponentially as t tends to infinity due to the recursive equations of (σ_t, α_t) and the ranges of β_1 and γ_1. In the proofs of Theorems 2 and 3, one can see that the consistency and asymptotic normality of MLE do not require known (σ_1^0, α_1^0).

The log-likelihood function based on arbitrary initial values $(\tilde{\sigma}_1, \tilde{\alpha}_1)$ with observations $\{Q_t\}_{t=1}^n$, denoted by $\tilde{L}_n(\theta)$, is

$$\tilde{L}_n(\theta) = \frac{1}{n}\sum_{t=1}^{n} \tilde{l}_t(\theta) = \frac{1}{n}\sum_{t=1}^{n} \left[\log \tilde{\alpha}_t + \tilde{\alpha}_t \log \tilde{\sigma}_t - (\tilde{\alpha}_t + 1)\log(Q_t - \mu) - \tilde{\sigma}_t^{\tilde{\alpha}_t}(Q_t - \mu)^{-\tilde{\alpha}_t}\right] \tag{3.9}$$

where $(\tilde{\sigma}_t, \tilde{\alpha}_t)$ is generated from $(\tilde{\sigma}_1, \tilde{\alpha}_1)$ through (3.5) and (3.6).

Theorem 2 *(Consistency) Assume the parameter space Θ is a compact set of Θ_s. Suppose the observations $\{Q_t\}_{t=1}^n$ are generated by a stationary and ergodic process defined in Θ with true parameter θ_0 which is in the interior of Θ, then there exists a sequence of $\hat{\theta}_n$, the local maximizer of $\tilde{L}_n(\theta)$, such that $\hat{\theta}_n \xrightarrow{p} \theta_0$ and $\left\|\hat{\theta}_n - \theta_0\right\| \leq \tau_n$, where $\tau_n = O_p\left(n^{-r}\right), 0 < r < 1/2$. Therefore $\hat{\theta}_n$ is consistent.*

Theorem 2 indicates that there always exists a sequence of consistent MLE $\hat{\theta}_n$ which is a local maximizer of $\tilde{L}_n(\theta)$ near the true parameters θ_0. Additionally, Theorem 3 shows the asymptotic normality of MLE $\hat{\theta}_n$. It is noted that both Theorems 2 and 3 do not depend on whether (σ_1^0, α_1^0) is known or not.

Theorem 3 *(Asymptotic normality) Under the conditions in Theorem 2, we have $\sqrt{n}\left(\hat{\theta}_n - \theta_0\right) \xrightarrow{d} N\left(0, M_0^{-1}\right)$, where $\hat{\theta}_n$ is the same as in Theorem 2 and M_0 is the Fisher Information matrix evaluated at θ_0. Further, the sample variance of plug-in estimated score functions $\left\{\frac{\partial}{\partial\theta} l_t\left(\hat{\theta}_n\right)\right\}_{t=1}^n$ is a consistent estimator of M_0.*

It is obvious that μ, β_3, γ_3 influence the support of the observations Q_t ($Q_t > \max(\mu, e/\beta_3, e/\gamma_3)$). Thus, MLE is irregular in the proposed model and the uniqueness of MLE becomes a problem. Zhao et al. (2018) briefly discussed the consistency and asymptotic normality for such irregular MLE for Fréchet distribution, with i.i.d. observations was proved by Smith (1985). They further extended the existing results to AcF model with exponential function under stationary and ergodic conditions. Here we provide a partial answer for our modified model following the proof of Zhao et al. (2018).

Proposition 1 *(Asymptotic uniqueness) Denote $V_n = \{\theta \in \Theta | \mu \leq cQ_{n,1} + (1-c)\mu_0\}$ where $Q_{n,1} = \min_{1\leq t\leq n} Q_t$, under the conditions in Theorem 2, for any fixed $0 < c < 1$, there exists a sequence of $\hat{\theta}_n = \arg\max_{\theta\in V_n} \tilde{L}_n(\theta)$ such that, $\hat{\theta}_n \xrightarrow{p} \theta_0$, $\left\|\hat{\theta}_n - \theta_0\right\| \leq \tau_n$, where $\tau_n = O_p\left(n^{-r}\right)$, $0 < r < 1/2$, and $P\left(\hat{\theta}_n \text{ is the unique global maximizer of } V_n\right) \to 1$.*

Notice that $\tilde{L}_n(\theta)$ is defined on $Q_t > \max(\mu, e/\beta_3, e/\gamma_3)$. It is obvious that $V_n \subseteq \Theta_n$ because $\mu_0 < cQ_{n,1} + (1-c)\mu_0 < Q_{n,1}$. Proposition 1 shows that there exists an asymptotic unique MLE $\hat{\theta}_n = \arg\max_{\theta \in V_n} \tilde{L}_n(\theta)$ over V_n with the probability going to 1.

All the proofs of Theorems 1, 2, 3, and Proposition 1 can be found in Chapter 6

3.3 Simulation

In this section, we study the finite sample performance of maximum likelihood estimators (MLEs) by six simulation examples. We simulate data from an AcFL model with the parameters obtained from the real data analysis in part 1 (without solar flare), part 12 (without solar flare), part 33(first solar flare), part 34 (first solar flare), part 44 (second solar flare), and part 45 (second solar flare), with lengths of 1000 and 5000 respectively. For each sample size, we repeat 500 times. Table 3.1 presents the estimated mean values and standard deviations from 500 simulated time series.

According to Table 3.1, one can see that the bias and standard deviation of MLEs decrease as the sample size increases. It denotes the consistency of the estimator under correct model specification. It is worth noting that when the sample size is 1000, the performance of MLE is acceptable.

In order to compare simulated data from AcFL model with real data, we draw histogram plots as shown in Figure 3.1. Since our data is highly skewed with long right tail, we use log transformation to emphasize large numbers. Top graph compares the simulated data and true values in part 1. One can see that simulated data approximate real data well in tail index, scale, and location. There is one extreme large value in simulated data which is due to a random unit Fréchet Y score. Although we may get such large value in simulation, the means of simulated parameters do not have large bias comparing to setting parameters. Similar to the top graph, the middle one indicates that simulated data in subareas with weak solar flare can also catch the characteristics of real data. As one can see, there also exist extreme large values in simulated data but they do not affect the performance of MLEs. For part 45 which has strong solar flare, the simulated data have several large values. The distribution of simulated data is similar to real data, especially for right tail part.

Remark 1: Since we have constraints of parameters β_3, γ_3, and μ based on real data $\{Q_t\}$, we check them by using simulated data in Section 3.3. All constraints are held in simulated data.

Part 1	γ_0	γ_1	γ_2	γ_3	β_0	β_1	β_2	β_3	μ
True Value	-2.717	0	22.495	5.519	5.961	0	3.315	0.047	94.065
Mean(S1)	-2.747	0	22.325	5.594	6.025	0	3.823	0.061	94.213
Std. Dev.(S1)	0.446	–	4.093	2.270	0.369	–	1.694	0.031	3.959
Mean(S2)	-2.717	0	22.676	5.591	5.978	0	3.474	0.052	94.156
Std. Dev(S2)	0.306	–	3.334	2.203	0.237	–	1.129	0.021	1.765
Part 12	γ_0	γ_1	γ_2	γ_3	β_0	β_1	β_2	β_3	μ
True Value	-2.868	0.198	27.896	35.571	7.749	0	-14.547	0.290	119.747
Mean(S1)	-2.784	0.200	26.803	32.722	7.712	0	-14.634	0.366	120.283
Std. Dev.(S1)	0.325	0.108	2.981	4.152	0.516	–	4.513	0.266	2.532
Mean(S2)	-2.850	0.200	27.519	33.753	7.769	0	-14.949	0.347	120.050
Std. Dev(S2)	0.175	0.044	1.754	4.289	0.426	–	3.795	0.193	1.008
Part 33	γ_0	γ_1	γ_2	γ_3	β_0	β_1	β_2	β_3	μ
True Value	-0.451	0.084	2.016	0.022	10.781	0	-51.947	38.623	41.730
Mean(S1)	-0.570	0.086	2.525	0.028	10.725	0	-51.466	39.233	40.902
Std. Dev.(S1)	0.148	0.071	0.545	0.020	0.312	–	3.098	3.990	10.526
Mean(S2)	-0.563	0.079	2.454	0.026	10.807	0	-52.438	40.298	42.162
Std. Dev(S2)	0.058	0.036	0.197	0.002	0.1672	–	1.773	3.538	4.728
Part 34	γ_0	γ_1	γ_2	γ_3	β_0	β_1	β_2	β_3	μ
True Value	-0.764	0.122	4.103	0.090	10.554	0	46.724	22.210	35.694
Mean(S1)	-0.704	0.120	3.965	0.102	10.441	0	45.121	20.004	35.612
Std. Dev.(S1)	0.289	0.043	1.760	0.066	0.310	–	3.081	3.795	9.223
Mean(S2)	-0.747	0.121	4.072	0.094	10.472	0	45.410	20.117	35.452
Std. Dev(S2)	0.155	0.034	0.991	0.036	0.181	–	2.280	3.512	4.152
Part 44	γ_0	γ_1	γ_2	γ_3	β_0	β_1	β_2	β_3	μ
True Value	-1.296	0.209	6.570	0.089	11.021	0	-59.495	94.416	68.211
Mean(S1)	-1.163	0.215	6.114	0.102	10.891	0	-56.613	76.102	68.769
Std. Dev.(S1)	0.457	0.090	2.890	0.083	0.259	–	2.084	22.926	12.633
Mean(S2)	-1.297	0.207	6.765	0.106	10.909	0	-57.084	77.815	68.119
Std. Dev(S2)	0.285	0.039	1.955	0.068	0.154	–	2.077	17.671	6.435
Part 45	γ_0	γ_1	γ_2	γ_3	β_0	β_1	β_2	β_3	μ
True Value	-1.694	0.144	11.989	0.532	12.286	0	70.687	77.882	55.75580
Mean(S1)	-1.684	0.143	12.015	0.568	12.217	0	69.908	77.936	54.074
Std. Dev.(S1)	0.319	0.044	2.532	0.224	0.345	–	3.769	1.889	10.026
Mean(S2)	-1.685	0.143	11.889	0.533	12.277	0	70.551	77.717	55.159
Std. Dev(S2)	0.201	0.034	1.747	0.160	0.210	–	2.356	1.822	5.458

Table 3.1: The performance of MLE with the sample size of 1000 (S1) and 5000 (S2) using the parameters from analysis in part 1, 12, 33, 34, 44, and 45. Mean and Std. Dev. are the sample mean and standard deviation of the MLE's obtained from 500 simulations.

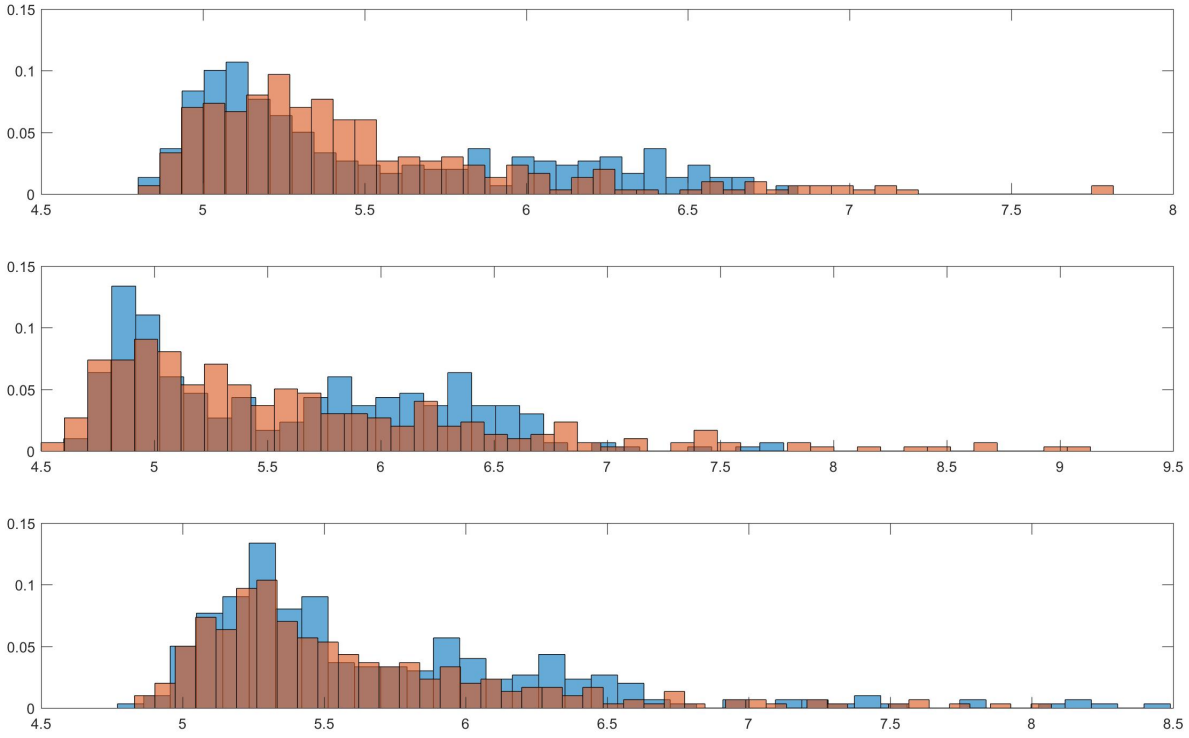

Figure 3.1: Histogram plots of simulated data (orange) and real data (blue) in part 1 (top), part 34 (middle), and part 45 (bottom)

3.4 Empirical Application

First we fit the established model in one hundred and twenty-two subareas. In this section, we will only show the results of part 1 (without solar flare), part 12 (without solar flare), part 33 (first solar flare), part 34 (first solar flare), part 44 (second solar flare), and part 45 (second solar flare). The fitted parameters are displayed in Table 3.2. Figures 3.2 and 3.3 show the plots of σ_t and α_t in three parts. Section 7.1 includes the fitting results and plots for all other subareas.

We note that β_1 is not significant in six subareas and γ_1 is not significant in part 1 when we fitted the data with all parameters. Therefore we set those parameters to be zero and all other parameters are significant this time. The standard deviations shown in Table 3.2 are

Part 1	γ_0	γ_1	γ_2	γ_3	β_0	β_1	β_2	β_3	μ
Est. Value	-2.714	0	22.325	5.594	6.025	0	3.823	0.061	94.213
Std. Dev.	0.170	–	0.512	0.762	0.197	–	0.272	0.010	9.447
Part 12	γ_0	γ_1	γ_2	γ_3	β_0	β_1	β_2	β_3	μ
Est. Value	-2.868	0.198	27.896	35.571	7.749	0	-14.547	0.290	119.747
Std. Dev.	0.805	0.089	6.279	7.100	0.262	–	0.676	0.040	8.375
Part 33	γ_0	γ_1	γ_2	γ_3	β_0	β_1	β_2	β_3	μ
Est. Value	-0.451	0.084	2.016	0.022	10.781	0	-51.947	38.623	41.730
Std. Dev.	0.063	0.010	0.174	0.002	0.262	–	1.429	0.313	6.999
Part 34	γ_0	γ_1	γ_2	γ_3	β_0	β_1	β_2	β_3	μ
Est. Value	-0.764	0.122	4.103	0.090	10.554	0	46.724	22.210	35.694
Std. Dev.	0.121	0.030	0.490	0.024	0.076	–	0.680	1.809	7.475
Part 44	γ_0	γ_1	γ_2	γ_3	β_0	β_1	β_2	β_3	μ
Est. Value	-1.296	0.209	6.570	0.089	11.021	0	-59.495	94.4164	68.211
Std. Dev.	0.179	0.098	0.725	0.009	0.135	–	0.836	0.499	10.259
Part 45	γ_0	γ_1	γ_2	γ_3	β_0	β_1	β_2	β_3	μ
Est. Value	-1.694	0.144	11.989	0.532	12.286	0	70.687	77.882	55.75580
Std. Dev.	0.186	0.028	0.936	0.125	0.122	–	0.794	0.151	8.422

Table 3.2: Estimated parameter values of standard AcFL model.

obtained by the following methods. We first calculate differences and randomly select 100 pixels in part 1, part 12, part 33, part 34, part 44, and part 45 at each time point. Then we obtain the maximum values based on these 100 data points and fit AcFL models. The procedure is repeated 500 times. The standard deviations are calculated from 500 estimates.

We use the same method to fit the data in other subareas and calculate their standard deviations. In Section 7.1, we see that for all parts, β_1 is not significant and we set it to be zero. γ_1 is not significant in 20% subareas.

Figure 3.2 includes six plots with the graphs of α_t on the left and the graphs of σ_t on the right. In the plots of α_t, it is obvious that the α_t changes dynamically in three parts. The horizontal lines exhibit the smallest value of α_t (α_{small}) in $t = 1 \sim 185$ when solar flare doesn't happen. The first vertical line in second (part 34) and third (part 45) plot indicate the time when the α_t is smaller than α_{small}.It is worth noting that the time in part 34 is 188 and the first solar flare happens at $t = 186$. The time in part 45 is 216 and the second solar flare occurs at $t = 215$. In addition, the second vertical lines show the last time that α_t is

less than α_{small}. In part 34, $t = 196$ is close to the time when first solar flare is brightest, $t = 197$. In part 45, $t = 235$ for second vertical line and second solar flare is brightest at $t = 229$.

In Figure 3.3, we show other six plots about α_t on the left and σ_t on the right. In part 12, although the value of α_t is below α_{small} at $t = 214$, it increases after that time point. When we look at original data, it can be seen that the maximum value in part 12 is at $t = 214$. We can also compare the α_t plot of part 33 and part 34 in Figure 3.2. The solar flare in part 34 looks brighter and has longer time than that in part 33. As a result, the value of α_t in part 33 is smaller than α_{small} at $t = 191$ and it is larger than the smallest value after $t = 196$. The starting time ($t = 191$) is behind that in part 34 which is $t = 188$. The ending time ($t = 196$) shown in Figure 3.3 is the same as that in part 44 ($t = 196$). Therefore the interval that α_t is smaller than α_{small} is short than part 34. Comparing part 44 and part 45, the α_t plots indicate solar flare first started in part 45 at $t = 216$ then "transferred" the energy to part 44 at $t = 222$. In part 44, solar flare ends at $t = 231$ earlier than that in part 45.

σ_t changes in opposite direction but is still sensitive to solar flare. The horizontal lines in right plots indicate the largest value of σ_t (σ_{large}) in $t = 1 \sim 185$. The first vertical lines display the first time when the σ_t is larger than σ_{large} and the second vertical lines indicate the last σ_t that is bigger than σ_{large}.

When we look at α_t and σ_t plots in Section 7.1, part 22 and part 96 do not have normal α_t curve if we use all the values. Therefore we show the plots for these two parts separately in Figure 3.4. After we change the large value in the beginning, one can see the α_t plot is normal again and tail index can be used to detect solar flare again. This is consistent with Theorems 2 and 3 that we do not need to know the true start point. On the other hand, there is no problem in σ_t plots. σ_t plots show that solar flare does not happen in these parts.

The results are coincident with original video in which solar flare appears quickly, lasts sometime, then vanishes. According to Figure 3.2 and Figure 3.3, the α_t decreases and σ_t

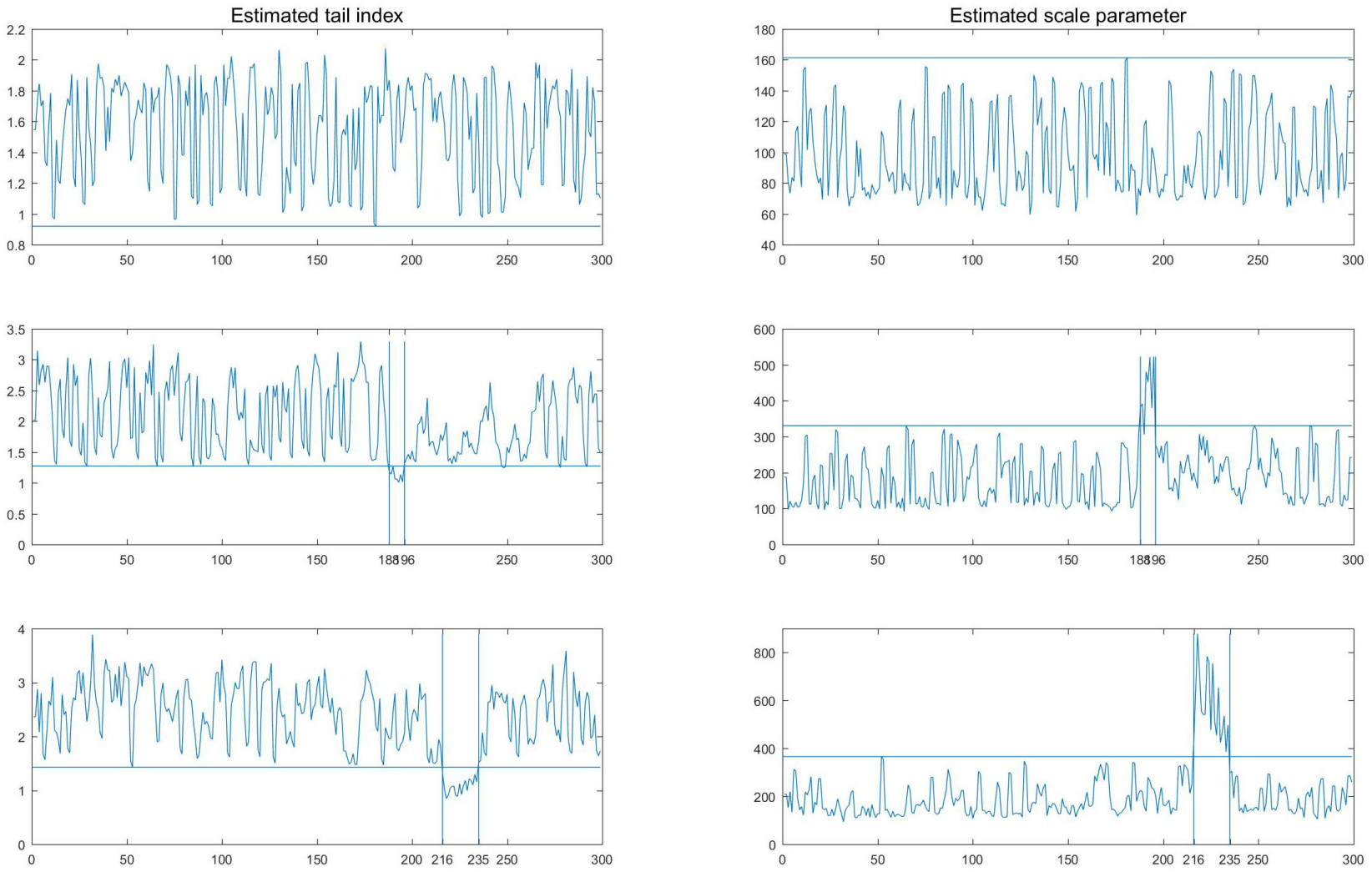

Figure 3.2: Estimated α_t (left) and σ_t(right) in part 1 (top), part 34 (middle), and part 45 (bottem) using standard AcFL model. For the plots of α_t, the horizontal lines indicate the smallest α_t in $t = 1 \sim 185$ (α_{small}). The first vertical line in each plot displays the first time when the α_t is smaller than α_{small}. And the second vertical line shows the the last α_t which is smaller α_{small} after α_t goes beyond the smallest value.The σ_t is shown in the same way with opposite direction.

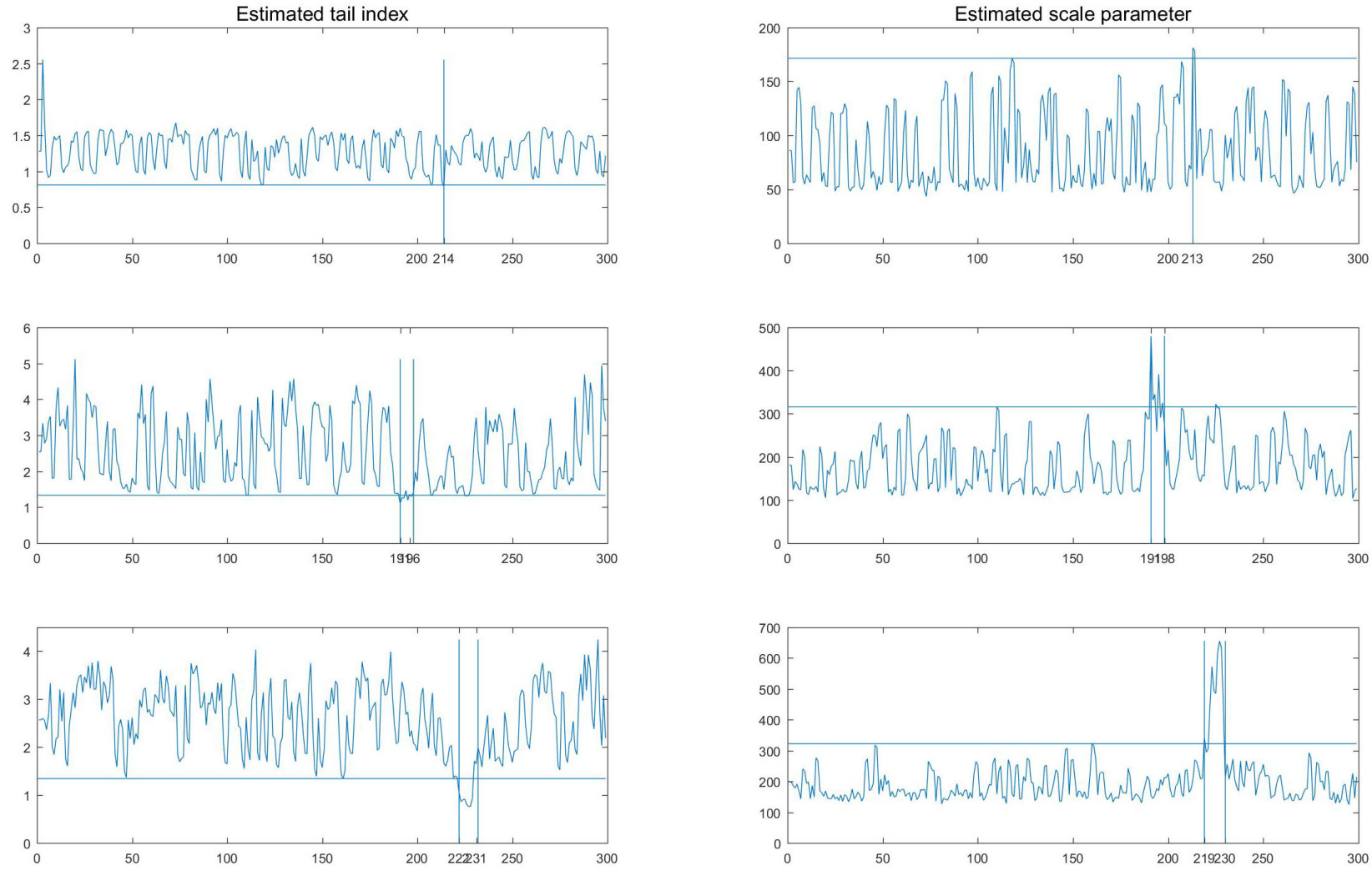

Figure 3.3: Estimated α_t (left) and σ_t(right) in part 12 (top), part 33 (middle), and part 44 (bottem) using AcFL model. For the plots of α_t, the horizontal lines indicate the smallest α_t in $t = 1 \sim 185$ (α_{small}). The first vertical line in each plot displays the first time when the α_t is smaller than α_{small}. And the second vertical line shows the the last α_t which is smaller α_{small} after α_t goes beyond the smallest value.The σ_t is shown in the same way with opposite direction.

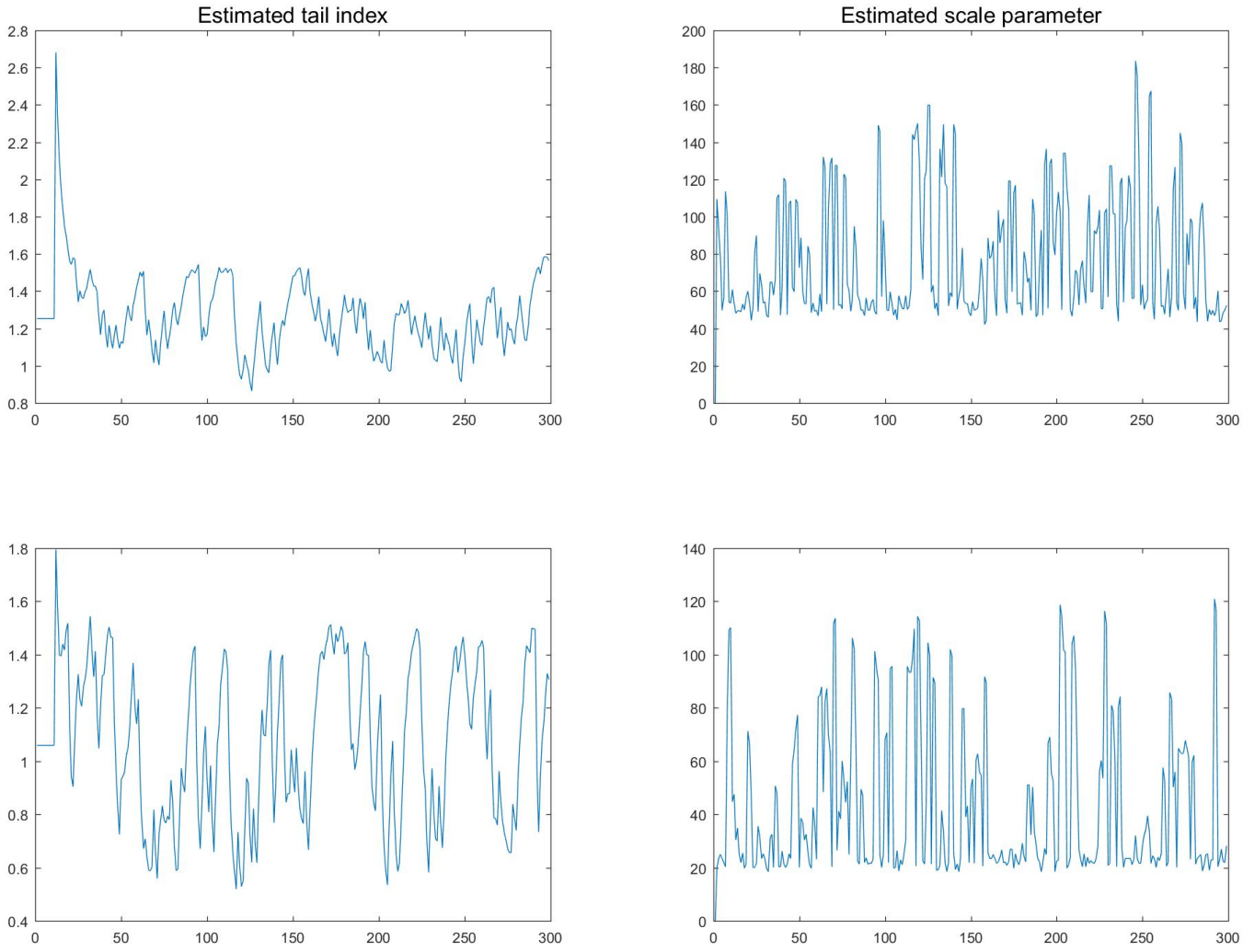

Figure 3.4: Estimated α_t (left) and σ_t(right) in part 22 (top) and part 99 (bottem) using AcFL model after removing large value in the beginning.

increases rapidly when solar flare occurs. As a result, the differences or variations are large when solar flare becomes brighter, hence it appears quickly. Then the variations change to small values and the solar flare lasts some seconds then disappears.

Therefore, we can use these two parameters α_t and σ_t to detect the solar flare one time before happening. In other words, we predict the first solar flare will happen immediately in 12 seconds at $t = 187$ for difference and the second solar will occur instantly in 12 seconds at $t = 215$ for difference. We compare our results with TRAS algorithm in Liu et al. (2015) and methods in Xie et al.(2013) in Table 3.3 using the same data set.

Detection time	First solar flare	Second solar flare
True time	$t = 188$	$t = 216$
Our model	$t = 189$(188 for diff)	$t = 217$ (216 for diff)
Wang et al. (2018)	$t = 190$	–
Liu et al. (2015)	$t = 190$	$t = 221$
Xie et al.(2013)	$t = 191$	$t = 217$

Table 3.3: Solar Flare Detection Time Comparison.

As shown in Table 3.3, our AcFL model has the best performance among four methods. In addition, our method uses 120 data in each frame, while Wang et al.(2018) uses 500 data which is the smallest number in other three methods. Since α_t and σ_t changes over time, it can be used for online application. Additionally, by the recursive formula of α_t and σ_t, we can detect the solar flare one time earlier.

3.5 AcFL model with $k = 2$

3.5.1 Extended Version of AcFL Model

By replacing Q_{t-1} with Q_{t-k} where $k > 1$, we can estimate $\{\sigma_t, \alpha_t\}$ with much earlier observations and then may detect solar flare much earlier. The proposed model is as following:

$$Q_t = \mu + \sigma_t Y_t^{1/\alpha_t} \tag{3.10}$$

$$\log \sigma_t = \beta_0 + \beta_1 \log \sigma_{t-1} - \beta_2 / \log (\beta_3 Q_{t-k}) \tag{3.11}$$

$$\log \alpha_t = \gamma_0 + \gamma_1 \log \alpha_{t-1} + \gamma_2 / \log (\gamma_3 Q_{t-k}) \tag{3.12}$$

where $\{Y_t\}$ is a sequence of i.i.d. unit Fréchet random variables, $\mu < \min(Q_t)$, $0 \leq \beta_1, \gamma_1 < 1$, $\beta_2 > 0$, $\beta_3 > e/\min(Q_t)$, $\gamma_2 > 0$, and $\gamma_3 > e/\min(Q_t)$.

Same as the standard AcFL model, $\{\sigma_t, \alpha_t\}$ also form a homogeneous Markov chain in $\mathbb{R}^2$. Under the same general sufficient conditions in Theorem 1, $\{\sigma_t, \alpha_t\}$ is stationary and geometrically ergodic.

Theorem 4 *(Stationarity and ergodicity) For an extended version of AcFL model with* $\beta_0, \gamma_0 \in \mathbb{R}$ *and* $0 \leq \beta_1, \gamma_1 < 1$, $\beta_2, \gamma_2 > 0$,$\beta_3, \gamma_3 > e/min(Q_t), \mu < min(Q_t)$, *e is the base of the natural logarithm, the latent process* $\{\sigma_t, \alpha_t\}$ *is stationary and geometrically ergodic.*

Since the proof is the same as that of Theorem 1, we skip it. Therefore, $\{Q_t\}$ is also stationary and ergodic.

In the following section, we use extended version of AcFL model with $k = 2$. We fit the solar are data set in part 1, part 12, part 33, part 34, part 44, and part 45 with following

model:

$$Q_t = \mu + \sigma_t Y_t^{1/\alpha_t} \tag{3.13}$$

$$\log \sigma_t = \beta_0 + \beta_1 \log \sigma_{t-1} - \beta_2 / \log (\beta_3 Q_{t-2}) \tag{3.14}$$

$$\log \alpha_t = \gamma_0 + \gamma_1 \log \alpha_{t-1} + \gamma_2 / \log (\gamma_3 Q_{t-2}) \tag{3.15}$$

3.5.2 Theoretical Properties

We set arbitrary parameters by $\theta = (\beta_0, \beta_1, \beta_2, \beta_3, \gamma_0, \gamma_1, \gamma_2, \gamma_3, \mu)$ and set $\Theta_s = \{\theta | \beta_0, \gamma_0 \in \mathbb{R}, 0 \leq \beta_1, \gamma_1 < 1, \beta_2, \gamma_2 > 0, \beta_3, \gamma_3 > e/\min(Q_t), \mu < \min(Q_t)\}$. In addition, We assume all allowable parameters including true parameters $\theta_0 = (\beta_0^0, \beta_1^0, \beta_2^0, \beta_3^0, \gamma_0^0, \gamma_1^0, \gamma_2^0, \gamma_3^0, \mu_0)$ are in Θ_s. We also denote the true value of (σ_1, α_1) as (σ_1^0, α_1^0). We denote the log-likelihood function, which is the same formula as (3.9) by $\tilde{L}_n(\theta)$,

Then we have Theorems 5 and 6 which show the consistency and asymptotic normality of MLE for extended version of AcFL model. Moreover, Proposition 2 indicates the existence of an asymptotic unique MLE $\hat{\theta}_n = \arg\max_{\theta \in V_n} \tilde{L}_n(\theta)$ for the extended model.

Theorem 5 *(Consistency) Assume the parameter space Θ is a compact set of Θ_s. Suppose the observations $\{Q_t\}_{t=1}^n$ are generated by a stationary and ergodic process defined in Θ with true parameter θ_0 which is in the interior of Θ, then there exists a sequence of $\hat{\theta}_n$, the local maximizer of $\tilde{L}_n(\theta)$, such that $\hat{\theta}_n \xrightarrow{p} \theta_0$ and $\left\| \hat{\theta}_n - \theta_0 \right\| \leq \tau_n$, where $\tau_n = O_p\left(n^{-r}\right), 0 < r < 1/2$. Therefore $\hat{\theta}_n$ is consistent.*

Theorem 6 *(Asymptotic normality) Under the conditions in Theorem 5, we have $\sqrt{n}\left(\hat{\theta}_n - \theta_0\right) \xrightarrow{d} N\left(0, M_0^{-1}\right)$, where $\hat{\theta}_n$ is the same as in Theorem 5 and M_0 is the Fisher Information matrix evaluated at θ_0. Further, the sample variance of plug-in estimated score functions $\left\{\frac{\partial}{\partial \theta} l_t\left(\hat{\theta}_n\right)\right\}_{t=1}^n$ is a consistent estimator of M_0.*

Proposition 2 *(Asymptotic uniqueness) Denote $V_n = \{\theta \in \Theta | \mu \leq c Q_{n,1} + (1-c)\mu_0\}$ where $Q_{n,1} = \min_{1 \leq t \leq n} Q_t$, under the conditions in Theorem 6, for any fixed $0 < c < 1$, there exists a*

sequence of $\hat{\theta}_n = \arg\max_{\theta \in V_n} \tilde{L}_n(\theta)$ *such that,* $\hat{\theta}_n \xrightarrow{p} \theta_0$, $\left\|\hat{\theta}_n - \theta_0\right\| \leq \tau_n$, *where* $\tau_n = O_p\left(n^{-r}\right)$, $0 < r < 1/2$, *and* $P\left(\hat{\theta}_n \text{ is the unique global maximizer of } V_n\right) \to 1$.

The proofs of Theorems 5, 6, and Proposition 2 are the same as that for the standard AcFL model. Hence we skip them.

3.5.3 Simulation

Simulation results are shown in Table 3.4. The simulation data is obtained from the extended version of AcFL model using the parameters from empirical applications. The sample sizes are the same as that in Section 3.3, 1000 and 5000. The simulation is repeated 500 times to calculate sample means and standard deviation. From Table 3.4, we see that as sample size increases, the bias and standard deviations of most MLEs reduces. The estimator consistency under the extended verions of AcFL model has been shown.

Like Section 3.3, we also show the histogram plots of simulated data and real data wiht log transformation in part 1 (top), part 34 (middle), and part 45 (bottom) for extended version of AcFL model with $k = 2$ in Figure 3.5. We see that the simulated data in these three subareas catch the characteristics of original data in tail index, scale and locations. There are more extreme values in simulated data for part 1 comparing with the standard AcFL model which is due to the small sample size and uncertainty of Fréchert distribution. Moreover, the simulated data in part 33 also include some huge values but the main part of simulation approximates real data well in tail index, scale, and location. In part 45, the simulated data of the extended version is even better than that of the standard AcFL model. Simulated data not only catch the characteristics of real data in tail index, scale, and location but also has similar large values in right tails.

Remark 2: Similar to the standard AcFL model, we check the constraints of parameters β_3, γ_3, and μ which is based on real data $\{Q_t\}$ through simulated data in this section. All parameter constraints are held in simulated data.

Part 1	γ_0	γ_1	γ_2	γ_3	β_0	β_1	β_2	β_3	μ
True Value	-0.427	0	1.288	0.022	5.592	0	1.766	0.024	95.448
Mean(S1)	-0.430	0	1.338	0.023	5.537	0	1.631	0.023	95.569
Std. Dev.(S1)	0.126	–	0.401	0.006	0.146	–	0.398	0.005	3.885
Mean(S2)	-0.429	0	1.315	0.023	5.567	0	1.707	0.024	95.656
Std. Dev(S2)	0.088	–	0.307	0.005	0.098	–	0.291	0.003	1.690
Part 12	γ_0	γ_1	γ_2	γ_3	β_0	β_1	β_2	β_3	μ
True Value	-0.304	0	1.239	0.023	5.513	0	1.340	0.020	91.463
Mean(S1)	-0.273	0	1.178	0.023	5.484	0	1.285	0.020	91.573
Std. Dev.(S1)	0.120	–	0.348	0.007	0.139	–	0.323	0.004	4.940
Mean(S2)	-0.281	0	1.214	0.023	5.501	0	1.335	0.020	91.578
Std. Dev(S2)	0.235	–	0.280	0.006	0.114	–	0.238	0.003	2.057
Part 33	γ_0	γ_1	γ_2	γ_3	β_0	β_1	β_2	β_3	μ
True Value	-0.487	0	1.941	0.056	7.272	0	22.902	17.387	97.677
Mean(S1)	-0.431	0	1.745	0.056	7.257	0	22.667	16.826	97.905
Std. Dev.(S1)	0.166	–	0.769	0.031	0.278	–	2.073	2.799	3.620
Mean(S2)	-0.471	0	1.922	0.059	7.267	0	22.765	16.997	97.717
Std. Dev(S2)	0.131	–	0.689	0.028	0.177	–	1.543	2.847	1.518
Part 34	γ_0	γ_1	γ_2	γ_3	β_0	β_1	β_2	β_3	μ
True Value	-1.365	0	14.032	27.993	5.499	0	1.286	0.026	74.935
Mean(S1)	-1.349	0	13.832	27.205	5.467	0	1.258	0.026	75.029
Std. Dev.(S1)	0.199	–	1.722	2.446	0.271	–	0.336	0.006	5.147
Mean(S2)	-1.357	0	13.853	27.932	5.492	0	1.286	0.026	75.094
Std. Dev(S2)	0.121	–	1.104	0.929	0.084	–	0.259	0.004	1.723
Part 44	γ_0	γ_1	γ_2	γ_3	β_0	β_1	β_2	β_3	μ
True Value	-1.7063	0.580	19.710	87.176	2.654	0.684	6.165	0.838	112.596
Mean(S1)	-1.852	0.511	21.597	88.040	2.785	0.666	6.457	0.928	112.457
Std. Dev.(S1)	0.186	0.129	1.990	1.974	0.603	0.081	1.566	0.291	6.502
Mean(S2)	-1.791	0.551	20.752	88.130	2.713	0.676	6.345	0.916	112.747
Std. Dev(S2)	0.113	0.049	1.226	1.799	0.262	0.033	1.003	0.289	2.778
Part 45	γ_0	γ_1	γ_2	γ_3	β_0	β_1	β_2	β_3	μ
True Value	-2.239	0.134	23.946	32.606	10.048	0	52.439	99.514	90.423
Mean(S1)	-2.153	0.141	23.234	31.509	10.112	0	52.868	98.240	91.013
Std. Dev.(S1)	0.548	0.115	1.678	1.707	0.442	–	1.011	4.111	5.432
Mean(S2)	-2.200	0.134	23.456	31.300	10.080	0	52.745	98.728	90.781
Std. Dev(S2)	0.132	0.056	1.264	1.509	0.090	–	0.855	3.812	2.521

Table 3.4: The performance of MLE with the sample size of 1000 (S1) and 5000 (S2) using the parameters from extended version of AcFL models. Mean and Std. Dev. are the sample mean and standard deviation of the MLE's obtained from 500 simulations.

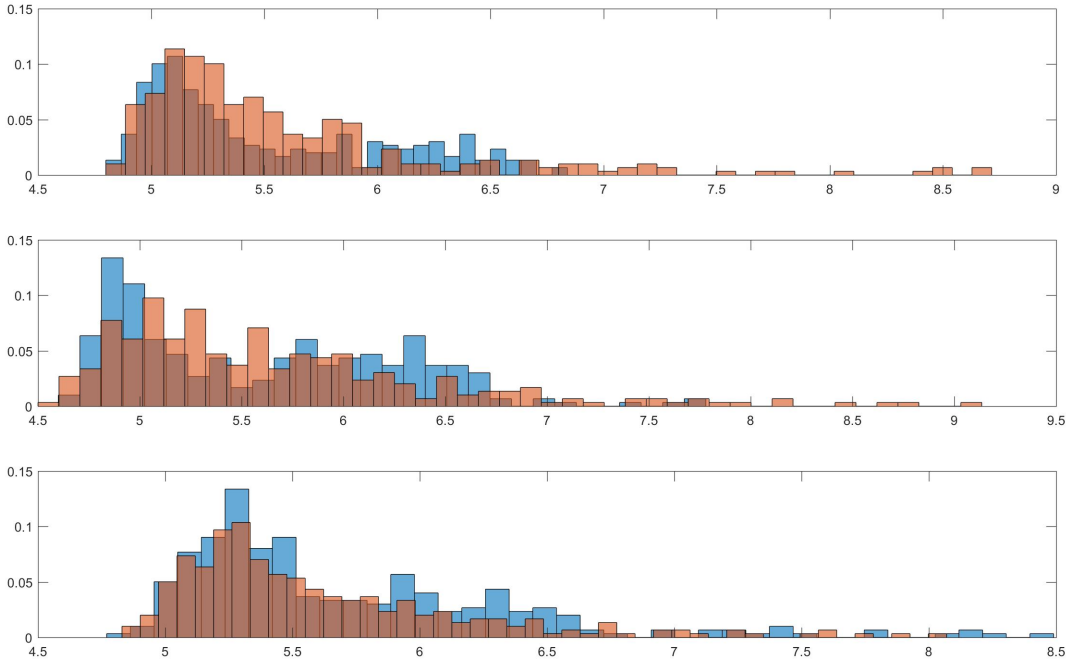

Figure 3.5: Histogram plots of simulated data (orange) and real data (blue) in part 1 (top), part 34 (middle), and part 45 (bottom)

3.5.4 Solar flare detection

The estimated parameters are shown in Table 3.5. We notice that comparing with standard AcFL model, models in part 1 and part 45 keep the same structure (β_1 is not significant in both models and γ_1 is not significant in the model of part 1), while γ_1s in the models of part 12, part 33, part 34 are not significant, hence set to zero this time (γ_1 and β_1 are not significant). In part 44, β_1 becomes significant this time. The standard deviations are calculated using the same method: we sample 100 pixels in each subareas at each time point and calculate maximum values based on 100 samples. Then we fit the the new data with the extended version of AcFL models. We repeat this procedure 500 times and finally obtained standard deviations.

We draw the plots of tail index α_t (left) and scale parameter σ_t (right) in the same way as the standard AcFL model. In Figure 3.6, the top two are the graphs of part 1, the middle

Part 1	γ_0	γ_1	γ_2	γ_3	β_0	β_1	β_2	β_3	μ
Est. Value	-0.427	0	1.288	0.022	5.592	0	1.766	0.024	95.448
Std. Dev.	0.017	–	0.271	0.004	1.028	–	0.123	0.003	7.446
Part 12	γ_0	γ_1	γ_2	γ_3	β_0	β_1	β_2	β_3	μ
Est. Value	-0.304	0	1.239	0.023	5.513	0	1.340	0.020	91.463
Std. Dev.	0.102	–	0.206	0.010	0.316	–	0.109	0.010	6.304
Part 33	γ_0	γ_1	γ_2	γ_3	β_0	β_1	β_2	β_3	μ
Est. Value	-0.487	0	1.941	0.056	7.272	0	22.902	17.387	97.677
Std. Dev.	0.058	–	0.111	0.003	0.075	–	0.473	0.661	5.453
Part 34	γ_0	γ_1	γ_2	γ_3	β_0	β_1	β_2	β_3	μ
Est. Value	-1.365	0	14.032	27.993	5.499	0	1.286	0.026	74.935
Std. Dev.	0.117	–	0.719	0.923	0.109	–	0.068	0.005	6.701
Part 44	γ_0	γ_1	γ_2	γ_3	β_0	β_1	β_2	β_3	μ
Est. Value	-1.7063	0.580	19.710	87.176	2.654	0.684	6.165	0.838	112.596
Std. Dev.	0.083	0.044	0.943	0.714	0.213	0.025	0.918	0.266	13.566
Part 45	γ_0	γ_1	γ_2	γ_3	β_0	β_1	β_2	β_3	μ
Est. Value	-2.239	0.134	23.946	32.606	10.048	0	52.439	99.514	90.423
Std. Dev.	0.226	0.031	0.758	1.717	0.389	–	2.327	2.219	8.812

Table 3.5: Estimated parameter values of AcFL model with $k = 2$

two are those of part 34 and the bottom plots are those of part 45. In Figure 3.7, the order is part 12 (top), part 33 (middle), and part 44 (bottom), respectively.

The horizontal lines display the smallest α_t (α_{small}) and the largest σ_t (σ_{large}) in $t = 1 \sim 185$. First vertical lines in the left plots shows the first time when α_t is smaller than α_{small} and the second vertical lines represents the last time when α_t is less than α_{small}. In the plots of σ_t, the first time when σ_t is larger than σ_{large} is displayed by the first vertical lines and the second lines exhibit the last time when σ_t is larger than σ_{large}.

According to the plots, when a solar flare happens, the tail index α_t decreases and scale parameter σ_t increases immediately. We can detect first solar flare happens at $t = 189$ and second solar flare occurs at $t = 217$. In other words, we predict first solar flare will appear in 24 seconds at $t = 187$ and second solar flare will take place in 24 seconds at $t = 215$.

Comparing with the plots in Section 3.4, it is worth noting that all prediction time (the starting time and the time when solar flare is brightest) in AcFL model with $k = 2$ is one time unit behind those in standard AcFL model due to the change of model structure. This

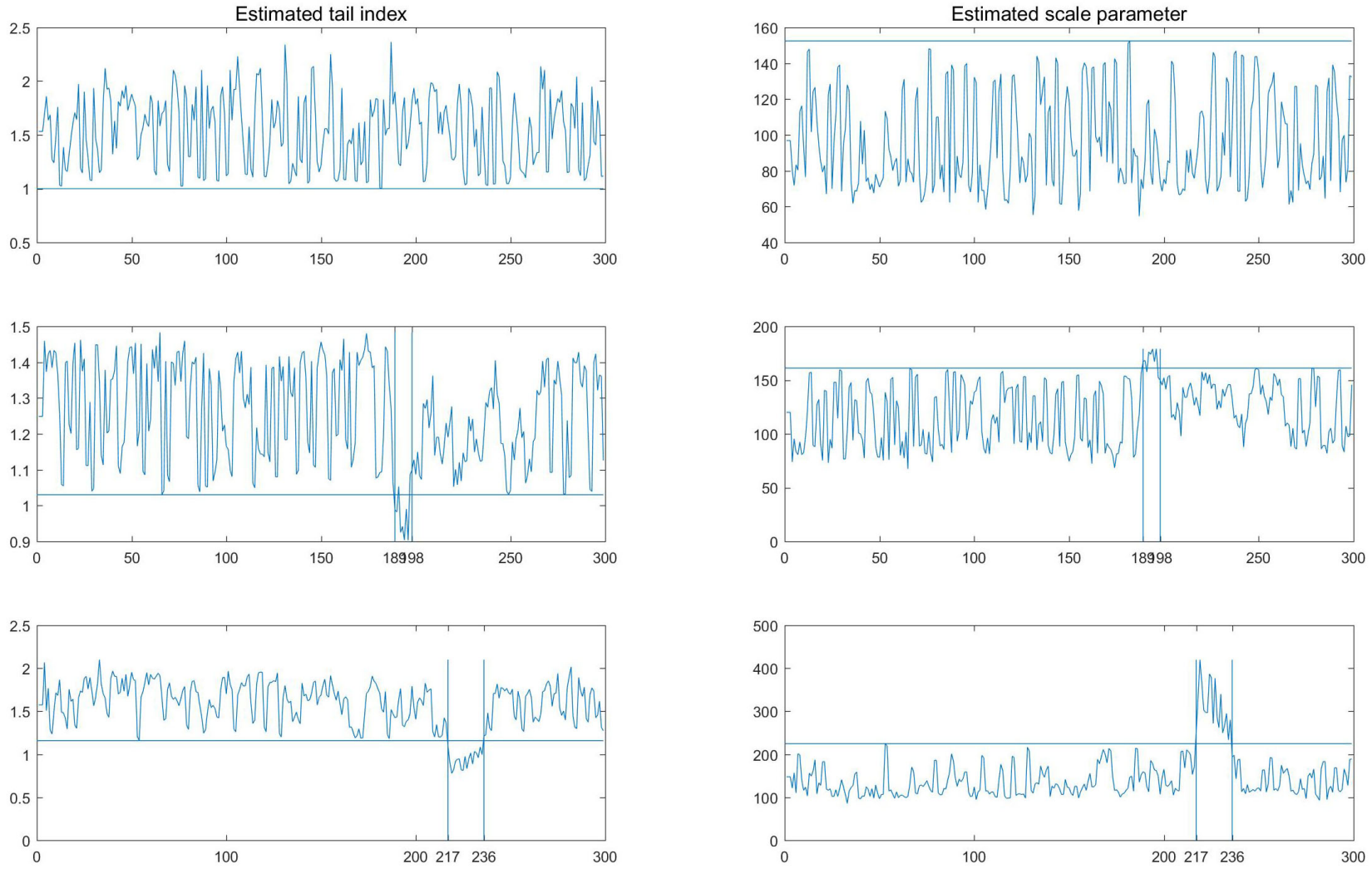

Figure 3.6: Estimated α_t (left) and σ_t(right) in part 1 (top), part 34 (middle), and part 45 (bottem) using Acf model with log function and $k = 2$. For the plots of α_t, the horizontal lines indicate the smallest α_t in $t = 1 \sim 185$ (α_{small}). The first vertical line in each plot displays the first time when the α_t is smaller than α_{small}. And the second vertical line shows the the last α_t which is smaller α_{small} after α_t goes beyond the smallest value.The σ_t is shown in the same way with opposite direction.

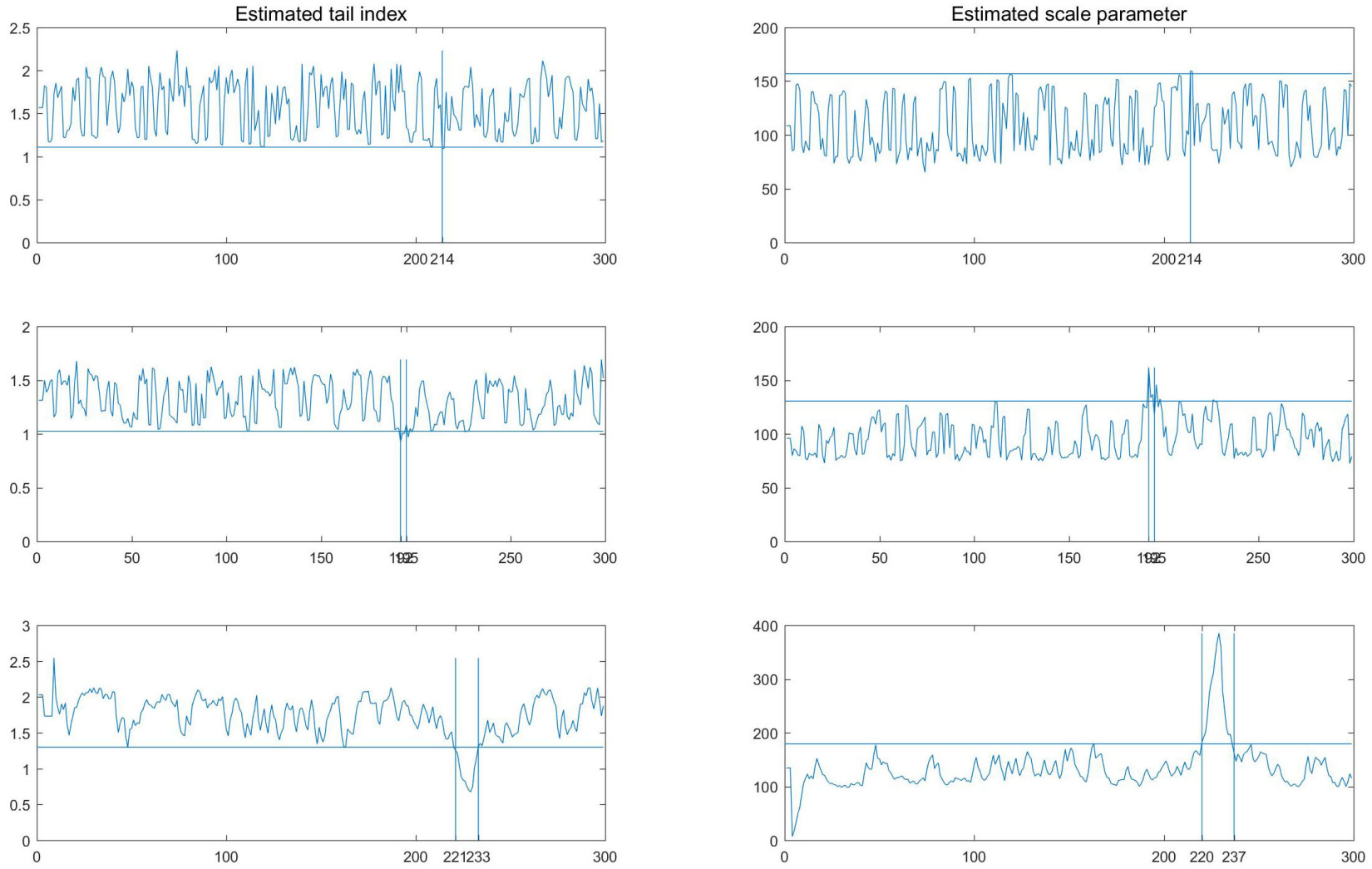

Figure 3.7: Estimated α_t (left) and σ_t(right) in part 12 (top), part 33 (middle), and part 44 (bottem) using Acf model with log function and $k = 2$. For the plots of α_t, the horizontal lines indicate the smallest α_t in $t = 1 \sim 185$ (α_{small}). The first vertical line in each plot displays the first time when the α_t is smaller than α_{small}. And the second vertical line shows the the last α_t which is smaller α_{small} after α_t goes beyond the smallest value.The σ_t is shown in the same way with opposite direction.

prediction delay not only happens in the subareas where solar flare occurs earlier than other areas for example part 34 and part 45, but also happens in part 33 and part 44.

The parameter results and plots for other subareas can be found in Section 7.2. There are 30% subareas that have insignificant γ_1 and we set thoese values to be zero. In nearly 60% parts, β_1 is not significant. Comparing to the standard AcFL model, AcFL model with more lag shows autoregressive effects for σ_t in some parts.

In addition, some α_t and σ_t plots have abnormal large values in the beginning which influence the whole graphs such as α_t plots in part 2, part 4, part 9, part 19, part 22, part 25, part 26, part 30, part 39, part 40, part 46, part 47, part 50, part 56, part 68, part 95, part 96, part 113, part 114, part 117 and σ_t plots in part 3, part 9, part 25, part 36, part, 39, part 52, part 56, part 63, part 68, part 78, part 113. If we remove these abnormal values from the start, the plots become normal again.

Moreover, σ_t plots in part 2, part 19, part 21, part 30, part 38, part 46, part 50, part 74, part 99 have upward trend. α_t plots in part 75, part 100,part 118 have downward trend. α_t plots in part 14, part 53, part 71, part 92, part 93, part 97 show sudden huge values in the middle of the graphs and becomes normal again. We consider those plots can not be used to detect solar flare. However, the subareas with abnormal σ_t plots (α_t plots) have normal α_t plots (σ_t plots) which we can use to detect solar activities.

The change of α_t and σ_t when solar flare appears are also smaller in Figure 3.6 (Figure 3.7) than those in Figure 3.2 (Figure 3.3). Moreover, maximum likelihood values of second group of models are all smaller than those of the standard AcFL models. Thus, we think the results in Section 3.5.4 are less accurate than those in Section 3.4. It is reasonable because we want to predict the events that happen in farther future in Section 3.5.4.

Chapter 4

Models with Spatial Correlations

4.1 Spatial Correlations

Now our AcFL model treated all subareas as independent and does not consider any spatial correlations. From previous literature, one can see that the method with spatial information e.g., Spatail Adaptive Sampling and Monitoring procedure (aka SASAM, Wang et al. 2018) has better detection performance than the similar technology without spatial correlations such as Top-r based Adaptive Sampling (aka TRAM, Liu et al. 2015). The detection delay of SASAM algorithm is clearly shorter than TRAM procedure.

Moreover, we check the original data by scatter plots. When we look at the original video and histogram plots of subareas with solar flare, it is easy to see there exists spatial correlations and tail dependence between adjacent parts. Figure 4.1 displays the scatter graphs of the original data in part 33 (first solar flare), part 34 (first solar flare), part 43 (without solar flare), part 44 (second solar flare). From Figure 4.1, one can see that there is some potential relationship between brightness values in adjacent areas specially for large values.

Therefore, we consider the following model based on the standard AcFL model in Chapter

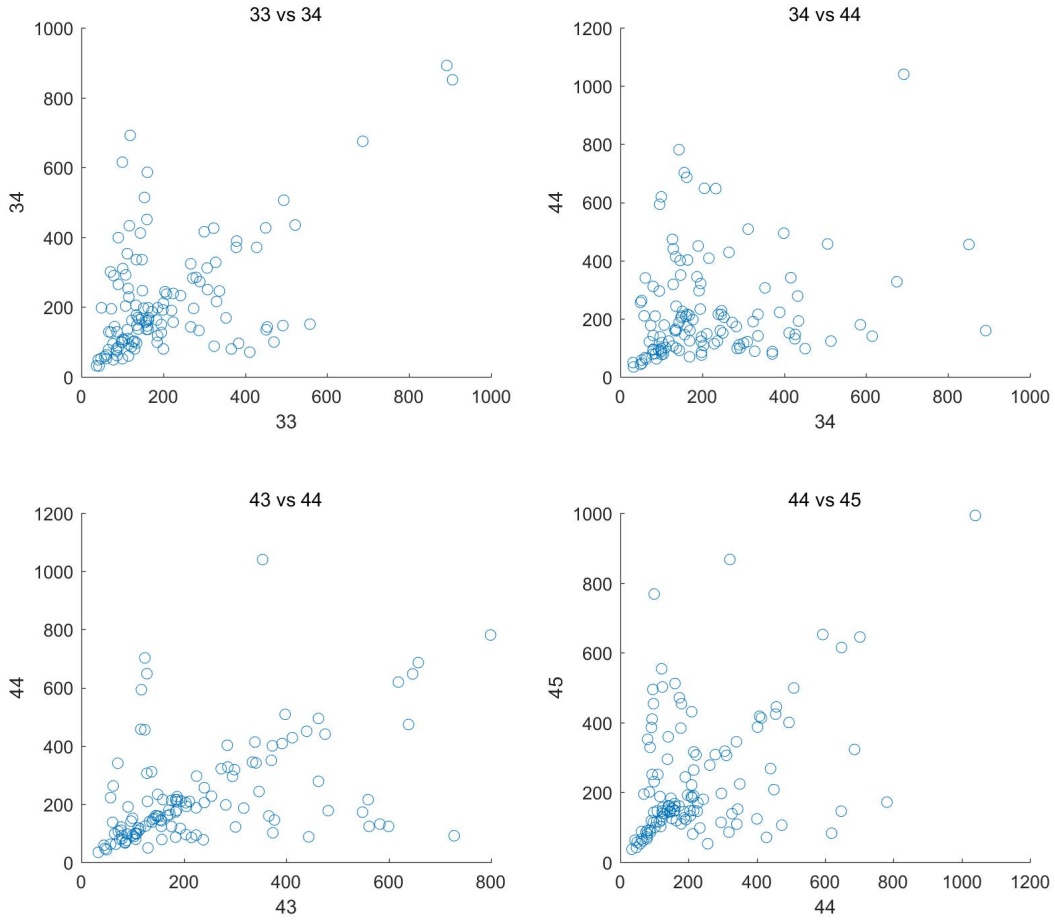

Figure 4.1: The scatter plots of original data in part 33 (first solar flare), part 34 (first solar flare), part 43 (without solar flare), and part 44 (second solar flare).

3:

$$Q_t = \mu + \sigma_t Y_t^{1/\alpha_t} \tag{4.1}$$

$$\log \sigma_t = \beta_0 + \beta_1 \log \sigma_{t-1} - \beta_2 / \log\left(\beta_3 Q_{t-1}\right) - \beta_4 / \log\left(\beta_5 Q_{t-1}^*\right) \tag{4.2}$$

$$\log \alpha_t = \gamma_0 + \gamma_1 \log \alpha_{t-1} + \gamma_2 / \log\left(\gamma_3 Q_{t-1}\right) + \gamma_4 / \log\left(\gamma_5 Q_{t-1}^*\right) \tag{4.3}$$

where $\{Y_t\}$ is a sequence of i.i.d. unit Fréchet random variables, $\mu < \min(Q_t)$, $0 \leq \beta_1, \gamma_1 < 1$, $\beta_2 > 0$, $\beta_3 > e/\min(Q_t)$, $\beta_4 \geq 0$, $\beta_5 > e/\min(Q_t^*)$, $\gamma_2 > 0$, $\gamma_3 > e/\min(Q_t)$, $\gamma_4 \geq 0$, $\gamma_5 > e/\min(Q_t^*)$, and e is the base of the natural logarithm. The restriction of β_3, β_5, γ_3,

and γ_5 makes sure the boundedness of logarithm functions.

$\{Q_t^*\}$ is the maximum value of adjacent parts around $\{Q_t\}$. For most subareas, there are 8 adjacent parts. For areas in the corner like part 1, there are 4 adjacent parts. For subareas on each side like part 2 and 11, there are 5 adjacent areas. Notice that when γ_4 and β_4 are both zero, the model is the same as the standard AcFL model in Chapter 3. Therefore, we can also obtain correct models for the subareas which are not affected by adjacent areas.

We note that $\{\sigma_t, \alpha_t\}$ in spatial AcFL model also form a homogeneous Markov chain in $\mathbb{R}^2$. Theorem 7 provides a sufficient condition for the staionarity and ergodicity of the sequence $\{\sigma_t, \alpha_t\}$

Theorem 7 *(Stationarity and ergodicity) For an AcFL model with spatial correlations, if* $\beta_0, \gamma_0 \in \mathbb{R}$ *and* $0 \leq \beta_1, \gamma_1 < 1$, $\beta_2, \gamma_2, \beta_4, \gamma_4 > 0$, $\beta_3, \gamma_3 > e/min(Q_t)$, $\beta_5, \gamma_5 > e/min(Q_t^*)$, *and* $\mu < min(Q_t)$, *e is the base of the natural logarithm, the latent process* $\{\sigma_t, \alpha_t\}$ *is stationary and geometrically ergodic.*

The proof of Theorem 7 can be found in Section 6.2.1. Since $\{Q_t\}$ is a coupled process of $\{\sigma_t, \alpha_t\}$, it is also stationary and ergodic.

4.2 Parameter Estimations

Let $\theta = (\beta_0, \beta_1, \beta_2, \beta_3, \beta_4, \beta_5, \gamma_0, \gamma_1, \gamma_2, \gamma_3, \gamma_4, \gamma_5, \mu)$ be arbitrary parameters. Let $\Theta_s = \{\theta | \beta_0, \gamma_0 \in \mathbb{R}, 0 \leq \beta_1, \gamma_1 < 1, \beta_2, \gamma_2, \beta_4, \gamma_4 > 0, \beta_3, \gamma_3 > e/\min(Q_t), \beta_5, \gamma_5 > e/\min(Q_t^*), \mu < \min(Q_t)\}$ and the true value of (σ_1, α_1) be (σ_1^0, α_1^0). We assume all allowable parameters including true parameters $\theta_0 = (\beta_0^0, \beta_1^0, \beta_2^0, \beta_3^0, \beta_4^0, \beta_5^0, \gamma_0^0, \gamma_1^0, \gamma_2^0, \gamma_3^0, \gamma_4^0, \gamma_5^0, \mu_0)$ are in Θ_s. The log-likelihood function for spatial AcFL model is the same as that for the standard AcFL model as shown in formula (3.9), denoted by $\tilde{L}_n(\theta)$.

Theorems 8 and 9 indicate the consistency and asymptotic normality of MLE for spatial AcFL model.

Theorem 8 *(Consistency) Suppose the parameter space Θ is a compact set of Θ_s. If the observations $\{Q_t\}_{t=1}^n$ are generated by a stationary and ergodic spatial AcFL defined in Θ with true parameter θ_0 being in the interior of Θ, then there exists a sequence of $\hat{\theta}_n$, the local maximizer of $\tilde{L}_n(\theta)$, such that $\hat{\theta}_n \xrightarrow{p} \theta_0$ and $\left\|\hat{\theta}_n - \theta_0\right\| \leq \tau_n$, where $\tau_n = O_p\left(n^{-r}\right), 0 < r < 1/2$. Hence $\hat{\theta}_n$ is consistent.*

Theorem 9 *(Asymptotic normality) Under the conditions in Theorem 8, we have $\sqrt{n}\left(\hat{\theta}_n - \theta_0\right) \xrightarrow{d} N\left(0, M_0^{-1}\right)$. $\hat{\theta}_n$ is the same as in Theorem 8 and M_0 is the Fisher Information matrix evaluated at θ_0. Further, the sample variance of plug-in estimated score functions $\left\{\frac{\partial}{\partial\theta} l_t\left(\hat{\theta}_n\right)\right\}_{t=1}^n$ is a consistent estimator of M_0.*

Theorem 8 shows the existence of a sequence of consistent MLE $\hat{\theta}_n$ which is a local maximizer of $\tilde{L}_n(\theta)$. In addition, Theorem 9 shows the asymptotic normality of the sequece of consistent MLE $\hat{\theta}_n$. It should be noticed that both Theorems 8 and 9 do not depend on the initial value (σ_1^0, α_1^0).

Proposition 3 *(Asymptotic uniqueness) Denote $V_n = \{\theta \in \Theta | \mu \leq cQ_{n,1} + (1-c)\mu_0\}$ where $Q_{n,1} = \min_{1\leq t\leq n} Q_t$, under the conditions in Theorem 8, for any fixed $0 < c < 1$, there exists a sequence of $\hat{\theta}_n = \arg\max_{\theta\in V_n} \tilde{L}_n(\theta)$ such that, $\hat{\theta}_n \xrightarrow{p} \theta_0$, $\left\|\hat{\theta}_n - \theta_0\right\| \leq \tau_n$, where $\tau_n = O_p\left(n^{-r}\right)$, $0 < r < 1/2$, and $P\left(\hat{\theta}_n \text{ is the unique global maximizer of } V_n\right) \to 1$.*

Proposition 3 indicates there exists an asymptotic unique MLE $\hat{\theta}_n = \arg\max_{\theta\in V_n} \tilde{L}_n(\theta)$ over V_n with the probability going to 1.

All the proofs of Theorems 8, 9, and Proposition 3 can be found in Section 6.2.2.

4.3 Simulation

In this section, our goal is to investigate the performance of maximum likelihood estimators (MLEs) under finite sample. We simulate data from the AcFL model with spatial relationship using the parameters calculated from real data analysis in all subareas. Since the new model

contains information from adjacent parts, the simulation procedure is more complex than standard version. First, we simulate the Q_1 in all 120 areas, then we calculate Q_1^*. As a result, we simulate data in 120 subareas simultaneously.

Different from what we did for standard and extended version of AcFL model, we provide a threshold for simulation because an abnormal large value not only influence consecutive value in this area but also affect the value in adjacent areas. After some time, it will influence all areas and make the whole simulation abnormal. In this part, we use 10^3 times largest value in real data as the threshold.

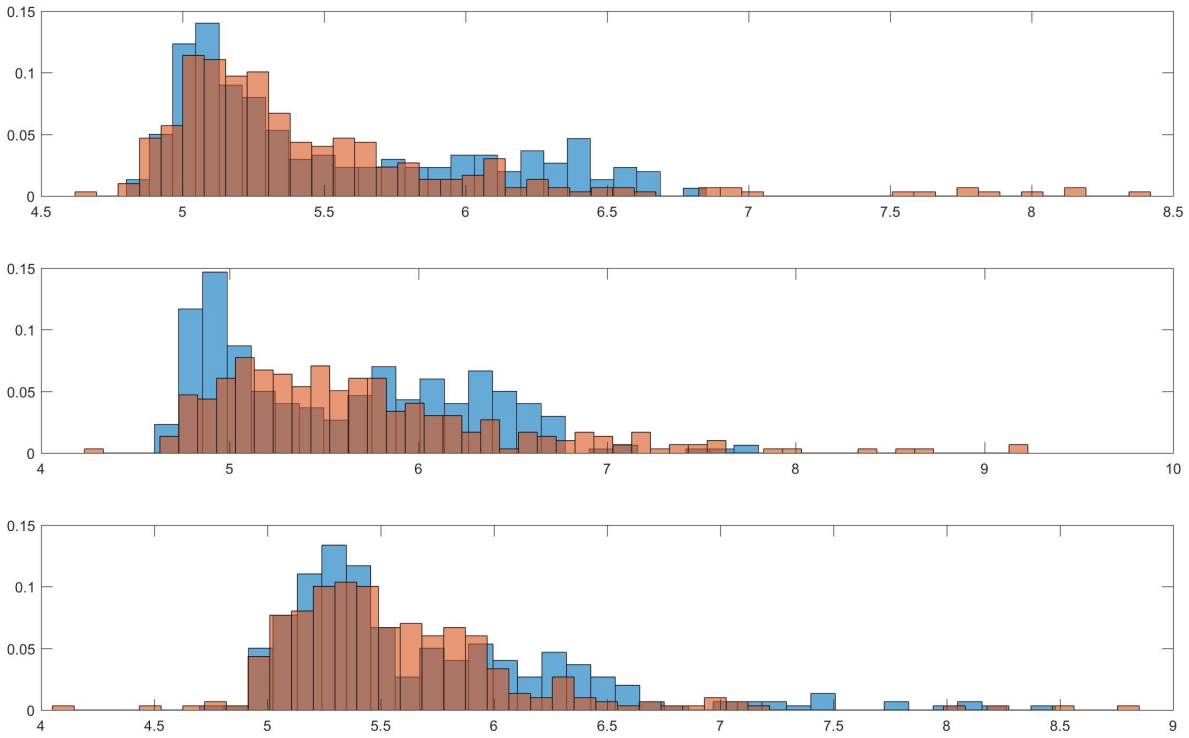

Figure 4.2: Histogram plots of simulated data (orange) and real data (blue) in part 1 (top), part 34 (middle), and part 45 (bottom)

We show the simulation results in part 1 (without solar flare), part 12 (without solar flare), part 33 (first solar flare), part 34 (first solar flare), part 44 (second solar flare), and part 45 (second solar flare). The sample size is 1000 and 5000 respectively. The procedure

is repeated 500 times. The estimated mean values and standard deviations are shown in Table 4.1. From Table 4.1, we see that when sample size increases, the bias and uncertainty of MLEs reduces. The consistency of the estimator under correct model specification has been shown. The performance of MLE is acceptable even when the sample size is not large. Moreover, it should be noticed that μs in all subareas are a little underestimated due to the threshold.

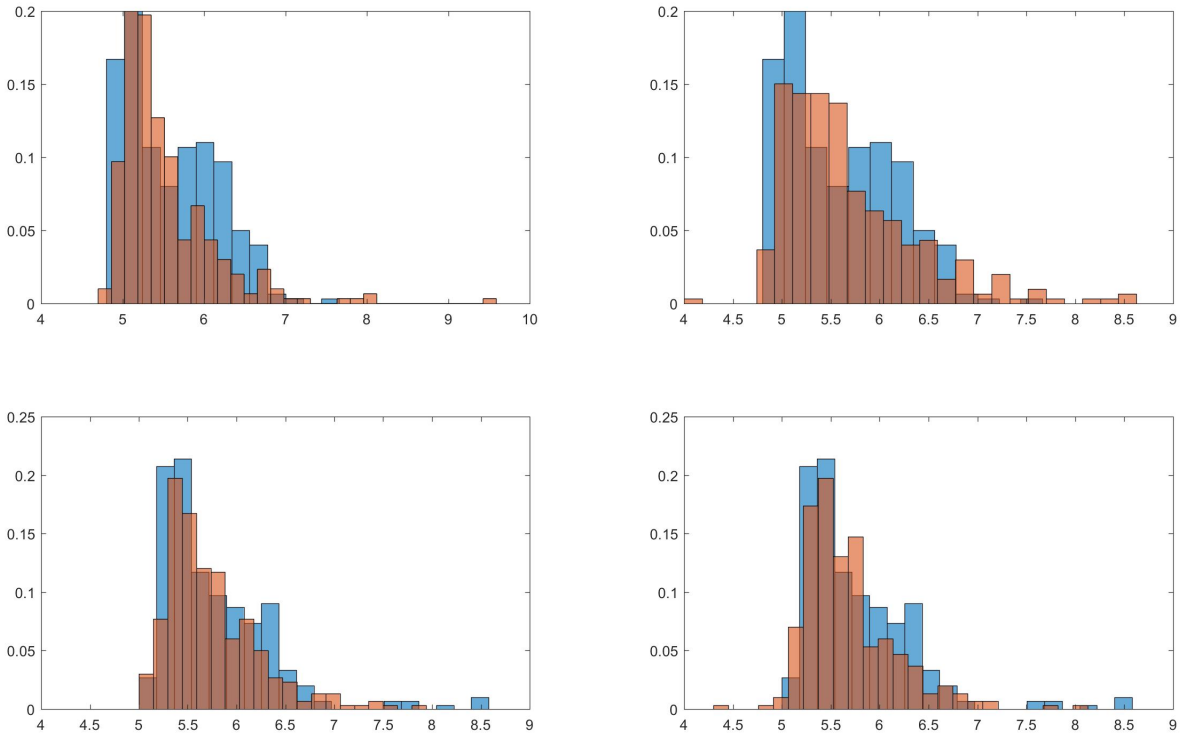

Figure 4.3: Histogram plots of simulated data (orange) and real data (blue) in part 33 (top), and part 44 (bottom) for AcFL model (left) and spatial ACFL model (right)

In order to compare the distribution of simulated data and real data, we draw the histogram plots. Figure 4.2 shows simulated data (orange) and real data (blue) in part 1 (top), part 34 (middle), and part 45 (bottom). According to the top graph, the distribution of simulated data in part 1 is similar to that of real data. Like previous two models, there are some extreme values in the simulation but they do not affect the estimation of whole model

when we look at the mean and standard deviation in Table 4.1. The simulated data in part 34 and 45 also catch the characteristics of real data. For part 33, the range of simulated value is smaller than other models which is more similar to real data. The simulation in subarea 45 approximates real data better than that of standard AcFL model.

Since in Section 4.4 we find the solar flare detection of AcFL model with spatial relationship in part 33 and 44 is better than that of the standard model, we also compare the simulated data in these two subareas in Figure 4.3. One can easily see that the distribution of simulated data in spatial AcFL model is more similar to that of the standard AcFL model in part 33 and part 44.

Remark 3: Since we have constraints of parameters β_3, γ_3, β_5, γ_5, and μ based on real data $\{Q_t\}$, we check them by using simulated data in Section 4.3. All constraints are held in simulated data.

Part 1	γ_0	γ_1	γ_2	γ_3	γ_4	γ_5	β_0	β_1	β_2
True Value	-3.914	0	29.023	15.782	6.632	21.873	5.404	0	1.523
Mean(S1)	-3.689	0	27.676	16.308	6.358	22.527	5.341	0	1.415
Std. Dev.(S1)	0.229	–	0.906	1.481	1.638	1.544	0.259	–	0.765
Mean(S2)	-3.849	0	28.312	15.356	6.681	22.138	5.406	0	1.583
Std. Dev(S2)	0.147	–	0.197	1.172	1.252	1.269	0.139	–	0.441
Part 1	β_3	β_4	β_5	μ					
True Value	0.022	0	–	102.532					
Mean(S1)	0.022	0	–	101.682					
Std. Dev.(S1)	0.010	–	–	4.331					
Mean(S2)	0.022	0	–	102.703					
Std. Dev(S2)	0.006	–	–	1.702					

Part 12	γ_0	γ_1	γ_2	γ_3	γ_4	γ_5	β_0	β_1	β_2
True Value	-2.813	0.197	25.662	25.552	0.173	0.016	8.266	0	14.692
Mean(S1)	-2.601	0.171	24.217	26.016	0.118	0.016	8.107	0	13.859
Std. Dev.(S1)	0.137	0.076	1.124	1.300	0.078	0.005	0.295	–	1.411
Mean(S2)	-2.730	0.195	24.948	25.146	0.154	0.017	8.148	0	13.963
Std. Dev(S2)	0.058	0.048	0.389	1.113	0.068	0.004	0.206	–	1.171
Part 12	β_3	β_4	β_5	μ					
True Value	0.298	4.612	15.557	119.911					
Mean(S1)	0.294	4.425	15.447	119.162					
Std. Dev.(S1)	0.071	1.675	1.382	3.137					
Mean(S2)	0.295	4.604	15.462	120.202					
Std. Dev(S2)	0.063	1.276	1.107	1.316					

Part 33	γ_0	γ_1	γ_2	γ_3	γ_4	γ_5	β_0	β_1	β_2
True Value	-0.540	0.023	2.334	0.025	0	–	10.859	0	48.896
Mean(S1)	-0.514	0.023	2.333	0.026	0	–	10.803 7	0	48.397
Std. Dev.(S1)	0.157	0.010	0.512	0.005	–	–	0.227	–	1.941
Mean(S2)	-0.524	0.023	2.246	0.025	0	–	10.827	0	48.682
Std. Dev(S2)	0.081	0.009	0.271	0.002	–	–	0.134	–	1.302
Part 33	β_3	β_4	β_5	μ					
True Value	23.956	0.290	0.007	53.349					
Mean(S1)	24.298	0.269	0.007	51.346					
Std. Dev.(S1)	1.776	0.058	0.001	7.316					
Mean(S2)	24.050	0.287	0.007	52.854					
Std. Dev(S2)	1.668	0.038	0.001	4.300					

Part 34	γ_0	γ_1	γ_2	γ_3	γ_4	γ_5	β_0	β_1	β_2
True Value	-2.197	0.097	24.053	65.603	0	–	12.372	0	59.881
Mean(S1)	-2.101	0.088	23.310	65.194	0	–	12.241	0	59.083
Std. Dev.(S1)	0.154	0.019	1.487	2.617	–	–	0.269	–	2.219
Mean(S2)	-2.185	0.092	23.924	65.300	0	–	12.351	0	59.919
Std. Dev(S2)	0.115	0.018	1.156	2.272	–	–	0.187	–	1.654

Part 34	β_3	β_4	β_5	μ					
True Value	69.024	15.657	59.961	71.869					
Mean(S1)	70.458	15.144	59.171	70.566					
Std. Dev.(S1)	1.819	1.624	3.819	3.065					
Mean(S2)	70.058	15.482	60.139	71.715					
Std. Dev(S2)	1.774	1.077	3.117	1.420					
Part 44	γ_0	γ_1	γ_2	γ_3	γ_4	γ_5	β_0	β_1	β_2
True Value	-1.262	0.180	6.826	0.105	0	–	12.109	0	53.882
Mean(S1)	-1.122	0.177	6.014	0.090	0	–	11.986	0	52.781
Std. Dev.(S1)	0.207	0.069	1.361	0.037	–	–	0.227	–	1.718
Mean(S2)	-1.211	0.182	6.528	0.101	0	–	12.049	0	53.280
Std. Dev(S2)	0.176	0.039	1.236	0.034	–	–	0.155	–	1.376
Part 44	β_3	β_4	β_5	μ					
True Value	50.633	13.541	45.522	72.549					
Mean(S1)	50.236	13.168	45.186	69.058					
Std. Dev.(S1)	1.877	1.360	1.779	7.667					
Mean(S2)	50.343	13.385	45.214	71.119					
Std. Dev(S2)	1.771	0.667	1.741	3.975					
Part 45	γ_0	γ_1	γ_2	γ_3	γ_4	γ_5	β_0	β_1	β_2
True Value	-3.275	0.074	31.800	9.025	0.120	0.013	12.438	0	59.915
Mean(S1)	-3.215	0.070	31.391	9.072	0.108	0.013	12.365	0	59.435
Std. Dev.(S1)	0.205	0.010	1.355	1.567	0.054	0.005	0.211	–	1.623
Mean(S2)	-3.258	0.074	31.695	9.062	0.110	0.013	12.406	0	59.656
Std. Dev(S2)	0.121	0.009	1.194	1.304	0.047	0.004	0.147	–	1.360
Part 45	β_3	β_4	β_5	μ					
True Value	72.122	10.871	21.867	41.841					
Mean(S1)	72.684	10.506	20.887	39.814					
Std. Dev.(S1)	1.563	1.260	1.526	5.737					
Mean(S2)	72.503	10.752	21.070	40.942					
Std. Dev(S2)	1.434	0.667	1.381	3.412					

Table 4.1: The performance of MLE with the sample size of 1000 (S1) and 5000 (S2) using the parameters from analysis in part 1, 12, 33, 34, 44, and 45. Mean and Std. Dev. are the sample mean and standard deviation of the MLE's obtained from 500 simulations.

4.4 Empirical Application

Like Chapter 3, we use the AcFL model with spatial correlation to fit one hundred and twenty-two parts and obtian 120 different models. We include parameter results and plots for part 1 (without solar flare), part 12 (without solar flare), part 33 (first solar flare), part 34 (first solar flare), part 44 (second solar flare), and part 45 (second solar flare). One can

see the fitted parameters and their standard deviations in Table 4.2.

The standard deviations are calculated by bootstrapping method. We randomly select 100 pixels in each part at each time point and then obtain the maximum values based on these 100 data points. Then we fit the spatial AcFL model to new data set and get the parameters. We repeat 500 times and obtain 500 models for each subareas. The standard deviations are calculated through these 500 models.

Same as the standard AcFL model, β_1 is not significant in six parts and γ_1 is not significant in part 1. γ_4 is not significant for part 33, 34, and 44. β_4 is not significant in part 1. Hence we set these parameters to be zero and other parameters are significant. The results indicate that all six subareas are influenced by adjacent parts.

Section 7.3 contains parameter results and plots for other subareas. Similar to the standard AcFL model, all β_1s are not significant in 120 subareas. γ_1 is not significant in 22% subareas. Nearly 50% parts have α_t that are not influenced by neighborhoods and around 40% σ_t are not affected by adjacent subareas.

Figure 4.4 and Figure 4.5 includes α_t (left) and σ_t (right) plots for six parts. Figure 4.4 is similar to Figure 3.2. Based on α_t and σ_t indices, in part 34 first solar flare "occurs" at $t = 188$ with is closed to real solar flare time $t = 186$. The second solar flare appears at $t = 215$ and in part 45 α_t and σ_t demonstrate solar activity time $t = 216$. Additionally, $t = 196$ in part 34 is near to the brightest time $t = 197$ of first solar flare. $t = 235$ is closed to time $t = 229$ when second solar flare is brightest.

Figure 4.5 and Figure 3.3 have some differences. The α_t and σ_t plots indicate first solar flare in part 33 happens at $t = 188$ which is the same as that in part 34. The ending time $t = 196$ keeps the same. For second solar flare in part 44, starting time becomes $t = 219$ which is the same as that in part 45. The plots show that second solar flare ends at $t = 231$ in part 44 which is earlier than that in part 45. In order to compare the prediction accuracy of the standard AcFL model and AcFL with spatial correlation, we check the original data plots in Figure 4.6.

Part 1	γ_0	γ_1	γ_2	γ_3	γ_4	γ_5	β_0	β_1	β_2
Est. Value	-3.914	0	29.023	15.782	6.632	21.873	5.404	0	1.523
Std. Dev.	0.259	–	0.787	1.245	1.577	1.688	0.353	–	0.208
Part 1	β_3	β_4	β_5	μ					
Est. Value	0.022	0	–	102.532					
Std. Dev.	0.004	–	–	7.516					
Part 12	γ_0	γ_1	γ_2	γ_3	γ_4	γ_5	β_0	β_1	β_2
Est. Value	-2.813	0.197	25.662	25.552	0.173	0.016	8.266	0	14.692
Std. Dev.	0.296	0.076	2.059	1.981	0.077	0.004	0.390	–	0.327
Part 12	β_3	β_4	β_5	μ					
Est. Value	0.298	4.612	15.557	119.911					
Std. Dev.	0.051	1.970	1.540	5.035					
Part 33	γ_0	γ_1	γ_2	γ_3	γ_4	γ_5	β_0	β_1	β_2
Est. Value	-0.540	0.023	2.334	0.025	0	–	10.859	0	48.896
Std. Dev.	0.214	0.009	0.616	0.004	–	–	0.472	–	1.747
Part 33	β_3	β_4	β_5	μ					
Est. Value	23.956	0.290	0.007	53.349					
Std. Dev.	1.750	0.072	0.002	6.786					
Part 34	γ_0	γ_1	γ_2	γ_3	γ_4	γ_5	β_0	β_1	β_2
Est. Value	-2.197	0.097	24.053	65.603	0	–	12.372	0	59.881
Std. Dev.	0.238	0.019	0.259	0.857	–	–	0.560	–	0.610
Part 34	β_3	β_4	β_5	μ					
Est. Value	69.024	15.657	59.961	71.869					
Std. Dev.	0.608	0.819	0.793	4.640					
Part 44	γ_0	γ_1	γ_2	γ_3	γ_4	γ_5	β_0	β_1	β_2
Est. Value	-1.262	0.180	6.826	0.105	0	–	12.109	0	53.882
Std. Dev.	0.148	0.034	0.237	0.009	–	–	0.531	–	0.713
Part 44	β_3	β_4	β_5	μ					
Est. Value	50.633	13.541	45.522	72.549					
Std. Dev.	0.560	0.607	0.748	7.114					
Part 45	γ_0	γ_1	γ_2	γ_3	γ_4	γ_5	β_0	β_1	β_2
Est. Value	-3.275	0.074	31.800	9.025	0.120	0.013	12.438	0	59.915
Std. Dev.	0.451	0.026	2.521	1.219	0.040	0.001	0.944	–	2.534
Part 45	β_3	β_4	β_5	μ					
Est. Value	72.122	10.871	21.867	41.841					
Std. Dev.	3.428	1.615	2.806	6.462					

Table 4.2: Estimated parameter values of AcFL model with spatial correlation

From Figure 4.6, one can easily see that first solar flare happens in part 33 and part 34 at the same time and ends simultaneously. Second solar flare occurs in part 44 and part 45 at almost the same time and it ends earlier in part 44 than in part 45. Moreover, maximized log-likelihoods for AcFL model with spatial relationship in part 33 and part 44 are higher than standard model. Therefore we think the spatial AcFL model is more accurate for subareas 33 and 44 than the standard AcFL model.

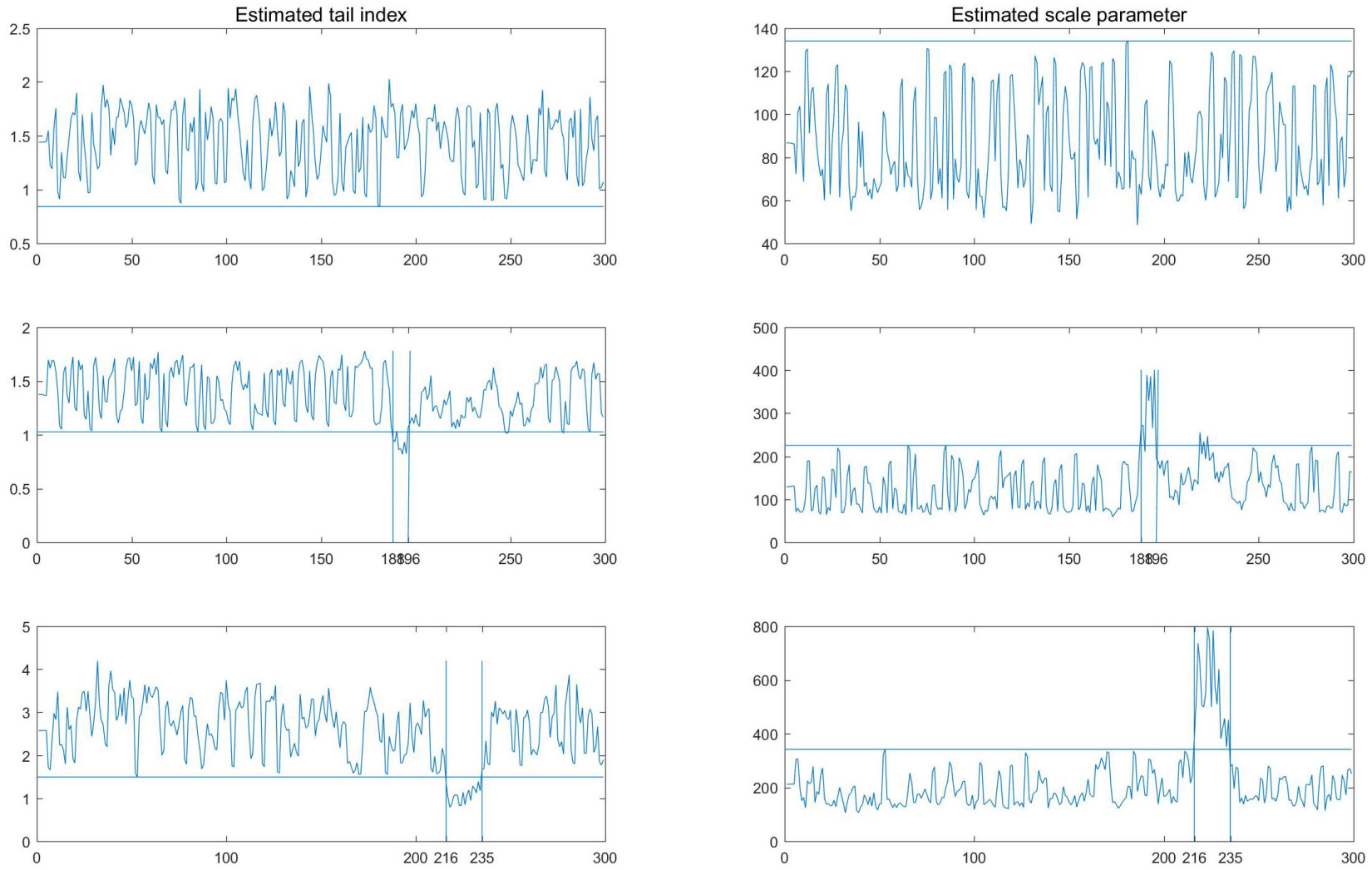

Figure 4.4: Estimated α_t (left) and σ_t(right) in part 1 (top), part 34 (middle), and part 45 (bottem) using spatial AcFL model. For the plots of α_t, the horizontal lines indicate the smallest α_t in $t = 1 \sim 185$ (α_{small}). The first vertical line in each plot displays the first time when the α_t is smaller than α_{small}. And the second vertical line shows the the last α_t which is smaller α_{small} after α_t goes beyond the smallest value.The σ_t is shown in the same way with opposite direction.

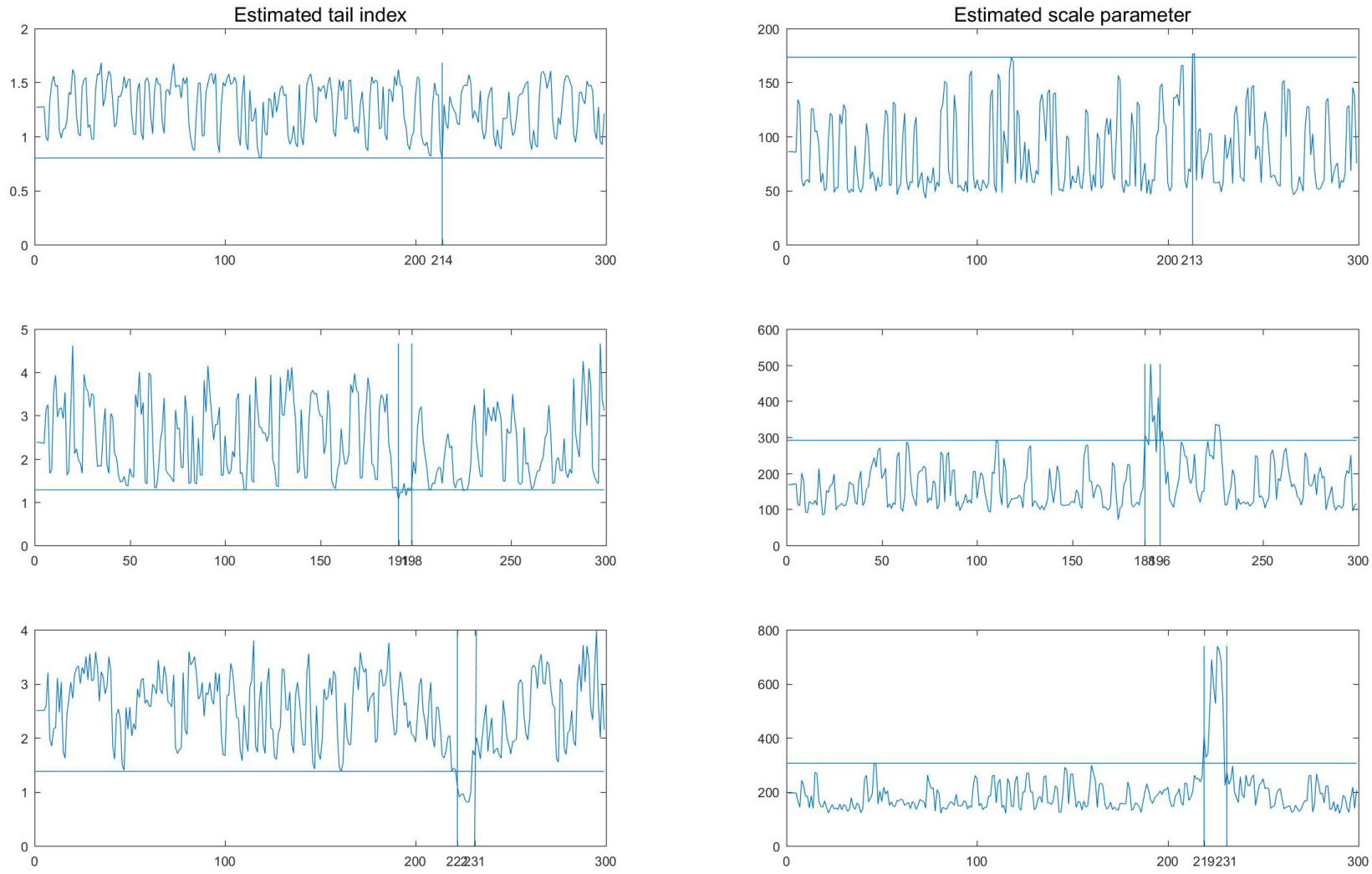

Figure 4.5: Estimated α_t (left) and σ_t(right) in part 12 (top), part 33 (middle), and part 44 (bottem) using saptial AcFL model. For the plots of α_t, the horizontal lines indicate the smallest α_t in $t = 1 \sim 185$ (α_{small}). The first vertical line in each plot displays the first time when the α_t is smaller than α_{small}. And the second vertical line shows the the last α_t which is smaller α_{small} after α_t goes beyond the smallest value.The σ_t is shown in the same way with opposite direction.

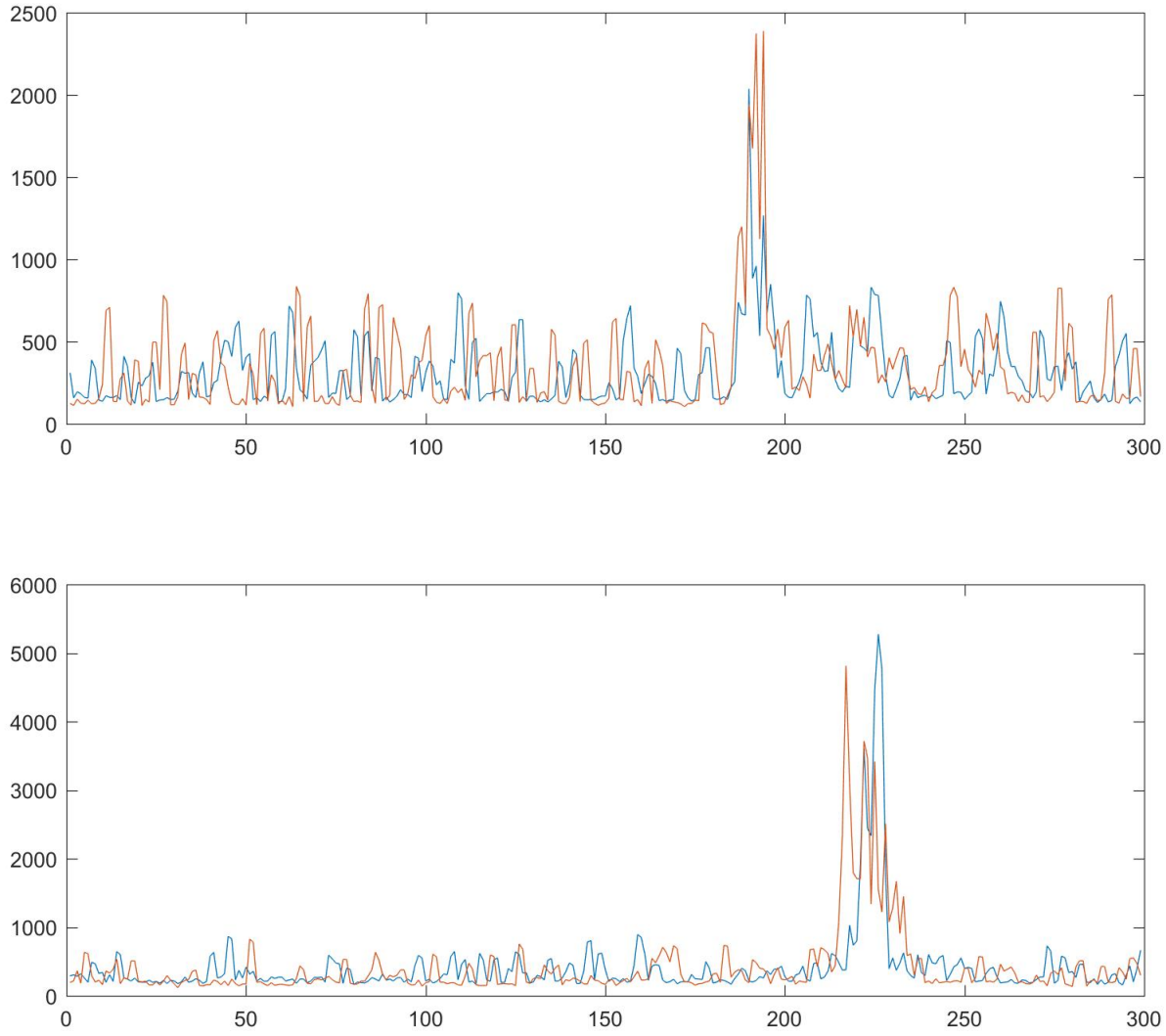

Figure 4.6: Top plot shows the original data in part 33 (blue) and part 34 (orange); bottom plot shows original data in part 44 (blue) and part 45 (orange)

Chapter 5

Discussion

Solar flare detection can help human society and researchers minimize the damage of this solar activity on Earth. Since the image data of Sun is natural time series, dynamic modeling can be an effective way to deal with the data. There are two advantages for dynamic model. First, it involves time effects and can catch more characteristics of solar image data than constant model. Second, this dynamic model does not need huge amount of data like machine learning and deep learning model. Thus the computation efficiency of dynamic model is higher.

In the dissertation, we use a new and direct way to remove the background information and extract the maximum value as feature of solar flare data set to reduce high dimensions. The method is different from the existing literature and it keeps more information without any assumption about original data. In addition, we use the characteristics derived from maximum values as the feature to detect solar flare instead of mean. This change is consistent with the nature of solar activity.

We propose new autoregressive conditional Fréchet model with logarithm function and fit the solar flare data frame with this dynamic conditional model. We find tail index α_t and scale parameter σ_t can be used to detect, even predict the solar flare. The proposed models improve the solar flare detection results and provide useful information about distribution

of extreme values of solar flare data set.

In addition, we extend the standard AcfL model to a more general version in order to make prediction as soon as possible. There is a trade-off between predicted time and prediction accuracy. Moreover, since there exists spatial correlation, we include spatial component in our AcFL model. The spatial AcFL model provides more accurate prediction results in real data analysis.

There are some other possible extension of AcFL model, for example multivariate AcFL model. In the paper we assume the maxima are asymptotically independent between subareas, equivalent to assume Y's in 120 models (subareas) are independent. In the literature, assuming asymptotic independence has been widely applied in researches. If we can catch the correlation between these Y's, we can build a dynamic framework which may improve the prediction accuracy.

Besides solar flare detection, our model may also be used in brain research. The process in this dissertation is similar to filtering and detection in spike sorting while the latter method usually has Gaussian distribution assumption. Moreover, our research inspires us that statistical model for society activity like economics and finance may also be used in natural science analysis, and vice versa.

Chapter 6

Appendix A

6.1 Proofs for AcFL model

6.1.1 Proof of stationarity and ergodicity

Proof of Theorem 1: The proof is mainly based on theory of general state space Markov Chain. We first prove $\{\log(\alpha_t)\}/\{\log(\sigma_t)\}$ is an aperiodic positive recurrent Harris Chains. By convergence theorem for aperiodic positive recurrent Harris Chain, it can be shown that there is a unique stationary distribution for $\{\log(\alpha_t)\}/\{\log(\sigma_t)\}$ and $\{\log(\alpha_t)\}/\{\log(\sigma_t)\}$ converges to the stationary distribution regardless of the initial distribution on $\{\log(\alpha_1)\}/\{\log(\sigma_t)\}$.

We set $G = \left(\frac{\beta_0-\beta_2}{1-\beta_1}, \frac{\beta_0}{1-\beta_1}\right) \times \left(\frac{\gamma_0}{1-\gamma_1}, \frac{\gamma_0+\gamma_2}{1-\gamma_1}\right)$, which is an open area in $\mathbb{R}^2$. Then we have Lemma 1 as following:

Lemma 1 *G is absorbing for $\mathbf{X}_t$.*

Proof: Suppose $\log \alpha_t > \frac{\gamma_0}{1-\gamma_1}$ then $\log \alpha_{t+1} = \gamma_0 + \gamma_1 \log \alpha_t + \gamma_2 / \log(\gamma_3 Q_t) > \gamma_0 + \gamma_1 \frac{\gamma_0}{1-\gamma_1} = \frac{\gamma_0}{1-\gamma_1}$ since $\gamma_3 > e/min(Q_t)$. Similarly, if $\log \alpha_t < \frac{\gamma_0+\gamma_2}{1-\gamma_1}$, then $\log \alpha_{t+1} < \gamma_0 + \gamma_1 \frac{\gamma_0+\gamma_2}{1-\gamma_1} + \gamma_2 = \frac{\gamma_0+\gamma_2}{1-\gamma_1}$. The proof of σ_t is the same.

Note here $\{\log(\alpha_t)\}$ and $\{\log(\sigma_t)\}$ are both bounded. First we prove that $\{\log \alpha_t\}$ is a

Harris Chain. WOLG, for simplicity, we assume $\beta_0 = \beta_1 = \beta_2 = 0$ and $\mu = 0$ in the following proof. As will be seen later in the proof, only the boundedness of $\{\log(\sigma_t)\}$ will be used. We continue the proof of $\{\log(\alpha_t)\}$ being a Harris Chain by following the definition of Harris Chain in R. Durrett (2010).

Definition 1 *We say that a Markov Chain $\{X_n\}$ is a Harris chain if we can find sets $A, B \in \mathcal{S}$, a function q with $q(x,y) \geq \epsilon > 0$ for $x \in A, y \in B$, and a probability measure ρ concentrated on B so that:*

(i) If $\tau_A = \inf\{n \geq 0 : X_n \in A\}$, then $P_z(\tau_A < \infty) > 0$ for all $z \in S$;

(ii) If $x \in A$ and $C \subset B$ then $p(x, C) \geq \int_C q(x,y)\rho(dy)$.

Lemma 2 *$\{\log \alpha_t\}$ is a Harris Chain.*

Proof: We set $q(x,y)$ be the transition probability density function and $\rho(x)$ to be the normalized Lebesgue measure concentrated on set B and $\beta_0 = \beta_1 = \beta_2 = 0$ and $\mu = 0$. Then we define

$$A = \left[\frac{\gamma_0 + \Delta_1}{1-\gamma_1}, \frac{\gamma_0 + \gamma_2 - \Delta_2}{1-\gamma_1}\right] = [L_A, U_A].$$

For $\log \alpha_t$, the range of $\log \alpha_{t+1}$ will be $(\gamma_0 + \gamma_1 \log \alpha_t, \gamma_0 + \gamma_1 \log(\alpha_t) + \gamma_2)$. It is easy to see that this range is a monotone function of $\log \alpha_t$ and the length is always γ_2. Due to the monotonicity of $(\gamma_0 + \gamma_1 \log \alpha_t, \gamma_0 + \gamma_1 \log \alpha_t + \gamma_2)$, we can make set B to be the intersection between the interval $(\gamma_0 + \gamma_1 \log \alpha_t, \gamma_0 + \gamma_1 \log \alpha_t + \gamma_2)$, for $\log \alpha_t = \frac{\gamma_0 + \Delta_1}{1-\gamma_1}$ and $\log \alpha_t = \frac{\gamma_0 + \gamma_2 - \Delta_2}{1-\gamma_1}$ in order to make sure that the transition probability $p(\log \alpha_t, \log \alpha_{t+1}) > \epsilon, \forall \log \alpha_t \in A, \log \alpha_{t+1} \in B$. Since we want two intervals to have intersections, we need to make

$$\gamma_0 + \gamma_1 \frac{\gamma_0 + \gamma_2 - \Delta_2}{1-\gamma_1} < \gamma_0 + \gamma_1 \frac{\gamma_0 + \Delta_1}{1-\gamma_1} + \gamma_2.$$

In other words, $\frac{\gamma_1}{1-\gamma_1}(\gamma_2 - \Delta_2 - \Delta_1) < \gamma_2$. One can easily find $\Delta_2 + \Delta_1 < \gamma_2$ to satisfy the above inequality for all $\gamma_1 < 1$ and $\gamma_2 > 0$. Then we can take B as a proper subset of

$$\left[\gamma_0 + \gamma_1 \frac{\gamma_0 + \gamma_2 - \Delta_2}{1-\gamma_1}, \gamma_0 + \gamma_1 \frac{\gamma_0 + \Delta_1}{1-\gamma_1} + \gamma_2\right] = \left[\frac{\gamma_0 + \gamma_1(\gamma_2 - \Delta_2)}{1-\gamma_1}, \frac{\gamma_0 + \gamma_1 \Delta_1}{1-\gamma_1} + \gamma_2\right].$$

By the definition of Harris Chain, we need to prove $P_x(\tau_A < \infty) > 0$. We apply the equations of $\log(\alpha_t)$ t times and get

$$\log \alpha_t = \frac{\gamma_0 (1-\gamma_1^t)}{1-\gamma_1} + \gamma_1^t \log \alpha_0 + \gamma_2 \sum_{i=1}^{t} \gamma_1^{i-1} (\log (\gamma_3 Q_{t-i}))^{-1}.$$

The latter part of $\log \alpha_t$ can be rewrote as

$$\gamma_2 \sum_{i=1}^{t} \gamma_1^{i-1} (\log \left(\gamma_3 Q_{t-i}\right)^{-1}) = \gamma_2 \sum_{i=1}^{t} \gamma_1^{i-1} (\log \left(\gamma_3 Y_{t-i}^{1/\alpha_{t-i}}\right).$$

Since $\{\log(\alpha_t)\}$ is bounded, for each $\epsilon > 0$, there exists a T_1 such that $\forall t > T_1$, $\left| \frac{\gamma_0 \left(1-\gamma_1^t\right)}{1-\gamma_1} + \gamma_1^t \alpha_0 - \frac{\gamma_0}{1-\gamma_1} \right| < \epsilon$. We also know $\gamma_2 \sum_{i=1}^{t} \gamma_1^{i-1} = \frac{\gamma_2 \left(1-\gamma_1^t\right)}{1-\gamma_1} \to \frac{\gamma_2}{1-\gamma_1}$. Hence we can find a $T_2 > T_1$ such that for all $\gamma_2 \sum_{i=1}^{t} \gamma_1^{i-1} - \frac{\gamma_2}{1-\gamma_1} > -\epsilon$, for all $t > T_2$. Moreover, depending on the value of Y_{t-i}, $(\log \left(\gamma_3 Y_{t-i}^{1/\alpha_{t-i}}\right))^{-1}$ can be any number between 0 and 1 due to the boundedness of $\{\log \alpha_t\}$. In other words, there is a uniform interval $[Y_L, Y_U]$ such that $(\log \left(\gamma_3 Y_{t-i}^{1/\alpha_{t-i}}\right))^{-1} \leq \epsilon$ and $(\log(\gamma_3 Y_U^{1/\alpha_t})^{-1} \geq 1-\epsilon$, regardless of $\log \alpha_t$. Therefore, for any value of $\log \alpha_0$, the range of $\gamma_2 \sum_{i=1}^{t} \gamma_1^{i-1} (\log \left(\gamma_3 Y_{t-i}^{1/\alpha_{t-i}}\right))^{-1}$ covers $\left[\epsilon, \frac{\gamma_2}{1-\gamma_1} - \epsilon\right]$, for $(Y_0, Y_1, \ldots, Y_{T_2-1}) \in [Y_L, Y_U]^{T_2}$. It should be noticed that $\gamma_2 \sum_{i=1}^{t} \gamma_1^{i-1} (\log \left(\gamma_3 Y_{t-i}^{1/\alpha_{t-i}}\right))^{-1}$ is a continuity function of $\left\{\{Y_{t-i}\}_{i=1}^{t}, \log \alpha_0\right\}$. Hence by generalized Intermediate Value Theorem, for every $\log \alpha_0$, there exists a sequence of positive constants $\left(K_0^{\alpha_0}, K_1^{\alpha_0}, \ldots, K_{T_2-1}^{\alpha_0}\right)$ such that if $(Y_0, Y_1, \ldots, Y_{T_2-1}) = \left(K_0^{\alpha_0}, K_1^{\alpha_0}, \ldots, K_{T_2-1}^{\alpha_0}\right)$, then

$$\begin{aligned} \gamma_2 \sum_{i=1}^{T_2} \gamma_1^{i-1} (\log(\gamma_3 Y_{T_2-i}^{1/\alpha_{T_2-i}})^{-1}) = \text{ singleton } &\in \left(\frac{\Delta_1}{1-\gamma_1} + 2\epsilon, \frac{\gamma_2 - \Delta_2}{1-\gamma_1} - 2\epsilon \right) \\ &= \left(L_A - \frac{\gamma_0}{1-\gamma_1} + 2\epsilon, U_A - \frac{\gamma_0}{1-\gamma_1} - 2\epsilon \right). \end{aligned}$$

We can extend $\left(\alpha_0, K_0^{\alpha_0}, K_1^{\alpha_0}, \ldots, K_{T_2-1}^{\alpha_0}\right)$ to a small set $D_{\alpha_0} = (\log \alpha_0 \pm \delta_{\alpha_0}, K_0^{\alpha_0} \pm \delta_0^{\alpha_0}, \ldots, K_{T_2-1}^{\alpha_0}$

$\pm\delta_{T_{-1}}^{\alpha_0}$), such that for all $(\log\alpha_0, Y_0, Y_1, \ldots, Y_{T_2-1})$ in the set. So we have

$$\gamma_2 \sum_{i=1}^{T_2} \gamma_1^{i-1} (\log(\gamma_3 Q_{T_2-i}))^{-1} \in \left(\frac{\Delta_1}{1-\gamma_1} + \epsilon, \frac{\gamma_2 - \Delta_2}{1-\gamma_1} - \epsilon \right) = \left(L_A - \frac{\gamma_0}{1-\gamma_1} + \epsilon, U_A - \frac{\gamma_0}{1-\gamma_1} - \epsilon \right).$$

Since $\left| \frac{\gamma_0\left(1-\gamma_1^{T_2}\right)}{1-\gamma_1} + \gamma_1^{T_2} \log\alpha_0 - \frac{\gamma_0}{1-\gamma_1} \right| < \epsilon$, for $\forall \log\alpha_0 \in S$, we have $P_{\alpha_0}(\log\alpha_{T_2} \in A) > 0$ i.e. $P_x(\tau_A < \infty) = 1 > 0$. Thus $\{\log\alpha_t\}$ is a Harris Chain.

Now we define a new Chain based on $\{\log\alpha_t\}$ by adding an artificial element $\{\beta\}$ in $S = \left(\frac{\gamma_0}{1-\gamma_1}, \frac{\gamma_0+\gamma_2}{1-\gamma_1} \right)$ and define the new transitional probability as follows:

1. if $x \in S \backslash A, \bar{p}(x, C) = p(x, C)$ for $C \in S$;
2. if $x \in A$, we have $\bar{p}(x, \{\beta\}) = \epsilon, \bar{p}(x, C) = p(x, C) - \epsilon\rho(C)$ for $C \in S$, where ρ is the normalized Lebsegue measure on A;
3. if $x = \beta, \bar{p}(\beta, D) = \int \bar{p}(x, D)\rho(dx)$ for $D \in \bar{S}$.

Lemma 3 *$\{\beta\}$ is positive recurrent in the new Chain.*

Proof: Since $\log\alpha_0 \in S = \left(\frac{\gamma_0}{1-\gamma_1}, \frac{\gamma_0+\gamma_2}{1-\gamma_1} \right)$ which is bounded, there is a compact set $S_K = \left[\frac{\gamma_0}{1-\gamma_1} + \delta, \frac{\gamma_0+\gamma_2}{1-\gamma_1} - \delta \right]$, where δ is sufficiently small. Then $\bigcup_{\alpha_0 \in S} (\log\alpha_0 - \delta_{\alpha_0}, \log\alpha_0 + \delta_{\alpha_0}($ is an open cover of S_K. According to the compactness of S_K, we can find a finite number of α_0 such that $\bigcup_{\text{finite } \log\alpha_0} (\log\alpha_0 - \delta_{\alpha_0}, \log\alpha_0 + \delta_{\alpha_0})$ covers S_K. For all $\log\alpha_0 \in S_K$ there is a uniform lower bound, denoted as ρ_1 such that $P_{\log\alpha_0}(\log\alpha_{T_2} \in A) > \rho_1 > 0$. Additionally, since δ is sufficiently small, there is a uniform lower bound, denoted as ρ_2 such that for $\log\alpha_0 \in S, P_{\log\alpha_0}(\log\alpha_1 \in S_K) > \rho_2$. For $\forall\alpha_0 \in S$, we have a uniform probability bound, say ρ_3 such that $p^{T_2+1}(\log\alpha_0, A) > \rho_3$.

Since $A \cap B \neq \varnothing$, $\{\beta\}$ is aperiodic, and $\{\log\alpha_t\}$ is aperiodic. We can prove that $\{\log\alpha_t\}$ is an aperiodic, positive recurrent Harris Chain. According to Theorem 17.1.7 in Meyn and Tweedie (2005), $\{\log\alpha_t\}$ will have a unique stationary distribution and it will converge to the stationary distribution and then $\{\log\alpha_t\}$ is ergodic. Similarly, we can prove $\{\log\sigma_t\}$ is stationary and ergodic.

6.1.2 Proof of consistency and asymptotic normality

We follow the proof of Theorem 2, 3 and Proposition 2 in Zhao et al. (2018) by giving technical lemmas (lemma 4-16) first. We assume the conditions in Theorem 2 hold in the following proof, which means the parameter space Θ is a compact set of Θ_s, which contains true parameter θ_0. Also we assume the observations $\{Q_t\}_{t=1}^n$ come from a stationary and ergodic AcFL defined in Θ. We denote the kth order statistics of $\{Y_t\}_{t=1}^n$ and $\{Q_t\}_{t=1}^n$ by $Y_{n,k}$ and $Q_{n,k}$. Moreover, we use $\tau_n \sim n^{-r}$ to represent $\tau_n/n^{-r} \to 1$ as $n \to \infty$. We use $C_b < 1$ to denote the upper bound of β_1, γ_1 in Θ and set C to be a generic positive constant.

In Lemma 4, we will prove the identifiability of AcFL. In other words, each parameter value θ defines a unique AcFL.

Lemma 4 *(Identifiability) If $Q_t(\theta_1) = Q_t(\theta_2)$ a.s. for all t, then $\theta_1 = \theta_2$. Here a.s. is for the infinite product space generated by $\{\ldots, Y_{-1}, Y_0, Y_1, Y_2, \ldots\}$, where Y_i's are i.i.d. unit Fréchet random variables.*

Proof: We set $\sigma_t(\theta_1)$ to be σ_t^1, $\alpha_t(\theta_1)$ to be α_t^1, $\sigma_t(\theta_2)$ to be σ_t^2, and $\alpha_t(\theta_2)$ to be α_t^2. Suppose there exists θ_1 and θ_2 such that $Q_t(\theta_1) = Q_t(\theta_2)$ a.s., then

$$\mu_1 + \sigma_t^1 Y_t^{1/\alpha_t^1} = \mu_2 + \sigma_t^2 Y_t^{1/\alpha_t^2} \text{ a.s.},$$

since $Y_{n,1} \searrow 0$ a.s., (σ_t^1, α_t^1) and (σ_t^2, α_t^2) are bounded, $\mu_1 = \mu_2$. Now we can rearrange the equation as following:

$$Y_t^{1/\alpha_t^1 - 1/\alpha_t^2} = \sigma_t^2/\sigma_t^1 \text{ a.s.}.$$

Let $\mathcal{F}_t$ be $\sigma(Y_t, Y_{t-1}, \ldots)$. Since $Y_t \perp \mathcal{F}_{t-1}$ and $\alpha_t^1, \alpha_t^2 \in \mathcal{F}_{t-1}$, previous equation holds if and only if $\sigma_t^1 = \sigma_t^2$ and $\alpha_t^1 = \alpha_t^2$ a.s. Based on AcFL model of $\log \alpha_t$, we know that if $\alpha_t^1 = \alpha_t^2$ a.s., then

$$\gamma_0^1 + \gamma_1^1 \log \alpha_{t-1} + \gamma_2^1 / \log\left(\gamma_3^1 Q_{t-1}\right) = \gamma_0^2 + \gamma_1^2 \log \alpha_{t-1} + \gamma_2^2 / \log\left(\gamma_3^2 Q_{t-1}\right),$$

$$\gamma_0^1 - \gamma_0^2 + \left(\gamma_1^1 - \gamma_1^2\right) \log \alpha_{t-1} = \gamma_2^2 / \log\left(\gamma_3^2 Q_{t-1}\right) - \gamma_2^1 / \log\left(\gamma_3^1 Q_{t-1}\right).$$

Since $\alpha_{t-1} \in \mathcal{F}_{t-2}$ and $Q_{t-1} \notin \mathcal{F}_{t-2}$, $\gamma_0^1 = \gamma_0^2, \gamma_1^1 = \gamma_1^2, \gamma_2^1 = \gamma_2^2$ and $\gamma_3^1 = \gamma_3^2$. Similarly, we can prove $\beta_0^1 = \beta_0^2, \beta_1^1 = \beta_1^2, \beta_2^1 = \beta_2^2$ and $\beta_3^1 = \beta_3^2$. Therefore AcFL model is uniquely defined by the value of θ.

In Lemma 5 we discuss the behavior of score function and Fisher information matrix at the true parameter θ_0 given initial value (σ_1^0, α_1^0).

Lemma 5 *Under the conditions in Theorem 2,* $E_{\theta_0}\left(\frac{\partial}{\partial\theta} l_t\left(\theta_0\right)\right) = 0$ *and for* M_0*, the Fisher information matrix at* θ_0*, we have* $M_0 = \mathrm{Var}_{\theta_0}\left(\frac{\partial}{\partial\theta} l_t\left(\theta_0\right)\right) = -E_{\theta_0}\left(\frac{\partial^2}{\partial\theta\partial\theta^T} l_t\left(\theta_0\right)\right)$ *and* M_0 *is well defined and positive definite.*

Proof: By interchanging the integration operator with differential operator, we have

$$\begin{aligned} E_{\theta_0}\left(\frac{\partial}{\partial\theta} l_t\left(\theta_0\right)\right) &= E_{\theta_0} \frac{\partial \log f_t\left(Q_t, \theta_0 | \sigma_t, \alpha_t\right)}{\partial\theta} = \int \frac{\partial \log f_t\left(q_t, \theta_0 | \sigma_t, \alpha_t\right)}{\partial\theta} f\left(q_t, \theta_0 | \sigma_t, \alpha_t\right) dq_t \\ &= \int \frac{1}{f_t\left(q_t, \theta_0 | \sigma_t, \alpha_t\right)} \frac{\partial f_t\left(q_t, \theta_0 | \sigma_t, \alpha_t\right)}{\partial\theta} f\left(q_t, \theta_0 | \sigma_t, \alpha_t\right) dq_t = \int \frac{\partial f_t\left(q_t, \theta_0 | \sigma_t, \alpha_t\right)}{\partial\theta} dq_t. \end{aligned}$$

For any $x \in (0,1)$ there exists a $c > 0$ such that $|\log(x)| \leq \frac{c}{x}$. One can easily find a $g\left(q_t\right)$ such that $\left|\frac{\partial f_t\left(q_t, \theta | \sigma_{t,} \alpha_t\right)}{\partial\theta}\right| \leq g\left(q_t\right)$ and $\int g\left(q_t\right) dq_t < \infty$ for all $\theta \in (\theta_0 - \epsilon, \theta_0 + \epsilon)$ with some poisitve ϵ. By dominate convergence theorem, $E_{\theta_0}\left(\frac{\partial}{\partial\theta} l_t\left(\theta_0\right)\right) = \int \frac{\partial f_t\left(q_t, \theta_\theta | v_t, \alpha_t\right)}{\partial\theta} dq_t = \frac{\partial}{\partial\theta} \int f_t\left(q_t, \theta_0 | \sigma_t, \alpha_t\right) dq_t = 0$. For $M_0 = \mathrm{Var}_{\theta_0}\left(\frac{\partial}{\partial\theta} l_t\left(\theta_0\right)\right)$, we have

$$\begin{aligned} &E_{\theta_0}\left(\frac{\partial^2 \log f_t\left(q_t, \theta_0 | \sigma_t, \alpha_t\right)}{\partial\theta\partial\theta'}\right) = \int \frac{\partial}{\partial\theta}\left(\frac{1}{f_t\left(q_t, \theta_0 | \sigma_t, \alpha_t\right)} \frac{\partial f_t\left(q_t, \theta_0 | \sigma_t, \alpha_t\right)}{\partial\theta'}\right) f_t\left(q_t, \theta_0 | \sigma_t, \alpha_t\right) dq_t \\ &= -\int \left[\frac{1}{f_t\left(q_t, \theta_0 | \sigma_t, \alpha_t\right)} \frac{\partial f_t\left(q_t, \theta_0 | \sigma_t, \alpha_t\right)}{\partial\theta}\right] \left[\frac{1}{f_t\left(q_t, \theta_0 | \sigma_t, \alpha_t\right)} \frac{\partial f_t\left(q_t, \theta_0 | \sigma_t, \alpha_t\right)}{\partial\theta'}\right] f_t\left(q_t, \theta_0 | \sigma_t, \alpha_t\right) dq_t \\ &+ \int \frac{\partial^2 f_t\left(q_t, \theta_0 | \sigma_t, \alpha_t\right)}{\partial\theta\partial\theta'} dq_t = -\mathrm{Var}_{\theta_0}\left(\frac{\partial}{\partial\theta} l_t\left(\theta_0\right)\right). \end{aligned}$$

Now, we have $M_0 = \mathrm{Var}_{\theta_0}\left(\frac{\partial}{\partial\theta} l_t\left(\theta_0\right)\right) = -E_{\theta_0}\left(\frac{\partial^2}{\partial\theta\partial\theta^T} l_t\left(\theta_0\right)\right)$. When t goes to infinity, the sequence $\frac{\partial^2}{\partial\theta\partial\theta^T} l_t\left(\theta_0\right)$ is strictly stationary, and then their expectations are the same. Hence M_0 has no relationship with t and is well defined, i.e. $M_0 < \infty$. Moreover, it is easy to prove

there doesn't exist a $c \in R^9$ such that $c^T \frac{\partial}{\partial \theta} l_t(\theta_0) = 0$. Thus M_0 is positive definite.

In Lemma 6, we will show the expectations of the items in $\frac{\partial^2}{\partial \theta_j \partial \theta_j} L_n(\theta_0)$ exist, which serve as building blocks for the following lemmas.

Lemma 6 *Under the conditions in Theorem 2, we have (a) for any* $\frac{1}{n}\sum_{t=1}^{n}(Q_t - \mu_0)^{-\alpha} \xrightarrow{p} E_{\theta_0}(Q_1 - \mu_0)^{-\alpha} < \infty$*, (b) for any positive integer k,* $\frac{1}{n}\sum_{t=1}^{n}[\log(Q_t - \mu_0)]^k \xrightarrow{p} E_{\theta_0}[\log(Q_1 - \mu_0)]^k < \infty$.

Proof: the proof of Lemma 6 is the same as Lemma 5 in Zhao et al.(2018).

Lemma 7 provides an asymptotic bound on the distance between $Q_{n,1}$ and μ_0. It indicates that $Q_{n,1}$ converges to μ_0 at a rate that is larger than $(\log n)^{-1/\alpha_L}$

Lemma 7 *Under the conditions in Theorem 2,* $Q_{n,1} - \mu_0 \geq O_p\left((\log n)^{-1/\alpha_L}\right)$.

Proof: the proof of Lemma 7 is the same as Lemma 6 in Zhao et al.(2018).

In Lemma 8, we give the foundation for the uniform convergence result in Lemma 12 and Lemma 15.

Lemma 8 *Denote* $S_n^{\alpha}(\mu) = n^{-1}\sum_{k=1}^{n}(Q_{n,k} - \mu)^{-\alpha}, \alpha > 0$ *or* $S_n^{\alpha}(\mu) = n^{-1}\sum_{k=1}^{n}\log(Q_{n,k} - \mu)$ *or* $S_n^{\alpha}(\mu) = n^{-1}\sum_{k=1}^{n}(Q_{n,k} - \mu)^{-\alpha}[\log(Q_{n,k} - \mu)]^m$ *for* $m = 1, 2, 3$*. Under the conditions in Theorem 2, given positive sequence* τ_n, *s.t.* $\tau_n \sim n^{-r}, r > 0$*, the following result holds uniformly over* $|\mu_n - \mu_0| < \tau_n$,

$$|S_n^{\alpha}(\mu_n) - S_n^{\alpha}(\mu_0)| \leq O_p(\tau_n).$$

Proof: the proof of Lemma 8 is the same as Lemma 7 in Zhao et al.(2018).

Lemmas 9 and 10 state that the supremum of $|\alpha_t - \alpha_t^0|$ and $|\sigma_t - \sigma_t^0|$, which are influenced by the parameter difference $|\theta - \theta_0|$, converges at the rate of τ_n over t.

Lemma 9 *Denote* $\Phi = (\gamma_0, \gamma_1, \gamma_2, \gamma_3)$ *and* $\Phi_0 = (\gamma_0^0, \gamma_1^0, \gamma_2^0, \gamma_3^0)$*, if* $\|\Phi - \Phi_0\| < \tau_n$ *and* $\tau_n \searrow$

0, *under the conditions in Theorem 2, we have*

$$(a)\ \sup_{1\le t\le n}\left|\alpha_t-\alpha_t^0\right|=O\left(\tau_n\right),\quad (b)\ \sup_{1\le t\le n}\left|\frac{\partial\alpha_t}{\partial\Phi}-\frac{\partial\alpha_t^0}{\partial\Phi}\right|=O\left(\tau_n\right),(c)\ \sup_{1\le t\le n}\left|\frac{\partial^2\alpha_t}{\partial\Phi_i\partial\Phi_j}-\frac{\partial^2\alpha_t^0}{\partial\Phi_i\partial\Phi_j}\right|=O\left(\tau_n\right)$$

uniformly over $\|\Phi-\Phi_0\|<\tau_n$.

Proof: We will only prove (a), since the proofs of other equations are similar but more complex. The domain of α_t is bounded and the function $\exp(\cdot)$ is continuously differentiable. Hence $\exp(\cdot)$ defined on this compact set is Lipschitz continuous. Therefore, we only need to verify $\sup_{1\le t\le n}\left|\log\alpha_t-\log\alpha_t^0\right|=O\left(\tau_n\right)$. By the iteration of autoregressive equation, we have

$$\log\alpha_t=\gamma_0\sum_{k=1}^{t-1}\gamma_1^{k-1}+\gamma_2\sum_{k=1}^{t-1}\gamma_1^{k-1}/\log\left(\gamma_3Q_{t-k}\right)+\gamma_1^{t-1}\log\alpha_1^0,$$

and than we calculate the difference

$$\begin{aligned}\left|\log\alpha_t-\log\alpha_t^0\right|\le&\left|\gamma_0\sum_{k=1}^{t-1}\gamma_1^{k-1}-\gamma_0^0\sum_{k=1}^{t-1}\left(\gamma_1^0\right)^{k-1}\right|+\left|\gamma_1^{t-1}\log\alpha_1^0-\left(\gamma_1^0\right)^{t-1}\log\alpha_1^0\right|\\&+\left|\gamma_2\sum_{k=1}^{t-1}\gamma_1^{k-1}/\log\left(\gamma_3Q_{t-k}\right)-\gamma_2^0\sum_{k=1}^{t-1}\left(\gamma_1^0\right)^{k-1}/\log\left(\gamma_3^0Q_{t-k}\right)\right|.\end{aligned}$$

Since

$$\sum_{k=1}^{t}\gamma_1^{k-1}<1/\left(1-\gamma_1\right)\le1/\left(1-C_b\right),$$

and

$$\left|\sum_{k=1}^{t-1}\left(\gamma_1^0\right)^{k-1}-\sum_{k=1}^{t-1}\left(\gamma_1\right)^{k-1}\right|\le\left|\frac{1}{1-\gamma_1^0}-\frac{1}{1-\gamma_1}\right|\le\frac{\tau_n}{\left(1-C_b\right)^2}=O\left(\tau_n\right),$$

the first two terms of the sum are $O(\tau_n)$ for any $1 \leq t \leq n$. Then for the third term, we get

$$\begin{aligned}
&\left|\gamma_2 \sum_{k=1}^{t-1} \gamma_1^{k-1} / \log(\gamma_3 Q_{t-k}) - \gamma_2^0 \sum_{k=1}^{t-1} \left(\gamma_1^0\right)^{k-1} / \log\left(\gamma_3^0 Q_{t-k}\right)\right| \\
&\leq \left|\gamma_2 - \gamma_2^0\right| \sum_{k=1}^{t-1} \gamma_1^{k-1} / \log(\gamma_3 Q_{t-k}) + \gamma_2^0 \sum_{k=1}^{t-1} \left|\gamma_1^{k-1} - \left(\gamma_1^0\right)^{k-1}\right| / \log(\gamma_3 Q_{t-k}) \\
&+ \gamma_2^0 \sum_{k=1}^{t-1} \left(\gamma_1^0\right)^{k-1} \left|1/\log(\gamma_3 Q_{t-k}) - 1/\log\left(\gamma_3^0 Q_{t-k}\right)\right|.
\end{aligned}$$

The first two terms of right part are $O(\tau_n)$ for any $1 \leq t \leq n$ because of the boundedness of $1/\log(-\gamma_3 Q_{t-k})$. For the third term we have,

$$\begin{aligned}
&\gamma_2^0 \sum_{k=1}^{t-1} \left(\gamma_1^0\right)^{k-1} \left|1/\log(\gamma_3 Q_{t-k}) - 1/\log\left(\gamma_3^0 Q_{t-k}\right)\right| \\
&= \gamma_2^0 \sum_{k=1}^{t-1} \left(\gamma_1^0\right)^{k-1} Q_{t-k} / \log(\gamma'_{3k} Q_{t-k}) \left|\gamma_3 - \gamma_3^0\right| \\
&= O(\tau_n), \text{ for any } 1 \leq t \leq n
\end{aligned}$$

where $\gamma'_{3k} > 0$ is a number between γ_3 and γ_3^0 depending on Q_{t-k}, and $\gamma'_{3k} \to \gamma_3^0$ uniformly over all $k \geq 1$. Since Θ is compact, $\gamma'_{3k} \geq C > 0$ for all $k \geq 1$. We use Mean value theorem to get the first equality. For the second equation, the boundedness of $Q_{t-k}/\log(\gamma'_{3k} Q_{t-k})$ is used.

Lemma 10 *Denote* $\Psi = (\beta_0, \beta_1, \beta_2, \beta_3)$ *and* $\Psi_0 = (\beta_0^0, \beta_1^0, \beta_2^0, \beta_3^0)$, *if* $\|\Psi - \Psi_0\| < \tau_n$ *and* $\tau_n \searrow 0$, *under the conditions in Theorem 2, we have*

$$(a) \sup_{1 \leq t \leq n} \left|\sigma_t - \sigma_t^0\right| = O(\tau_n), \quad (b) \sup_{1 \leq t \leq n} \left|\frac{\partial \sigma_t}{\partial \Psi} - \frac{\partial \sigma_t^0}{\partial \Psi}\right| = O(\tau_n), (c) \sup_{1 \leq t \leq n} \left|\frac{\partial^2 \sigma_t}{\partial \Psi_i \partial \Psi_j} - \frac{\partial^2 \sigma_t^0}{\partial \Psi_i \partial \Psi_j}\right| = O(\tau_n)$$

uniformly over $\|\Psi - \Psi_0\| < \tau_n$.

Proof: the proof of Lemma 10 is the same as that of Lemma 9.

Lemma 11 *Suppose* $\tau_n \sim n^{-r}, r > 0$ *and* $\sup_{1 \leq t \leq n} |\alpha_t - \alpha'_t| = O(\tau_n)$ *where* $\{\alpha_t\}$ *and* $\{\alpha'_t\}$

represent two different series of tail index. Under the conditions in Theorem 2, we have

$$\frac{1}{n}\sum_{t=1}^{n}\left|(Q_t-\mu_n)^{-\alpha_t}-(Q_t-\mu_n)^{-\alpha_t'}\right|=O_p\left(\tau_n\right)$$

uniformly over $|\mu_n-\mu_0|<\tau_n$. *The same result holds for*

$$\frac{1}{n}\sum_{t=1}^{n}\left|(Q_t-\mu_n)^{-\alpha_t}-(Q_t-\mu_n)^{-\alpha_t'}\right|\left[\log\left(Q_t-\mu_n\right)\right]^k, k=1,2.$$

Proof: We assume $\alpha_t<\alpha_t^{'}$. By Mean Value Theorem and Lemma 8,

$$\begin{aligned}\frac{1}{n}\sum_{t=1}^{n}\left|(Q_t-\mu_n)^{-\alpha_t}-(Q_t-\mu_n)^{-\alpha_t'}\right| &\leq \frac{C}{n}\sum_{t=1}^{n}(Q_t-\mu_n)^{-\alpha_t^*}\left|\log\left(Q_t-\mu_n\right)\right|\tau_n\\ &\leq \frac{\tau_n C}{n}\sum_{t=1}^{n}\left((Q_t-\mu_n)^{-\alpha_L}+(Q_t-\mu_n)^{-\alpha_U}\right)\left|\log\left(Q_t-\mu_n\right)\right|\\ &= O_p\left(\tau_n\right),\end{aligned}$$

where $\alpha_t^*\in(\alpha_t,\alpha_t')$. For another formula, we use the similar way to prove the result as following:

$$\begin{aligned}&\frac{1}{n}\sum_{t=1}^{n}\left|(Q_t-\mu_n)^{-\alpha_t}-(Q_t-\mu_n)^{-\alpha_t'}\right|\left[\log\left(Q_t-\mu_n\right)\right]^k\\ &\leq \frac{C}{n}\sum_{t=1}^{n}(Q_t-\mu_n)^{-\alpha_t^*}\left|\log\left(Q_t-\mu_n\right)\right|\tau_n\left[\log\left(Q_t-\mu_n\right)\right]^k\\ &\leq \frac{\tau_n C}{n}\sum_{t=1}^{n}\left((Q_t-\mu_n)^{-\alpha_L}+(Q_t-\mu_n)^{-\alpha_U}\right)\left|\log\left(Q_t-\mu_n\right)\right|^{k+1}, k=1,2\\ &= O_p\left(\tau_n\right),\end{aligned}$$

by Mean Value Theorem and Lemma 8.

Lemma 12 proves the uniform convergence result of the second order derivatives of $L_n(\theta)$ over a neighborhood of θ_0. We will use Lemma 12 in the proof of Lemma 13 (a). Additionally we denote $m_{\theta_1\theta_j}(\theta_0)=-E_{\theta_0}\left(\frac{\partial^2}{\partial\theta_i\partial\theta_j}l_1(\theta_0)\right)$.

Lemma 12 *Under the conditions in Theorem 2, for all second order derivatives of* $L_n(\theta_n)$, *we have* $\frac{\partial^2}{\partial\theta_i\partial\theta_j}L_n(\theta_n) \xrightarrow{p} -m_{\theta_i\theta_j}(\theta_0)$,*uniformly over* $\|\theta_n - \theta_0\| < \tau_n$, *where* $\tau_n \sim n^{-r}, r > 0$.

Proof: the proof of Lemma 12 is the same as that of Lemma 11 in Zhao at el.(2018).

Lemma 13 *Under the conditions in Theorem 2, there exists a positive constant* C *such that for all* $\theta \in \Theta$ *and* $t \geq 1$,

$$(a)\,|\alpha_t - \tilde{\alpha}_t| \leq C \cdot C_b^{t-1}, \quad (b)\left|\frac{\partial\alpha_t}{\partial\Phi} - \frac{\partial\tilde{\alpha}_t}{\partial\Phi}\right| \leq C \cdot tC_b^{t-1}, \quad (c)\left|\frac{\partial^2\alpha_t}{\partial\Phi_i\partial\Phi_j} - \frac{\partial^2\tilde{\alpha}_t}{\partial\Phi_i\partial\Phi_j}\right| \leq C \cdot t^2C_b^{t-1}$$
$$(d)\,|\sigma_t - \tilde{\sigma}_t| \leq C \cdot C_b^{t-1}, \quad (e)\left|\frac{\partial\sigma_t}{\partial\Phi} - \frac{\partial\tilde{\sigma}_t}{\partial\Phi}\right| \leq C \cdot tC_b^{t-1}, \quad (f)\left|\frac{\partial^2\sigma_t}{\partial\Phi_i\partial\Phi_j} - \frac{\partial^2\tilde{\sigma}_t}{\partial\Phi_i\partial\Phi_j}\right| \leq C \cdot t^2C_b^{t-1}.$$

Proof: the proof is trivial so we skip it.

Lemma 14 *Under the conditions in Theorem 2, we have* $\frac{1}{n}\sum_{t=1}^{n}\left|(Q_t - \mu_n)^{-\alpha_t} - (Q_t - \mu_n)^{-\tilde{\alpha}_t}\right| \xrightarrow{p} 0$, *uniformly over* $|\mu_n - \mu_0| < \tau_n$, *where* $\tau_n \sim n^{-r}, r > 0$. *The same result holds for*

$$\frac{1}{n}\sum_{t=1}^{n}\left|(Q_t - \mu_n)^{-\alpha_t} - (Q_t - \mu_n)^{-\tilde{\alpha}_t}\right|[\log(Q_t - \mu_n)]^k, \quad k = 1, 2.$$

Proof: From Lemma 11, we know $|\alpha_t - \tilde{\alpha}_t| \leq C \cdot C_b^{t-1}$. Assume $\alpha < \tilde{\alpha}$, we have

$$\begin{aligned}\frac{1}{n}\sum_{t=1}^{n}\left|(Q_t - \mu_n)^{-\alpha_t} - (Q_t - \mu_n)^{-\tilde{\alpha}_t}\right| &\leq \frac{C}{n}\sum_{t=1}^{n}(Q_t - \mu_n)^{-\alpha_t^*}\left|\log(Q_t - \mu_n)\right|C_b^{t-1} \\ &\leq \frac{C}{n}\sum_{t=1}^{n}\left((Q_t - \mu_n)^{-\alpha_L} + (Q_t - \mu_n)^{-\alpha_U}\right)\left|\log(Q_t - \mu_n)\right|C_b^{t-1} \\ &\to_p 0,\end{aligned}$$

by Mean Value Theorem and Lemma 8. For another part of proof, we use the same method

as following:

$$\begin{aligned}
&\frac{1}{n}\sum_{t=1}^{n}\left|(Q_t-\mu_n)^{-\alpha_t}-(Q_t-\mu_n)^{-\tilde{\alpha}_t}\right|\left[\log\left(Q_t-\mu_n\right)\right]^k \\
&\leq \frac{C}{n}\sum_{t=1}^{n}\left(Q_t-\mu_n\right)^{-\alpha_t^*}\left|\log\left(Q_t-\mu_n\right)\right| C_b^{t-1}\left[\log\left(Q_t-\mu_n\right)\right]^k \\
&\leq \frac{C}{n}\sum_{t=1}^{n}\left(\left(Q_t-\mu_n\right)^{-\alpha_L}+\left(Q_t-\mu_n\right)^{-\alpha_U}\right)\left|\log\left(Q_t-\mu_n\right)\right|^{k+1} C_b^{t-1},\ k=1,2 \\
&\to_p 0.
\end{aligned}$$

In Lemma 15, we provide the main uniform convergence result which can be used in the proof of Theorems 2 and 3.

Lemma 15 *Under the conditions in Theorem 2, (a) for all second order derivatives of* $\tilde{L}_n(\theta)$*, we have* $\frac{\partial^2}{\partial\theta_i\partial\theta_j}\tilde{L}_n(\theta)\to_p -m_{\theta_i\theta_j}(\theta_0)$*, uniformly over* $\|\theta-\theta_0\|<\tau_n$*, where* $\tau_n\sim n^{-r}, r>0$ *(b) for the score function of* $\tilde{L}_n(\theta)$*, we have* $(\tau_n^*)^{-1}\left(\frac{\partial}{\partial\theta}\tilde{L}_n(\theta_0)-\frac{\partial}{\partial\theta}L_n(\theta_0)\right)\xrightarrow{p}0$ *if* $\tau_n^* n\to\infty, e.g. \tau_n^*=1/\sqrt{n}$.

Proof: For (a), we already know that $\frac{\partial^2}{\partial\theta_i\partial\theta_j}\tilde{L}_n(\theta)-\frac{\partial^2}{\partial\theta_i\partial\theta_j}L_n(\theta)\to_p 0$ uniformly according to Lemma 14 and 15. Moreover, one can easily see that $\frac{\partial^2}{\partial\theta_0\partial\theta_j}L_n\left(\widehat{\theta}_n\right)-\frac{\partial^2}{\partial\theta_i\partial\theta_j}L_n(\theta_0)\to_p 0$ uniformly over $\left\|\widehat{\theta}_n-\theta_0\right\|\leq\tau_n$. Therefore, $\frac{\partial^2}{\partial\theta_i\partial\theta_j}\tilde{L}_n\left(\widehat{\theta}_n\right)-\frac{\partial^2}{\partial\theta_i\partial\theta_j}L_n(\theta_0)\to_p 0$ over $\left\|\widehat{\theta}_n-\theta_0\right\|\leq\tau_n$.

For (b), we only prove the case of $\frac{\partial}{\partial\mu}\tilde{L}_n(\theta_0)$ as an example and the proof of other first order partial derivatives are similar. We set $g(\sigma_t,\alpha_t)=\frac{\alpha_t}{\sigma^2 t}$. Since $|\sigma_t-\tilde{\sigma}_t|\leq C\cdot C_b^{t-1}, |\alpha_t-\tilde{\alpha}_t|\leq C\cdot C_b^{t-1}$, we have $|g(\sigma_t,\alpha_t)-g(\tilde{\sigma}_t,\tilde{\alpha}_t)|\leq C\cdot C_b^{t-1}$. Then

$$\frac{1}{\tau_n^*}\left(\frac{\partial}{\partial\mu}\tilde{L}_n(\theta_0)-\frac{\partial}{\partial\mu}L_n(\theta_0)\right)=\frac{1}{n\tau_n^*}\sum_{t=1}^{n}\left(\frac{\alpha_t-\tilde{\alpha}_t}{Q_t-\mu_0}-\frac{g(\sigma_t,\alpha_t)}{(Q_t-\mu_0)^{\alpha_t+1}}+\frac{g(\tilde{\sigma}_t,\tilde{\alpha}_t)}{(Q_t-\mu_0)^{\tilde{\alpha}_t+1}}\right)$$
$$=\frac{1}{n\tau_n^*}\sum_{t=1}^{n}\left(\frac{\alpha_t-\tilde{\alpha}_t}{Q_t-\mu_0}-\frac{g(\sigma_t,\alpha_t)-g(\tilde{\sigma}_t,\tilde{\alpha}_t)}{(Q_t-\mu_0)^{\alpha_t+1}}+g(\tilde{\sigma}_t,\tilde{\alpha}_t)\left[(Q_t-\mu_0)^{-(\tilde{\alpha}_t+1)}-(Q_t-\mu_0)^{-(\alpha_t+1)}\right]\right)$$
$$=\frac{1}{n\tau_n^*}\sum_{t=1}^{n}(\frac{\alpha_t-\tilde{\alpha}_t}{Q_t-\mu_0})-\frac{1}{n\tau_n^*}\sum_{t=1}^{n}(\frac{g(\sigma_t,\alpha_t)-g(\tilde{\sigma}_t,\tilde{\alpha}_t)}{(Q_t-\mu_0)^{\alpha_t+1}})$$
$$+\frac{1}{n\tau_n^*}\sum_{t=1}^{n}(g(\tilde{\sigma}_t,\tilde{\alpha}_t)\left[(Q_t-\mu_0)^{-(\tilde{\alpha}_t+1)}-(Q_t-\mu_0)^{-(\alpha_t+1)}\right]).$$

It is easy to verify that $\frac{1}{n\tau_n^*}\sum_{t=1}^{n}(\frac{\alpha_t-\tilde{\alpha}_t}{Q_t-\mu_0})<\frac{C}{n\tau_n^*}\sum_{t=1}^{n}\frac{C_b^{t-1}}{Q_t-\mu_0}$ and $\frac{1}{n\tau_n^*}\sum_{t=1}^{n}(\frac{g(\sigma_t,\alpha_t)-g(\tilde{\sigma}_t,\tilde{\alpha}_t)}{(Q_t-\mu_0)^{\alpha_t+1}})<\frac{C}{n\tau_n^*}\sum_{t=1}^{n}\frac{C_b^{t-1}}{(Q_t-\mu_0)^{\alpha_t+1}}$. Since $n\tau_n^*\to\infty$ and $E_{\theta_0}\left[\sum_{t=1}^{\infty}C_b^{t-1}(Q_t-\mu_0)^{-\alpha}\right]<\infty$ for all $\alpha>0$, both first and second terms converge to 0 in probability. For third term, assume $\alpha_t>\tilde{\alpha}_t$ we use Mean Value Theorem as following:

$$\frac{1}{n\tau_n^*}\sum_{t=1}^{n}(g(\tilde{\sigma}_t,\tilde{\alpha}_t)\left[(Q_t-\mu_0)^{-(\tilde{\alpha}_t+1)}-(Q_t-\mu_0)^{-(\alpha_t+1)}\right])$$
$$<\frac{C\cdot C_b^{t-1}}{n\tau_n^*}\sum_{t=1}^{n}g(\tilde{\sigma}_t,\tilde{\alpha}_t)(Q_t-\mu_0)^{-(\alpha_t^*+1)}\log(Q_t-\mu_n)$$
$$<\frac{C\cdot C_b^{t-1}}{n\tau_n^*}\sum_{t=1}^{n}g(\tilde{\sigma}_t,\tilde{\alpha}_t)\left((Q_t-\mu_0)^{-\alpha_L}+(Q_t-\mu_0)^{-\alpha_U}\right)\log(Q_t-\mu_n)$$
$$\to_p 0,$$

where $\alpha_t^*\in(\tilde{\alpha}_t,\alpha_t)$.

Lemma 16 *Under the conditions in Theorem 2,*

$$\frac{1}{\sqrt{n}}\sum_{i=1}^{n}\frac{\partial l_t(\theta_0)}{\partial\theta}\Rightarrow N\left(0,M_0^{-1}\right)$$

where M is the Fisher Information matrix at θ_0.

Proof: We follow the proof of Lemma 15 in Zhao et al.(2018) by using CLT for martingale

difference (Billingsley (1961)). One can easily prove that

$$E_{\theta_0}\left(\frac{\partial l_t(\theta_0)}{\partial\theta}|\mathcal{F}_{t-1}\right)=0 \text{ and } \operatorname{Var}_{\theta_0}\left(\frac{\partial l_t(\theta_0)}{\partial\theta}\right)=M_0<\infty$$

For any $\lambda\in\mathbb{R}^9$, $\left\{\lambda\frac{\partial l_t(\theta_0)}{\partial\theta},\mathcal{F}_t\right\}_t$ is a square-integrable stationary martingale difference. Additionally, the sequences $\{\sigma_t,\alpha_t\}$ and $\{Q_t\}$ are both stationary and egodic, hence the sequences $\frac{\partial\alpha_t}{\partial\Phi}$ and $\frac{\partial\sigma_t}{\partial\Psi}$ follow the properties of strict stationarity and ergodicity because they are the measureable function. Therefore, $\frac{\partial l_t(\theta_0)}{\partial\theta_i}$(for $i=1,\cdots,9$), which are generated from $\alpha_t,\sigma_t,Q_t,\frac{\partial\alpha_t}{\partial\Phi},\frac{\partial\sigma_t}{\partial\Psi}$, are also stationary and egodic. According to CLT of (Billingsley, 1961) and Wold-Cramer device, Lemma 16 holds.

Proof of Theorem 2: Let $\{\tau_n\}$ be a sequence such that $\tau_n\sim n^{-r}$ and $n^{1/2}\tau_n\to\infty$ i.e. $0<r<1/2$. Let $t\in\mathbb{R},y\in\mathbb{R}^8$ and $f_n(t,y)=\tau_n^{-2}\tilde{L}_n\left(\mu_0+\tau_nt,\phi^0+\tau_ny\right)$, where we use ϕ^0 to denote $(\beta_0^0,\beta_1^0,\beta_2^0,\beta_3^0,\gamma_0^0,\gamma_1^0,\gamma_2^0,\gamma_3^0)$. Then by Taylor Expansion we have,

$$\begin{aligned}\frac{\partial}{\partial t}f_n(t,y)&=\tau_n^{-1}\frac{\partial\tilde{L}_n\left(\mu_0+\tau_nt,\phi^0+\tau_ny\right)}{\partial\mu}\\&=\tau_n^{-1}\frac{\partial\tilde{L}_n\left(\mu_0,\phi^0\right)}{\partial\mu}+\frac{\partial^2\tilde{L}_n\left(\mu^*,\phi^*\right)}{\partial\mu^2}t+\sum_{i=1}^{8}\frac{\partial^2\tilde{L}_n\left(\mu^*,\phi^*\right)}{\partial\mu\partial\phi_i}y_i\\&=\tau_n^{-1}\left(\frac{\partial\tilde{L}_n\left(\mu_0,\phi^0\right)}{\partial\mu}-\frac{\partial L_n\left(\mu_0,\phi^0\right)}{\partial t}\right)+\tau_n^{-1}\left(\frac{\partial L_n\left(\mu_0,\phi^0\right)}{\partial\mu}\right)+\frac{\partial^2\tilde{L}_n\left(\mu^*,\phi^*\right)}{\partial\mu^2}t\\&+\sum_{i=1}^{8}\frac{\partial^2\tilde{L}_n\left(\mu^*,\phi^*\right)}{\partial\mu\partial\phi_i}y_i,\end{aligned}$$

by the fact that $|\mu^*-\mu_0|<\tau_nt$, $\|\phi^*-\phi^0\|<\tau_n\|y\|$, and a Taylor expansion of $\frac{\partial\tilde{L}_n\left(\mu_0+\tau_nt,\phi^0+\tau_ny\right)}{\partial t}$ at (μ_0,ϕ^0). Based on Lemma 15 (b), the first term goes to 0. The second term converges to 0 because of Lemma 16 the fact that $\tau_n\sqrt{n}\to\infty$. Moreover, the third and forth terms

converge uniformly over $t^2 + \|y\|^2 \leq 1$ by Lemma 13 (a), which means

$$\frac{\partial^2 \tilde{L}_n(\mu^*, \phi^*)}{\partial \mu^2} t + \sum_i \frac{\partial^2 \tilde{L}_n(\mu^*, \phi^*)}{\partial \mu \partial \phi_i} y_i \to_p -m_{\mu\mu}(\theta_0)\, t - \sum_{i=1}^{8} m_{\mu\phi_i}(\theta_0)\, y_i.$$

Now we have $\frac{\partial}{\partial t} f_n(t,y) = -m_{\mu\mu}(\theta_0)\, t - \sum_{i=1}^{8} m_{\mu\phi_i}(\theta_0)\, y_i + o_p(1)$. In addition, we also have $\frac{\partial}{\partial y_k} f_n(t,y) = -m_{\phi_k\mu}(\theta_0)\, t - \sum_{i=1}^{8} m_{\phi_k\phi_i}(\theta_0)\, y_i + o_p(1)$, for $k = 1, \ldots, 8$, where $o_p(1)'$ s are uniformly decaying over $t^2 + \|y\|^2 \leq 1$. Consider $t^2 + \|y\|^2 = 1$, we get

$$t\frac{\partial f_n}{\partial t}(t,y) + \sum_i y_i \frac{\partial f_n}{\partial y_i}(t,y) = -t^2 m_{\mu\mu}(\theta_0) - 2t \sum_{i=1}^{8} y_i m_{\mu\phi_i}(\theta_0) - \sum_{i=1}^{8}\sum_{j=1}^{8} y_i y_j m_{\phi_i\phi_j}(\theta_0) + o_p(1) < 0,$$

based on the fact that the Fisher Information matrix M_0 is positive definite.

According to Lemma 5 in Smith (1985), we have that f_n has a local maximum over the open set $t^2 + \|y\|^2 < 1$ with probability going to 1. Therefore one can find a sequence of local maximizer $\hat{\theta}_n$ of $\tilde{L}_n(\theta)$ such that $\hat{\theta}_n \to_p \theta_0$ and $\left\|\hat{\theta}_n - \theta_0\right\| \leq \tau_n$, where $\tau_n \sim n^{-r}, 0 < r < 1/2$.

Proof of Theorem 3: We use similar method to prove Theorem 3. By Taylor expansion, we have

$$\frac{\partial \tilde{L}_n\left(\widehat{\theta}_n\right)}{\partial \theta} = \frac{\partial \tilde{L}_n(\theta_0)}{\partial \theta} + \frac{\partial^2 \tilde{L}_n(\theta^*)}{\partial \theta \partial \theta'}\left(\widehat{\theta}_n - \theta_0\right),$$

in which λ is a constant number with $0 \leq \lambda \leq 1$ such that $\theta^* = \lambda\widehat{\theta}_n + (1-\lambda)\theta_0$. Hence

$$\sqrt{n}\left(\widehat{\theta}_n - \theta_0\right) = -\left(\frac{\partial^2 \tilde{L}_n(\theta^*)}{\partial \theta \partial \theta'}\right)^{-1} \sqrt{n}\frac{\partial \tilde{L}_n(\theta_0)}{\partial \theta}.$$

Based on (a) of Lemma 15, $-\left(\frac{\partial^2 \bar{L}_n(\theta^*)}{\partial \theta \partial \theta'}\right) \to_p I(\theta_0) = -E_{\theta_0}\left(\frac{\partial^2}{\partial \theta \partial \theta^T} 1_t(\theta_0)\right)$. Moreover, $\sqrt{n}\frac{\partial \tilde{L}_n(\theta_0)}{\partial \theta}$ converges to $N(0, I(\theta_0))$ in distribution according to (b) in Lemma 15 and Lemma 16. By Slutsky theorem, one can easily prove that $\sqrt{n}\left(\hat{\theta}_n - \theta_0\right)$ converges to $N\left(0, M_0^{-1}\right)$ in distribution.

Proof of Proposition 1: Let δ be a generic small positive constant and let $\phi = (\beta_0, \beta_1, \beta_2, \beta_3, \gamma_0, \gamma_1, \gamma_2, \gamma_3)$. Denote $V_n = \{\theta \in \Theta | \mu \leq cQ_{n,1} + (1-c)\mu_0\}$. It is easily to see that $\mu_0 < cQ_{n,1} + (1-c)\mu_0 < Q_{n,1}$ and $cQ_{n,1} + (1-c)\mu_0 \searrow \mu_0$ a.s. for any $0 < c < 1$. Denote $\Theta_n^\delta = \{\theta \in V_n | \, \|\theta - \theta_0\| \geq \delta\}, \Theta_n^\mu = \{\theta \in V_n | \, \|\theta - \theta_0\| \geq \delta, \mu > \mu_0\}$ and $\Theta^\delta = \{\theta \in V_n | \, \|\theta - \theta_0\| \geq \delta, \mu \leq \mu_0\}$. Note that $\Theta_n^\delta = \Theta_n^\mu \cup \Theta^\delta$.

(I) first we prove for any $\delta > 0$,

$$P\left(\sup_{\Theta_n^\delta} \tilde{L}_n(\theta) \geq \tilde{L}_n(\theta_0)\right) \to 0, \text{ as } n \to \infty.$$

Based on Lemma 8 and Lemma 14, we have $\sup_{\Theta_n^\delta} \left|\tilde{L}_n(\theta) - L_n(\theta)\right| \to_p 0$ as $n \to \infty$. Additionally, by Lemma 9, $\sup_{\Theta_n^\mu} |L_n(\mu, \phi) - L_n(\mu_0, \phi)| \to_p 0$ as $n \to \infty$. Then we have

$$\begin{aligned}
\sup_{\Theta_n^\delta} \tilde{L}_n(\theta) &= \sup_{\Theta_n^\delta} L_n(\theta) + o_p(1) \\
&= \max\left(\sup_{\Theta^\delta} L_n(\theta), \sup_{\Theta_n^\mu} L_n(\theta)\right) + o_p(1) \\
&= \max\left(\sup_{\Theta^\delta} \sup_n(\theta), \sup_{\Theta_n^\mu} L_n(\mu_0, \phi)\right) + o_p(1) \\
&\leq \sup_{\Theta^{\delta/2}} L_n(\theta) + o_p(1).
\end{aligned}$$

The last inequality results from the fact that $\epsilon_n \searrow 0$. Then with probability going to 1, $\{\phi | \phi \in \Theta_n^\mu\} \subseteq \left\{\phi | \phi \in \Theta^{\delta/2}\right\}$. One can also prove that $\tilde{L}_n(\theta_0) = L_n(\theta_0) + o_p(1) \to_p E_{\theta_0}(l_1(\theta_0))$. The rest proof of the first part follows from the proof of Proposition 2 in Dombry (2015).

Now Denote $\Theta_n^{\delta c} = \{\theta \in V_n | \, \|\theta - \theta_0\| < \delta\}, \Theta_n^{\mu c} = \{\theta \in V_n | \, \|\theta - \theta_0\| < \delta, \mu > \mu_0\}$ and $\Theta^{\delta c} = \{\theta \in V_n | \, \|\theta - \theta_0\| < \delta, \mu \leq \mu_0\}$. Similarly, $\Theta_n^{\delta c} = \Theta_n^{\mu c} \cup \Theta^{\delta c}$.

(II) Next We prove that there exists a $\delta^* > 0$ such that

$$P\left(\text{ All Hessian matrices } \frac{\partial^2}{\partial\theta\partial\theta^T}\tilde{L}_n(\theta) \text{ over } \theta \in \Theta_n^{\delta^* c} \text{ is negative definite }\right) \to 1, \text{ as } n \to \infty.$$

Based on the results in Lemma 8 and Lemma 14, we can prove

$$\sup_{\Theta_n^{\delta c}} \left| \frac{\partial^2}{\partial\theta_i\partial\theta_j}\tilde{L}_n(\theta) - \frac{\partial^2}{\partial\theta_i\partial\theta_j}L_n(\theta) \right| \to_p 0, \text{ as } n \to \infty,$$

and

$$\sup_{\Theta_n^{\mu c}} \left| \frac{\partial^2}{\partial\theta_i\partial\theta_j}L_n(\mu,\phi) - \frac{\partial^2}{\partial\theta_i\partial\theta_j}L_n\left(\mu_0,\phi\right) \right| \to_p 0, \text{ as } n \to \infty,$$

since $\mu \leq \mu_0$ over $\Theta^{\delta c}$, we can prove that $\sup_{\Theta^{\delta c}} \left| \frac{\partial^2}{\partial\theta_i\partial\theta_j} l_t(\theta) \right|$ is integrable. Based on stationarity and ergodicity of AcFL model and Uniform Law of Large Numbers,

$$\sup_{\Theta^{\delta c}} \left| \frac{\partial^2}{\partial\theta_i\partial\theta_j}L_n(\mu,\phi) - E_{\theta_0}\left(\frac{\partial^2}{\partial\theta_i\partial\theta_j} l_1(\mu,\phi) \right) \right| \to_p 0, \text{ as } n \to \infty.$$

In addition, $E_{\theta_0}\left(\frac{\partial^2}{\partial\theta\partial\theta^T} l_1\left(\theta_0\right)\right) = -M_0$ is negative definite by Lemma 5. Since $E_{\theta_0}\left(\frac{\partial^2}{\partial\theta\partial\theta^T} l_1(\theta)\right)$ is continuous w.r.t. θ over $\Theta^{\delta c}$, there exists a $\delta^* > 0$ such that $E_{\theta_0}\left(\frac{\partial^2}{\partial\theta\partial\theta^T} l_1(\theta)\right)$ is negative definite for all $\theta \in \Theta^{\delta^* c}$. Therefore we can prove (II). From (I), we know that with probability going to 1, the global maximizer of $\tilde{L}_n(\theta)$ over V_n is located within $\Theta_n^{\delta^* c}$. By Theorem 2, one can find a sequence $\hat{\theta}_n$ of local maximizer of $\tilde{L}_n(\theta)$ such that $\left\|\hat{\theta}_n - \theta_0\right\| \leq \tau_n$ where $\tau_n = O_p\left(n^{-r}\right), 0 < r < 1/2$. Thus $P\left(\hat{\theta}_n \in \Theta_n^{\delta^* c}\right) \to 1$. Moreover, $\frac{\partial \tilde{L}_n}{\partial\theta}\left(\hat{\theta}_n\right) = 0$. Combining with (II) and Theorem 2.6 in Makelainen et al. (1981), we can prove the proposition.

6.2 Proofs for AcFL model with spatial correlations

6.2.1 Proof of stationarity and ergodicity

Proof of Theorem 7: For spatial AcFL model, we follow the proof of Theorem 1 and also apply Harris Chains to prove the staionarity and ergodicity of $\{\log(\alpha_t), \log(\sigma_t)\}$. We set $G^* = \left(\frac{\beta_0-\beta_2-\beta_4}{1-\beta_1}, \frac{\beta_0}{1-\beta_1}\right) \times \left(\frac{\gamma_0}{1-\gamma_1}, \frac{\gamma_0+\gamma_2+\gamma_4}{1-\gamma_1}\right)$, an open area in $\mathbb{R}^2$. Then Lemma 17 is as following:

Lemma 17 *G^* is absorbing for $\mathbf{X}_t$.*

Proof: If $\log \alpha_t > \frac{\gamma_0}{1-\gamma_1}$, $\log \alpha_{t+1} = \gamma_0 + \gamma_1 \log \alpha_t + \gamma_2 / \log(\gamma_3 Q_t) + \gamma_4 / \log(\gamma_5 Q_t^*) > \gamma_0 + \gamma_1 \frac{\gamma_0}{1-\gamma_1} = \frac{\gamma_0}{1-\gamma_1}$ because $\gamma_3 > e/\min(Q_t)$ and $\gamma_5 > e/\min(Q_t^*)$. Similarly, if $\log \alpha_t < \frac{\gamma_0+\gamma_2+\gamma_4}{1-\gamma_1}$, then $\log \alpha_{t+1} < \gamma_0 + \gamma_1 \frac{\gamma_0+\gamma_2+\gamma_4}{1-\gamma_1} + \gamma_2 + \gamma_4 = \frac{\gamma_0+\gamma_2+\gamma_4}{1-\gamma_1}$. The proof of σ_t is the same.

One can see that $\{\log(\alpha_t)\}$ and $\{\log(\sigma_t)\}$ are both bounded. We will prove that $\{\log \alpha_t\}$ is a Harris Chain first. WOLG, for simplicity, we set $\beta_0 = \beta_1 = \beta_2 = \beta_4 = 0$ and $\mu = 0$ in the following proof. Same as the proof of Theorem 1, only the boundedness of $\{\log(\sigma_t)\}$ will be used. We continue the proof of $\{\log(\alpha_t)\}$ being a Harris Chain by Definition 1 in Section 6.2.1.

Lemma 18 $\{\log \alpha_t\}$ *is a Harris Chain.*

Proof: Let $q(x, y)$ be the transition probability density function and $\rho(x)$ to be the normalized Lebesgue measure concentrated on set B and $\beta_0 = \beta_1 = \beta_2 = \beta_4 = 0$ and $\mu = 0$. We define

$$A = \left[\frac{\gamma_0 + \Delta_1}{1-\gamma_1}, \frac{\gamma_0 + \gamma_2 + \gamma_4 - \Delta_2}{1-\gamma_1} \right] = [L_A, U_A] .$$

For any $\log \alpha_t$, $\gamma_0 + \gamma_1 \log \alpha_t \leq \log \alpha_{t+1} \leq \gamma_0 + \gamma_1 \log(\alpha_t) + \gamma_2 + \gamma_4$. Since we want to make sure that the transition probability $p(\log \alpha_t, \log \alpha_{t+1}) > \epsilon, \forall \log \alpha_t \in A, \log \alpha_{t+1} \in B$, we can set B to be the intersection between $(\gamma_0 + \gamma_1 \log \alpha_t, \gamma_0 + \gamma_1 \log \alpha_t + \gamma_2 + \gamma_4)$, for $\log \alpha_t = \frac{\gamma_0+\Delta_1}{1-\gamma_1}$ and $\log \alpha_t = \frac{\gamma_0+\gamma_2+\gamma_4-\Delta_2}{1-\gamma_1}$. Therefore, in order to make two intervals have intersection, we need

$$\gamma_0 + \gamma_1 \frac{\gamma_0 + \gamma_2 + \gamma_4 - \Delta_2}{1-\gamma_1} < \gamma_0 + \gamma_1 \frac{\gamma_0 + \Delta_1}{1-\gamma_1} + \gamma_2 + \gamma_4.$$

It is obvious that $\Delta_2 + \Delta_1 < \gamma_2 + \gamma_4$ satisfy the above inequality for all $\gamma_1 < 1$, $\gamma_2 > 0$, and $\gamma_4 > 0$. Hence we can take B as a proper subset of

$$\left[\gamma_0 + \gamma_1 \frac{\gamma_0 + \gamma_2 + \gamma_4 - \Delta_2}{1-\gamma_1}, \gamma_0 + \gamma_1 \frac{\gamma_0 + \Delta_1}{1-\gamma_1} + \gamma_2 + \gamma_4 \right] = \left[\frac{\gamma_0 + \gamma_1 (\gamma_2 + \gamma_4 - \Delta_2)}{1-\gamma_1}, \frac{\gamma_0 + \gamma_1 \Delta_1}{1-\gamma_1} + \gamma_2 + \gamma_4 \right].$$

We need to prove $P_x(\tau_A < \infty) > 0$ next. Applying the equations of $\log(\alpha_t)$ t times, we get

$$\log \alpha_t = \frac{\gamma_0 \left(1-\gamma_1^t\right)}{1-\gamma_1} + \gamma_1^t \log \alpha_0 + \gamma_2 \sum_{i=1}^{t} \gamma_1^{i-1} (\log \left(\gamma_3 Q_{t-i}\right))^{-1} + \gamma_4 \sum_{i=1}^{t} \gamma_1^{i-1} (\log \left(\gamma_5 Q^*_{t-i}\right))^{-1}.$$

Due to the boundedness of $\{\log(\alpha_t)\}$, for each $\epsilon > 0$, there exists a T_1 such that $\forall t > T_1, \left| \frac{\gamma_0\left(1-\gamma_1^t\right)}{1-\gamma_1} + \gamma_1^t \log(\alpha_0) - \frac{\gamma_0}{1-\gamma_1} \right| < \epsilon$. Moreover, $\gamma_4 \sum_{i=1}^{t} \gamma_1^{i-1} = \frac{\gamma_4\left(1-\gamma_1^t\right)}{1-\gamma_1} \to \frac{\gamma_4}{1-\gamma_1}$. Hence we can find a $T_3 > T_1$ such that for all $\gamma_4 \sum_{i=1}^{t} \gamma_1^{i-1} - \frac{\gamma_4}{1-\gamma_1} > -\epsilon$, for all $t > T_3$. Then the range of $\gamma_4 \sum_{i=1}^{t} \gamma_1^{i-1} (\log \left(\gamma_5 Q^*_{t-i}\right))^{-1}$ is $\left[\epsilon, \frac{\gamma_4}{1-\gamma_1} - \epsilon\right]$ since the value of $\log(\alpha_0)$ does not affect $\{Q^*_t\}$. We can also find a $T_2 > \max(T_1, T_3)$ such that for all $\gamma_2 \sum_{i=1}^{t} \gamma_1^{i-1} - \frac{\gamma_2}{1-\gamma_1} > -\epsilon$, for all $t > T_2$.

Following the proof of Theorem 1, we have

$$\gamma_2 \sum_{i=1}^{T_2} \gamma_1^{i-1} (\log \left(\gamma_3 Q_{T_2-i}\right))^{-1} \in \left(\frac{\Delta_1}{1-\gamma_1} + \epsilon, \frac{\gamma_2 - \Delta_2}{1-\gamma_1} - \epsilon \right) = \left(L_A - \frac{\gamma_0}{1-\gamma_1} + \epsilon, U_A - \frac{\gamma_0 + \gamma_4}{1-\gamma_1} - \epsilon \right).$$

Since $\left| \frac{\gamma_0\left(1-\gamma_1^{T_2}\right)}{1-\gamma_1} + \gamma_1^{T_2} \log \alpha_0 - \frac{\gamma_0}{1-\gamma_1} \right| < \epsilon$, $\gamma_4 \sum_{i=1}^{t} \gamma_1^{i-1} (\log \left(\gamma_5 Q^*_{t-i}\right))^{-1} \in \left[\epsilon, \frac{\gamma_4}{1-\gamma_1} - \epsilon\right]$, for $\forall \log \alpha_0 \in S$, we have $P_{\alpha_0} (\log \alpha_{T_2} \in A) > 0$ i.e. $P_x (\tau_A < \infty) = 1 > 0$. Thus $\{\log \alpha_t\}$ is a Harris Chain.

Then we define a new Chain based on $\{\log \alpha_t\}$ by adding an artificial element $\{\beta\}$ in $S = \left(\frac{\gamma_0}{1-\gamma_1}, \frac{\gamma_0+\gamma_2++\gamma_4}{1-\gamma_1}\right)$ and define the new transitional probability as follows:

1. if $x \in S \backslash A, \bar{p}(x, C) = p(x, C)$ for $C \in S$;

2. if $x \in A$, we have $\bar{p}(x, \{\beta\}) = \epsilon, \bar{p}(x, C) = p(x, C) - \epsilon\rho(C)$ for $C \in S$, where ρ is the normalized Lebsegue measure on A;

3. if $x = \beta, \bar{p}(\beta, D) = \int \bar{p}(x, D)\rho(dx)$ for $D \in \bar{S}$.

Lemma 19 $\{\beta\}$ *is positive recurrent in the new Chain.*

Proof: The proof of Lemma 19 is the same as that of Lemma 3.

$\{\beta\}$ is aperiodic because $A \cap B \neq \varnothing$,, hence $\{\log \alpha_t\}$ is aperiodic. Therefore, we know $\{\log \alpha_t\}$ is an aperiodic, positive recurrent Harris Chain. By Theorem 17.1.7 in Meyn and Tweedie (2005), $\{\log \alpha_t\}$ will have a unique stationary distribution and it will converge to the stationary distribution and then $\{\log \alpha_t\}$ is ergodic. Similarly, we can prove $\{\log \sigma_t\}$ is stationary and ergodic.

6.2.2 Proof of consistency and asymptotic normality

The proofs of Theorems 8, 9 and Proposition 3 are based on technical lemmas (Lemma 20 - 32). Most lemmas in the section have the same proofs of lemmas in Section 6.1.2, so we skip and only show the contents of these lemmas. Similar to the proofs in Section 6.1.2, We assume the conditions in Theorem 8 hold in the following proof. The parameter space Θ is a compact set of Θ_s contains true parameter θ_0. We also assume the observations $\{Q_t\}_{t=1}^n$ come from a stationary and ergodic spatial AcFL defined in Θ. We denote the kth order statistics of $\{Y_t\}_{t=1}^n$ and $\{Q_t\}_{t=1}^n$ by $Y_{n,k}$ and $Q_{n,k}$. In addition, we use $\tau_n \sim n^{-r}$ to represent $\tau_n/n^{-r} \to 1$ as $n \to \infty$. We use $C_b < 1$ to denote the upper bound of β_1, γ_1 in Θ and set C to be a generic positive constant.

First, we prove the identifiability of spatial AcFL model in Lemma 20, which means each parameter value θ defines a unique AcFL with spatial correlations.

Lemma 20 *(Identifiability) If $Q_t(\theta_1) = Q_t(\theta_2)$ a.s. for all t, then $\theta_1 = \theta_2$. Here a.s. is for the infinite product space generated by $\{\ldots, Y_{-1}, Y_0, Y_1, Y_2, \ldots\}$, where Y_i's are i.i.d. unit Fréchet random variables.*

Proof: Let $\sigma_t(\theta_1)$ to be σ_t^1, $\alpha_t(\theta_1)$ be α_t^1, $\sigma_t(\theta_2)$ be σ_t^2, and $\alpha_t(\theta_2)$ be α_t^2. Suppose there exists θ_1 and θ_2 such that $Q_t(\theta_1) = Q_t(\theta_2)$ a.s., then

$$\mu_1 + \sigma_t^1 Y_t^{1/\alpha_t^1} = \mu_2 + \sigma_t^2 Y_t^{1/\alpha_t^2} \text{ a.s.},$$

since $Y_{n,1} \searrow 0$ a.s., (σ_t^1, α_t^1) and (σ_t^2, α_t^2) are bounded, $\mu_1 = \mu_2$. After rearranging the

equation, we obtain

$$Y_t^{1/\alpha_t^1-1/\alpha_t^2}=\sigma_t^2/\sigma_t^1 \text{ a.s..}$$

Let $\mathcal{F}_t$ denote $\sigma\left(Y_t,Y_{t-1},\ldots\right)$. Previous equation holds if and only if $\sigma_t^1=\sigma_t^2$ and $\alpha_t^1=\alpha_t^2$ a.s. because $Y_t\perp\mathcal{F}_{t-1}$ and $\alpha_t^1,\alpha_t^2\in\mathcal{F}_{t-1}$. Based on spatial AcFL model of $\log\alpha_t$, we know that if $\alpha_t^1=\alpha_t^2$ a.s., then

$$\gamma_0^1+\gamma_1^1\log\alpha_{t-1}+\gamma_2^1/\log\left(\gamma_3^1Q_{t-1}\right)+\gamma_4^1/\log\left(\gamma_5^1Q_{t-1}\right)=\gamma_0^2+\gamma_1^2\log\alpha_{t-1}+\gamma_2^2/\log\left(\gamma_3^2Q_{t-1}\right)+\gamma_4^2/\log\left(\gamma_5^2Q_{t-1}\right),$$

$$\gamma_0^1-\gamma_0^2+\left(\gamma_1^1-\gamma_1^2\right)\log\alpha_{t-1}=\gamma_2^2/\log\left(\gamma_3^2Q_{t-1}\right)-\gamma_2^1/\log\left(\gamma_3^1Q_{t-1}\right)+\gamma_4^2/\log\left(\gamma_5^2Q_{t-1}\right)-\gamma_4^1/\log\left(\gamma_5^1Q_{t-1}\right).$$

Because $\alpha_{t-1}\in\mathcal{F}_{t-2}$ and $Q_{t-1}\notin\mathcal{F}_{t-2}$, $\gamma_0^1=\gamma_0^2,\gamma_1^1=\gamma_1^2,\gamma_2^1=\gamma_2^2,\gamma_3^1=\gamma_3^2,\gamma_4^1=\gamma_4^2,\gamma_5^1=\gamma_5^2$. Similarly, we can prove $\beta_0^1=\beta_0^2,\beta_1^1=\beta_1^2,\beta_2^1=\beta_2^2,\beta_3^1=\beta_3^2,\beta_4^1=\beta_4^2,\beta_5^1=\beta_5^2$. Therefore spatial AcFL model is uniquely defined by the value of θ.

We discuss the behavior of score function and Fisher information matrix at the true parameter θ_0 given initial value (σ_1^0,α_1^0) in the following lemma.

Lemma 21 *Under the conditions in Theorem 8, $E_{\theta_0}\left(\frac{\partial}{\partial\theta}l_t\left(\theta_0\right)\right)=0$ and for M_0, the Fisher information matrix at θ_0, we have $M_0=\mathrm{Var}_{\theta_0}\left(\frac{\partial}{\partial\theta}l_t\left(\theta_0\right)\right)=-E_{\theta_0}\left(\frac{\partial^2}{\partial\theta\partial\theta^T}l_t\left(\theta_0\right)\right)$ and M_0 is well defined and positive definite.*

Proof: the proof of Lemma 21 is the same as that of Lemma 5.

Lemma 22 shows the expectations of the items in $\frac{\partial^2}{\partial\theta_j\partial\theta_j}L_n\left(\theta_0\right)$ exist, which serve as building blocks for the following lemmas.

Lemma 22 *Under the conditions in Theorem 8, we have (a) for any $\frac{1}{n}\sum_{t=1}^n\left(Q_t-\mu_0\right)^{-\alpha}\xrightarrow{p}E_{\theta_0}\left(Q_1-\mu_0\right)^{-\alpha}<\infty$, (b) for any positive integer k, $\frac{1}{n}\sum_{t=1}^n\left[\log\left(Q_t-\mu_0\right)\right]^k\xrightarrow{p}E_{\theta_0}\left[\log\left(Q_1-\mu_0\right)\right]^k<\infty$.*

Proof: the proof of Lemma 22 is the same as Lemma 5 in Zhao et al.(2018).

In Lemma 23, we will show an asymptotic bound on the distance between $Q_{n,1}$ and μ_0. It indicates that the convergence rate of $Q_{n,1}$ is larger than $(\log n)^{-1/\alpha_L}$.

Lemma 23 *Under the conditions in Theorem 8,* $Q_{n,1} - \mu_0 \geq O_p\left((\log n)^{-1/\alpha_L}\right)$.

Proof: the proof of Lemma 23 is the same as Lemma 6 in Zhao et al.(2018).

Lemma 24 provides the foundation for the uniform convergence result in Lemma 28 and Lemma 31.

Lemma 24 *Denote* $S_n^\alpha(\mu) = n^{-1}\sum_{k=1}^n (Q_{n,k} - \mu)^{-\alpha}, \alpha > 0$ *or* $S_n^\alpha(\mu) = n^{-1}\sum_{k=1}^n \log(Q_{n,k} - \mu)$ *or* $S_n^\alpha(\mu) = n^{-1}\sum_{k=1}^n (Q_{n,k} - \mu)^{-\alpha}[\log(Q_{n,k} - \mu)]^m$ *for* $m = 1, 2, 3$. *Under the conditions in Theorem 8, given positive sequence* τ_n, *s.t.* $\tau_n \sim n^{-r}, r > 0$, *the following result holds uniformly over* $|\mu_n - \mu_0| < \tau_n$,

$$|S_n^\alpha(\mu_n) - S_n^\alpha(\mu_0)| \leq O_p(\tau_n).$$

Proof: the proof of Lemma 24 is the same as Lemma 7 in Zhao et al.(2018).

Lemmas 25 and 26 show that the supremum of $|\alpha_t - \alpha_t^0|$ and $|\sigma_t - \sigma_t^0|$, which are influenced by the parameter difference $|\theta - \theta_0|$, converges at the rate of τ_n over t.

Lemma 25 *Denote* $\Phi = (\gamma_0, \gamma_1, \gamma_2, \gamma_3)$ *and* $\Phi_0 = (\gamma_0^0, \gamma_1^0, \gamma_2^0, \gamma_3^0)$, *if* $\|\Phi - \Phi_0\| < \tau_n$ *and* $\tau_n \searrow 0$, *under the conditions in Theorem 8, we have*

$$(a)\sup_{1\leq t\leq n}\left|\alpha_t - \alpha_t^0\right| = O(\tau_n), \quad (b)\sup_{1\leq t\leq n}\left|\frac{\partial\alpha_t}{\partial\Phi} - \frac{\partial\alpha_t^0}{\partial\Phi}\right| = O(\tau_n), (c)\sup_{1\leq t\leq n}\left|\frac{\partial^2\alpha_t}{\partial\Phi_i\partial\Phi_j} - \frac{\partial^2\alpha_t^0}{\partial\Phi_i\partial\Phi_j}\right| = O(\tau_n)$$

uniformly over $\|\Phi - \Phi_0\| < \tau_n$.

Proof: Here we only prove (a) because the proofs of other equations are similar but more complex. Since the domain of α_t is bounded and the function $\exp(\cdot)$ is continuously differentiable, $\exp(\cdot)$ defined on this compact set is Lipschitz continuous. Therefore, we only need to verify $\sup_{1\leq t\leq n}|\log\alpha_t - \log\alpha_t^0| = O(\tau_n)$. Applying autoregressive equation t times, we obtain

$$\log \alpha_t = \gamma_0 \sum_{k=1}^{t-1} \gamma_1^{k-1} + \gamma_2 \sum_{k=1}^{t-1} \gamma_1^{k-1} / \log\left(\gamma_3 Q_{t-k}\right) + \gamma_4 \sum_{k=1}^{t-1} \gamma_1^{k-1} / \log\left(\gamma_5 Q_{t-k}^*\right) + \gamma_1^{t-1} \log \alpha_1^0,$$

Then the difference is

$$\begin{aligned}
\left|\log \alpha_t - \log \alpha_t^0\right| \leq & \left|\gamma_0 \sum_{k=1}^{t-1} \gamma_1^{k-1} - \gamma_0^0 \sum_{k=1}^{t-1} \left(\gamma_1^0\right)^{k-1}\right| + \left|\gamma_1^{t-1} \log \alpha_1^0 - \left(\gamma_1^0\right)^{t-1} \log \alpha_1^0\right| \\
& + \left|\gamma_2 \sum_{k=1}^{t-1} \gamma_1^{k-1} / \log\left(\gamma_3 Q_{t-k}\right) - \gamma_2^0 \sum_{k=1}^{t-1} \left(\gamma_1^0\right)^{k-1} / \log\left(\gamma_3^0 Q_{t-k}\right)\right| \\
& + \left|\gamma_4 \sum_{k=1}^{t-1} \gamma_1^{k-1} / \log\left(\gamma_5 Q_{t-k}^*\right) - \gamma_4^0 \sum_{k=1}^{t-1} \left(\gamma_1^0\right)^{k-1} / \log\left(\gamma_5^0 Q_{t-k}^*\right)\right|.
\end{aligned}$$

In the proof of Lemma 9, we show the first three terms are $O\left(\tau_n\right)$. Here we focus on the last term.

$$\begin{aligned}
& \left|\gamma_4 \sum_{k=1}^{t-1} \gamma_1^{k-1} / \log\left(\gamma_5 Q_{t-k}^*\right) - \gamma_4^0 \sum_{k=1}^{t-1} \left(\gamma_1^0\right)^{k-1} / \log\left(\gamma_5^0 Q_{t-k}^*\right)\right| \\
& \leq \left|\gamma_4 - \gamma_4^0\right| \sum_{k=1}^{t-1} \gamma_1^{k-1} / \log\left(\gamma_5 Q_{t-k}^*\right) + \gamma_4^0 \sum_{k=1}^{t-1} \left|\gamma_1^{k-1} - \left(\gamma_1^0\right)^{k-1}\right| / \log\left(\gamma_3 Q_{t-k}^*\right) \\
& + \gamma_4^0 \sum_{k=1}^{t-1} \left(\gamma_1^0\right)^{k-1} \left|1/\log\left(\gamma_5 Q_{t-k}^*\right) - 1/\log\left(\gamma_5^0 Q_{t-k}^*\right)\right|.
\end{aligned}$$

Since $1/\log\left(\gamma_5 Q_{t-k}^*\right)$ is bounded, the first two terms of right part are $O\left(\tau_n\right)$ for any $1 \leq t \leq n$. Similar to the proof of Lemma 9, we can show the third term is also $O\left(\tau_n\right)$ by Mean Value Theorem.

Lemma 26 *Denote* $\Psi = (\beta_0, \beta_1, \beta_2, \beta_3)$ *and* $\Psi_0 = (\beta_0^0, \beta_1^0, \beta_2^0, \beta_3^0)$, *if* $\|\Psi - \Psi_0\| < \tau_n$ *and* $\tau_n \searrow 0$, *under the conditions in Theorem 8, we have*

$$(a) \sup_{1 \leq t \leq n} \left|\sigma_t - \sigma_t^0\right| = O\left(\tau_n\right), \quad (b) \sup_{1 \leq t \leq n} \left|\frac{\partial \sigma_t}{\partial \Psi} - \frac{\partial \sigma_t^0}{\partial \Psi}\right| = O\left(\tau_n\right), (c) \sup_{1 \leq t \leq n} \left|\frac{\partial^2 \sigma_t}{\partial \Psi_i \partial \Psi_j} - \frac{\partial^2 \sigma_t^0}{\partial \Psi_i \partial \Psi_j}\right| = O\left(\tau_n\right)$$

uniformly over $\|\Psi - \Psi_0\| < \tau_n$.

Proof: the proof of Lemma 26 is the same as that of Lemma 25.

Lemma 27 *Suppose* $\tau_n \sim n^{-r}, r > 0$ *and* $\sup_{1\leq t\leq n} |\alpha_t - \alpha_t'| = O(\tau_n)$ *where* $\{\alpha_t\}$ *and* $\{\alpha_t'\}$ *represent two different series of tail index. Under the conditions in Theorem 8, we have*

$$\frac{1}{n}\sum_{t=1}^{n}\left|(Q_t-\mu_n)^{-\alpha_t}-(Q_t-\mu_n)^{-\alpha_t'}\right| = O_p(\tau_n)$$

uniformly over $|\mu_n - \mu_0| < \tau_n$. *The same result holds for*

$$\frac{1}{n}\sum_{t=1}^{n}\left|(Q_t-\mu_n)^{-\alpha_t}-(Q_t-\mu_n)^{-\alpha_t'}\right|\left[\log(Q_t-\mu_n)\right]^k, k=1,2.$$

Proof: the proof of Lemma 27 is the same as that of Lemma 11.

In Lemma 28, we prove the uniform convergence result of the second order derivatives of $L_n(\theta)$ over a neighborhood of θ_0. Lemma 28 will be applied in the proof of Lemma 29 (a). Additionally we denote $m_{\theta_1\theta_j}(\theta_0) = -E_{\theta_0}\left(\frac{\partial^2}{\partial\theta_i\partial\theta_j} l_1(\theta_0)\right)$.

Lemma 28 *Under the conditions in Theorem 8, for all second order derivatives of* $L_n(\theta_n)$, *we have* $\frac{\partial^2}{\partial\theta_i\partial\theta_j} L_n(\theta_n) \xrightarrow{p} -m_{\theta_i\theta_j}(\theta_0)$,*uniformly over* $\|\theta_n - \theta_0\| < \tau_n$, *where* $\tau_n \sim n^{-r}, r > 0$.

Proof: the proof of Lemma 28 is the same as that of Lemma 11 in Zhao at el.(2018).

Lemma 29 *Under the conditions in Theorem 8, there exists a positive constant* C *such that for all* $\theta \in \Theta$ *and* $t \geq 1$,

$$(a)\,|\alpha_t - \tilde{\alpha}_t| \leq C\cdot C_b^{t-1}, \quad (b)\left|\frac{\partial\alpha_t}{\partial\Phi} - \frac{\partial\tilde{\alpha}_t}{\partial\Phi}\right| \leq C\cdot tC_b^{t-1}, \quad (c)\left|\frac{\partial^2\alpha_t}{\partial\Phi_i\partial\Phi_j} - \frac{\partial^2\tilde{\alpha}_t}{\partial\Phi_i\partial\Phi_j}\right| \leq C\cdot t^2C_b^{t-1}$$
$$(d)\,|\sigma_t - \tilde{\sigma}_t| \leq C\cdot C_b^{t-1}, \quad (e)\left|\frac{\partial\sigma_t}{\partial\Phi} - \frac{\partial\tilde{\sigma}_t}{\partial\Phi}\right| \leq C\cdot tC_b^{t-1}, \quad (f)\left|\frac{\partial^2\sigma_t}{\partial\Phi_i\partial\Phi_j} - \frac{\partial^2\tilde{\sigma}_t}{\partial\Phi_i\partial\Phi_j}\right| \leq C\cdot t^2C_b^{t-1}.$$

Proof: the proof is trivial so we skip it.

Lemma 30 *Under the conditions in Theorem 8, we have* $\frac{1}{n}\sum_{t=1}^{n}\left|(Q_t-\mu_n)^{-\alpha_t}-(Q_t-\mu_n)^{-\tilde{\alpha}_t}\right| \xrightarrow{p}$

0, *uniformly over* $|\mu_n - \mu_0| < \tau_n$, *where* $\tau_n \sim n^{-r}, r > 0$. *The same result holds for*

$$\frac{1}{n}\sum_{t=1}^{n}\left|(Q_t-\mu_n)^{-\alpha_t}-(Q_t-\mu_n)^{-\tilde{\alpha}_t}\right|\left[\log\left(Q_t-\mu_n\right)\right]^k, \quad k=1,2.$$

Proof: the proof of Lemma 30 is the same as that of Lemma 14.

Lemma 31 provides the main uniform convergence result which can be used in the proof of Theorems 8 and 9.

Lemma 31 *Under the conditions in Theorem 8, (a) for all second order derivatives of* $\tilde{L}_n(\theta)$, *we have* $\frac{\partial^2}{\partial\theta_i\partial\theta_j}\tilde{L}_n(\theta) \to_p -m_{\theta_i\theta_j}(\theta_0)$, *uniformly over* $\|\theta-\theta_0\| < \tau_n$, *where* $\tau_n \sim n^{-r}, r > 0$ *(b) for the score function of* $\tilde{L}_n(\theta)$, *we have* $(\tau_n^*)^{-1}\left(\frac{\partial}{\partial\theta}\tilde{L}_n(\theta_0) - \frac{\partial}{\partial\theta}L_n(\theta_0)\right) \xrightarrow{p} 0$ *if* $\tau_n^* n \to \infty, e.g. \tau_n^* = 1/\sqrt{n}$.

Proof: the proof of Lemma 31 is the same as that of Lemma 15.

Lemma 32 *Under the conditions in Theorem 8,*

$$\frac{1}{\sqrt{n}}\sum_{i=1}^{n}\frac{\partial l_t(\theta_0)}{\partial\theta} \Rightarrow N\left(0, M_0^{-1}\right)$$

where M *is the Fisher Information matrix at* θ_0.

Proof: the proof of Lemma 32 is the same as that of Lemma 16.

Proof of Theorem 8: The proof of Theorem 8 is similar to that of Theorem 2. We will also apply Taylor Expansion here. Suppose $\{\tau_n\}$ is a sequence such that $\tau_n \sim n^{-r}$ and $n^{1/2}\tau_n \to \infty$ i.e. $0 < r < 1/2$. Let $t \in \mathbb{R}, y \in \mathbb{R}^{12}$ and $f_n(t,y) = \tau_n^{-2}\tilde{L}_n\left(\mu_0+\tau_n t, \phi^0+\tau_n y\right)$, where we use ϕ^0 to denote $(\beta_0^0, \beta_1^0, \beta_2^0, \beta_3^0, \gamma_0^0, \gamma_1^0, \gamma_2^0, \gamma_3^0, \gamma_4^0, \gamma_5^0)$. Then by the fact that $|\mu^* - \mu_0| < \tau_n t$, $\|\phi^* - \phi^0\| < \tau_n\|y\|$, we have

$$\begin{aligned}\frac{\partial}{\partial t}f_n(t,y) &= \tau_n^{-1}\frac{\partial \tilde{L}_n\left(\mu_0+\tau_n t, \phi^0+\tau_n y\right)}{\partial \mu} \\ &= \tau_n^{-1}\left(\frac{\partial \tilde{L}_n\left(\mu_0,\phi^0\right)}{\partial \mu}-\frac{\partial L_n\left(\mu_0,\phi^0\right)}{\partial t}\right)+\tau_n^{-1}\left(\frac{\partial L_n\left(\mu_0,\phi^0\right)}{\partial \mu}\right)+\frac{\partial^2 \tilde{L}_n\left(\mu^*,\phi^*\right)}{\partial \mu^2}t \\ &+\sum_{i=1}^{12}\frac{\partial^2 \tilde{L}_n\left(\mu^*,\phi^*\right)}{\partial \mu \partial \phi_i}y_i,\end{aligned}$$

According to Lemma 31 (b) and Lemma 32, the first two terms go to 0. The third and forth terms converge uniformly over $t^2+\|y\|^2 \leq 1$ by Lemma 29 (a). Now we have $\frac{\partial}{\partial t}f_n(t,y) = -m_{\mu\mu}\left(\theta_0\right)t - \sum_{i=1}^{12} m_{\mu\phi_i}\left(\theta_0\right)y_i + o_p(1)$. Moreover, $\frac{\partial}{\partial y_k}f_n(t,y) = -m_{\phi_k\mu}\left(\theta_0\right)t - \sum_{i=1}^{12} m_{\phi_k\phi_i}\left(\theta_0\right)y_i + o_p(1)$, for $k = 1,\ldots,12$, where $o_p(1)'$ s are uniformly decaying over $t^2+\|y\|^2 \leq 1$. Consider $t^2+\|y\|^2 = 1$, we have

$$t\frac{\partial f_n}{\partial t}(t,y)+\sum_i y_i\frac{\partial f_n}{\partial y_i}(t,y) = -t^2 m_{\mu\mu}\left(\theta_0\right)-2t\sum_{i=1}^{12} y_i m_{\mu\phi_i}\left(\theta_0\right)-\sum_{i=1}^{12}\sum_{j=1}^{12} y_i y_j m_{\phi_i\phi_j}\left(\theta_0\right)+o_p(1) < 0,$$

based on the fact that the Fisher Information matrix M_0 is positive definite. Based on Lemma 5 in Smith (1985), we have that f_n has a local maximum over the open set $t^2+\|y\|^2 < 1$ with probability going to 1. Therefore there exists a sequence of local maximizer $\hat{\theta}_n$ of $\tilde{L}_n(\theta)$ such that $\hat{\theta}_n \to_p \theta_0$ and $\left\|\hat{\theta}_n-\theta_0\right\| \leq \tau_n$, where $\tau_n \sim n^{-r}, 0 < r < 1/2$.

Proof of Theorem 9: The proof of Theorem 9 is the same as that of Theorem 3 by applying Lemmas 31 and 32.

Proof of Proposition 3: The proof of Proposition 3 is the same as that of Proposition 1 by applying Lemmas 21, 24, 30, 32, and Theorem 8.

6.3 First and second order partial derivative of $l_t(\theta)$

In this section, we provide the formula for $\frac{\partial l_t(\theta)}{\partial \theta}$ and $\frac{\partial^2 l_t(\theta)}{\partial \theta \partial \theta^T}$, which are calculated in Zhao et al.(2018). We denote Φ as $(\gamma_0, \gamma_1, \gamma_2, \gamma_3)$ (or $(\gamma_0, \gamma_1, \gamma_2, \gamma_3, \gamma_4, \gamma_5)$ for spatial AcFl model). In other words, Φ is used to be a generic symbol for $(\gamma_0, \gamma_1, \gamma_2, \gamma_3)$ (or $(\gamma_0, \gamma_1, \gamma_2, \gamma_3, \gamma_4, \gamma_5)$ for spatial AcFl model). Similarly, we set $\Psi = (\beta_0, \beta_1, \beta_2, \beta_3)$ (or $(\beta_0, \beta_1, \beta_2, \beta_3, \beta_4, \beta_5)$ for spatial AcFL model). As a reminder, the likelihood function is

$$1_t(\theta) = \log \alpha_t + \alpha_t \log \sigma_t - (\alpha_t + 1) \log (Q_t - \mu) - \left(\frac{Q_t - \mu}{\sigma_t} \right)^{-\alpha_t}$$

. For the first order partial derivative, we have

$$\begin{aligned}
\frac{\partial l_t(\theta)}{\partial \mu} &= \frac{\alpha_t + 1}{Q_t - \mu} - \frac{\alpha_t}{\sigma_t} \left(\frac{Q_t - \mu}{\sigma_t} \right)^{-(\alpha_t + 1)}, \\
\frac{\partial l_t(\theta)}{\partial \Phi} &= \left[\frac{1}{\alpha_t} - \log \left(\frac{Q_t - \mu}{\sigma_t} \right) + \left(\frac{Q_t - \mu}{\sigma_t} \right)^{-\alpha_t} \log \left(\frac{Q_t - \mu}{\sigma_t} \right) \right] \frac{\partial \alpha_t}{\partial \Phi}, \\
\frac{\partial l_t(\theta)}{\partial \Psi} &= \left[\frac{\alpha_t}{\sigma_t} - \frac{\alpha_t}{\sigma_t} \left(\frac{Q_t - \mu}{\sigma_t} \right)^{-\alpha_t} \right] \frac{\partial \sigma_t}{\partial \Psi}.
\end{aligned}$$

For the second order partial derivative, we have

$$\frac{\partial^2 l_t(\theta)}{\partial \mu^2} = (\alpha_t + 1)(Q_t - \mu)^{-2} - \alpha_t(\alpha_t + 1)\sigma_t^{\alpha_t}(Q_t - \mu)^{-(\alpha_t+2)},$$

$$\frac{\partial^2 l_t(\theta)}{\partial \mu \partial \Phi} = \left[\frac{1}{Q_t - \mu} - \sigma_t^{\alpha_t}(Q_t - \mu)^{-(\alpha_t+1)} + \alpha_t \sigma_t^{\alpha_t}(Q_t - \mu)^{-(\alpha_t+1)} \log\left(\frac{Q_t - \mu}{\sigma_t}\right)\right] \frac{\partial \alpha_t}{\partial \Psi},$$

$$\frac{\partial^2 l_t(\theta)}{\partial \mu \partial \Psi} = -\frac{\alpha_t^2}{\sigma_t^2}\left(\frac{Q_t - \mu}{\sigma_t}\right)^{-(\alpha_t+1)} \frac{\partial \sigma_t}{\partial \Psi},$$

$$\frac{\partial^2 l_t(\theta)}{\partial \Phi \partial \Psi} = \left[\frac{1}{\sigma_t} - \frac{1}{\sigma_t}\left(\frac{Q_t - \mu}{\sigma_t}\right)^{-\alpha_t} + \frac{\alpha_t}{\sigma_t}\left(\frac{Q_t - \mu}{\sigma_t}\right)^{-\alpha_t} \log\left(\frac{Q_t - \mu}{\sigma_t}\right)\right] \frac{\partial \sigma_t}{\partial \Psi}\frac{\partial \alpha_t}{\partial \Phi},$$

$$\frac{\partial^2 l_t(\theta)}{\partial \Psi_i \partial \Psi_j} = \left[\frac{\alpha_t}{\sigma_t} - \frac{\alpha_t}{\sigma_t}\left(\frac{Q_t - \mu}{\sigma_t}\right)^{-\alpha_t}\right] \frac{\partial^2 \sigma_t}{\partial \Psi_i \partial \Psi_j} + \left[-\frac{\alpha_t}{\sigma_t^2} - \frac{\alpha_t(\alpha_t - 1)}{\sigma_t^2}\left(\frac{Q_t - \mu}{\sigma_t}\right)^{-\alpha_t}\right] \frac{\partial \sigma_t}{\partial \Psi_i}\frac{\partial \sigma_t}{\partial \Psi_j},$$

$$\frac{\partial^2 l_t(\theta)}{\partial \Phi_i \partial \Phi_j} = \left[\frac{1}{\alpha_t} - \log\left(\frac{Q_t - \mu}{\sigma_t}\right) + \left(\frac{Q_t - \mu}{\sigma_t}\right)^{-\alpha_t} \log\left(\frac{Q_t - \mu}{\sigma_t}\right)\right] \frac{\partial^2 \alpha_t}{\partial \Phi_i \partial \Phi_j},$$

$$+ \left[-\frac{1}{\alpha_t^2} + \left(\frac{Q_t - \mu}{\sigma_t}\right)^{-\alpha_t}\left[\log\left(\frac{Q_t - \mu}{\sigma_t}\right)\right]^2\right] \frac{\partial \alpha_t}{\partial \Phi_i}\frac{\partial \alpha_t}{\partial \Phi_j}.$$

Chapter 7

Appendix B

In Appendix B, we include the graph of max values in all 120 subareas. We also show the parameter results, tail index (α) and scale parameter (σ) plots for all sub-areas. X label indicates the index of each parts.

7.1 AcFL model

Part	γ_0	γ_1	γ_2	γ_3	β_0	β_1	β_2	β_3	μ
1	-2.717	0	22.495	5.519	5.961	0	3.314	0.047	94.065
2	-3.097	0	31.786	47.784	10.499	0	58.55	49.072	101.875
3	-3.376	0.083	34.195	59.401	7.489	0	16.186	1.02	60.402
4	-1.809	0.408	18.518	113.047	11.176	0	65.226	52.167	78.367
5	-3.049	0	30.144	50.778	5.364	0	2.918	0.056	79.326
6	-2.742	0.027	27.609	54.829	9.636	0	49.673	51.681	71.149
7	-3.016	0.216	33.075	105.811	9.181	0	45.22	89.255	36.466
8	-2.167	0.282	19.977	62.989	5.662	0	6.9	0.219	45.712
9	-2.496	0.173	26.875	116.724	8.168	0	40.786	105.447	24.82
10	-0.4	0.845	1.234	0.256	9.893	0	53.443	44.009	22.337
11	-0.735	0	1.873	0.02	12.658	0	87.359	146.7	113.278
12	-2.868	0.198	27.896	35.571	7.749	0	14.547	0.29	119.747
13	-2.957	0.025	31.748	51.451	5.964	0	3.319	0.062	59.792
14	-1.574	0.295	13.162	12.933	11.008	0	64.304	67.31	78.113
15	-3.72	0.447	39.37	135.525	12.179	0	74.858	54.377	92.267
16	-2.895	0.056	30.209	69.339	6.175	0	4.674	0.057	89.017
17	-3.192	0	37.661	219.958	5.349	0	1.812	0.037	55.26
18	-1.841	0.188	14.09	3.87	6.76	0	14.151	2.107	23.967
19	-2.185	0.096	21.268	59.012	5.998	0	9.409	0.459	32.778
20	-3.957	0	42.219	140.52	4.819	0	5.077	0.527	16.899
21	-3.332	0	33.207	52.897	10.486	0	59.221	49.321	100.618
22	-1.231	0.735	13.254	115.879	11.418	0	67.907	53.482	115.61
23	-3.964	0.059	50.971	332.053	9.27	0	28.571	2.236	75.318
24	-2.085	0.201	17.795	16.267	5.675	0	3.213	0.053	88.082
25	-2.418	0.492	24.227	68.809	8.855	0	27.515	1.698	94.429
26	-3.404	0.006	35.222	56.198	10.286	0	54.033	38.264	94.893
27	-1.906	0.12	14.328	5.38	5.68	0	4.01	0.077	62.592
28	-2.222	0.21	21.206	64.823	7.14	0	17.261	1.589	44.249
29	-1.918	0.256	22.219	47.995	7.182	0	23.046	49.106	-5.000
30	-0.73	0.058	2.534	0.142	8.404	0	44.609	69.603	22.607
31	-1.461	0.304	7.527	0.461	11.406	0	72.261	126.773	82.29
32	-2.294	0.409	23.23	92.039	9.253	0	33.328	2.945	98.609
33	-0.451	0.084	2.016	0.022	10.781	0	51.947	38.623	41.73
34	-0.764	0.122	4.103	0.09	10.554	0	46.724	22.21	35.694
35	-1.989	0	20.506	41.421	9.37	0	49.521	76.023	107.093

Part	γ_0	γ_1	γ_2	γ_3	β_0	β_1	β_2	β_3	μ
36	-1.472	0.583	12.771	5.045	9.912	0	47.621	58.214	64.096
37	-2.963	0	27.077	39.714	6.264	0	6.728	0.118	73.14
38	-0.567	0.237	1.477	0.047	9.537	0	48.221	43.822	49.65
39	-2.344	0.12	28.902	159.161	8.539	0	40.241	132.494	11.59
40	-2.489	0.559	26.052	205.028	10.932	0	69.858	145.151	27.765
41	-2.738	0	27.901	39.326	5.723	0	4.68	0.13	84.745
42	-3.003	0.38	31.435	192.633	6.661	0	8.506	0.095	113.665
43	-1.95	0.139	21.006	65.968	6.937	0	11.208	0.315	102.743
44	-1.296	0.209	6.57	0.089	11.021	0	59.495	94.416	68.211
45	-1.694	0.144	11.989	0.532	12.286	0	70.687	77.882	55.756
46	-3.785	0.033	43.375	83.103	9.581	0	46.309	54.299	76.431
47	-1.928	0.27	18.838	56.398	10.625	0	58.64	40.296	89.669
48	-3.034	0.139	30.43	54.795	9.695	0	50.314	52.823	68.154
49	-2.946	0.151	31.125	159.752	5.571	0	4.222	0.099	42.105
50	-1.745	0.089	14.835	9.155	6.077	0	8.728	0.443	26.912
51	-2.487	0.128	22.544	23.569	5.557	0	1.993	0.026	87.639
52	-2.332	0.333	23.048	49.075	10.797	0	59.383	45.078	95.778
53	-3.468	0.455	36.518	110.623	11.833	0	72.168	51.958	119.343
54	-2.9	0	21.676	1.855	9.668	0	52.463	128.435	104.418
55	-2.043	0.129	21.355	39.148	7.858	0	16.787	0.625	95.558
56	-2.606	0.015	29.096	47.814	9.301	0	42.784	46.292	85.137
57	-1.877	0.349	19.62	113.783	10.726	0	60.76	54.4	85.629
58	-2.078	0.344	21.914	47.269	8.887	0	37.335	46.068	39.879
59	-2.057	0.116	13.049	2.002	7.18	0	17.216	1.632	42.248
60	-2.379	0.197	19.17	22.55	5.644	0	7.751	0.371	36.421
61	-2.776	0.169	28.007	61.223	6.541	0	6.512	0.085	93.242
62	-3.304	0	35.168	87.606	6.689	0	8.27	0.095	131.144
63	-2.639	0	26.685	22.169	5.667	0	1.951	0.024	104.325
64	-0.486	0.112	1.566	0.032	10.463	0	56.317	49.228	96.65
65	-3.031	0	33.064	55.503	9.978	0	50.701	53.869	75.936
66	-3.773	0.27	42.816	108.92	10.412	0	53.694	52.558	78.766
67	-2.142	0.125	21.112	72.985	8.832	0	29.175	2.387	76.238
68	-2.069	0	17.951	38.99	6.899	0	17.061	1.76	62.8
69	-2.834	0.23	30.728	157.119	9.078	0	48.65	130.239	34.853
70	-2.485	0	26.2	56.574	5.826	0	4.133	0.102	39.632
71	-0.221	0	0.754	0.022	9.101	0	43.648	45.936	97.639
72	-1.233	0	5.965	0.134	10.191	0	48.678	21.991	109.35
73	-2.043	0.435	12.548	1.624	9.484	0	49.466	58.012	90.006
74	-2.303	0.394	22.224	44.954	10.247	0	53.566	39.931	70.626
75	-2.268	0	23.382	50.413	9.697	0	41.898	13.092	70.092

Part	γ_0	γ_1	γ_2	γ_3	β_0	β_1	β_2	β_3	μ
76	-3.535	0	36.053	37.312	6.863	0	8.455	0.209	62.616
77	-2.389	0.496	22.295	54.19	9.909	0	53.068	50.891	65.315
78	-1.198	0.358	5.99	0.716	9.907	0	49.62	26.006	57.083
79	-2.07	0.376	16.933	22.859	9.324	0	45.624	24.727	49.539
80	-2.848	0.311	28.793	48.787	9.348	0	43.823	47.584	32.815
81	-2.817	0.198	28.008	24.825	6.031	0	2.944	0.04	80.368
82	-3.015	0	33.513	79.104	6.974	0	8.996	0.152	101.239
83	-0.083	0.983	0.149	0.036	5.178	0	2.135	0.031	84.405
84	-2.528	0	24.209	52.583	9.997	0	54.752	60.591	61.251
85	-2.721	0.33	25.432	48.709	9.354	0	47.716	45.208	58.272
86	-1.695	0.333	15.361	71.573	8.429	0	23.864	1.028	72.582
87	-1.591	0.413	9.795	2.897	6.133	0	6.306	0.101	67.053
88	-0.571	0	1.209	0.053	12.344	0	88.586	195.809	60.116
89	-1.342	0.357	5.688	0.329	9.837	0	48.954	32.262	43.343
90	-1.22	0.387	5.991	0.725	9.671	0	55.626	103.989	43.042
91	-3.233	0.138	32.677	47.799	10.097	0	53.154	46.141	79.262
92	-4.399	0.059	56.941	331.73	7.193	0	9.778	0.281	56.812
93	-3.966	0.051	48.947	281.738	9.451	0	42.908	38.479	32.948
94	-2.281	0.235	22.673	78.966	6.191	0	7.523	0.197	51.611
95	-2.378	0.492	23.901	114.304	10.674	0	63.334	83.44	56.865
96	-2.813	0.698	33.97	1173.338	13.276	0	101.044	232.657	67.528
97	-0.609	0.076	0.81	0.04	10.254	0	64.178	99.811	65.098
98	-0.431	0.117	0.899	0.042	10.602	0	57.181	37.327	53.042
99	-2.138	0.322	18.866	43.508	9.597	0	50.288	40.026	47.227
100	-2.467	0.103	24.221	53.812	8.712	0	41.317	52.264	34.984
101	-0.462	0.527	0.974	0.035	9.362	0	45.472	46.579	64.778
102	-2.991	0.173	28.796	48.645	9.509	0	48.968	45.398	64.816
103	-3.105	0.337	31.394	115.656	10.471	0	62.787	84.768	51.633
104	-1.834	0.384	16.044	39.417	7.106	0	14.152	0.564	50.895
105	-0.391	0.369	0.814	0.043	5.729	0	4.935	0.115	52.668
106	-1.192	0.532	11.362	114.869	12.789	0	91.082	139.421	62.279
107	-2.604	0	21.668	18.893	6.641	0	11.607	0.4	53.392
108	-1.436	0.219	6.692	0.632	9.628	0	53.527	69.938	52.108
109	-1.662	0.458	11.52	5.852	10.271	0	59.322	74.45	45.135
110	-2.247	0.131	25.127	160.213	7.95	0	38.914	133.092	28.356
111	-2.057	0.3	18.961	21.856	7.698	0	15.371	0.706	40.879
112	-0.311	0.381	0.782	0.045	11.093	0	71.648	183.827	44.602
113	-1.074	0.38	9.635	12.264	11.031	0	67.783	138.752	38.689
114	-1.993	0.164	18.377	48.535	9.608	0	50.267	45.361	48.269
115	-1.774	0.196	19.932	29.344	6.956	0	11.443	1.565	-4.999

Part	γ_0	γ_1	γ_2	γ_3	β_0	β_1	β_2	β_3	μ
116	-2.136	0.412	26.264	183.566	8.901	0	39.779	130.999	-5.000
117	-2.267	0.203	21.455	53.859	9.693	0	50.479	50.834	47.425
118	-1.809	0.312	16.942	48.374	8.638	0	40.694	46.483	44.204
119	-0.231	0.358	0.62	0.048	9.374	0	41.424	17.174	43.784
120	-1.226	0.367	15.565	69.258	7.451	0	26.129	69.343	-5.000

Estimated tail index plots for 120 subareas

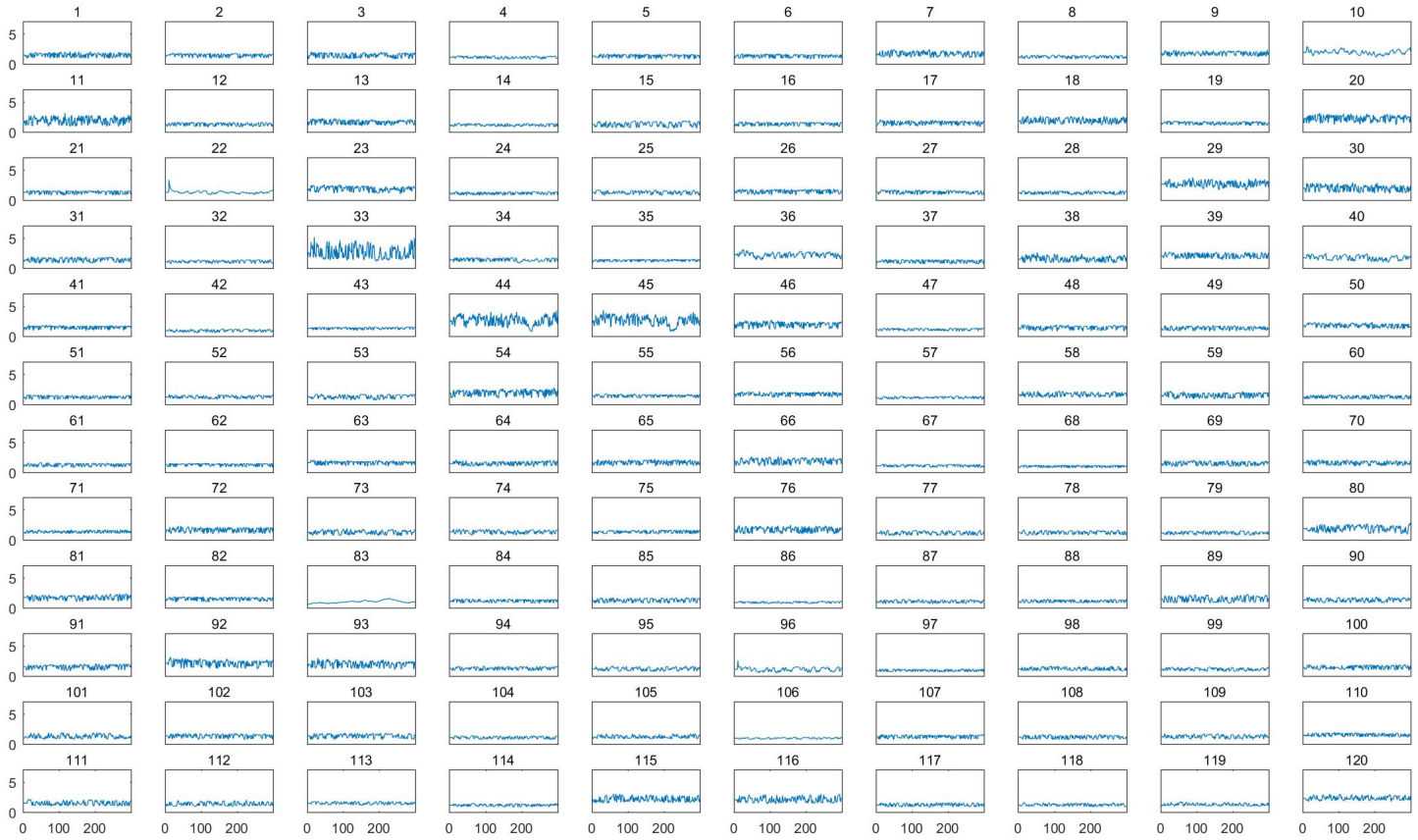

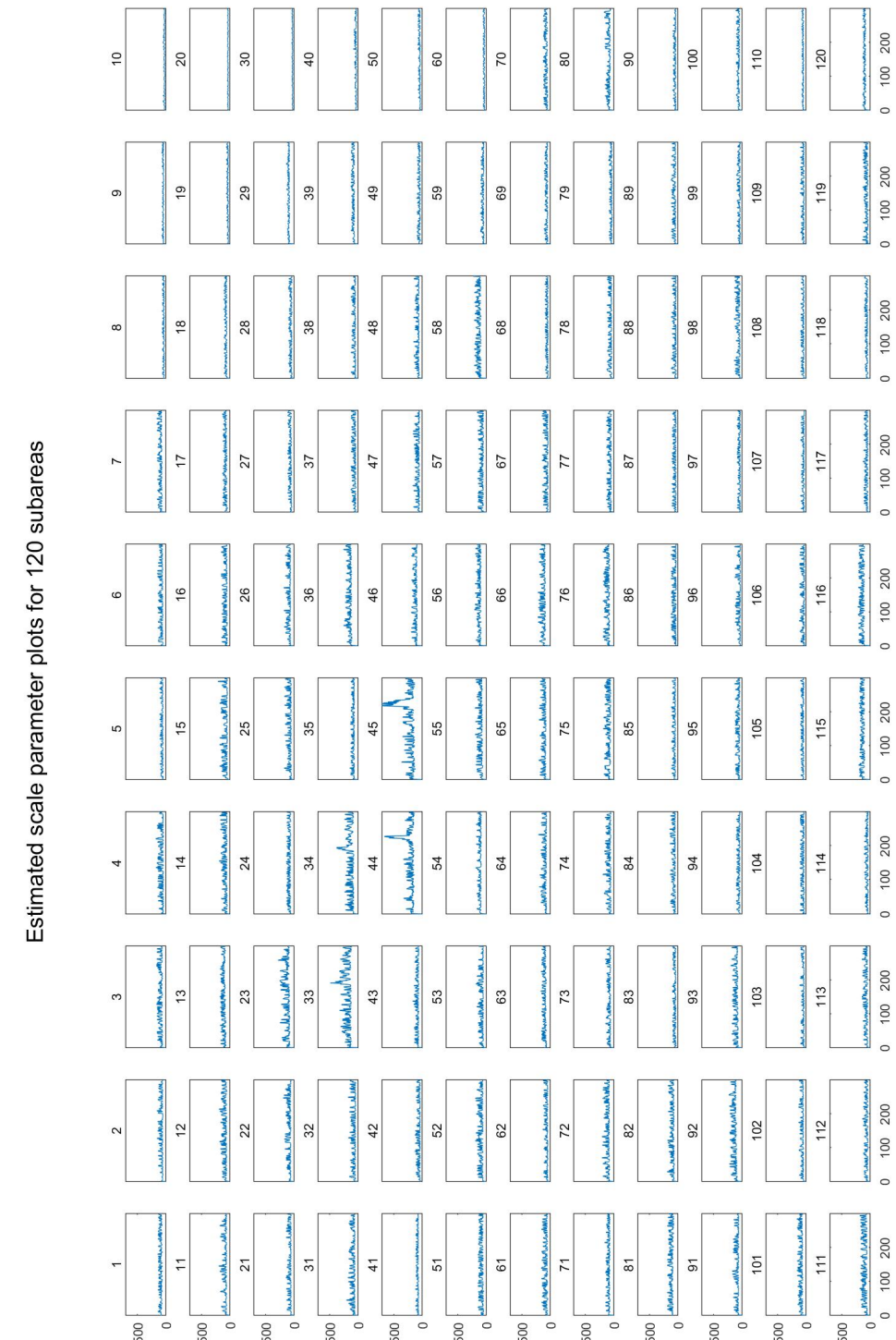
Estimated scale parameter plots for 120 subareas

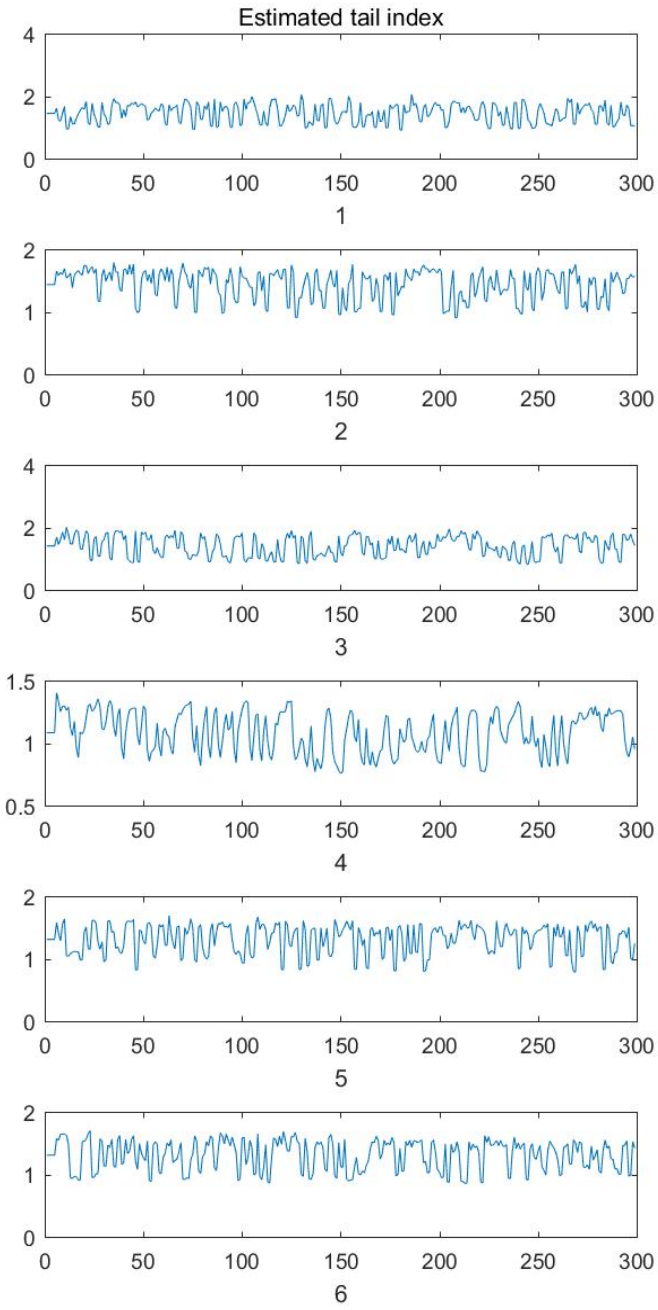
Estimated tail index
1
2
3
4
5
6

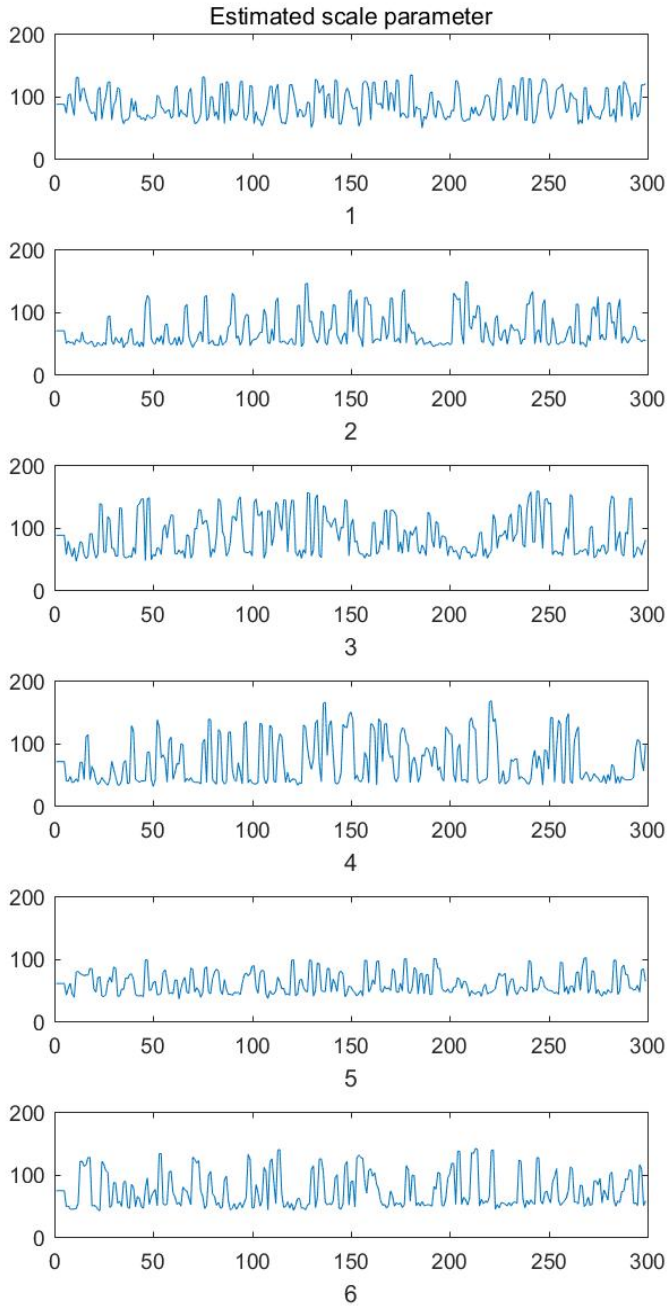
Estimated scale parameter
1
2
3
4
5
6

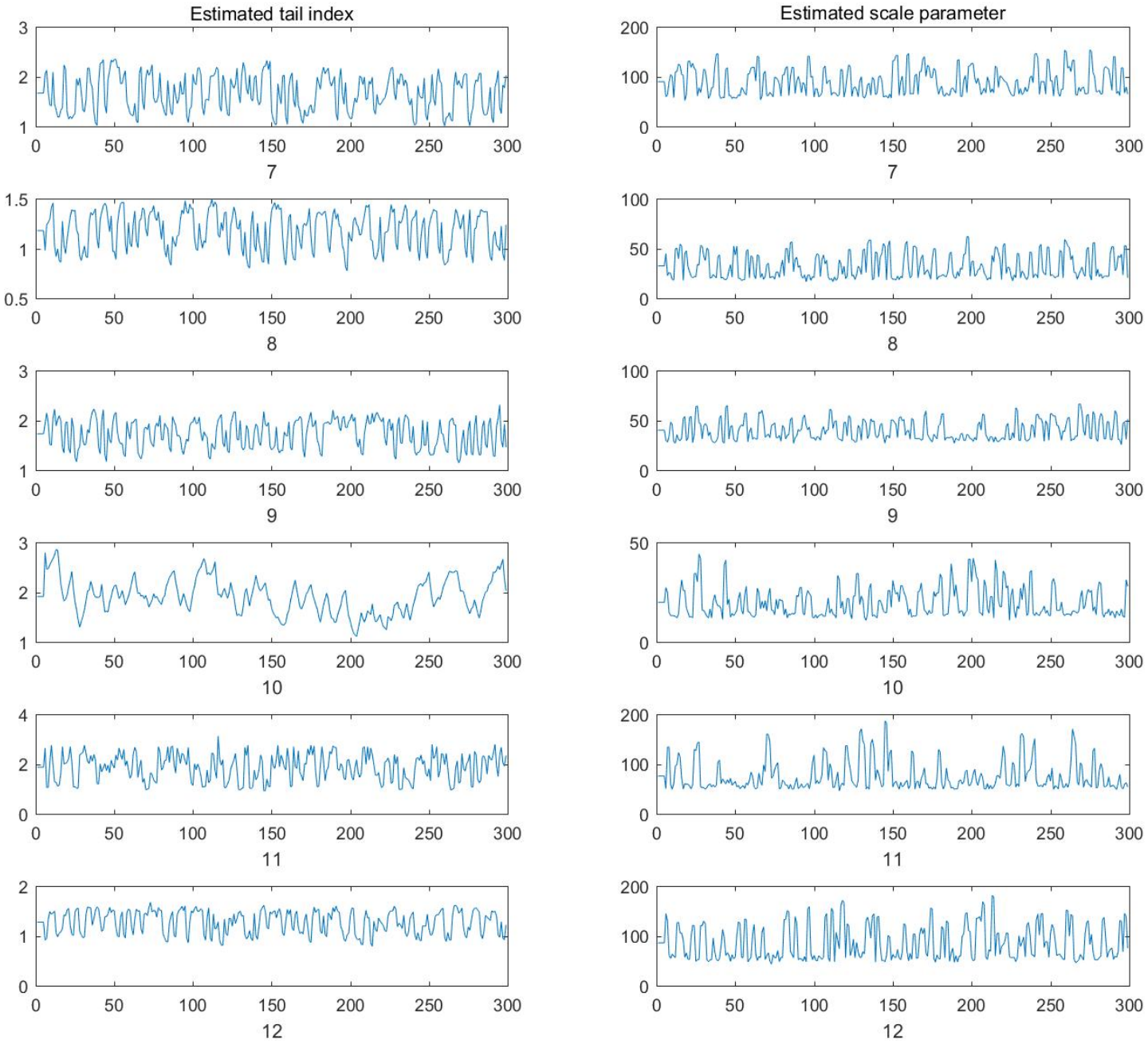
Estimated tail index
Estimated scale parameter
7
8
9
10
11
12

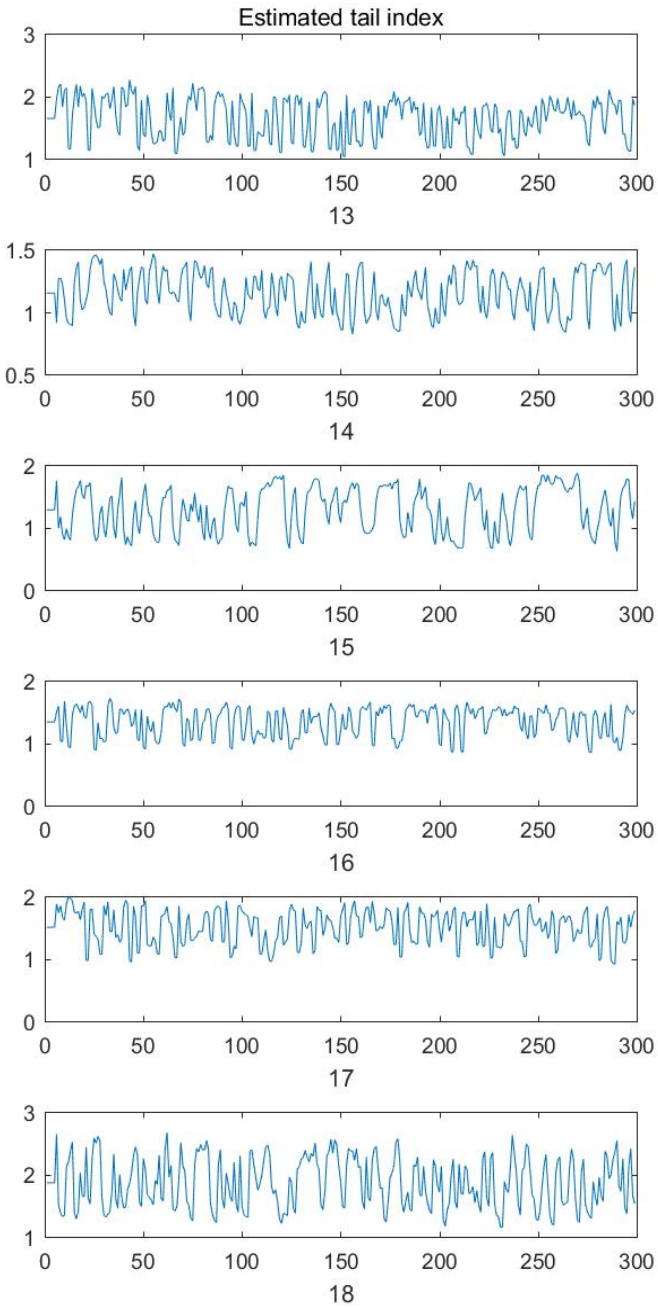
Estimated tail index
13
14
15
16
17
18

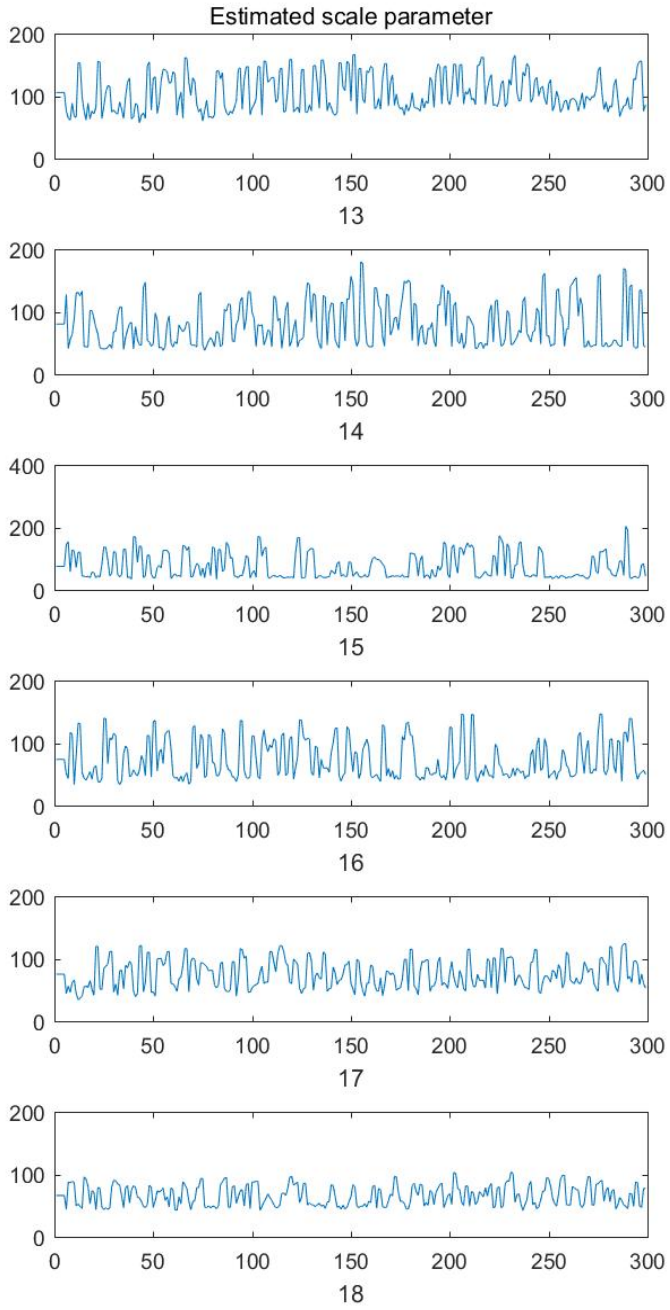
Estimated scale parameter
13
14
15
16
17
18

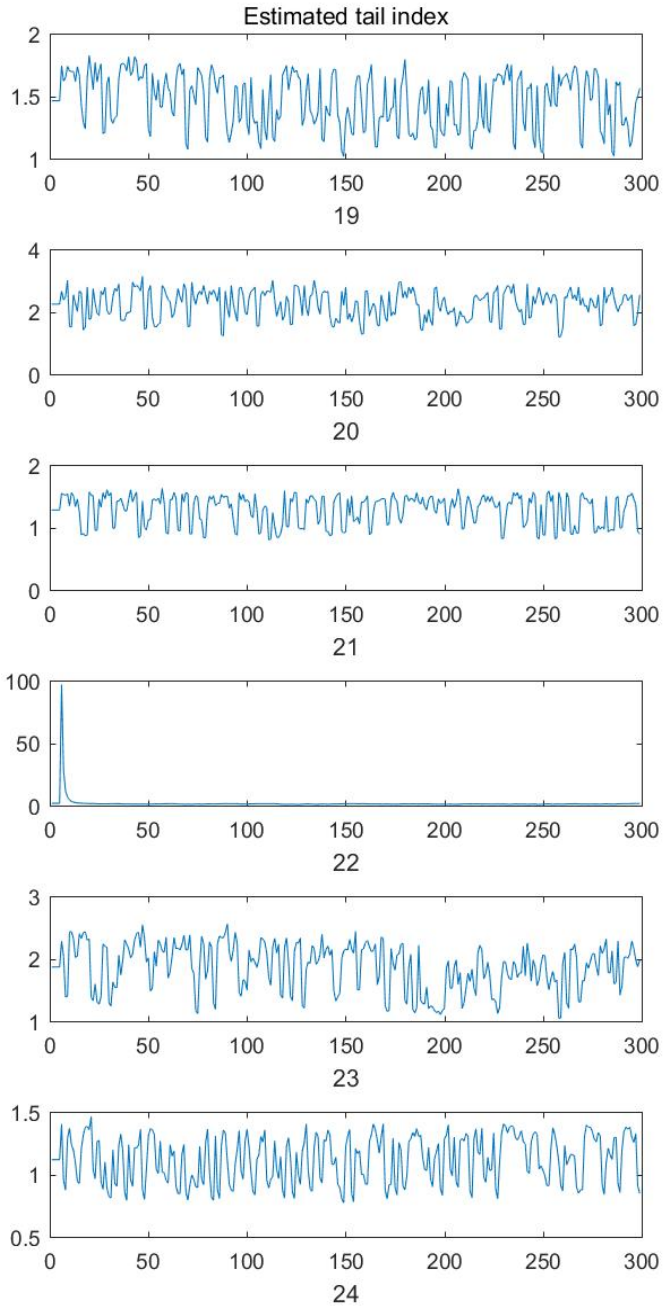
Estimated tail index
19
20
21
22
23
24

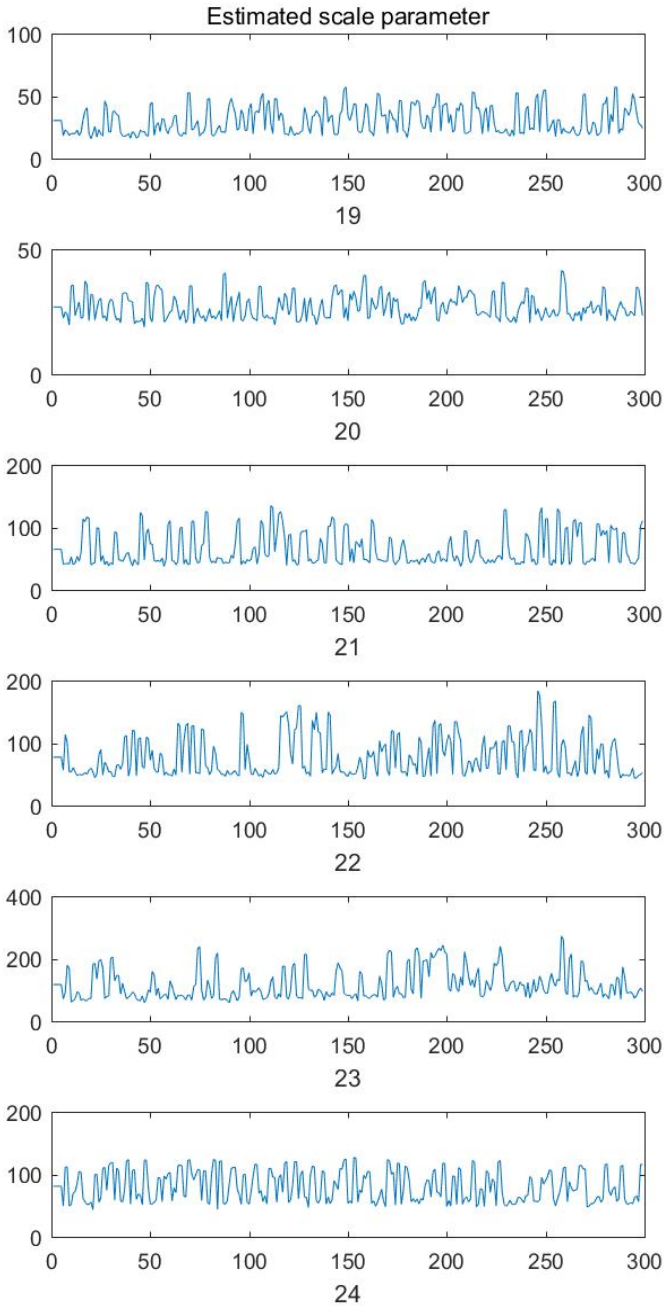
Estimated scale parameter
19
20
21
22
23
24

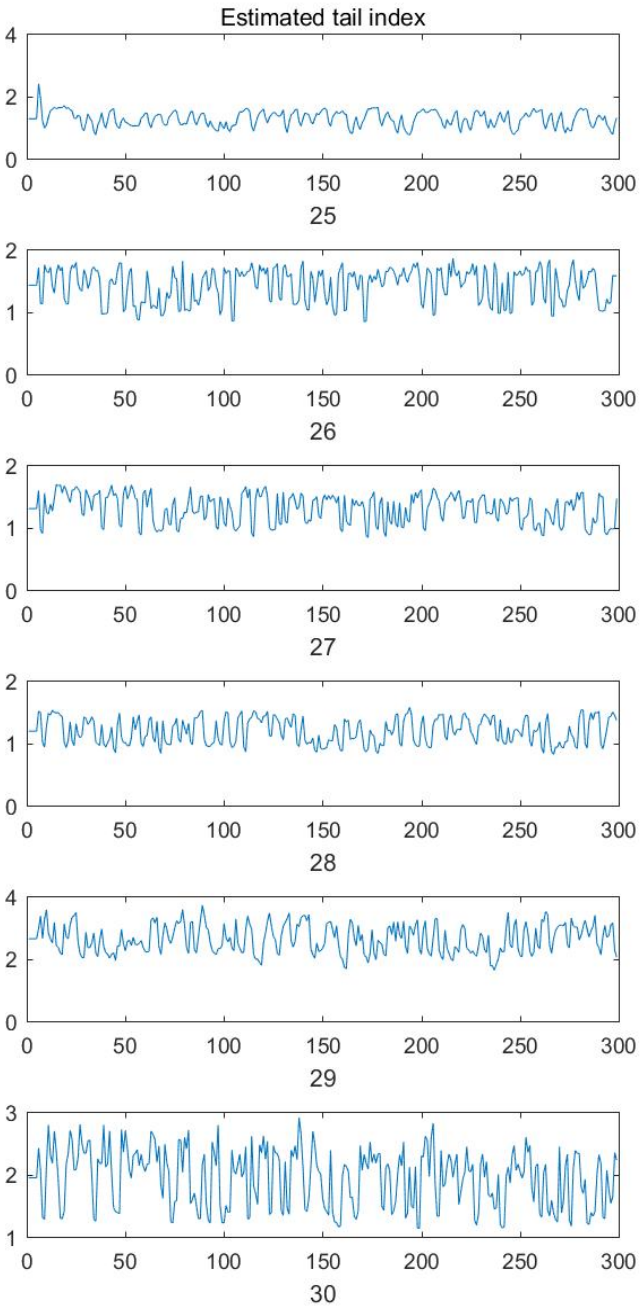
Estimated tail index
25
26
27
28
29
30

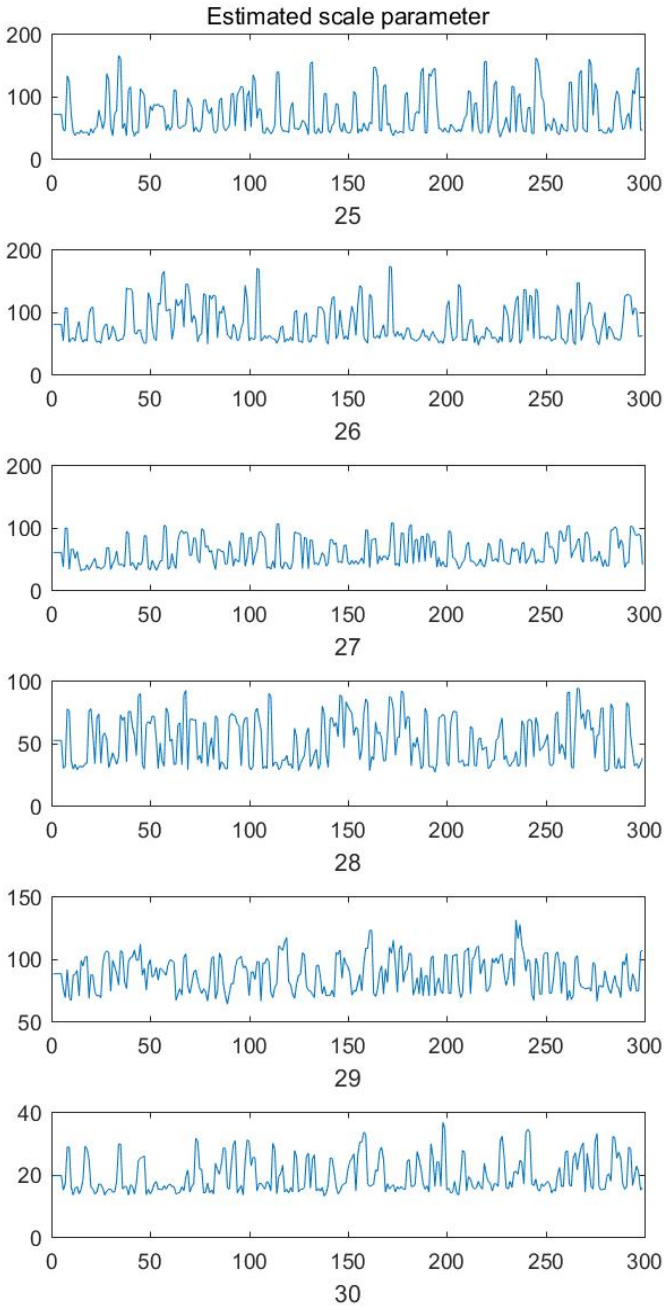
Estimated scale parameter
25
26
27
28
29
30

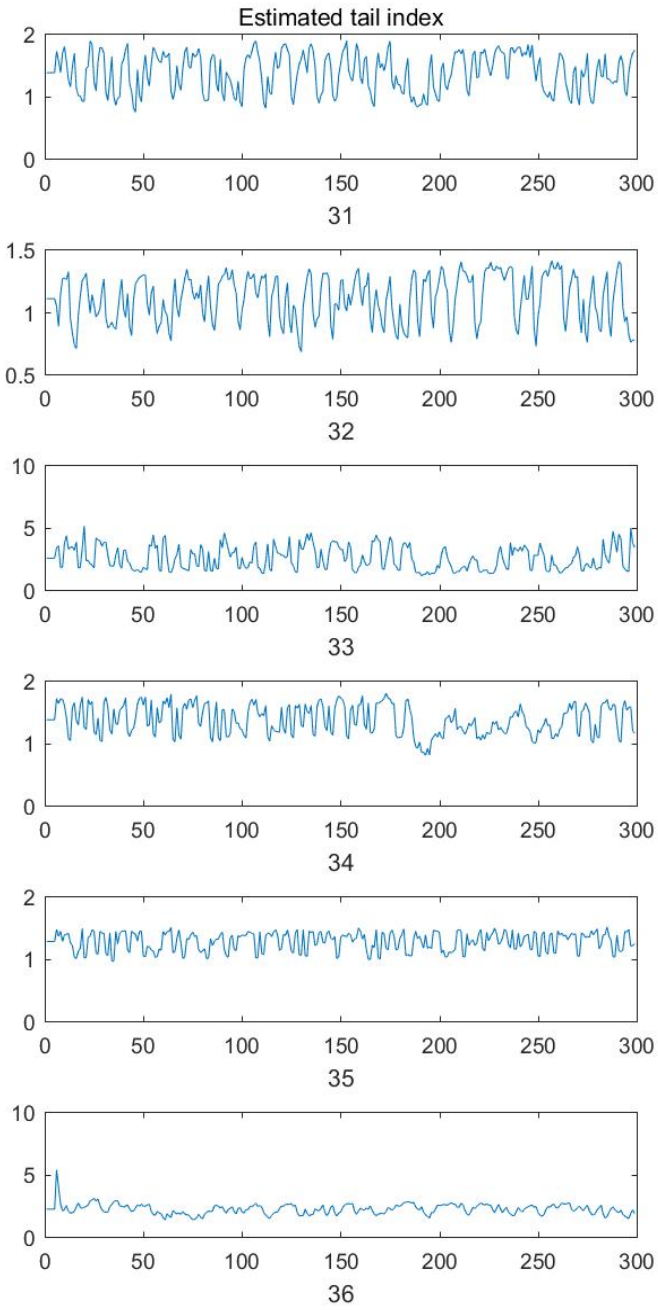
Estimated tail index
31
32
33
34
35
36

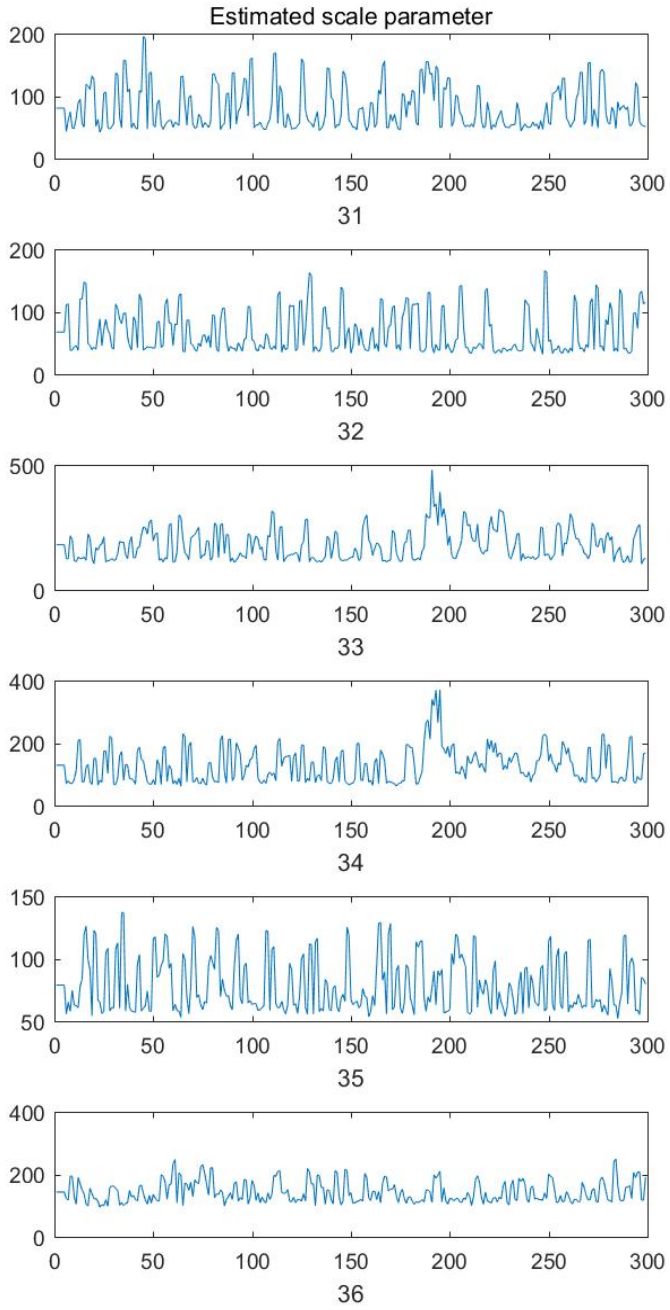
Estimated scale parameter
31
32
33
34
35
36

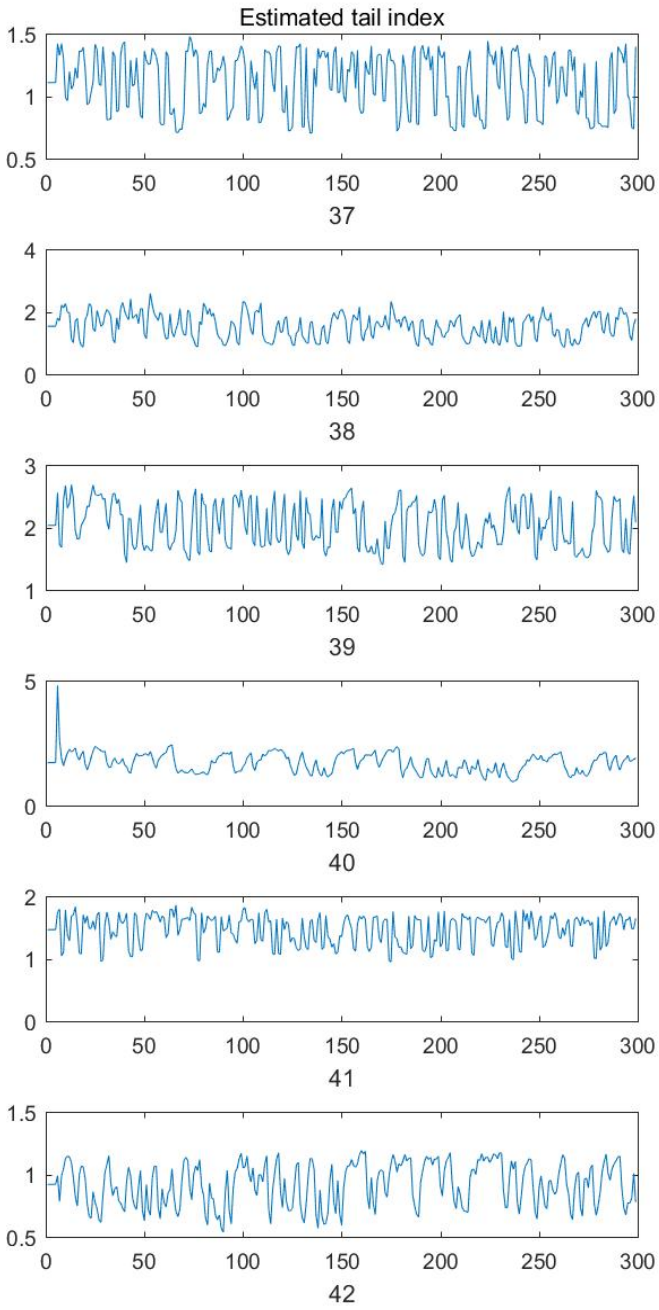
Estimated tail index
37
38
39
40
41
42

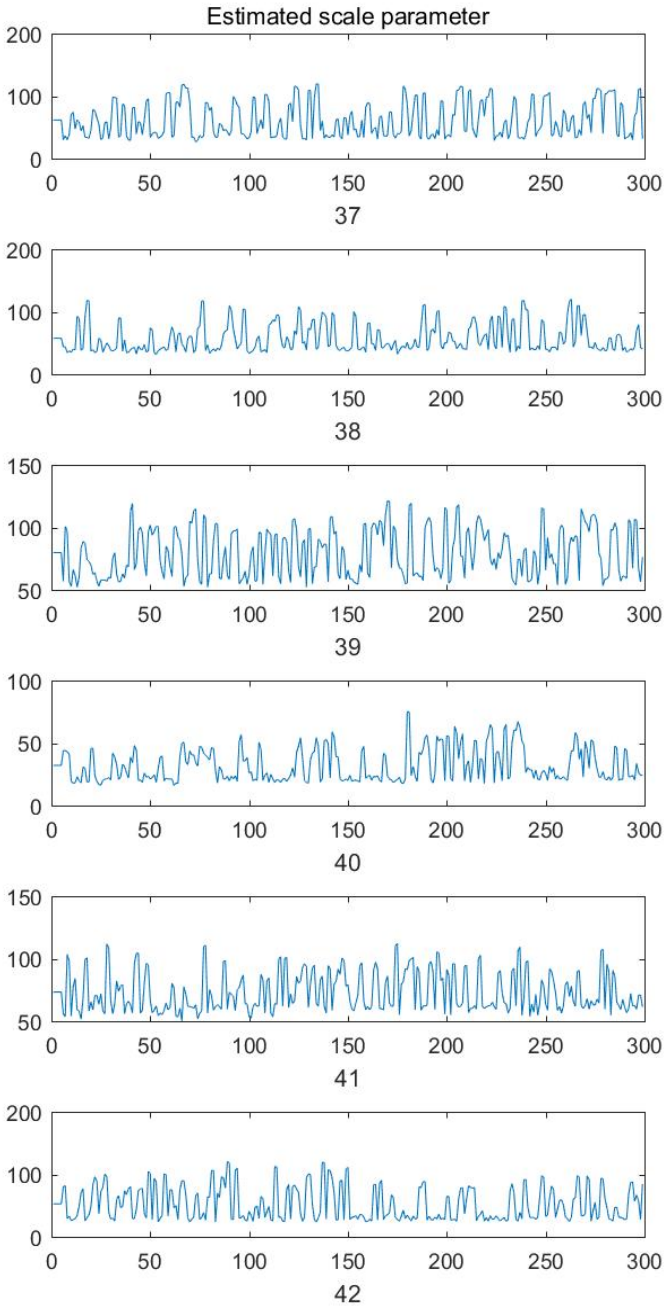
Estimated scale parameter
37
38
39
40
41
42

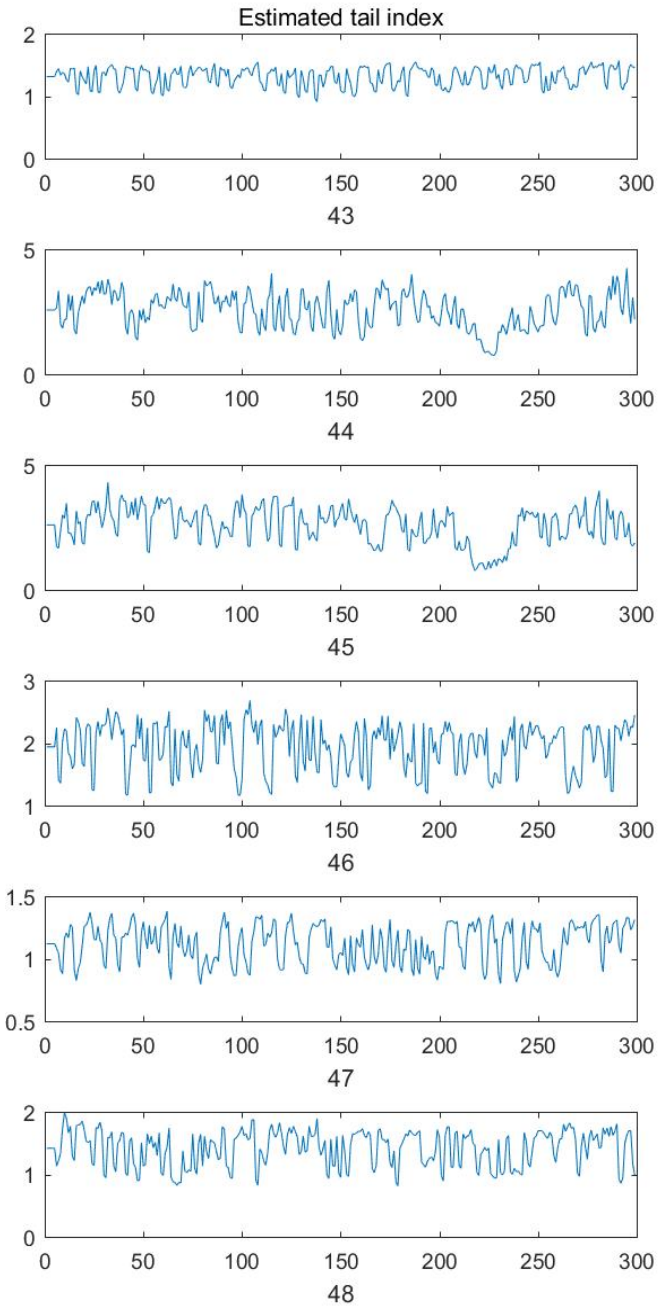
Estimated tail index
43
44
45
46
47
48

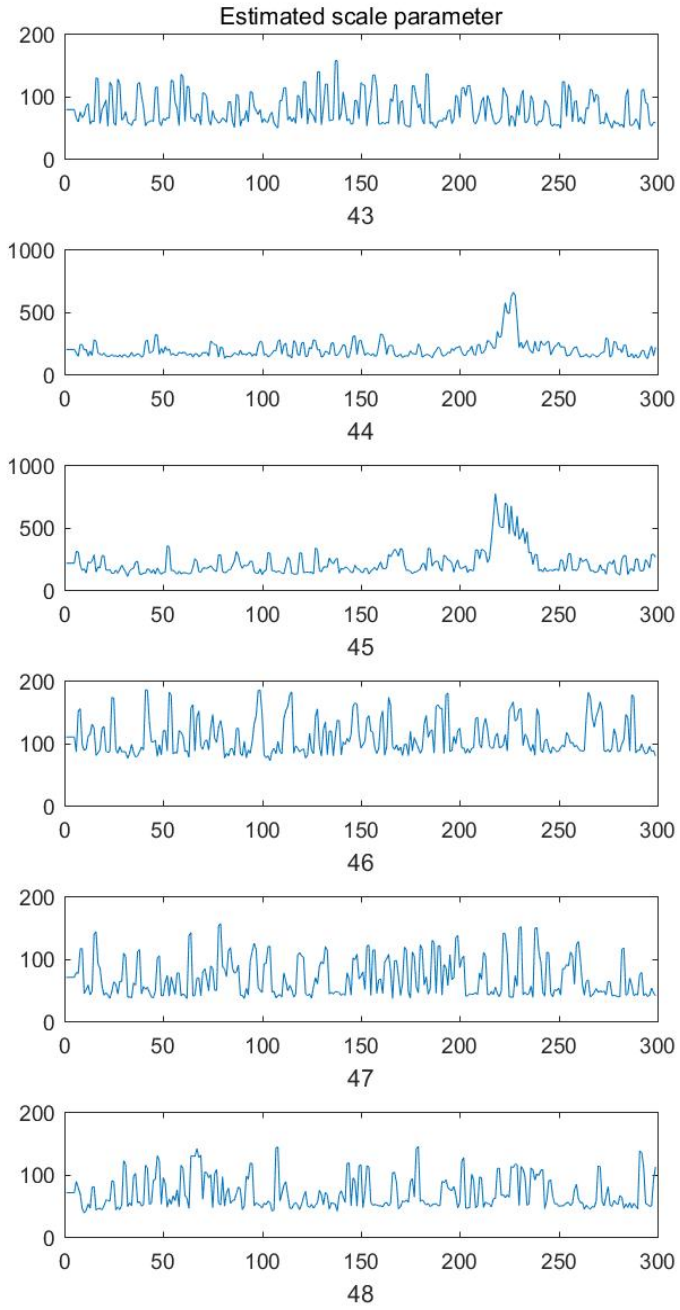
Estimated scale parameter
43
44
45
46
47
48

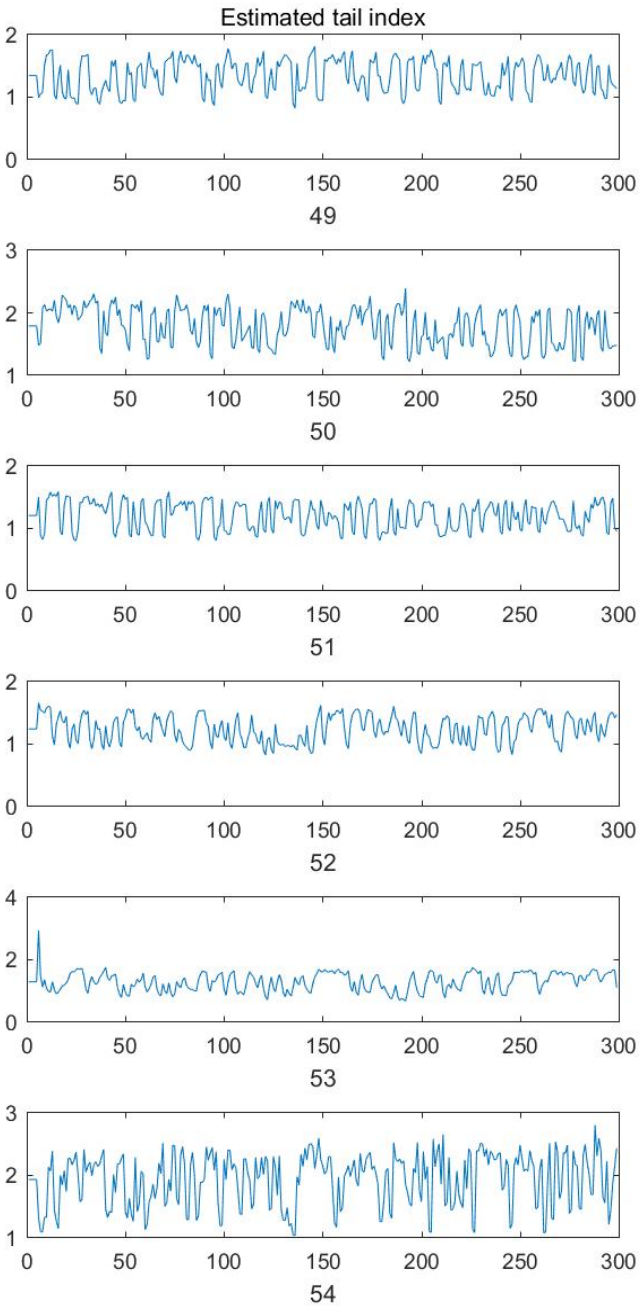
Estimated tail index
49
50
51
52
53
54

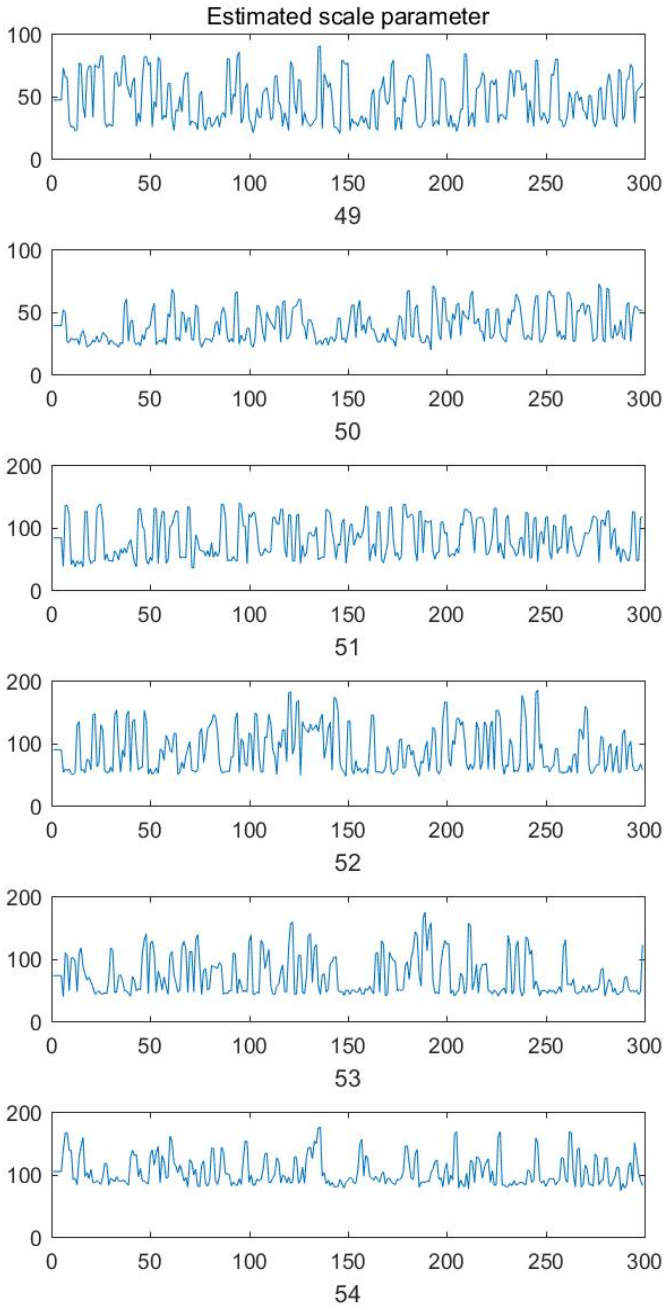
Estimated scale parameter
49
50
51
52
53
54

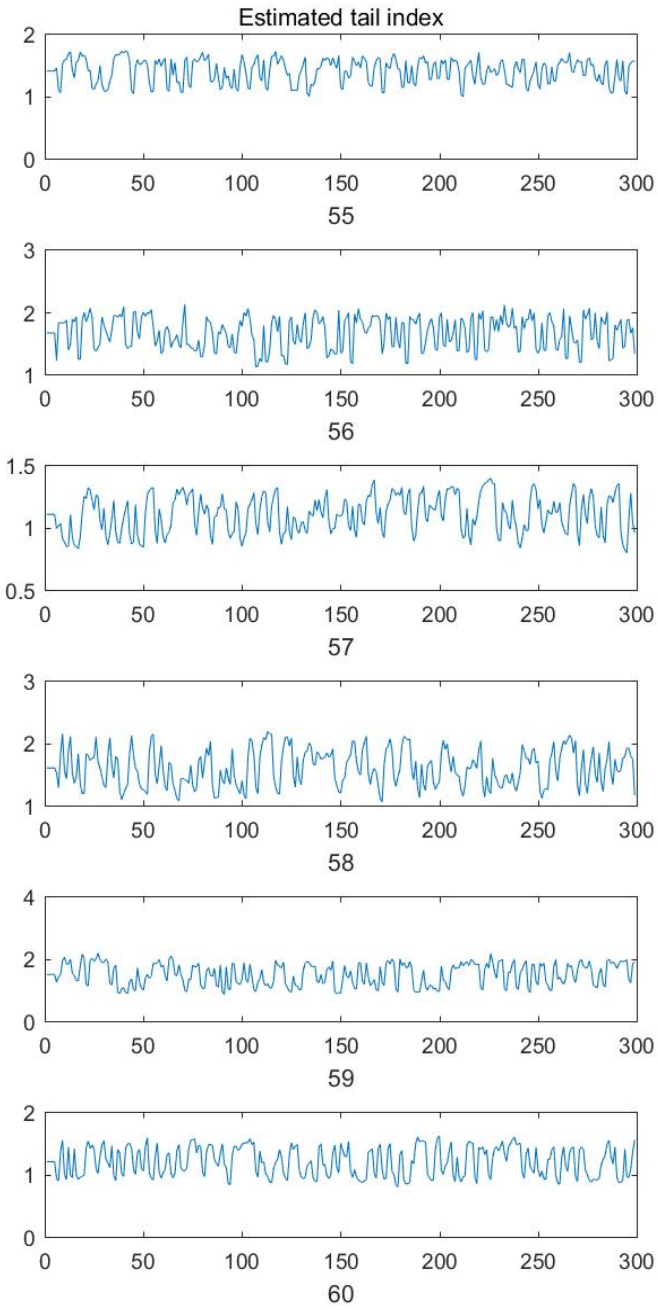
Estimated tail index
55
56
57
58
59
60

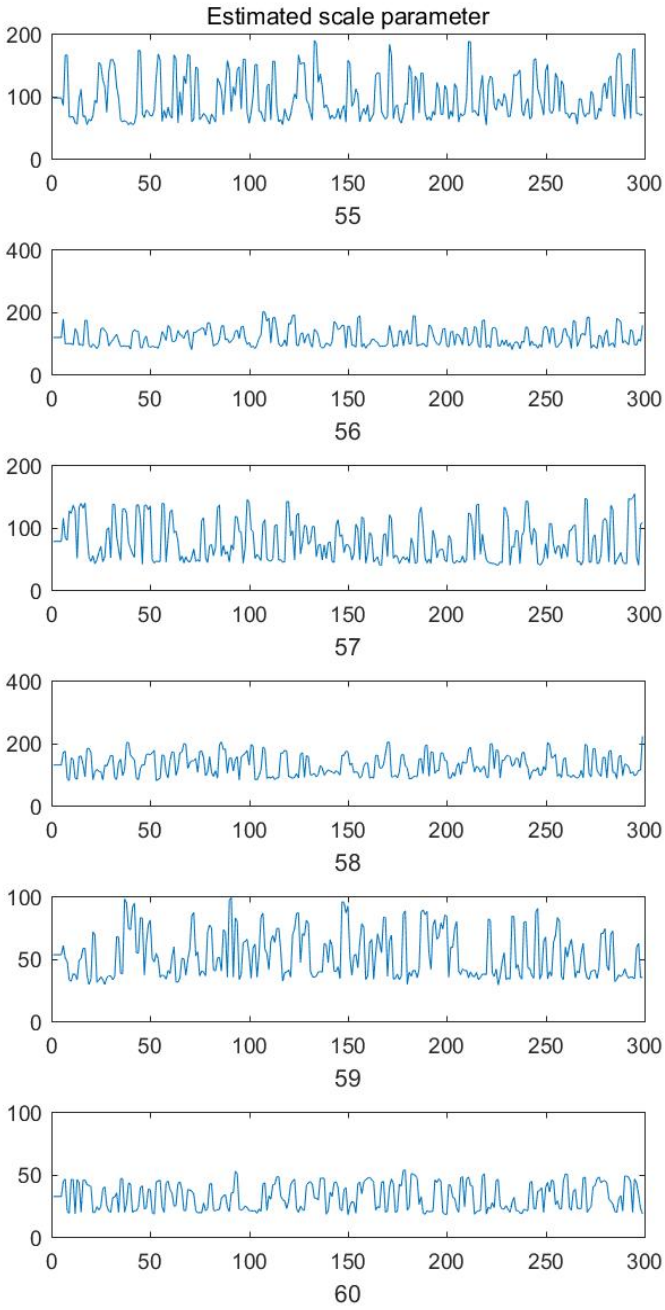
Estimated scale parameter
55
56
57
58
59
60

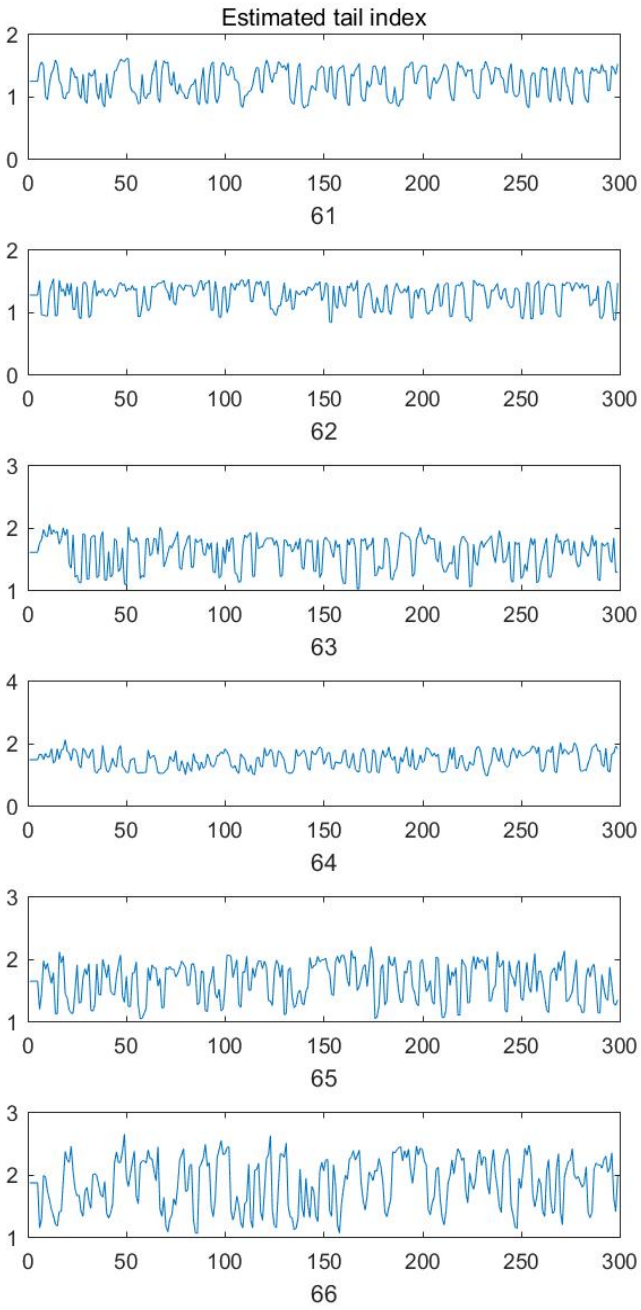
Estimated tail index
61
62
63
64
65
66

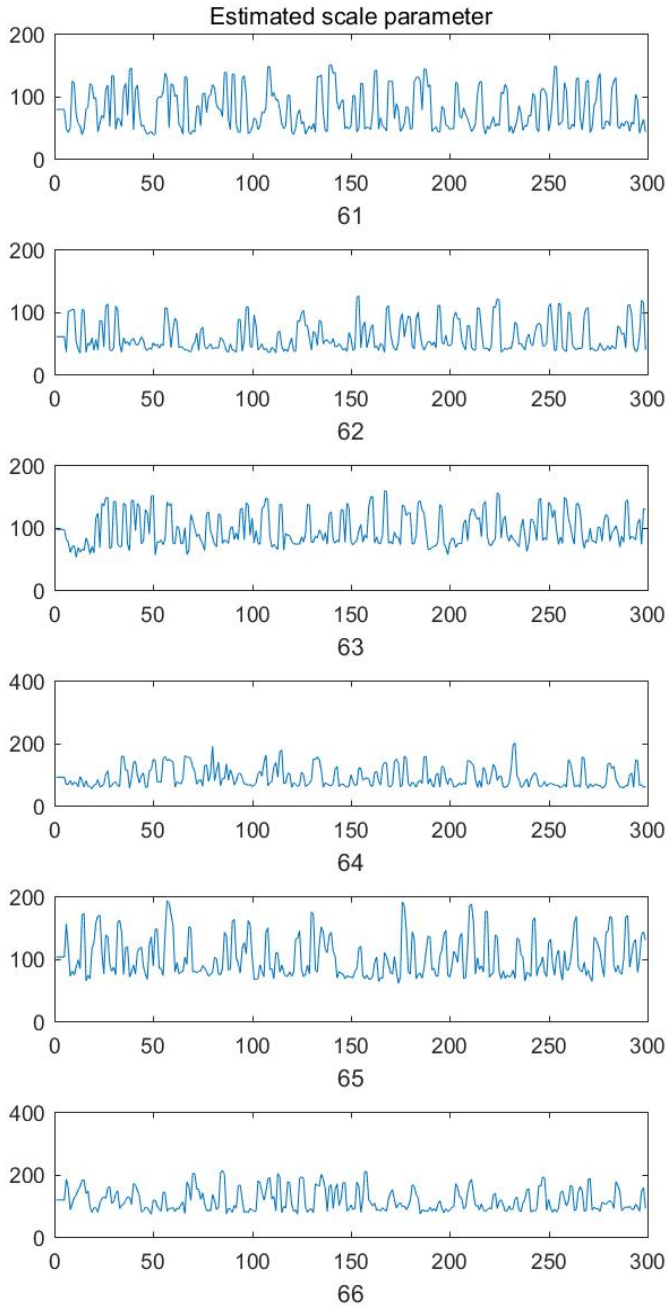
Estimated scale parameter
61
62
63
64
65
66

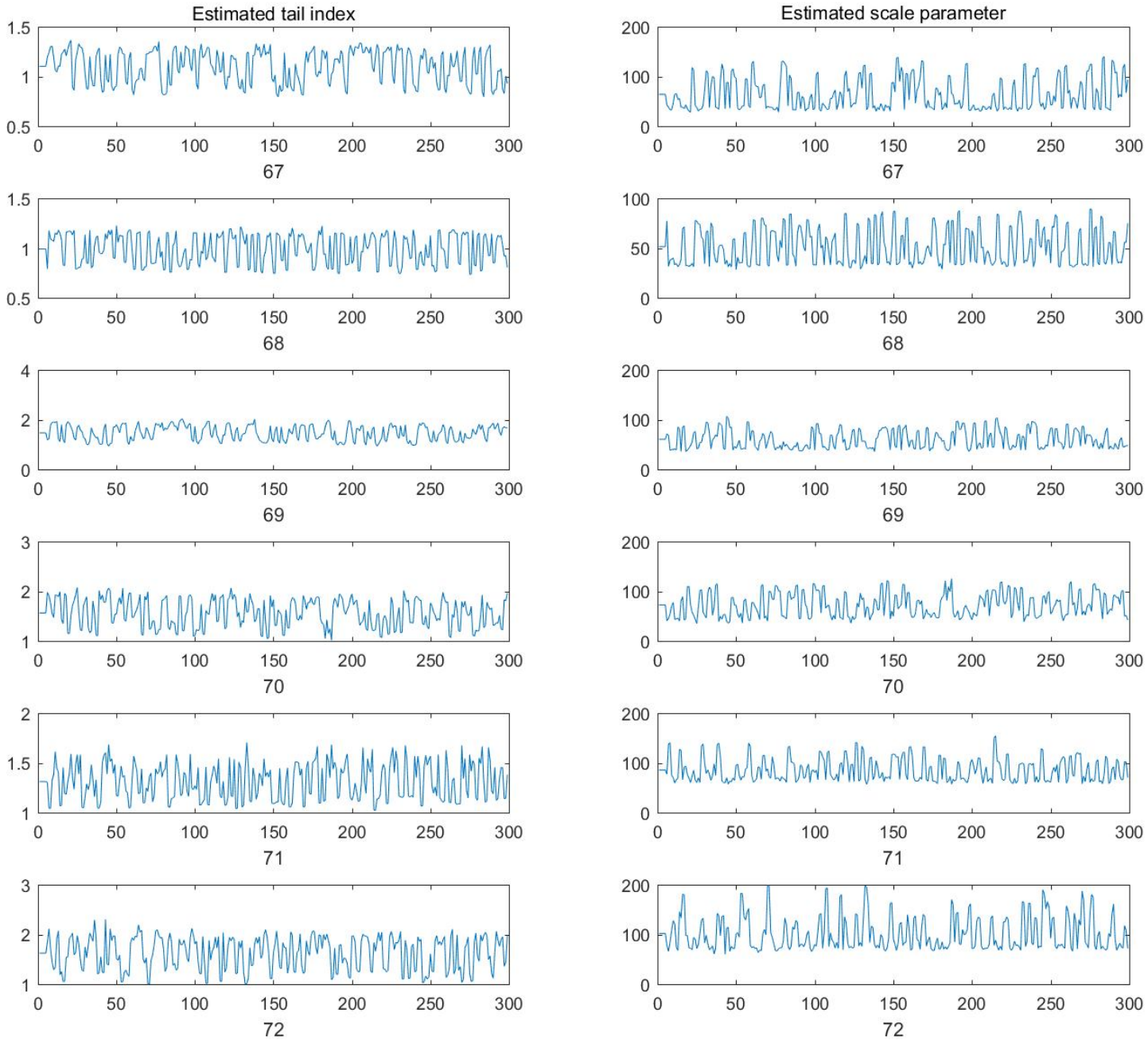
Estimated tail index
Estimated scale parameter
67
68
69
70
71
72

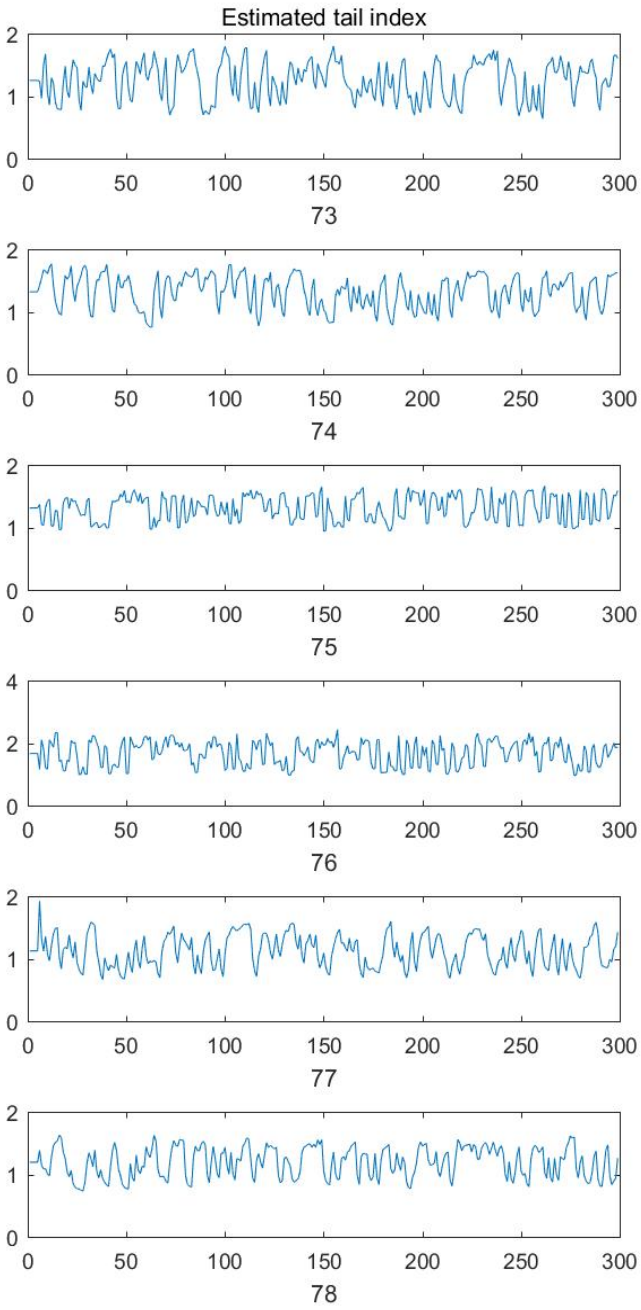
Estimated tail index
73
74
75
76
77
78

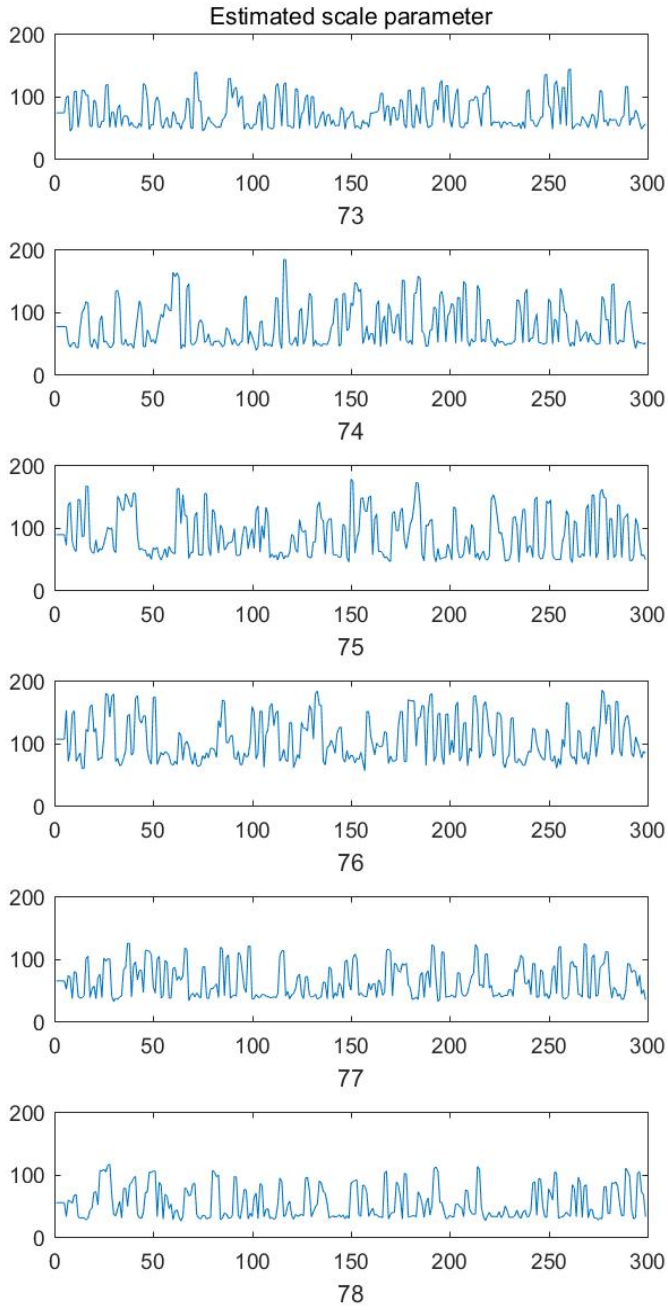
Estimated scale parameter
73
74
75
76
77
78

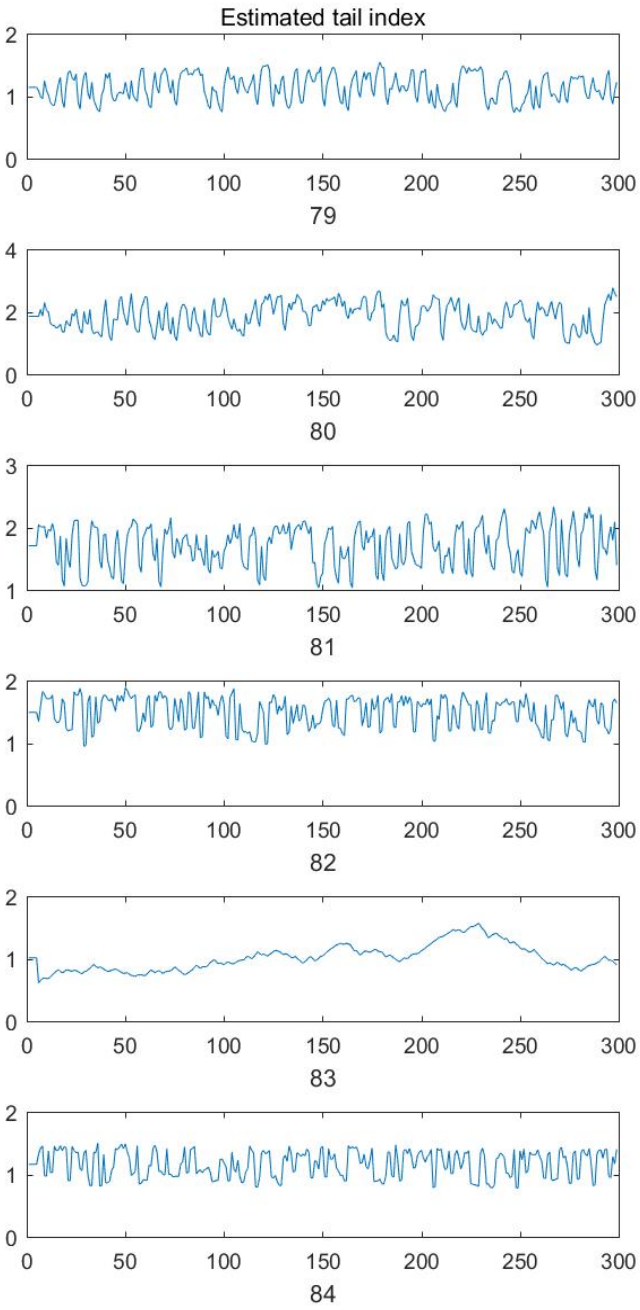
Estimated tail index
79
80
81
82
83
84

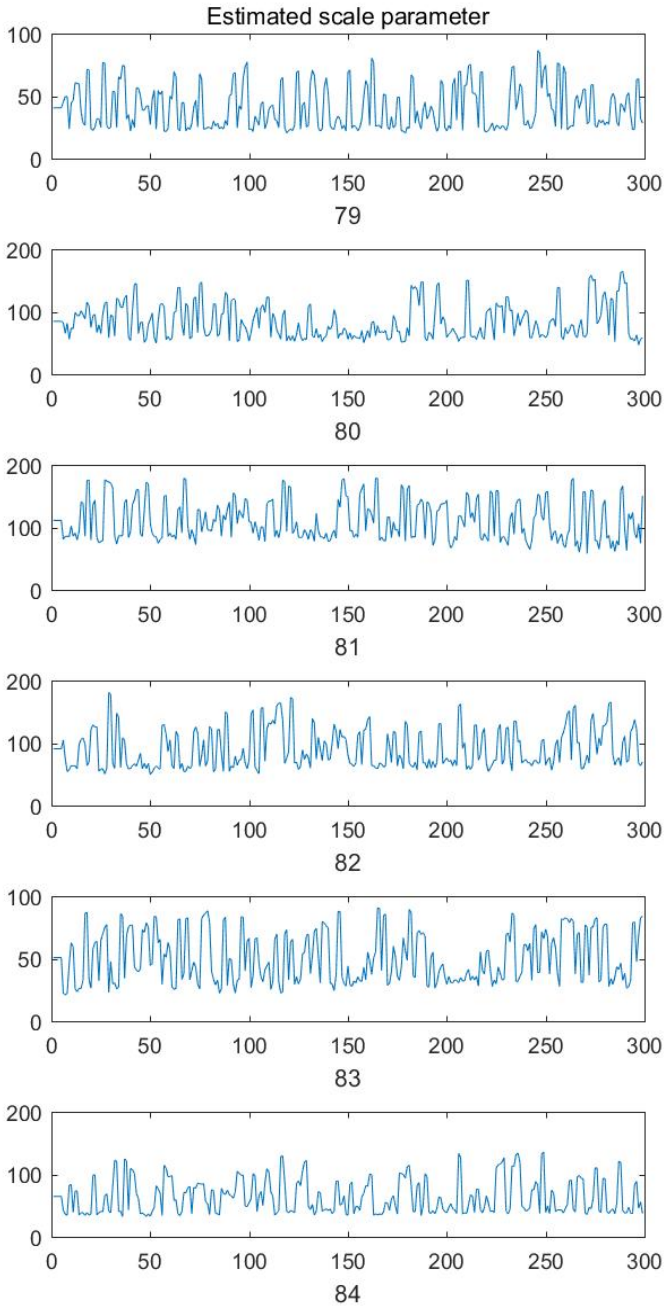
Estimated scale parameter
79
80
81
82
83
84

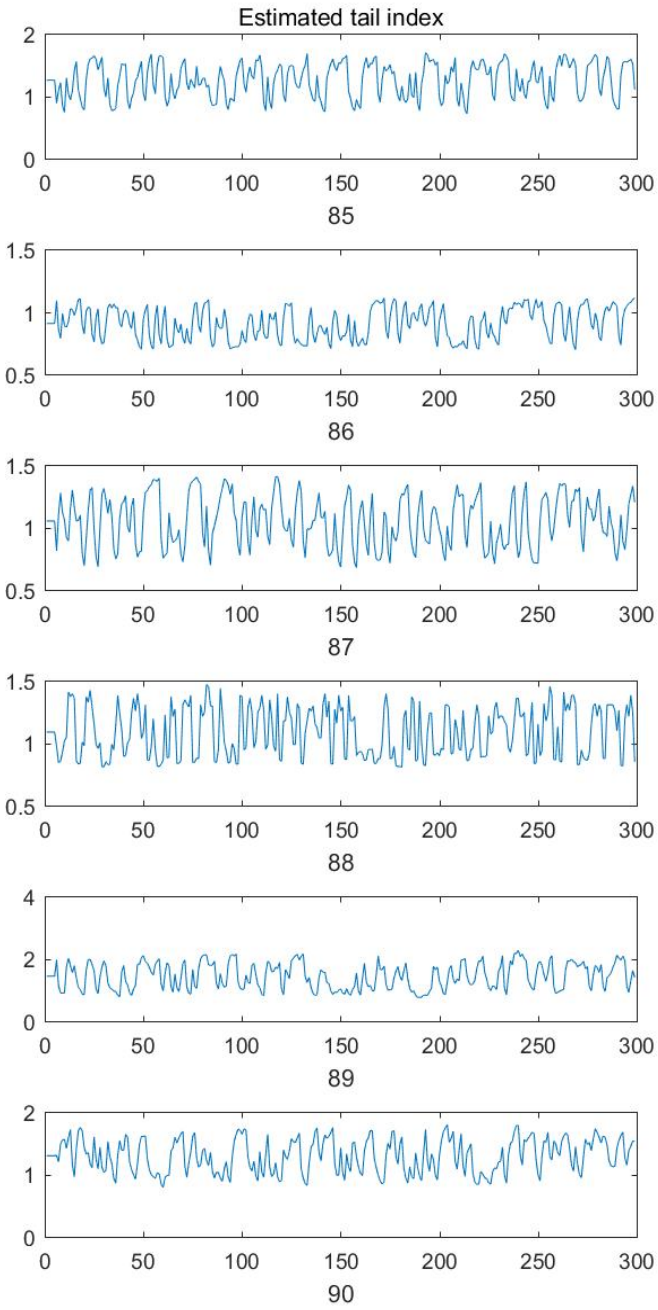
Estimated tail index
85
86
87
88
89
90

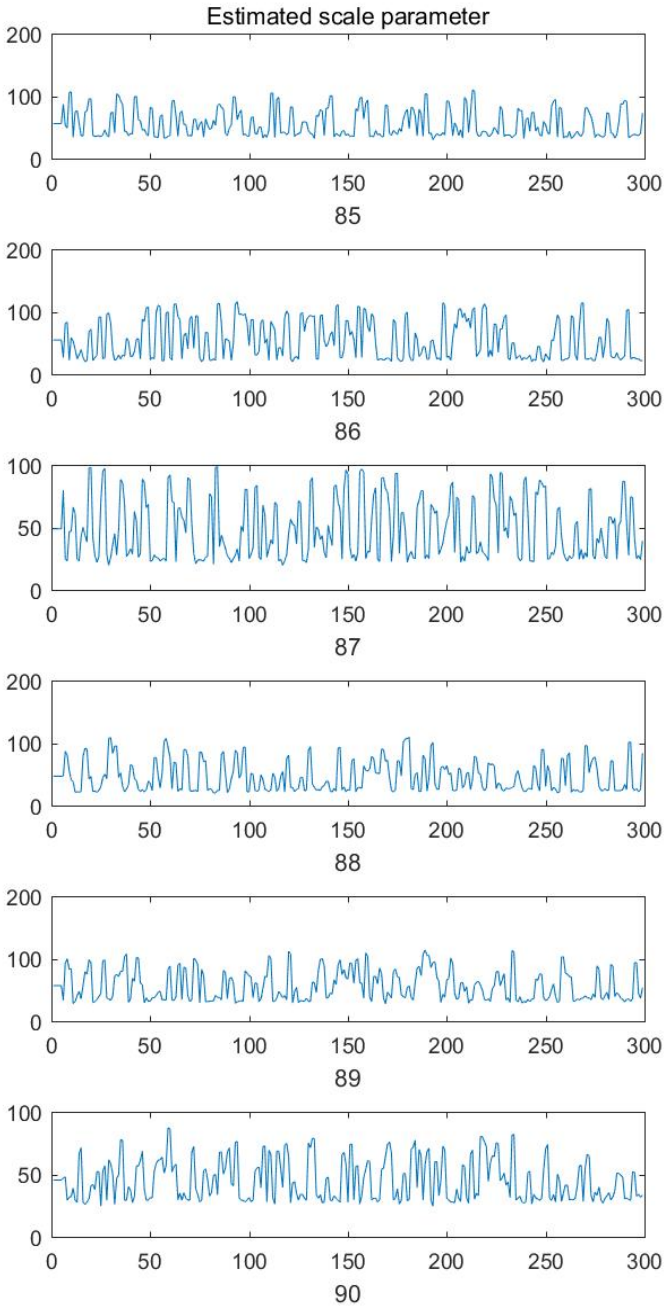
Estimated scale parameter
85
86
87
88
89
90

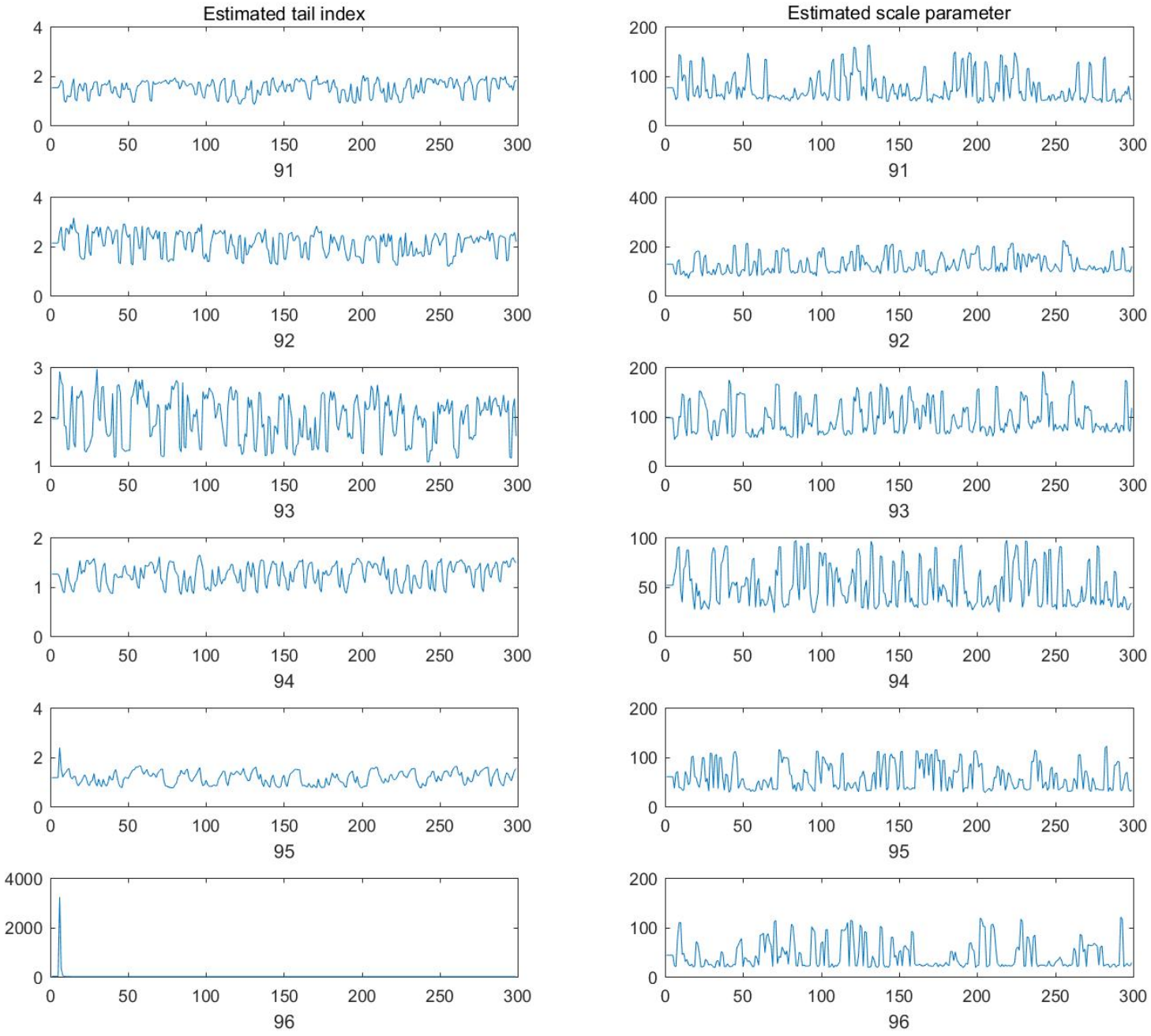
Estimated tail index
Estimated scale parameter
91
92
93
94
95
96

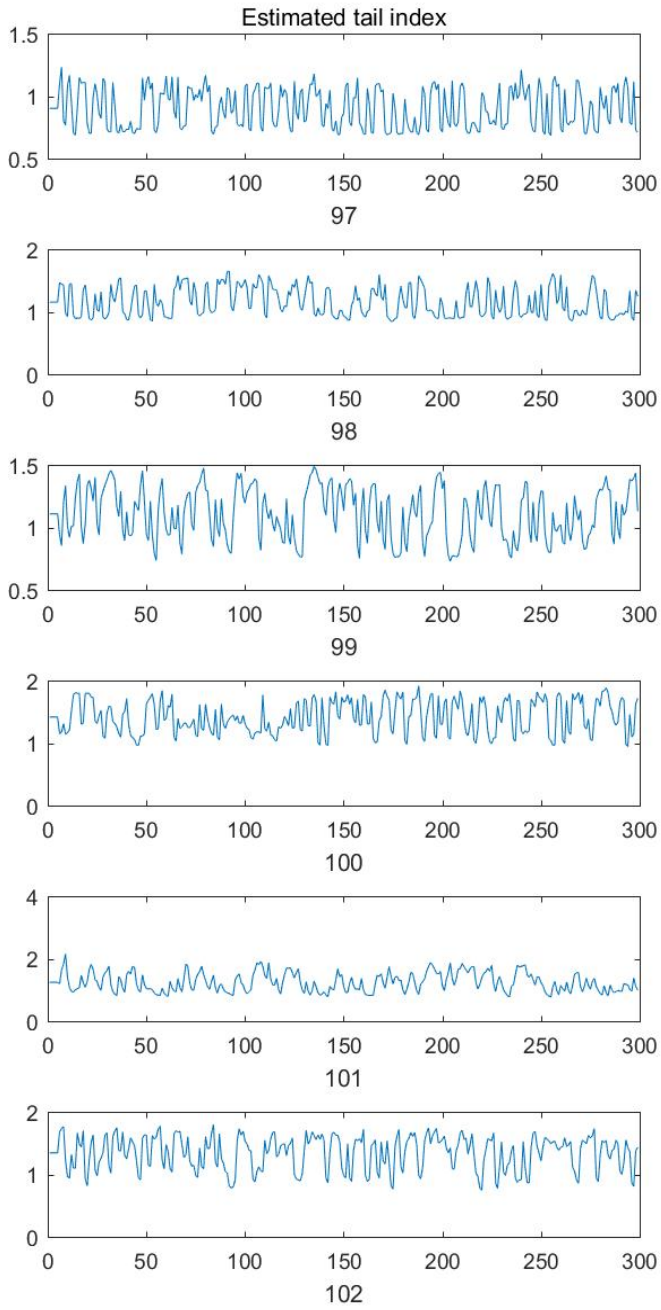
Estimated tail index
97
98
99
100
101
102

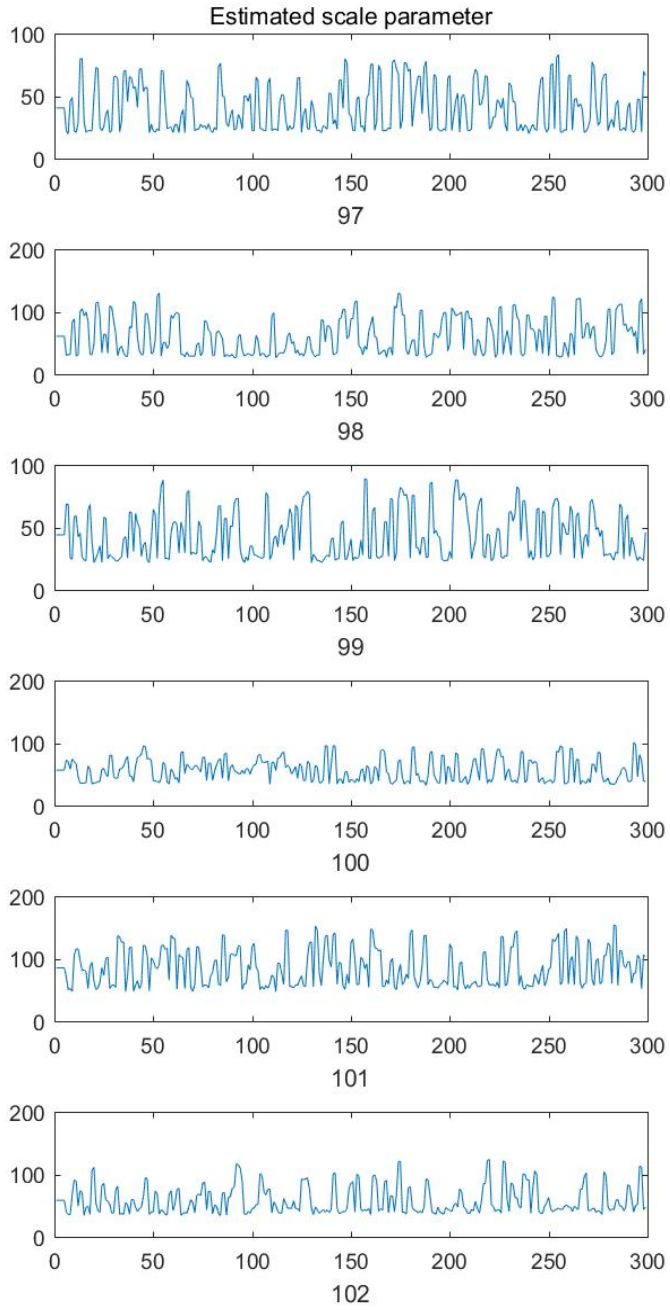
Estimated scale parameter
97
98
99
100
101
102

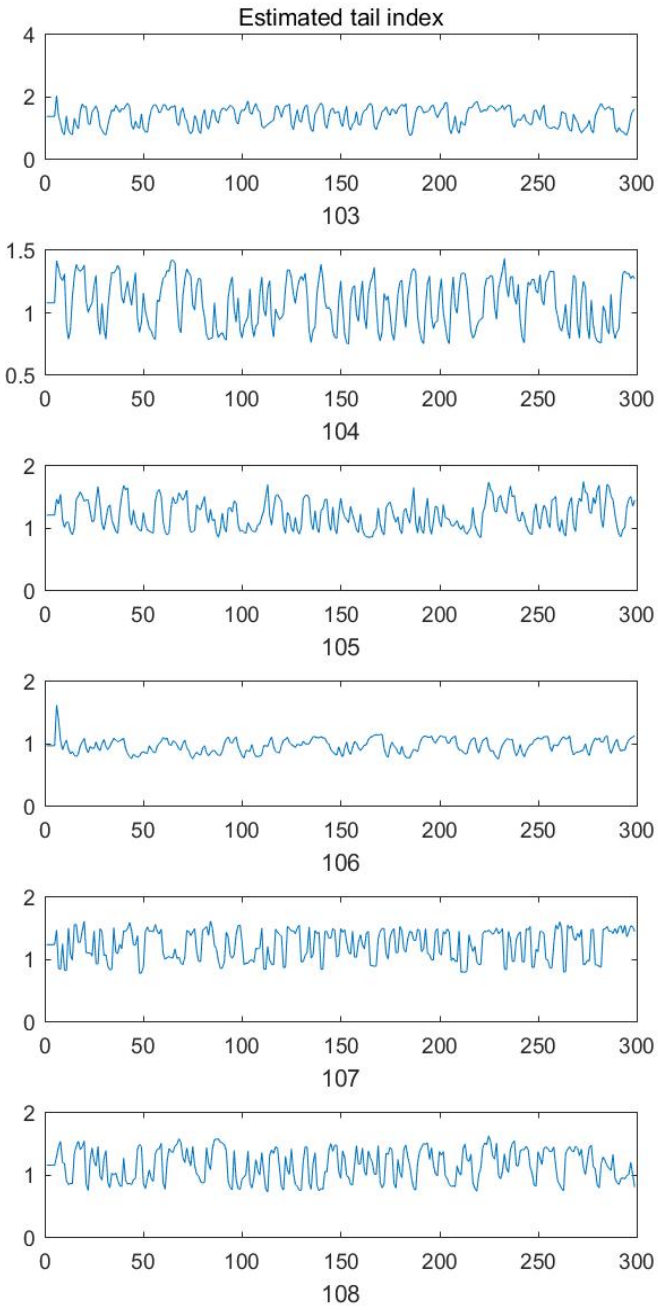
Estimated tail index
103
104
105
106
107
108

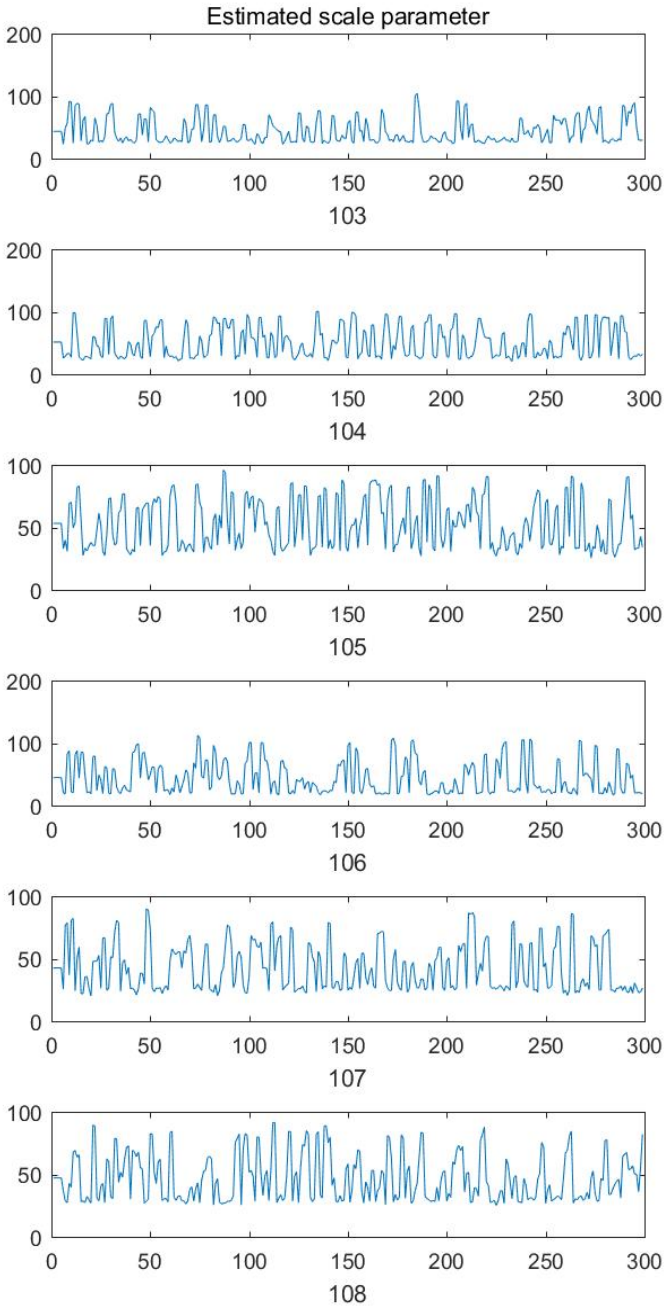
Estimated scale parameter
103
104
105
106
107
108

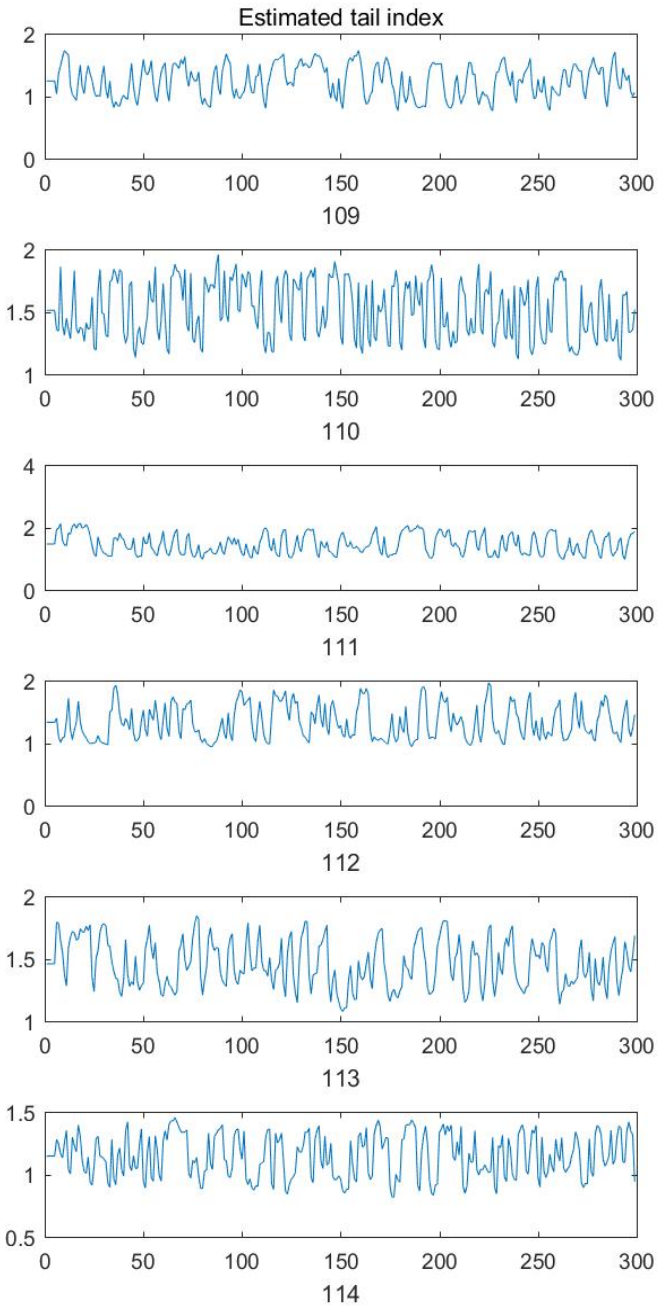
Estimated tail index
109
110
111
112
113
114

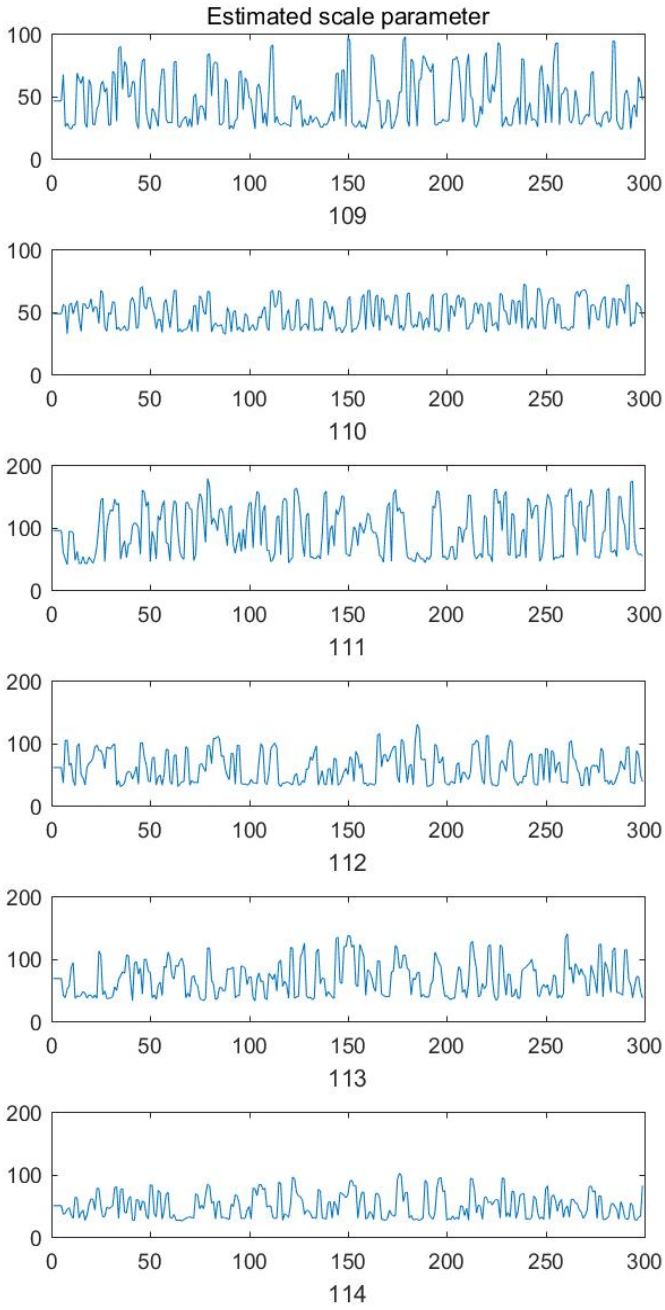
Estimated scale parameter
109
110
111
112
113
114

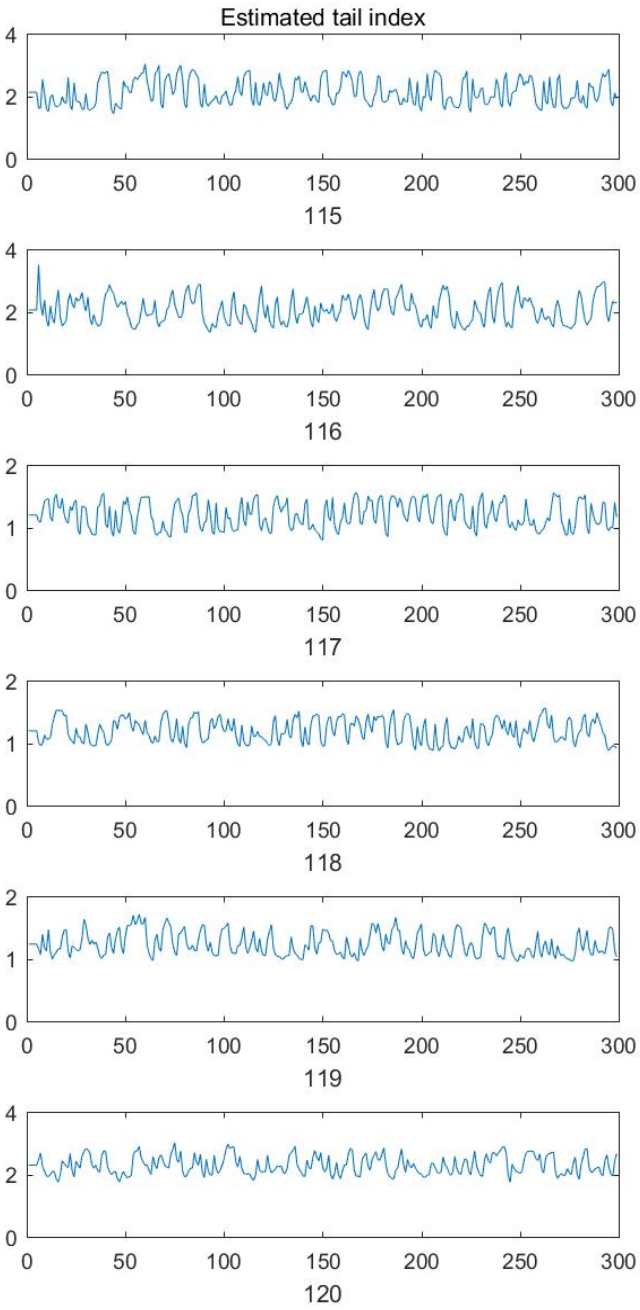
Estimated tail index
115
116
117
118
119
120

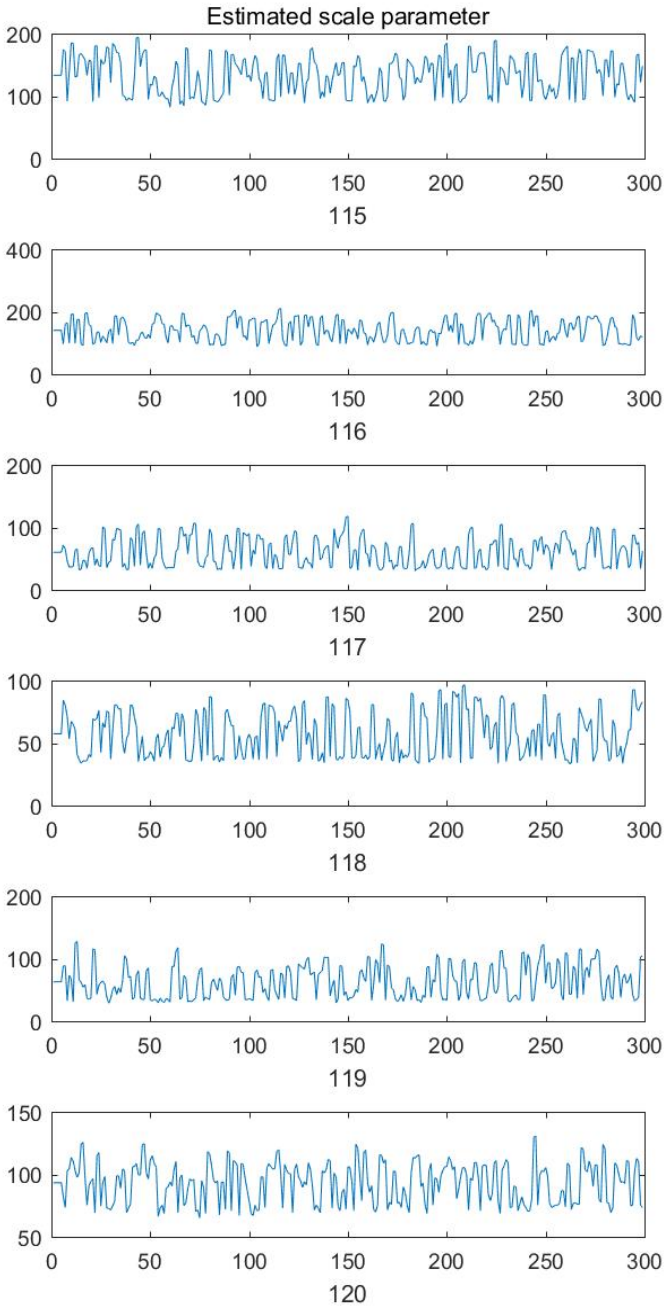
Estimated scale parameter
115
116
117
118
119
120

7.2 AcFL model with $k = 2$

Part	γ_0	γ_1	γ_2	γ_3	β_0	β_1	β_2	β_3	μ
1	-0.427	0	1.288	0.022	5.592	0	1.766	0.024	95.448
2	-0.018	0.916	0.364	416.548	0.049	0.989	0.021	148.655	107.201
3	-0.177	0.416	1.768	34.144	0.182	0.960	0.139	74.884	73.439
4	-0.051	0.889	0.390	50.403	0.100	0.982	0.075	0.093	80.722
5	0.124	0	0.001	18.981	3.944	0	0.001	28.977	82.794
6	0.075	0	0.001	25.851	4.070	0	0.001	20.211	76.744
7	-0.222	0	3.787	19.865	4.229	0	0.026	0.042	47.990
8	0.009	0.546	0.001	11.101	3.451	0	0.307	0.053	47.519
9	-0.103	0.823	1.378	50.376	0.661	0.848	1.081	56.809	28.739
10	-0.075	0.917	0.175	0.097	4.957	0	16.383	49.673	22.580
11	-0.698	0	7.520	12.073	6.312	0	23.234	82.222	126.125
12	-0.304	0	1.239	0.023	5.513	0	1.340	0.020	91.463
13	0.261	0	0.001	19.405	4.599	0	0.307	0.030	72.117
14	-0.045	0.071	0.001	0.002	7.106	0.002	16.454	0.707	91.710
15	-1.575	0.381	14.472	42.910	3.672	0.169	0.576	0.027	96.152
16	-0.019	0.992	0.034	0.027	4.022	0	0.001	6.062	95.611
17	0.235	0	0.001	22.595	4.162	0	0.001	20.982	59.178
18	0.227	0.237	0.224	0.021	6.454	0	10.120	1.197	11.881
19	-0.028	0.862	0.459	66.121	0.073	0.980	0.056	73.969	35.861
20	0.527	0	0.001	22.693	3.023	0	0.001	19.687	21.619
21	-0.051	0.805	0.399	3.806	0.082	0.980	0.026	4.284	105.651
22	-0.032	0.922	0.443	316.408	0.980	0.855	1.313	0.143	118.581
23	-0.311	0	5.978	60.860	6.444	0	15.858	11.968	89.591
24	-0.746	0.590	1.852	0.061	6.207	0	6.247	0.093	99.101
25	-0.246	0.842	2.356	34.554	0.391	0.915	0.460	247.918	94.758
26	-0.127	0.836	1.485	99.115	0.482	0.918	0.386	0.073	102.240
27	0.175	0.828	0.223	0.001	6.919	0	15.589	1.129	70.969
28	-2.180	0.013	17.234	9.678	6.152	0	7.554	0.254	41.584
29	0.090	0	5.877	16.865	4.444	0	0.001	15.517	-5.000
30	0.007	0.971	0.013	26.879	0.010	0.998	0.009	20.022	26.820

Part	γ_0	γ_1	γ_2	γ_3	β_0	β_1	β_2	β_3	μ
31	-0.061	0	1.081	7.313	4.186	0	0.803	21.775	89.212
32	-0.040	0	0.001	39.764	4.137	0	1.796	39.810	100.832
33	-0.487	0	1.941	0.056	7.272	0	22.902	17.387	97.677
34	-1.365	0	14.032	27.993	5.499	0	1.286	0.026	74.935
35	-0.001	0.994	0.003	0.022	4.256	0	0.001	18.355	110.028
36	-0.202	0.590	1.611	0.213	0.248	0.953	0.149	1.007	91.870
37	-0.276	0.861	0.989	0.268	3.856	0	0.001	68.848	78.036
38	0.017	0.125	0.180	0.042	0.049	0.988	0.023	28.036	57.228
39	0.006	0.960	0.091	35.350	0.145	0.967	0.052	83.146	21.199
40	-0.677	0.764	7.967	586.914	1.126	0.827	2.807	1.978	30.365
41	0.249	0	0.001	25.263	4.150	0	0.001	20.784	90.099
42	-0.036	0.989	0.065	0.035	3.130	0.144	0.001	5.683	115.784
43	0.175	0	0.001	27.279	4.236	0	0.001	29.008	105.084
44	-1.706	0.580	19.710	87.176	2.654	0.684	6.165	0.838	112.596
45	-2.239	0.134	23.946	32.606	10.048	0	52.439	99.514	90.423
46	0.018	0.935	0.059	18.988	0.022	0.995	0.006	17.424	94.538
47	-0.125	0.829	0.901	8.708	0.137	0.971	0.051	0.070	92.762
48	0.130	0	0.001	18.564	4.802	0	7.643	68.967	75.053
49	0.063	0.007	0.001	19.793	3.739	0	0.294	0.052	45.692
50	0.001	0.967	0.102	115.220	0.032	0.992	0.019	57.505	28.069
51	-0.035	0	0.497	29.012	4.223	0	0.001	17.671	90.600
52	-0.048	0.976	0.090	0.029	0.923	0.817	1.470	106.804	102.231
53	0.055	0.049	0.001	0.001	6.003	0.247	16.035	0.895	122.221
54	0.465	0	0.001	19.988	4.541	0	0.084	0.020	113.316
55	0.185	0	0.001	19.111	4.528	0	0.238	0.022	100.861
56	0.014	0.937	0.054	58.008	0.170	0.963	0.024	56.336	97.629
57	-0.023	0	0.001	19.394	4.210	0	0.594	29.853	88.043
58	-0.033	0.989	0.063	0.032	4.513	0	0.001	19.999	63.033
59	0.028	0	0.184	0.049	3.984	0	2.116	9.972	48.002
60	-0.262	0	1.041	0.713	3.219	0	0.001	16.208	39.133
61	0.006	0	0.001	19.454	4.081	0	0.001	19.983	99.002
62	0.084	0	0.001	28.642	3.890	0	0.001	29.813	134.232
63	-0.010	0.995	0.020	0.021	0.512	0.904	0.717	9.361	119.140
64	0.082	0	0.119	0.023	4.946	0	6.476	41.627	105.936
65	0.270	0	0.001	24.732	4.398	0	0.001	27.116	86.376
66	-0.516	0	7.373	25.853	4.567	0	0.179	0.022	96.327
67	-0.005	0.994	0.008	0.032	0.847	0.828	0.293	0.032	79.822
68	-0.093	0.879	0.721	58.124	0.245	0.942	0.181	26.749	64.052
69	-0.268	0	3.317	24.171	3.827	0	0.001	15.838	41.817
70	-0.525	0.479	1.913	0.079	5.842	0	3.542	0.084	35.204

Part	γ_0	γ_1	γ_2	γ_3	β_0	β_1	β_2	β_3	μ
71	0.069	0	0.029	0.008	7.198	0	19.225	3.142	102.424
72	-0.014	0.991	0.027	0.020	3.148	0.279	0.001	0.533	121.577
73	-0.805	0.439	5.070	1.940	4.098	0	0.001	18.528	93.859
74	-0.047	0.648	0.141	0.033	0.045	0.990	0.016	26.330	75.534
75	-0.003	0.999	0.006	9.468	2.118	0.589	1.881	0.630	79.203
76	-0.027	0.920	0.074	0.029	1.801	0.741	6.467	69.340	77.899
77	-0.611	0.643	4.045	4.861	3.940	0	0.001	29.788	67.388
78	-0.049	0.977	0.088	0.048	0.655	0.839	0.520	24.894	61.393
79	-0.306	0.529	1.728	2.741	3.462	0	0.001	15.780	51.243
80	-0.151	0.931	0.486	0.137	0.240	0.959	0.125	0.045	49.059
81	0.350	0	0.001	21.674	4.598	0	0.112	0.024	88.162
82	0.213	0	0.001	14.578	4.830	0	4.205	12.922	107.546
83	-0.658	0.712	1.765	0.070	6.408	0	6.682	0.095	79.885
84	-0.055	0	0.001	10.666	4.125	0	1.687	7.833	66.077
85	-0.258	0.395	2.312	18.223	3.872	0	0.268	0.140	61.607
86	-0.032	0.960	0.053	0.062	0.662	0.889	0.728	0.112	73.668
87	-0.162	0	0.515	28.728	3.597	0	0.001	27.479	68.395
88	-0.004	0.999	0.007	0.041	4.271	0	5.212	5.327	63.333
89	-0.485	0.344	1.404	0.142	3.829	0	0.359	0.048	50.836
90	-0.184	0	0.449	0.057	3.574	0	0.001	10.363	46.265
91	-0.004	0.995	0.012	0.440	4.023	0	0.001	7.906	90.162
92	0.741	0.055	0.001	0.003	6.599	0.001	13.473	3.603	76.458
93	0.147	0	0.207	0.014	5.910	0	3.491	0.057	54.194
94	0.018	0.748	0.001	6.444	3.804	0	0.747	19.998	53.832
95	-0.558	0.747	5.238	96.623	1.882	0.690	7.210	187.706	60.418
96	-0.674	0.736	5.451	37.650	2.684	0.444	6.948	29.006	69.938
97	-0.266	0.146	0.043	0.015	5.918	0.001	18.696	9.467	66.151
98	-0.026	0.983	0.047	0.056	0.410	0.920	0.183	0.042	58.664
99	-0.064	0.769	0.242	2.395	0.014	0.997	0.009	23.866	50.832
100	-0.001	0.992	0.008	31.994	0.504	0.906	0.599	0.454	42.912
101	-0.009	0.997	0.018	0.033	3.585	0.141	0.001	19.586	72.065
102	-0.098	0	0.265	0.036	3.786	0	0.001	28.438	70.663
103	-0.016	0.984	0.027	0.045	3.675	0	1.376	4.596	55.274
104	-1.714	0.233	12.337	7.493	7.317	0	18.106	1.430	49.198
105	-0.073	0	0.513	4.022	3.727	0	0.001	5.454	55.945
106	-0.209	0.089	0.071	0.041	4.100	0	4.758	17.223	62.934
107	0.519	0	0.755	0.001	7.443	0	19.769	1.179	57.897
108	-0.179	0	0.173	0.045	3.592	0	0.044	0.045	55.932
109	-0.143	0.568	0.222	0.049	3.571	0	0.110	0.049	48.996
110	0.826	0.058	1.002	0.001	6.296	0	14.582	3.070	33.392

Part	γ_0	γ_1	γ_2	γ_3	β_0	β_1	β_2	β_3	μ
111	-1.930	0.211	14.141	6.004	6.591	0	7.222	0.121	57.456
112	-0.110	0.849	0.177	0.045	3.252	0.169	0.281	0.045	52.740
113	-0.019	0.937	0.225	7.042	0.198	0.955	0.109	23.600	38.210
114	-0.009	0.926	0.030	19.193	2.318	0.419	0.364	0.046	52.731
115	-0.004	0.991	0.019	0.048	2.793	0.498	2.949	19.534	-5.000
116	0.777	0.427	0.589	0.001	7.648	0	19.277	7.140	-5.000
117	-0.019	0.938	0.090	3.431	0.457	0.889	0.348	87.331	53.356
118	-0.002	0.993	0.005	65.186	0.595	0.865	0.885	100.243	51.982
119	-0.007	0.990	0.013	0.051	4.422	0	3.726	6.796	47.526
120	0.757	0.001	0.001	19.217	2.770	0.396	0.417	19.511	-5.000

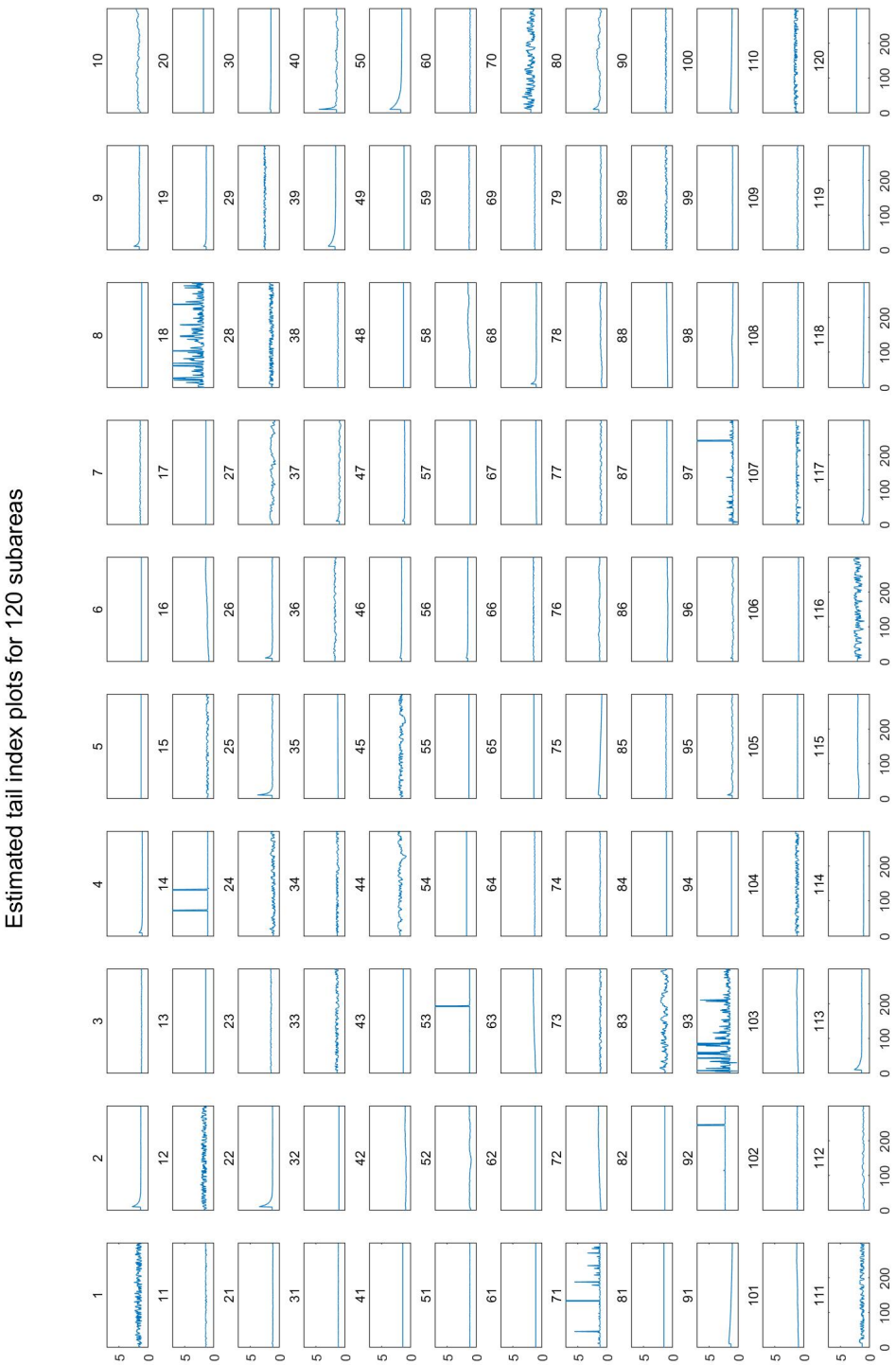
Estimated tail index plots for 120 subareas


Estimated scale parameter plots for 120 subareas

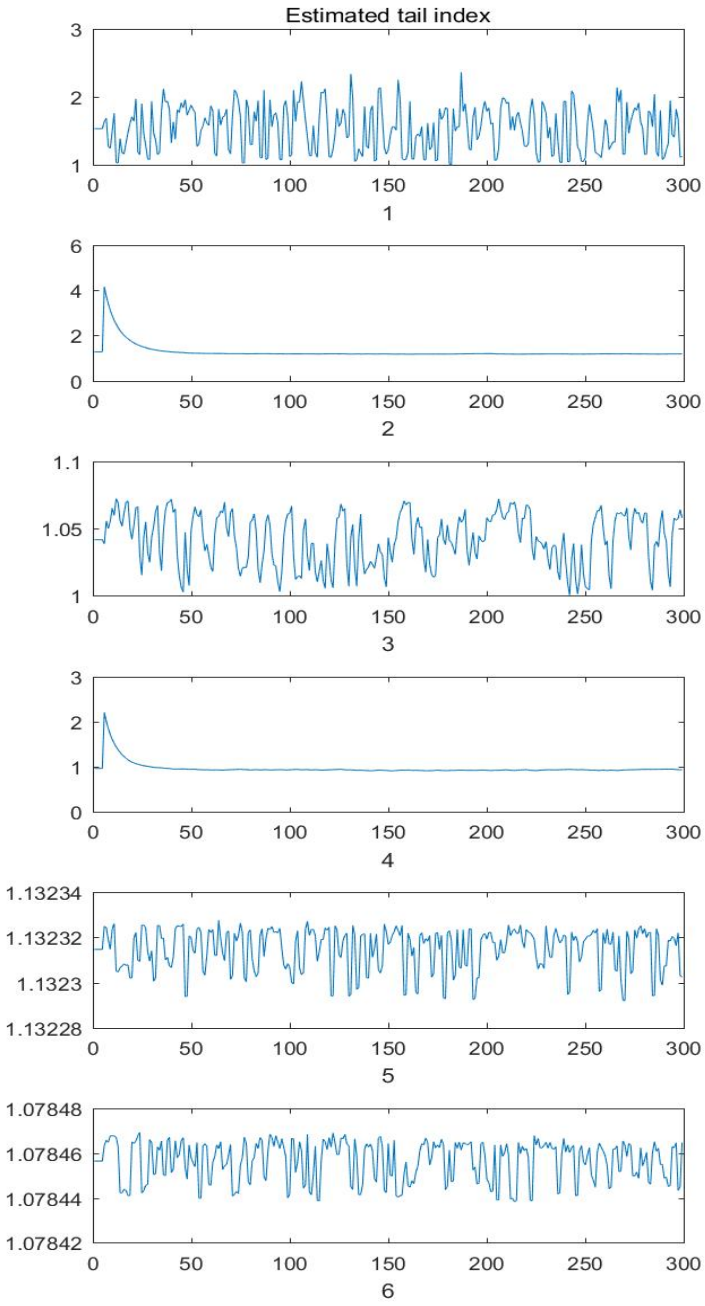
Estimated tail index
1
2
3
4
5
6

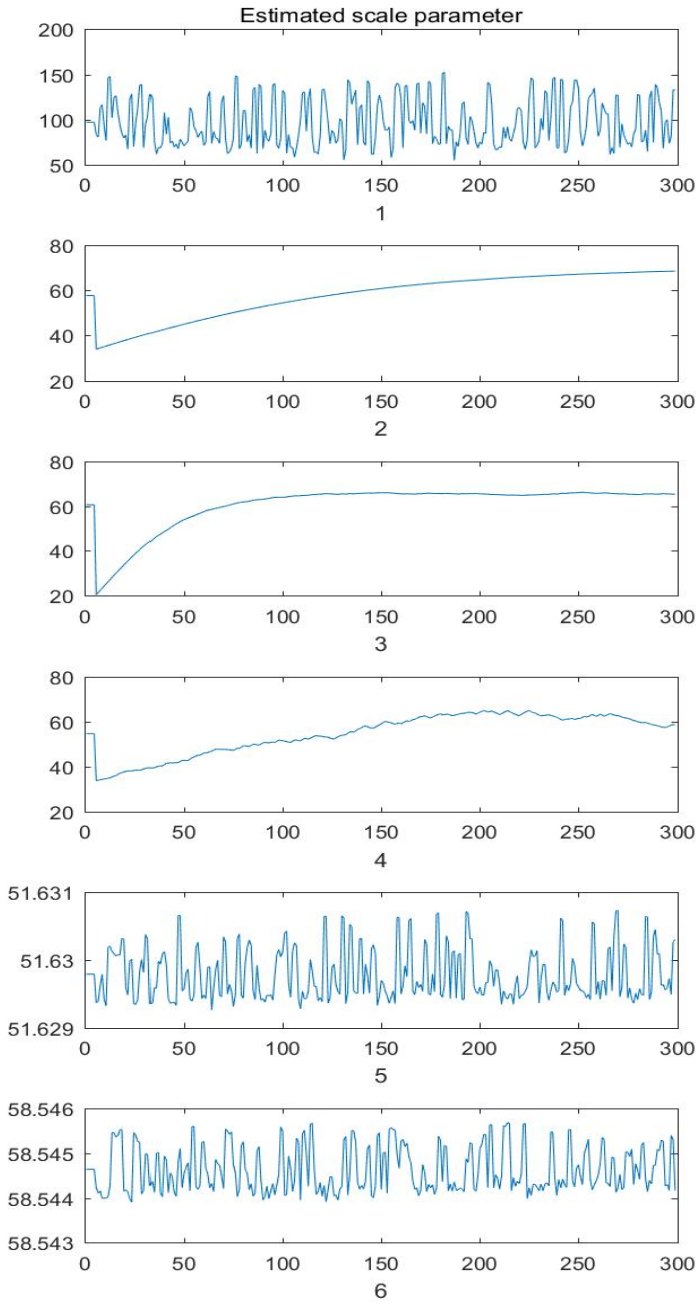
Estimated scale parameter
1
2
3
4
5
6

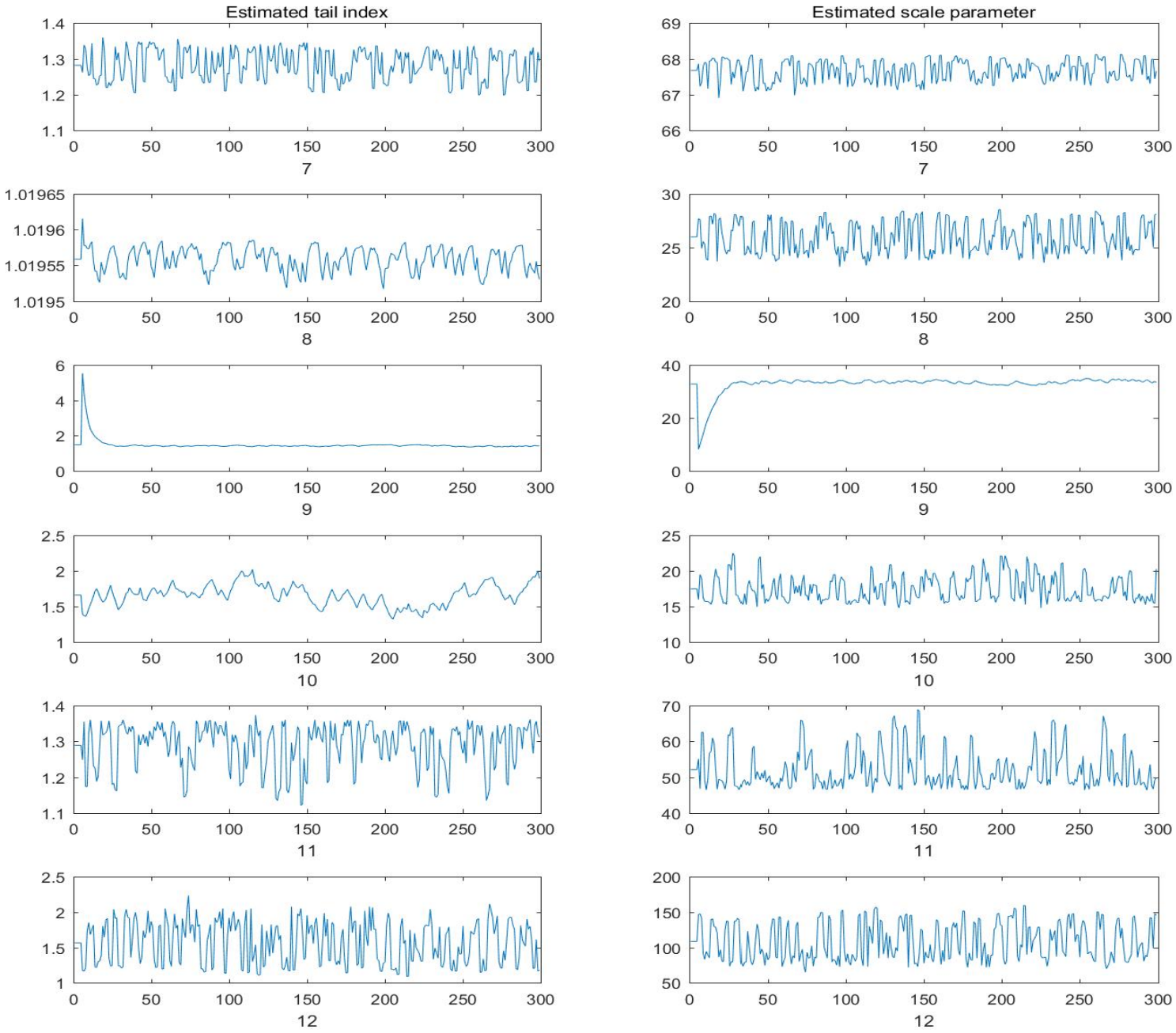
Estimated tail index
Estimated scale parameter
7
8
9
10
11
12

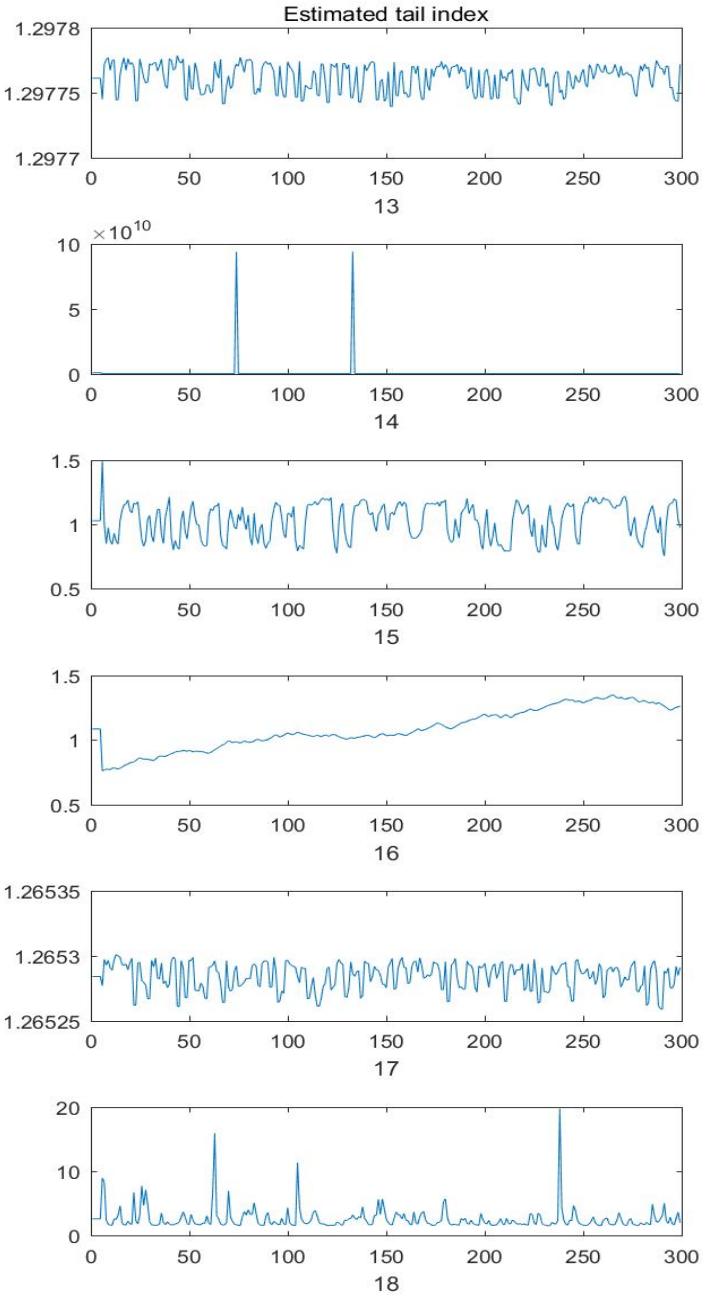
Estimated tail index
1.2978
1.29775
1.2977
0 50 100 150 200 250 300
13
×10^10
10
5
0
0 50 100 150 200 250 300
14
1.5
1
0.5
0 50 100 150 200 250 300
15
1.5
1
0.5
0 50 100 150 200 250 300
16
1.26535
1.2653
1.26525
0 50 100 150 200 250 300
17
20
10
0
0 50 100 150 200 250 300
18

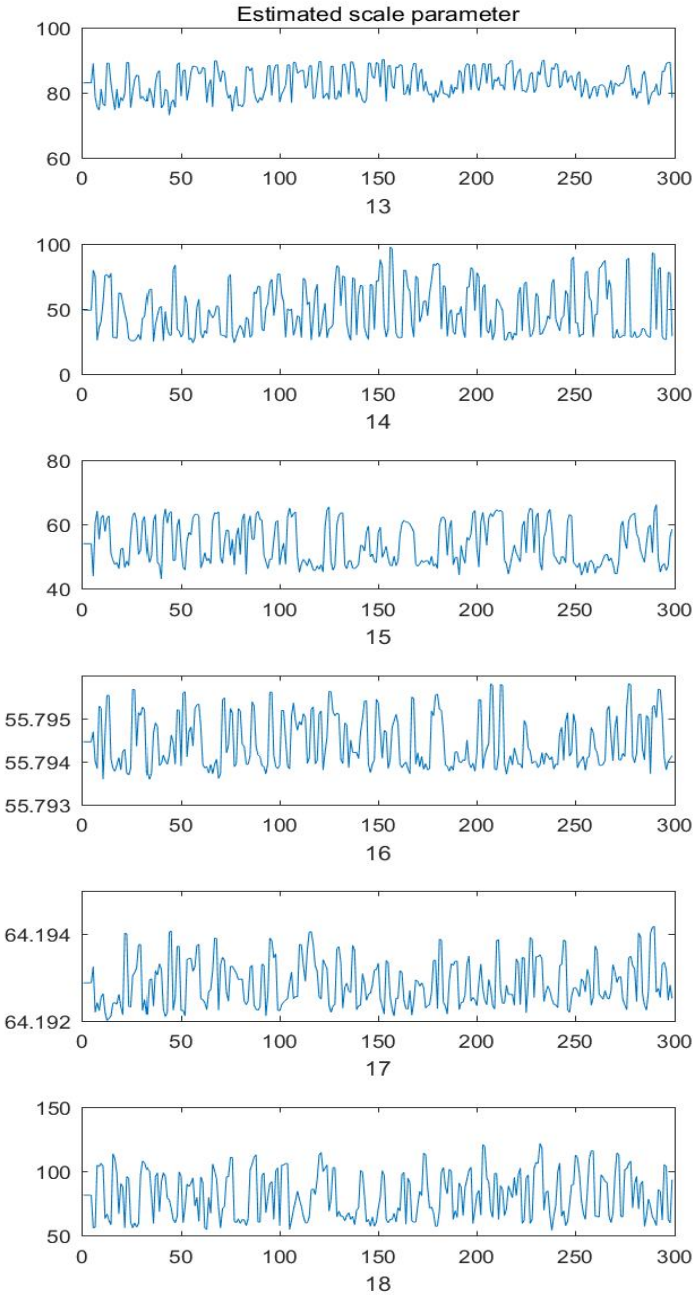
Estimated scale parameter
100
80
60
0 50 100 150 200 250 300
13
100
50
0
0 50 100 150 200 250 300
14
80
60
40
0 50 100 150 200 250 300
15
55.795
55.794
55.793
0 50 100 150 200 250 300
16
64.194
64.192
0 50 100 150 200 250 300
17
150
100
50
0 50 100 150 200 250 300
18

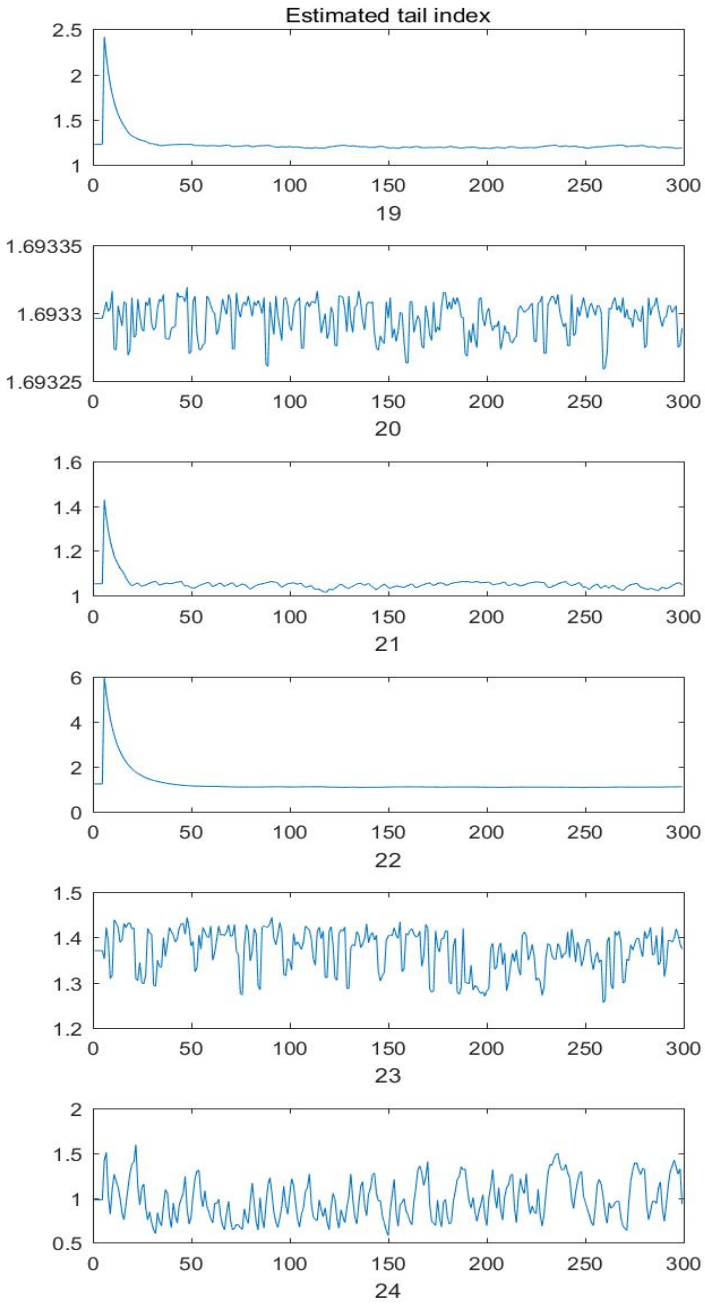
Estimated tail index
19
20
21
22
23
24

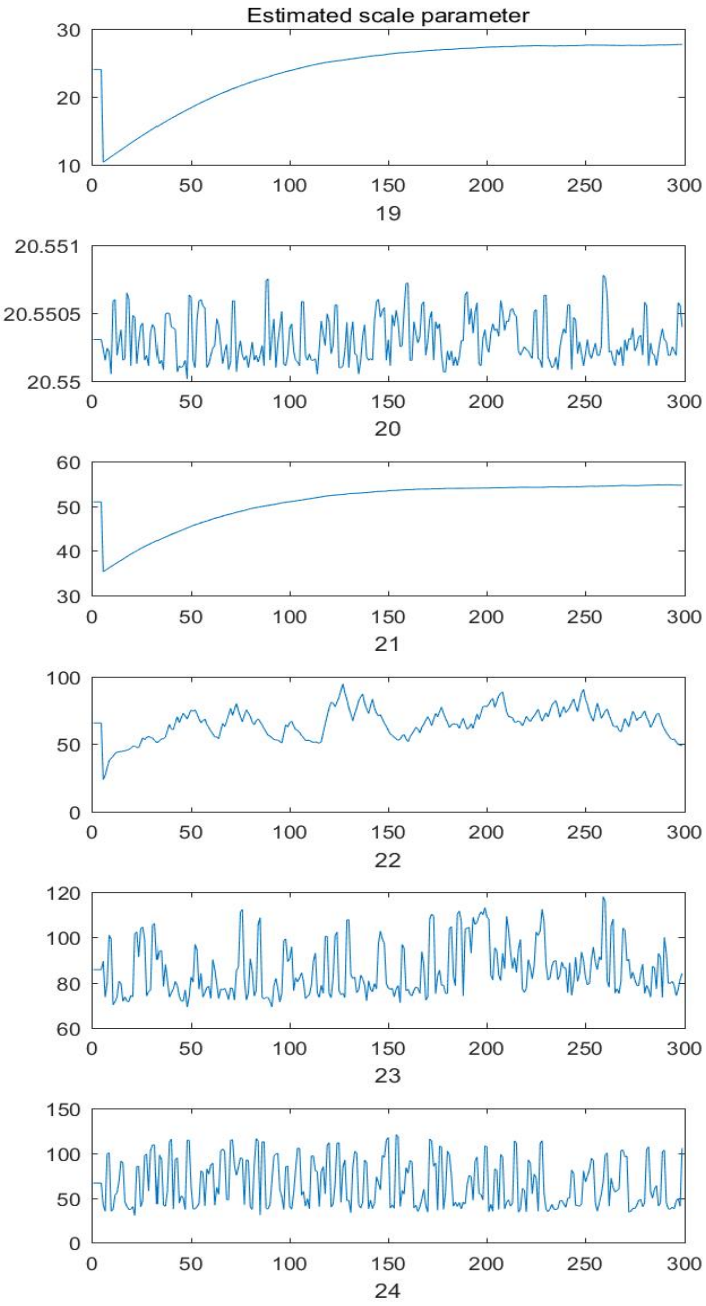
Estimated scale parameter
19
20
21
22
23
24

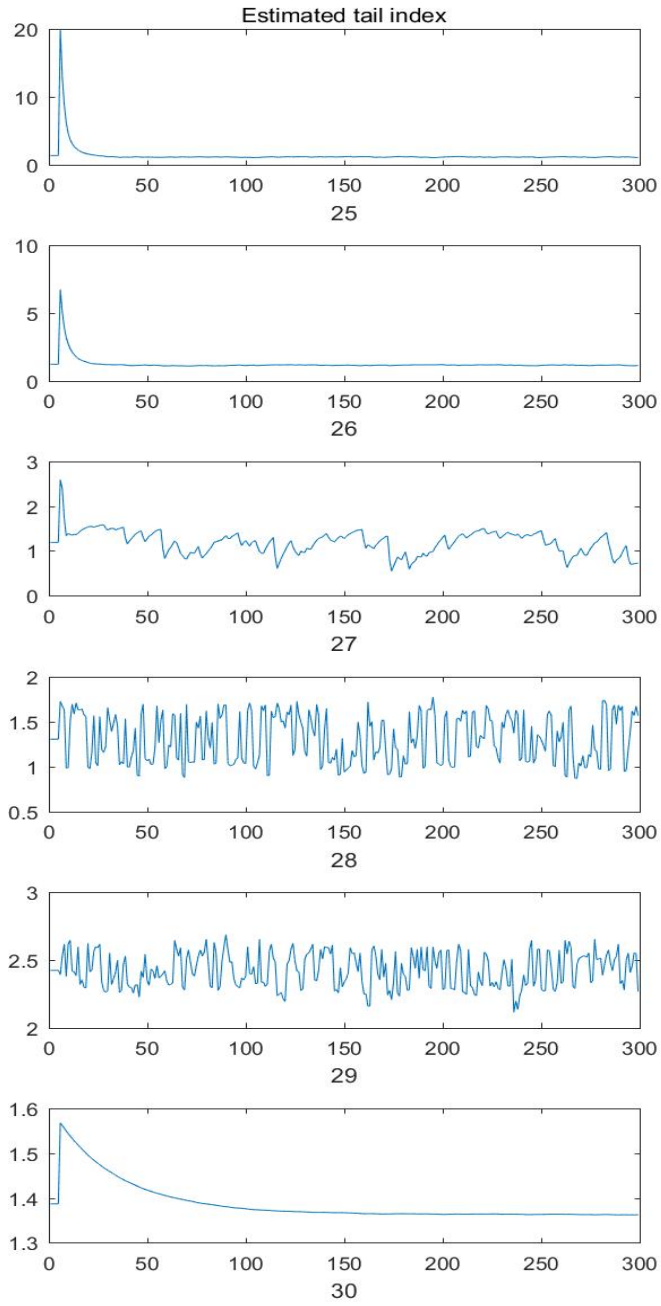
Estimated tail index
25
26
27
28
29
30

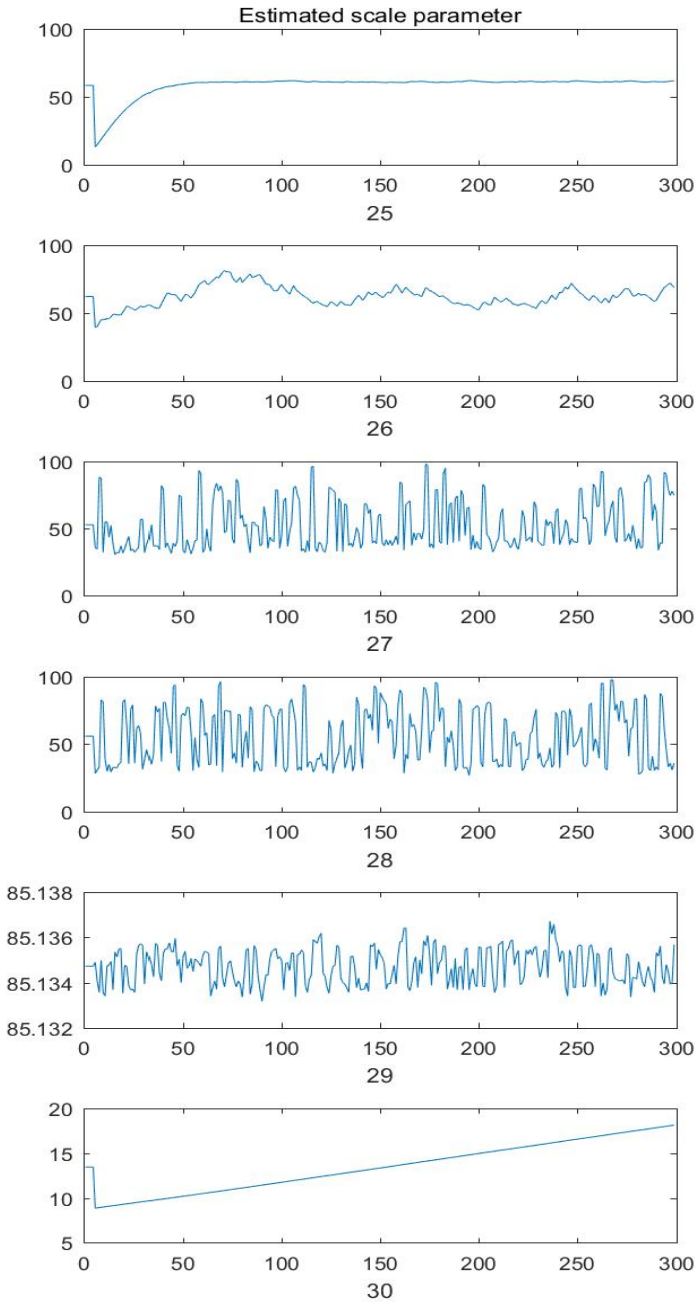
Estimated scale parameter
25
26
27
28
29
30

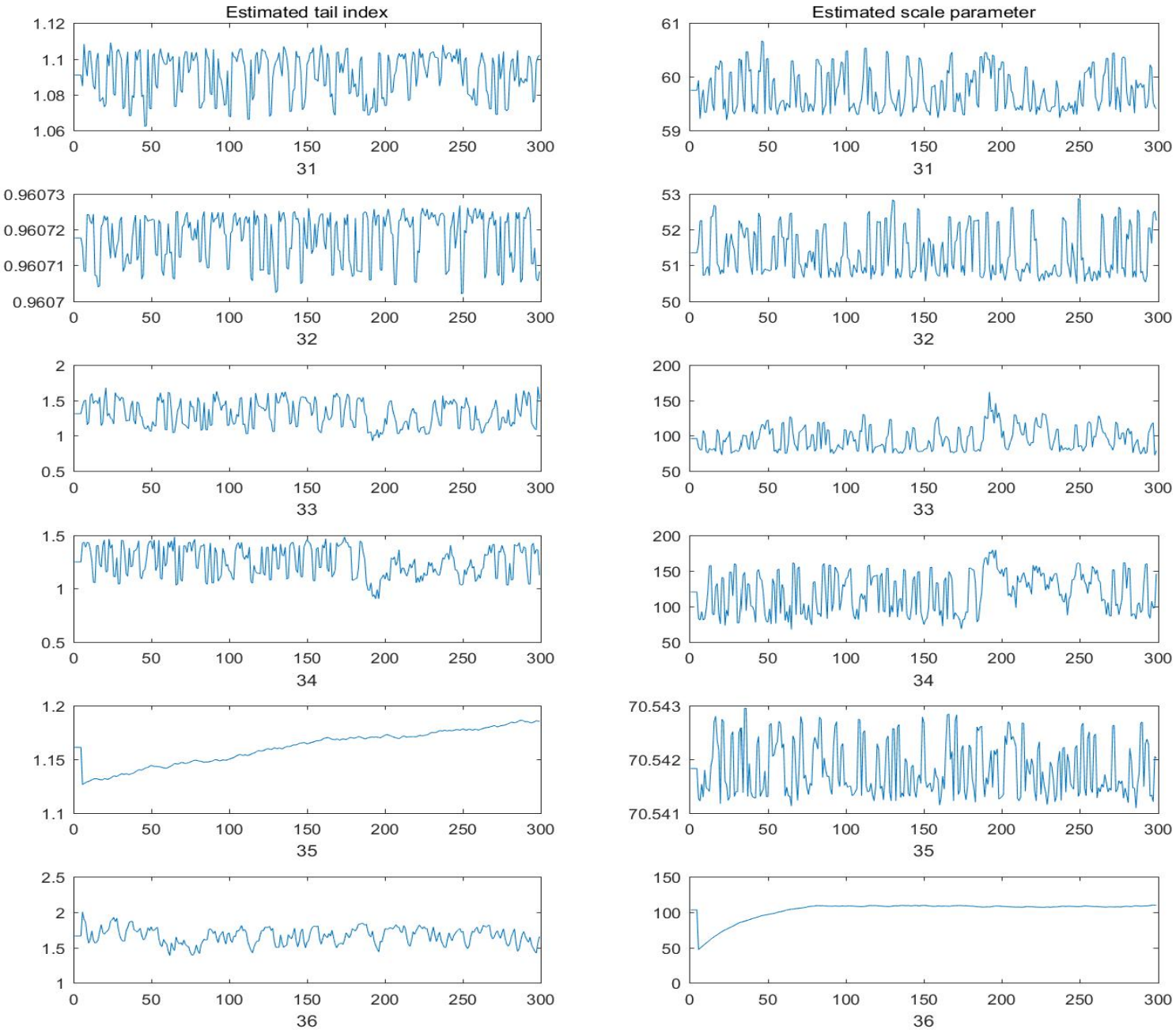
Estimated tail index
Estimated scale parameter
31
32
33
34
35
36

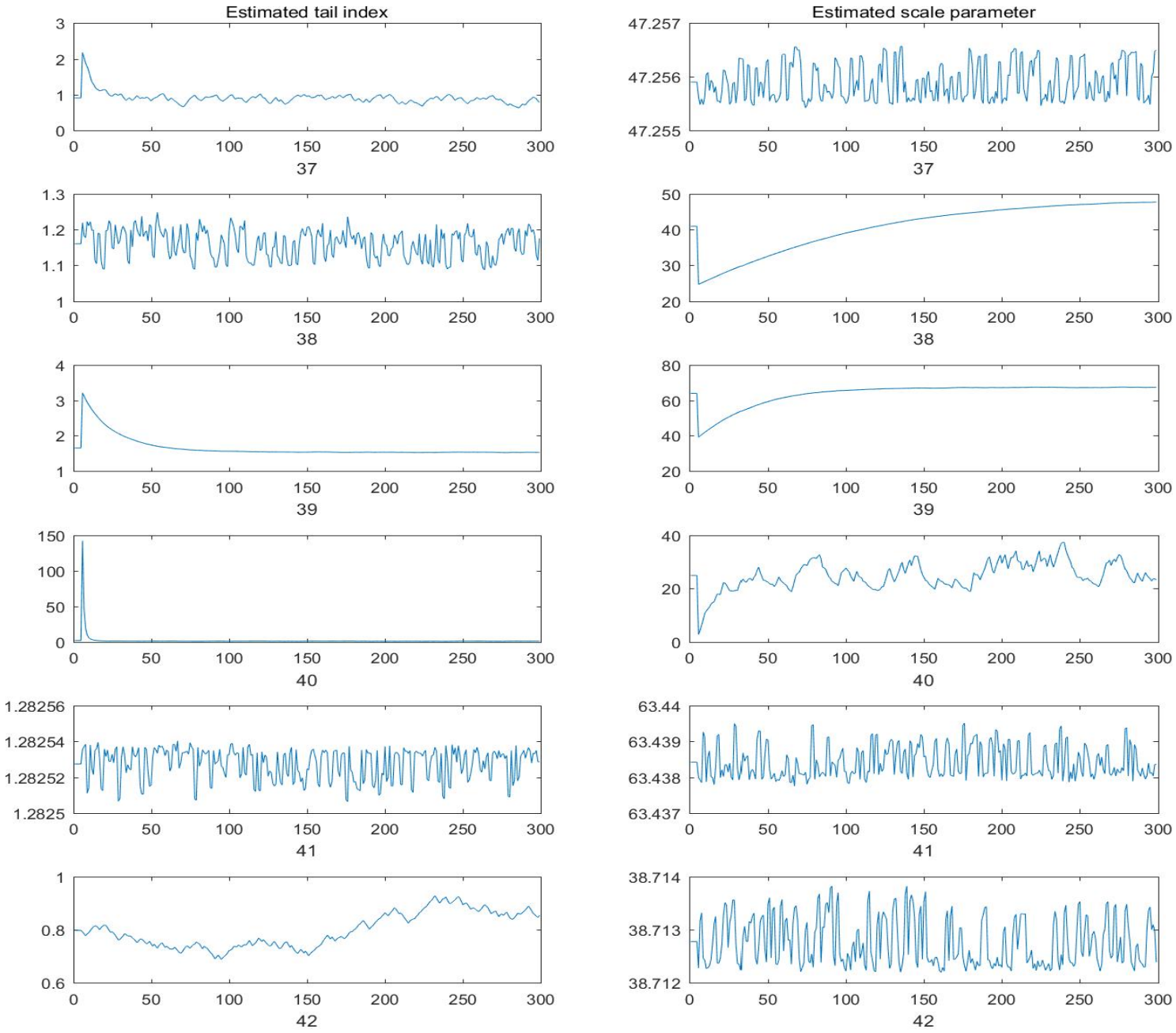
Estimated tail index
Estimated scale parameter
37
38
39
40
41
42

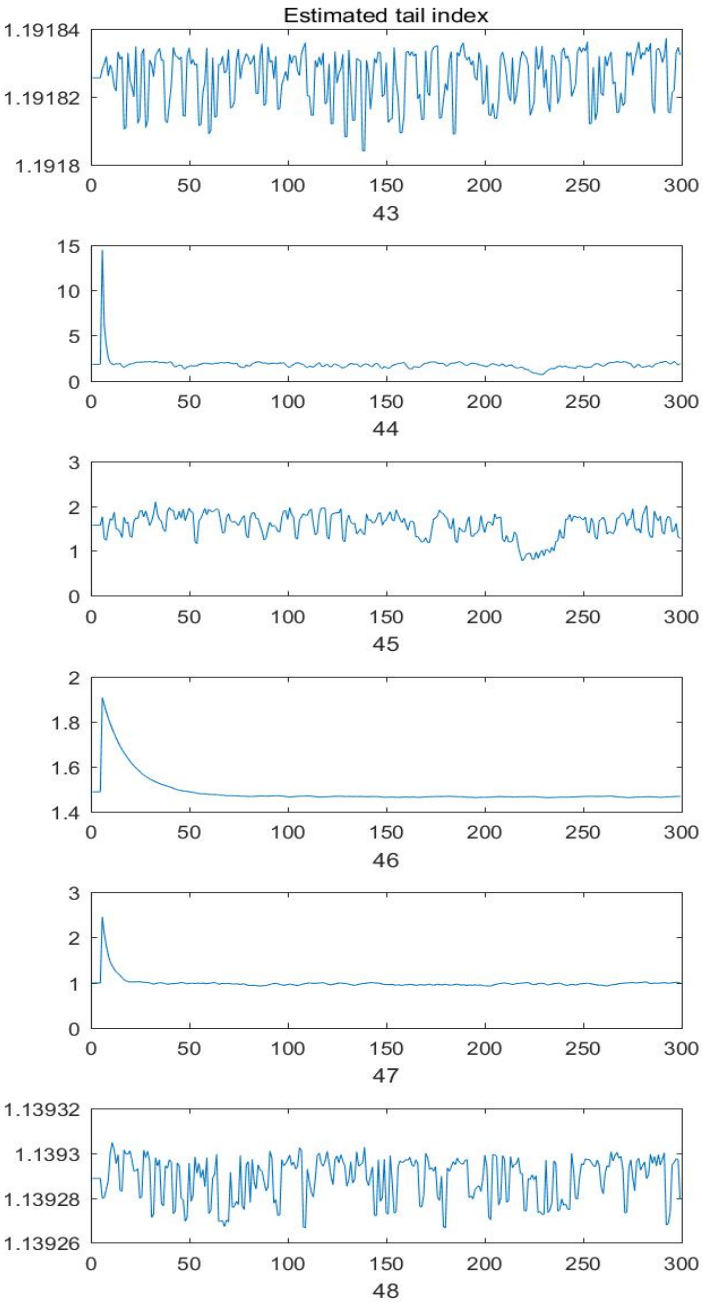
Estimated tail index
1.19184
1.19182
1.1918
0 50 100 150 200 250 300
43
15 10 5 0
0 50 100 150 200 250 300
44
3 2 1 0
0 50 100 150 200 250 300
45
2 1.8 1.6 1.4
0 50 100 150 200 250 300
46
3 2 1 0
0 50 100 150 200 250 300
47
1.13932
1.1393
1.13928
1.13926
0 50 100 150 200 250 300
48

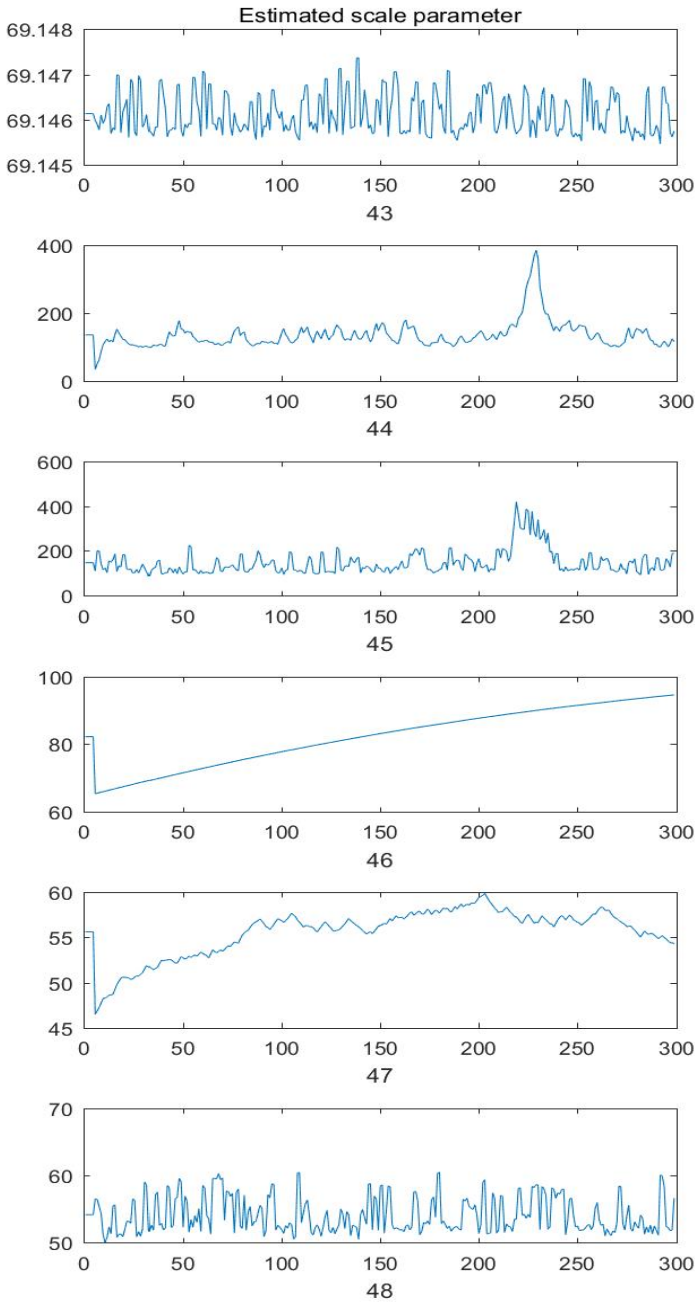
Estimated scale parameter
69.148
69.147
69.146
69.145
0 50 100 150 200 250 300
43
400 200 0
0 50 100 150 200 250 300
44
600 400 200 0
0 50 100 150 200 250 300
45
100 80 60
0 50 100 150 200 250 300
46
60 55 50 45
0 50 100 150 200 250 300
47
70 60 50
0 50 100 150 200 250 300
48

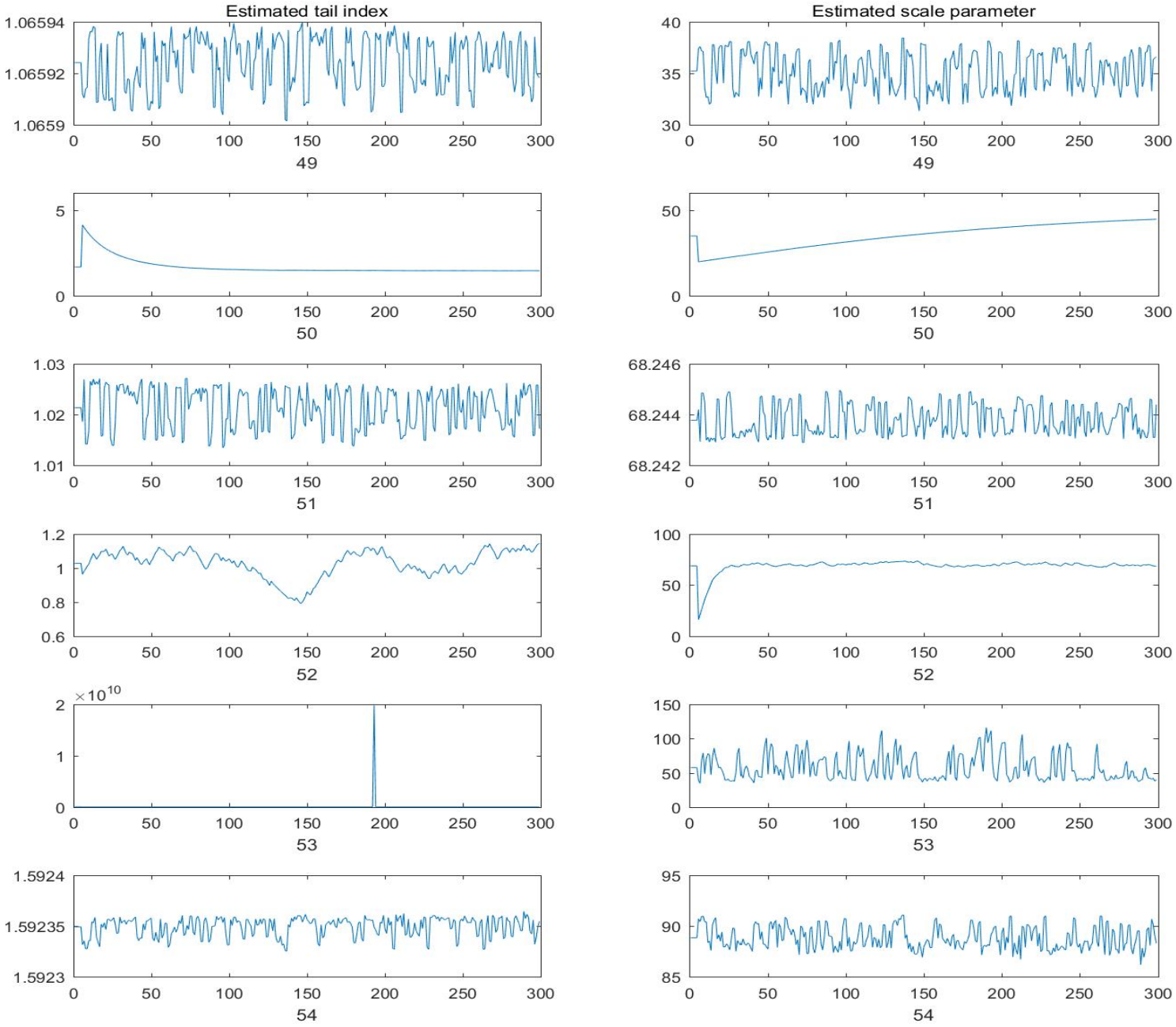
Estimated tail index
Estimated scale parameter
49
50
51
52
53
54
×10^10

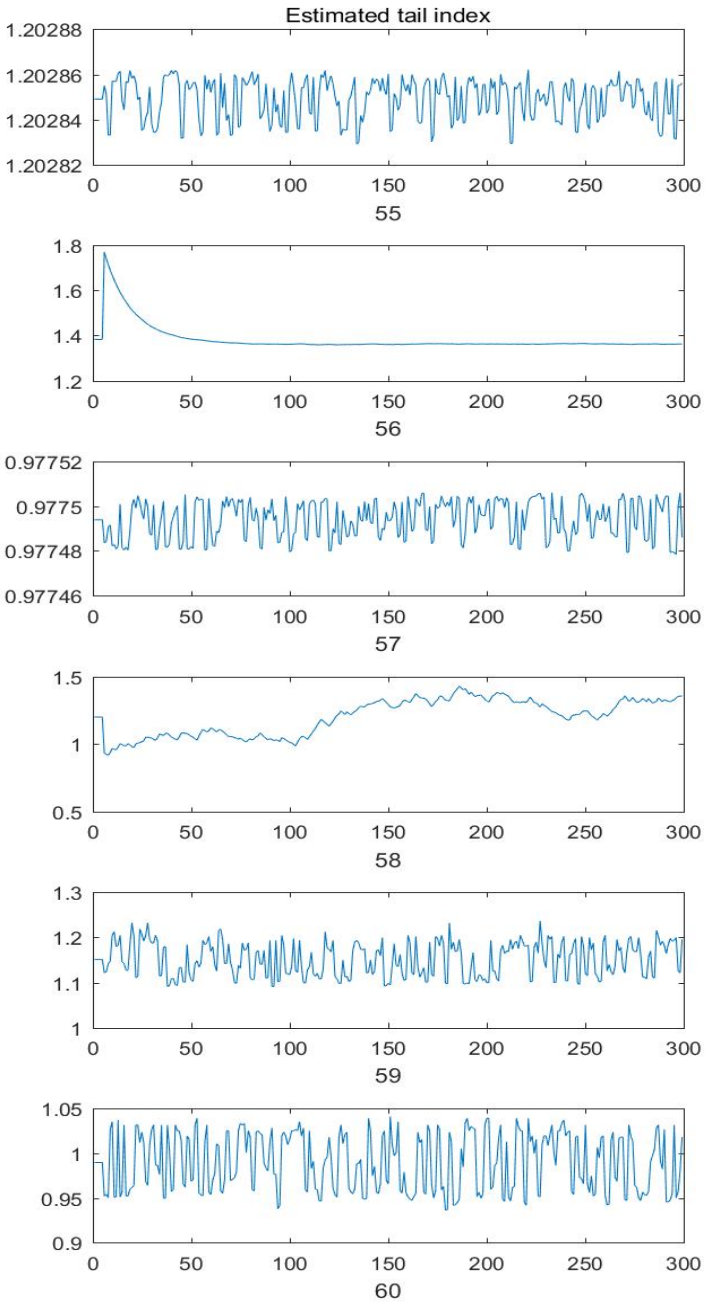
Estimated tail index
1.20288
1.20286
1.20284
1.20282
0 50 100 150 200 250 300
55
1.8
1.6
1.4
1.2
0 50 100 150 200 250 300
56
0.97752
0.9775
0.97748
0.97746
0 50 100 150 200 250 300
57
1.5
1
0.5
0 50 100 150 200 250 300
58
1.3
1.2
1.1
1
0 50 100 150 200 250 300
59
1.05
1
0.95
0.9
0 50 100 150 200 250 300
60

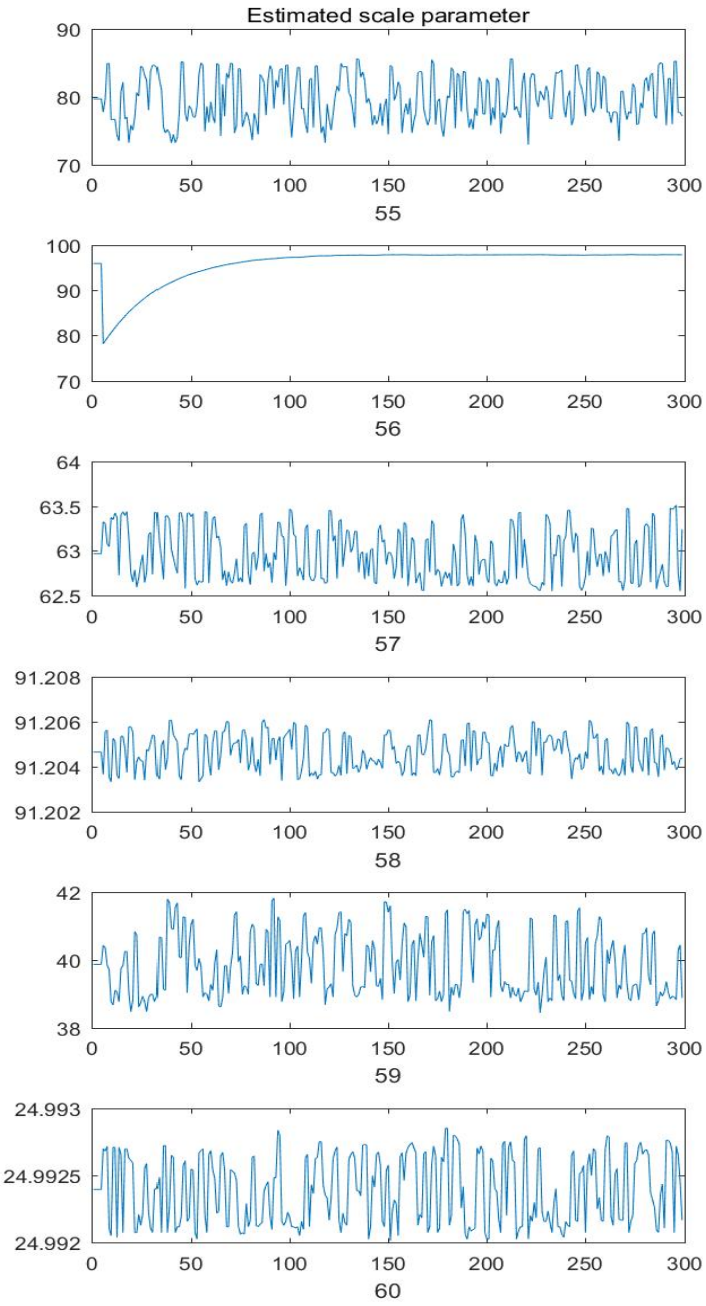
Estimated scale parameter
90
80
70
0 50 100 150 200 250 300
55
100
90
80
70
0 50 100 150 200 250 300
56
64
63.5
63
62.5
0 50 100 150 200 250 300
57
91.208
91.206
91.204
91.202
0 50 100 150 200 250 300
58
42
40
38
0 50 100 150 200 250 300
59
24.993
24.9925
24.992
0 50 100 150 200 250 300
60

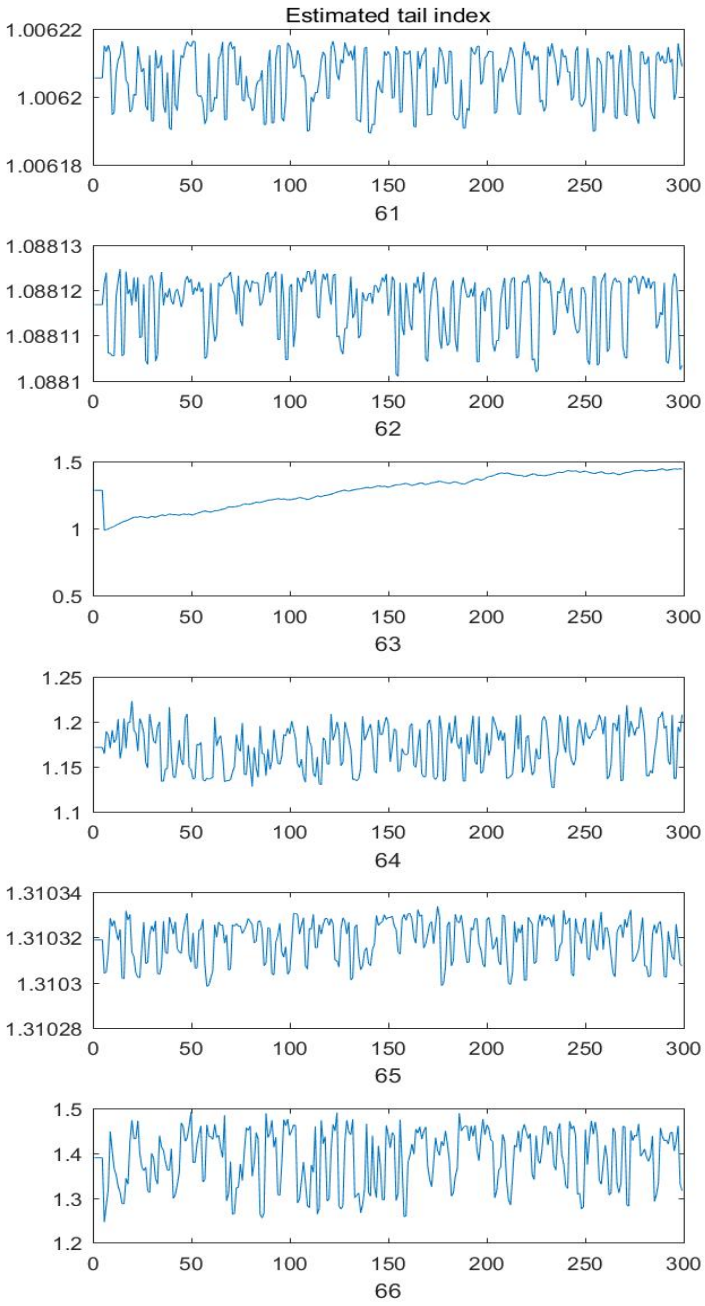
Estimated tail index
1.00622
1.0062
1.00618
0 50 100 150 200 250 300
61
1.08813
1.08812
1.08811
1.0881
0 50 100 150 200 250 300
62
1.5
1
0.5
0 50 100 150 200 250 300
63
1.25
1.2
1.15
1.1
0 50 100 150 200 250 300
64
1.31034
1.31032
1.3103
1.31028
0 50 100 150 200 250 300
65
1.5
1.4
1.3
1.2
0 50 100 150 200 250 300
66

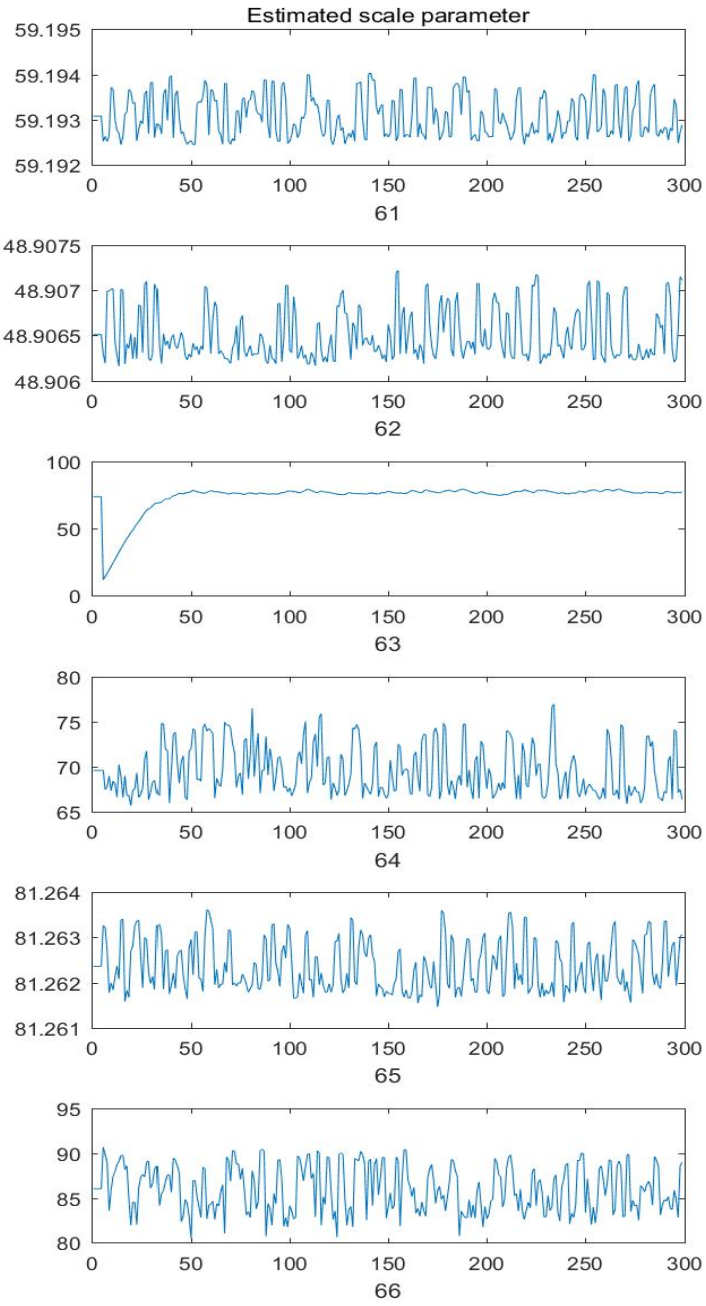
Estimated scale parameter
59.195
59.194
59.193
59.192
0 50 100 150 200 250 300
61
48.9075
48.907
48.9065
48.906
0 50 100 150 200 250 300
62
100
50
0
0 50 100 150 200 250 300
63
80
75
70
65
0 50 100 150 200 250 300
64
81.264
81.263
81.262
81.261
0 50 100 150 200 250 300
65
95
90
85
80
0 50 100 150 200 250 300
66

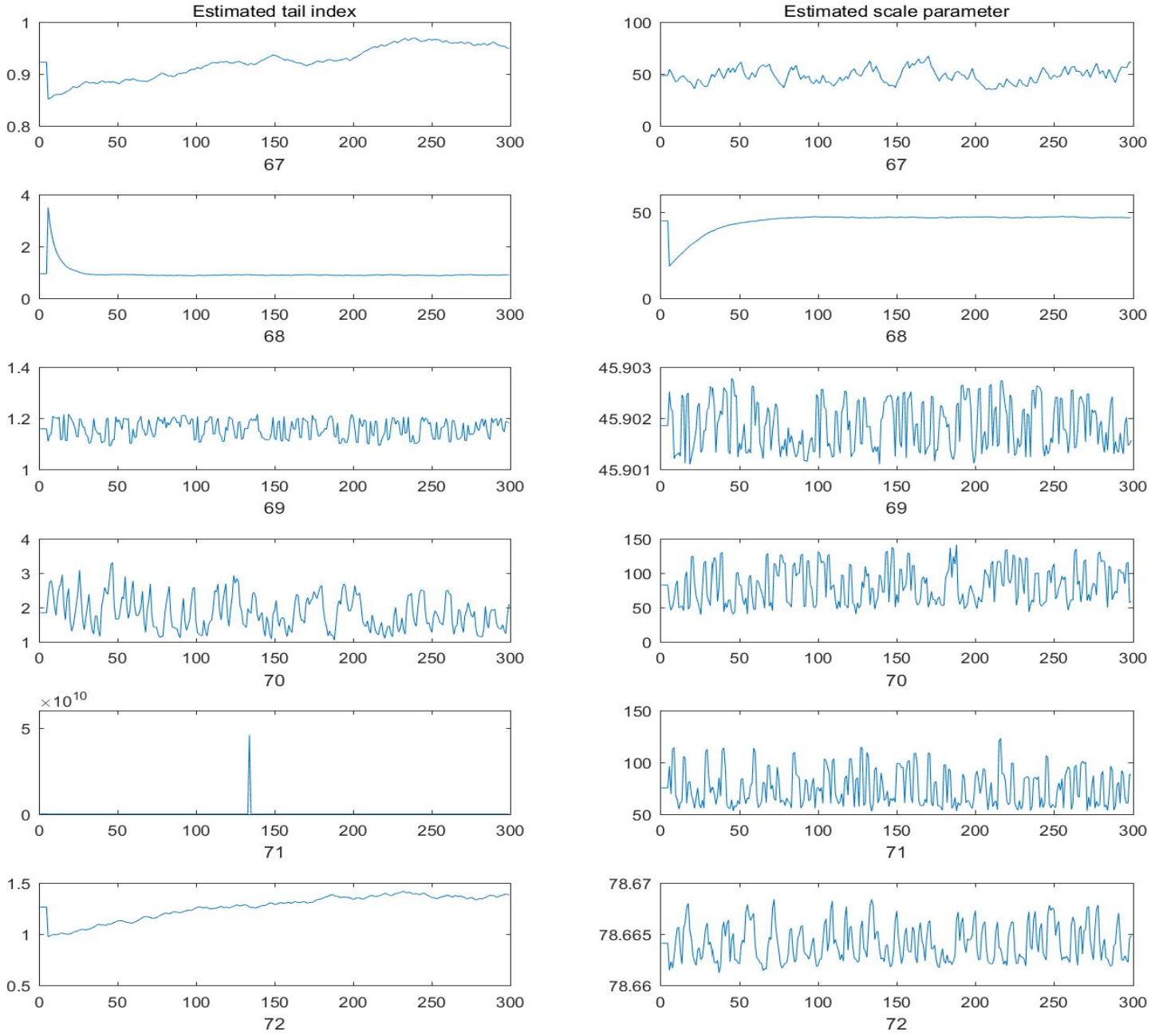
Estimated tail index
Estimated scale parameter
67
68
69
70
71
72
×10^10

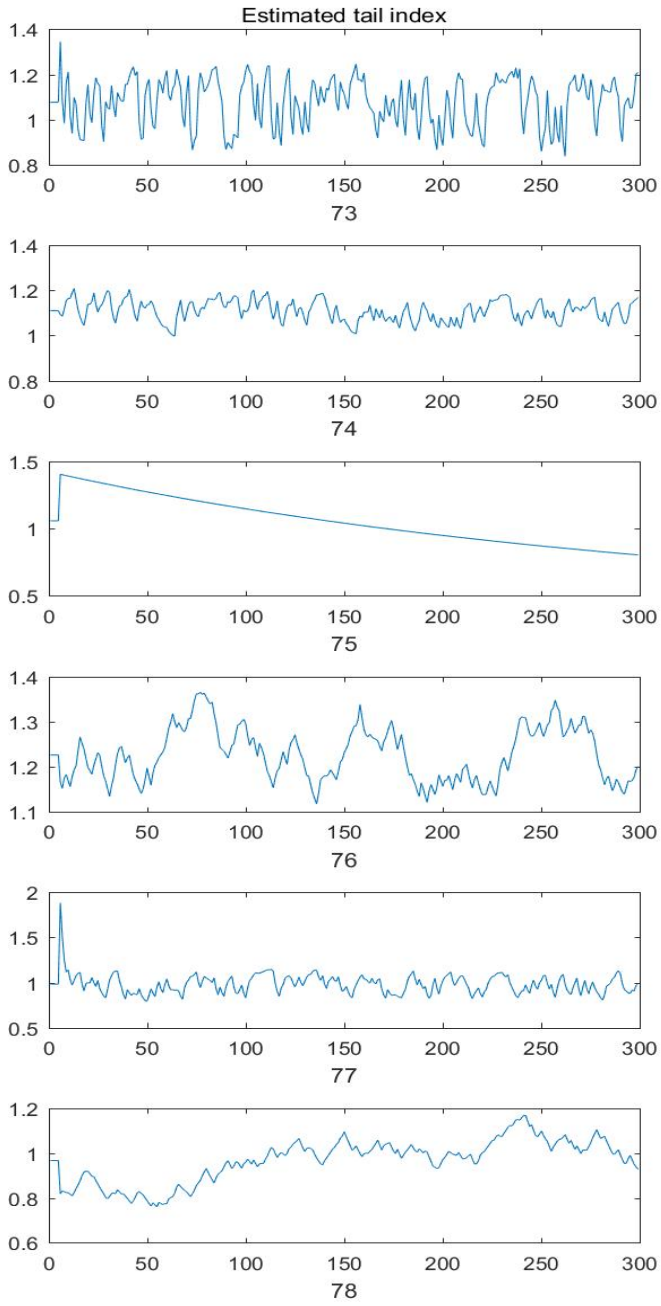
Estimated tail index
73
74
75
76
77
78

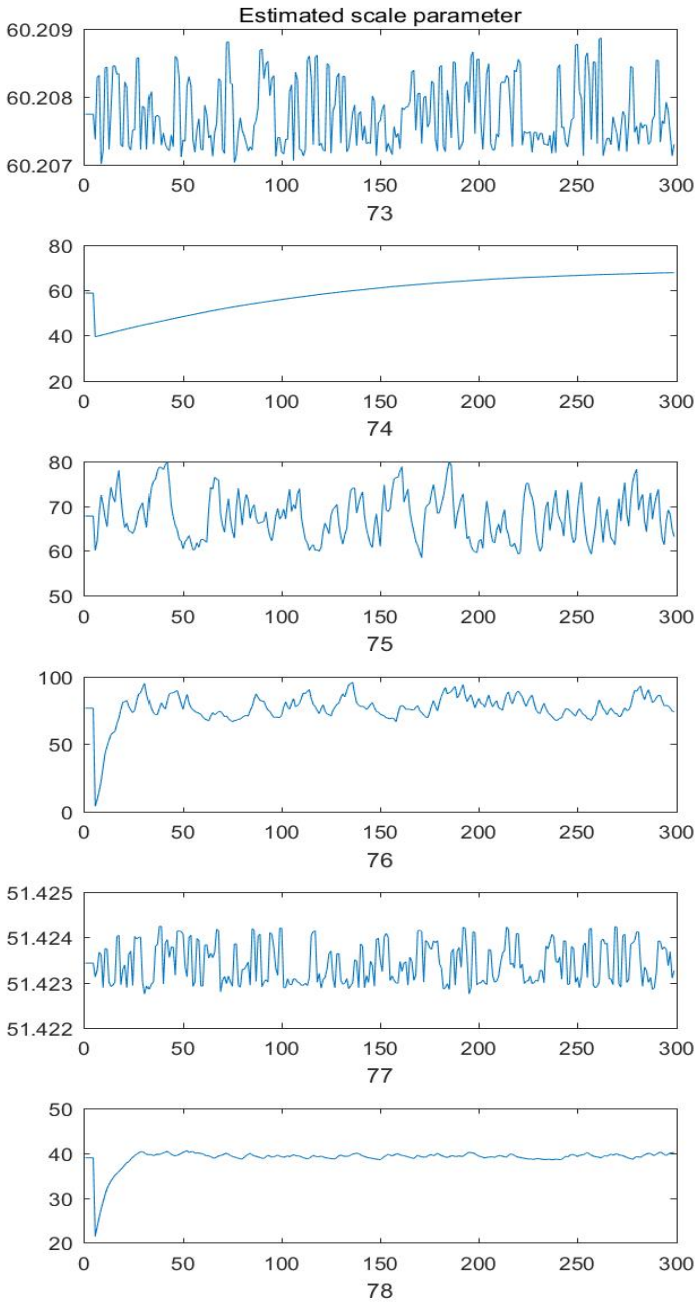
Estimated scale parameter
73
74
75
76
77
78

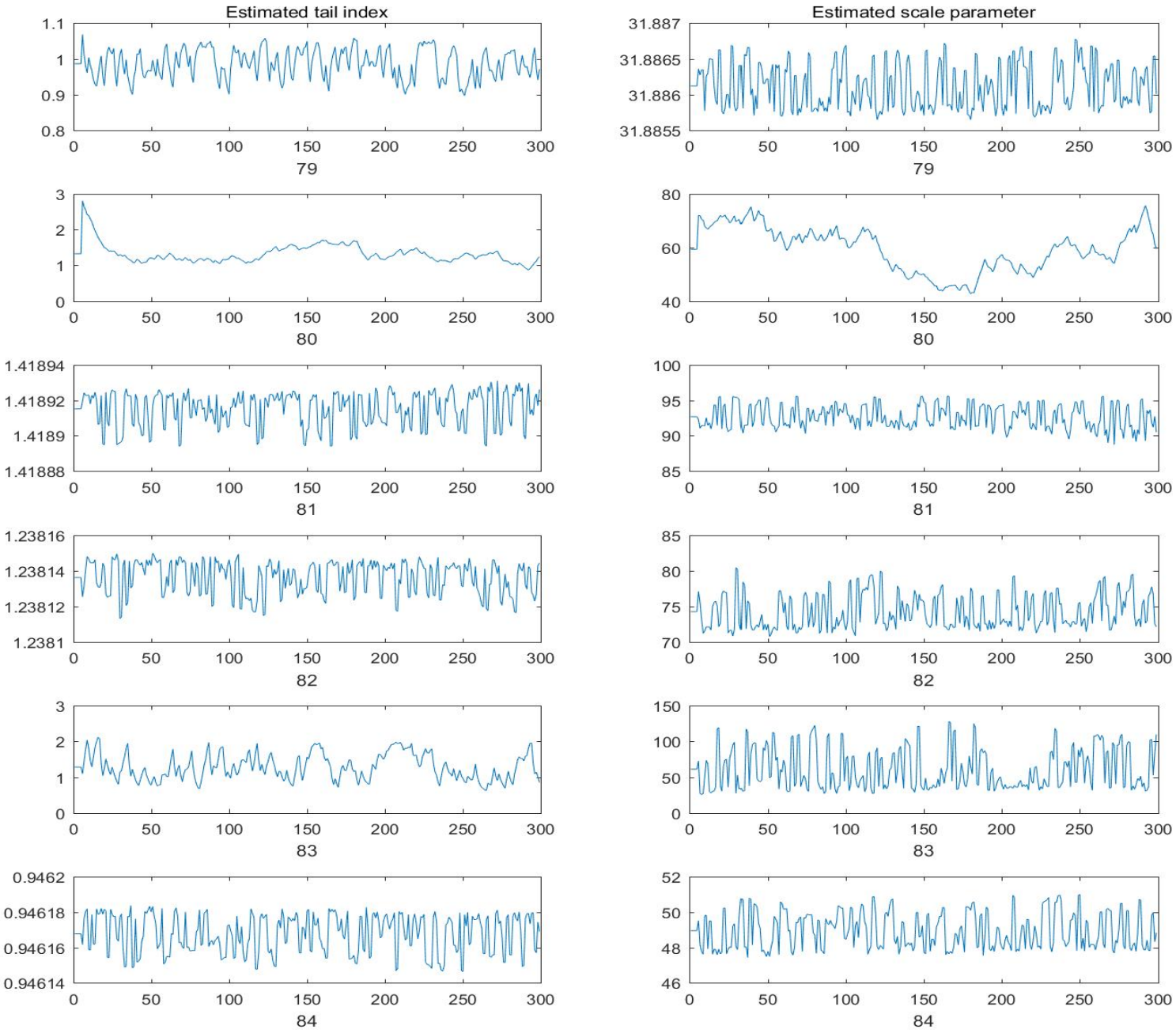
Estimated tail index
Estimated scale parameter
79
80
81
82
83
84

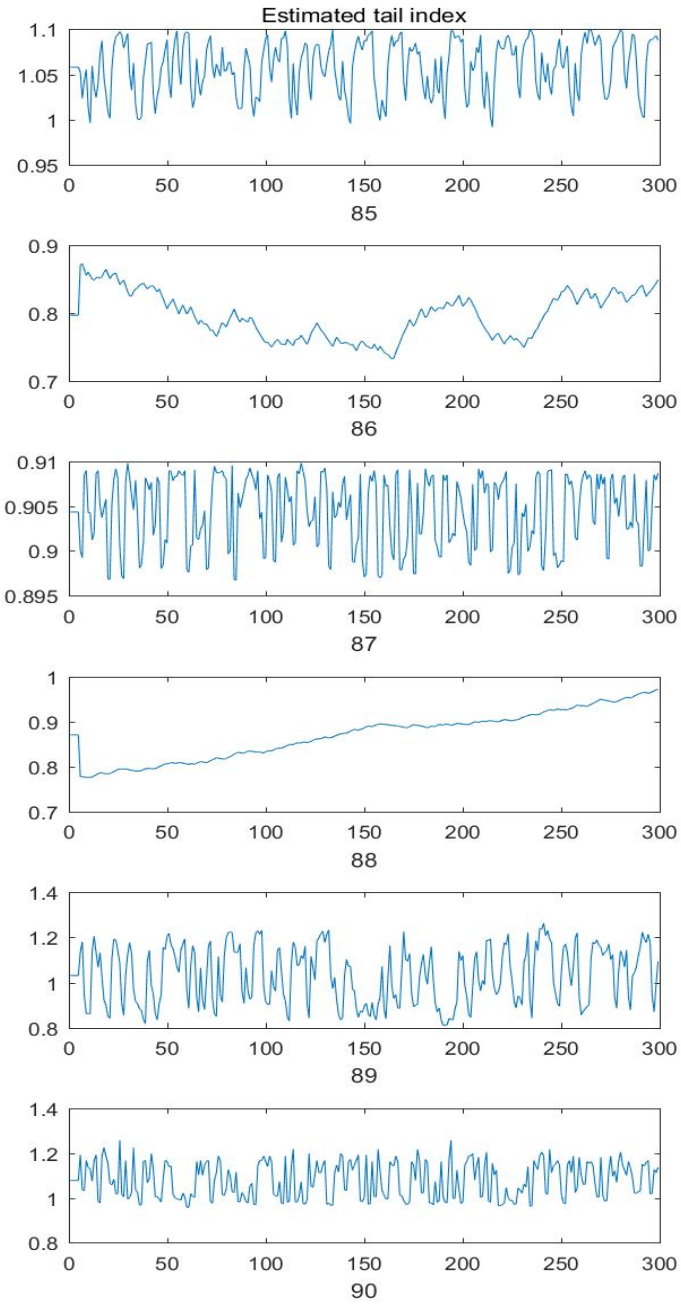
Estimated tail index
85
86
87
88
89
90

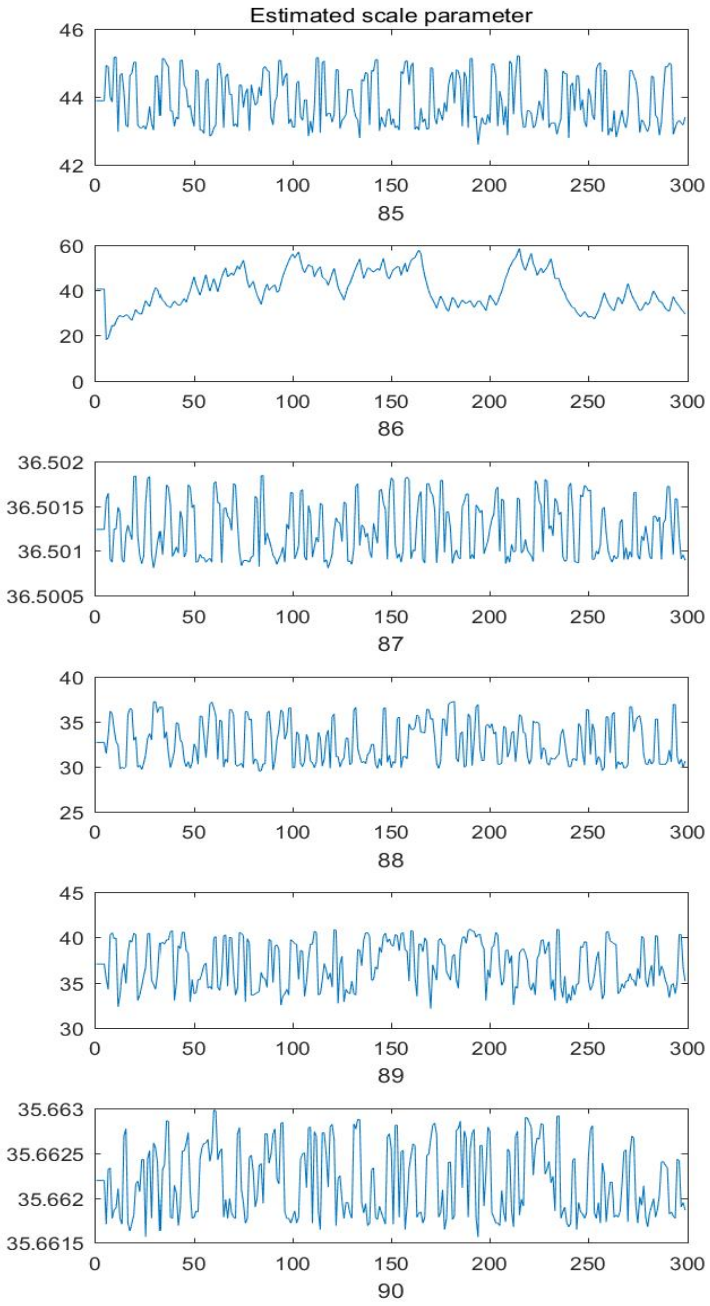
Estimated scale parameter
85
86
87
88
89
90

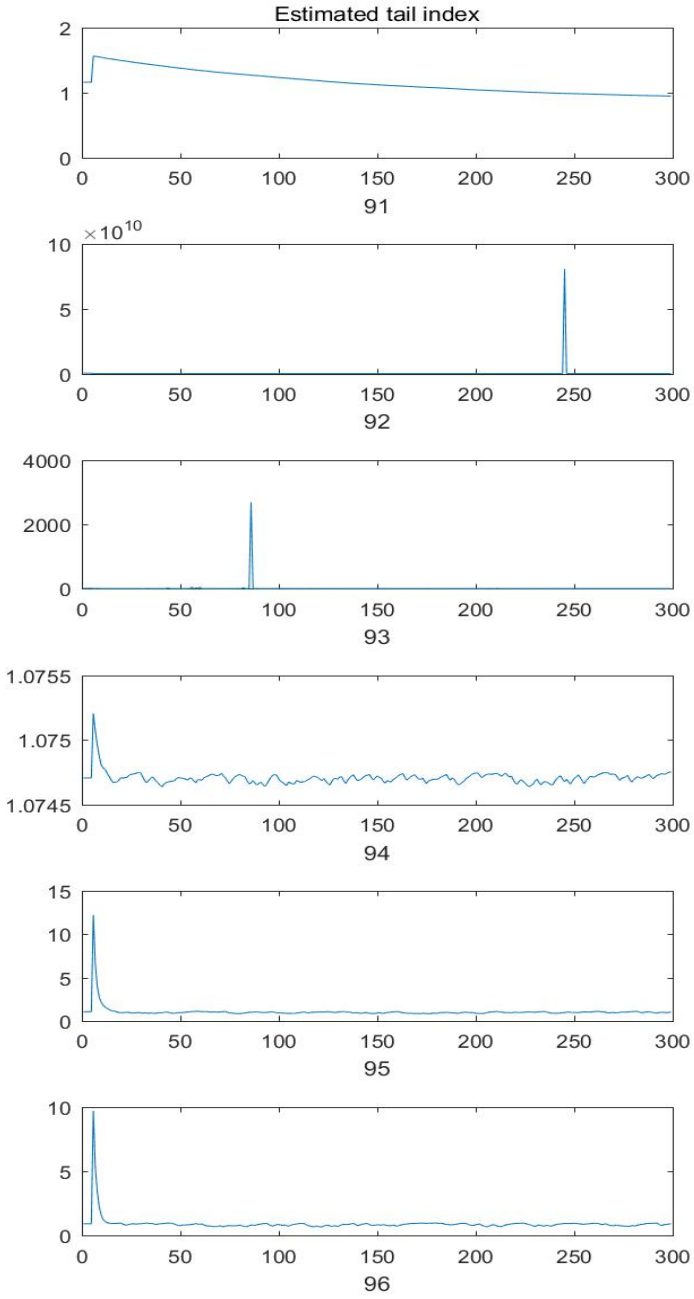
Estimated tail index
91
92
93
94
95
96

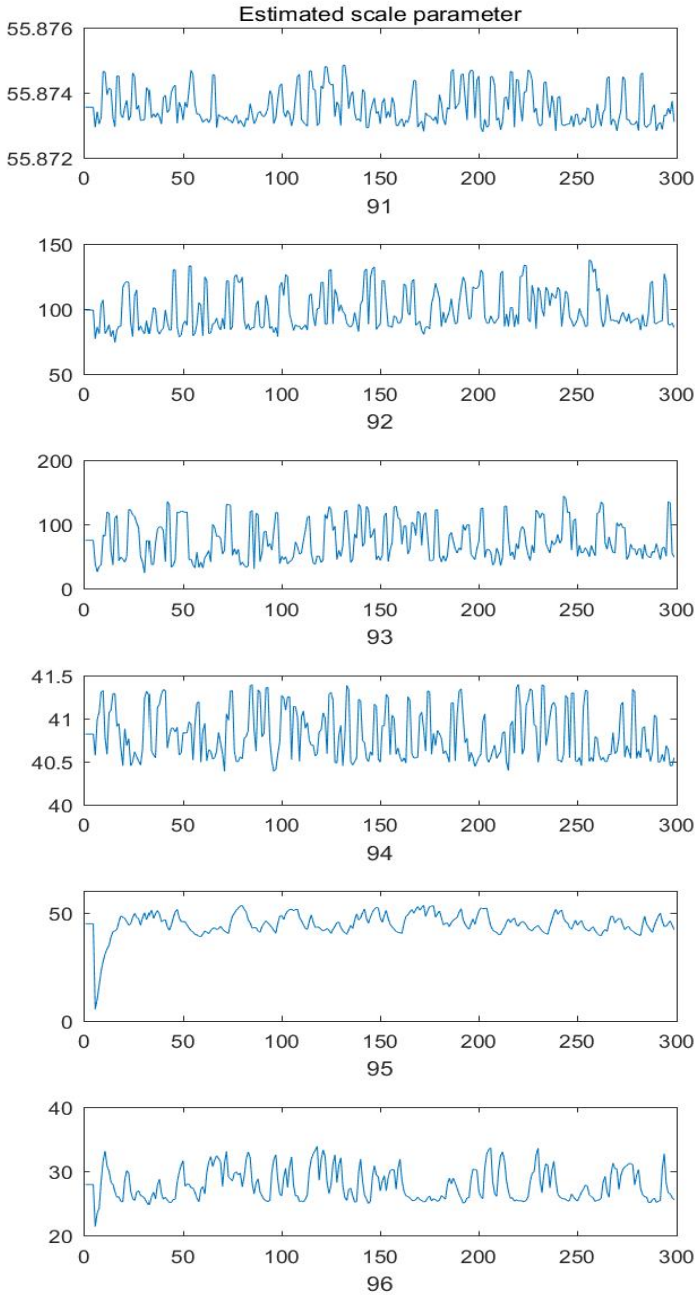
Estimated scale parameter
91
92
93
94
95
96

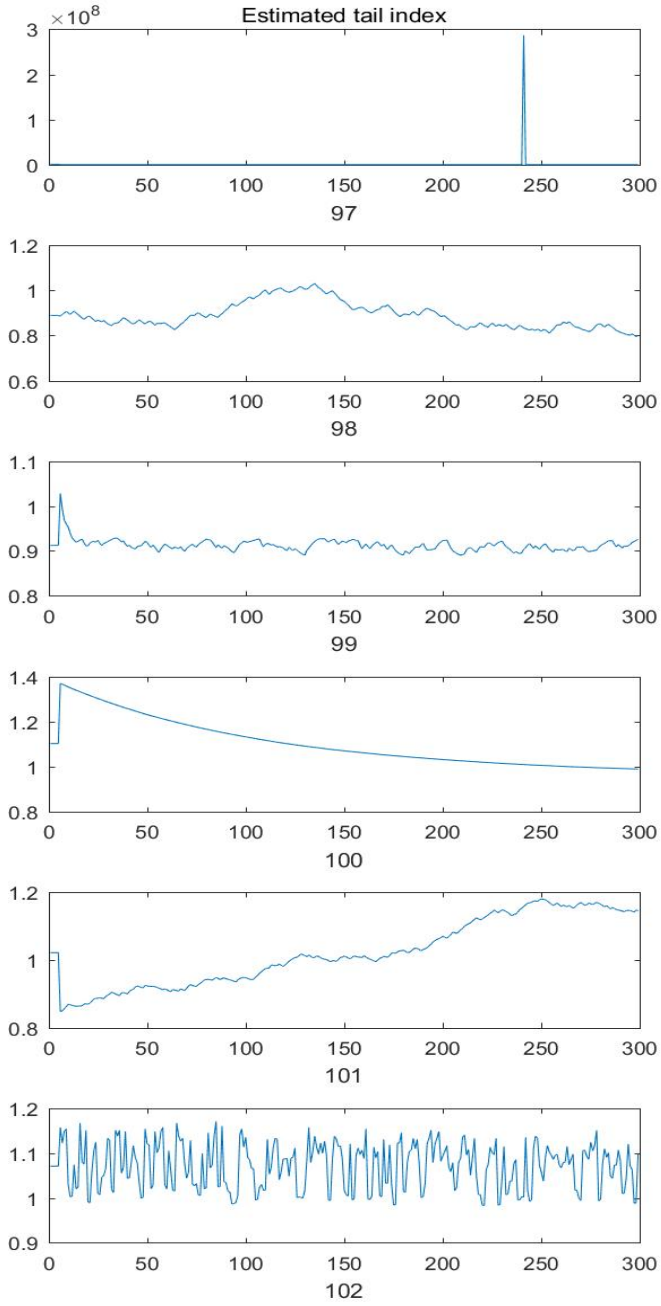
Estimated tail index
×10^8
97
98
99
100
101
102

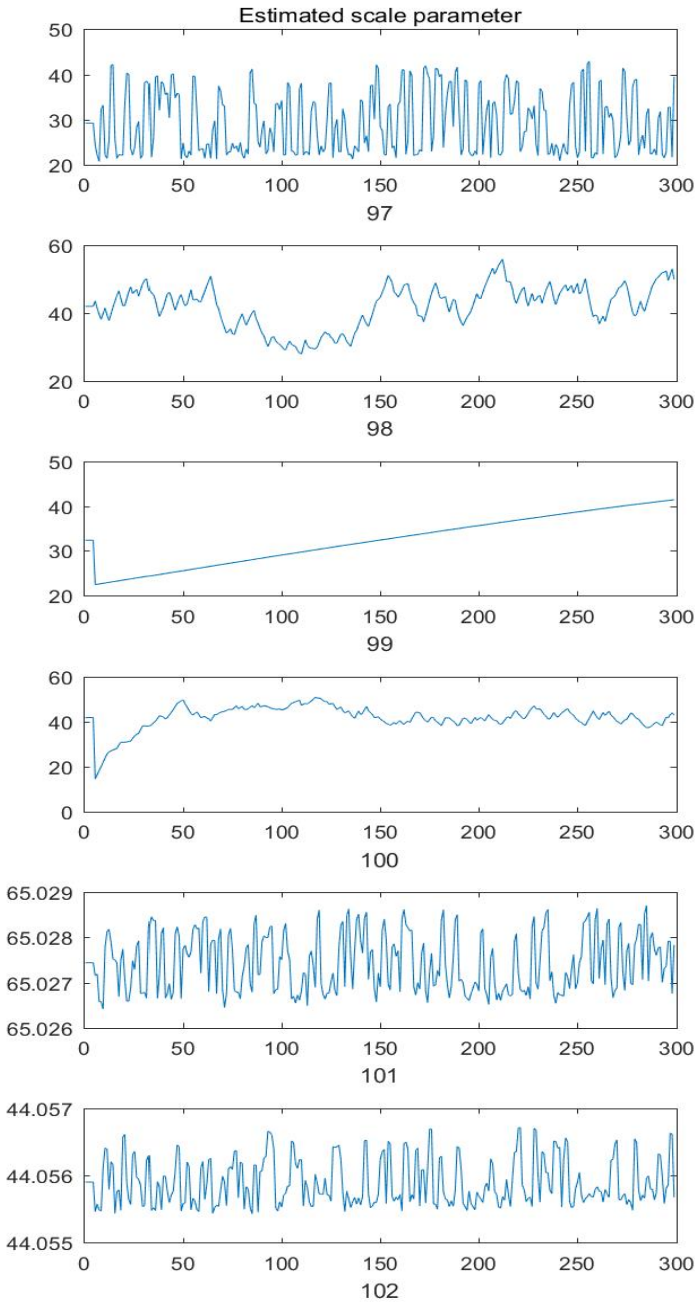
Estimated scale parameter
97
98
99
100
101
102

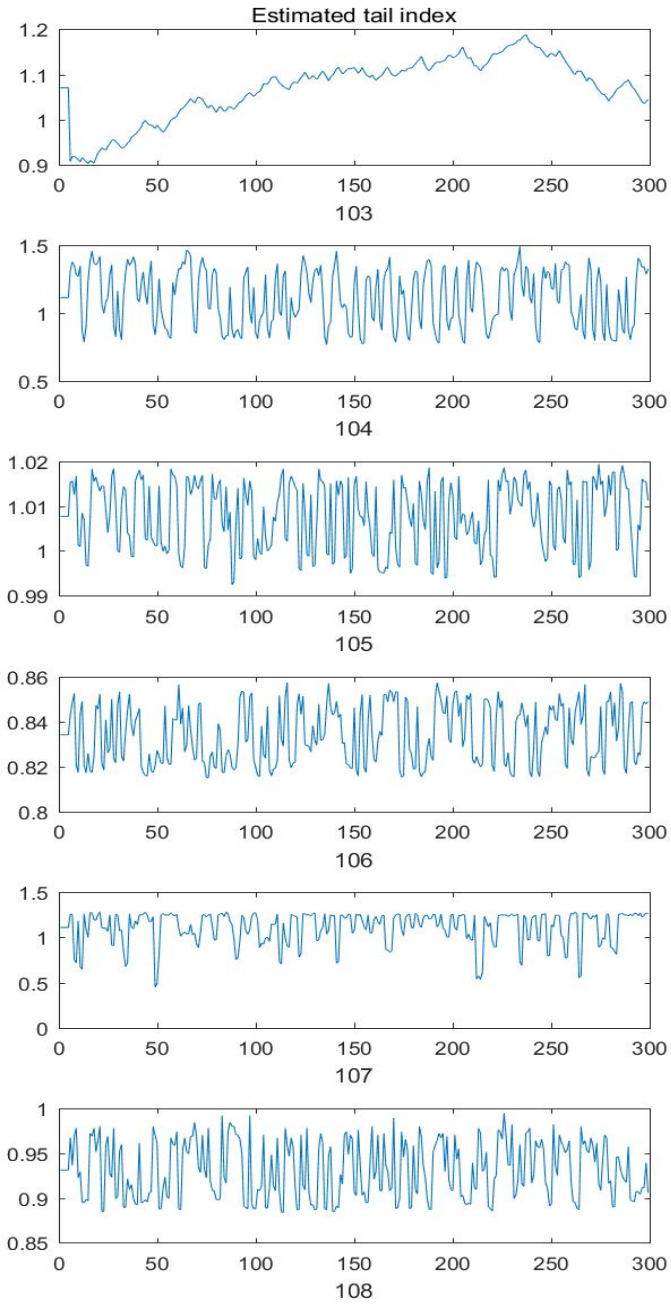
Estimated tail index
103
104
105
106
107
108

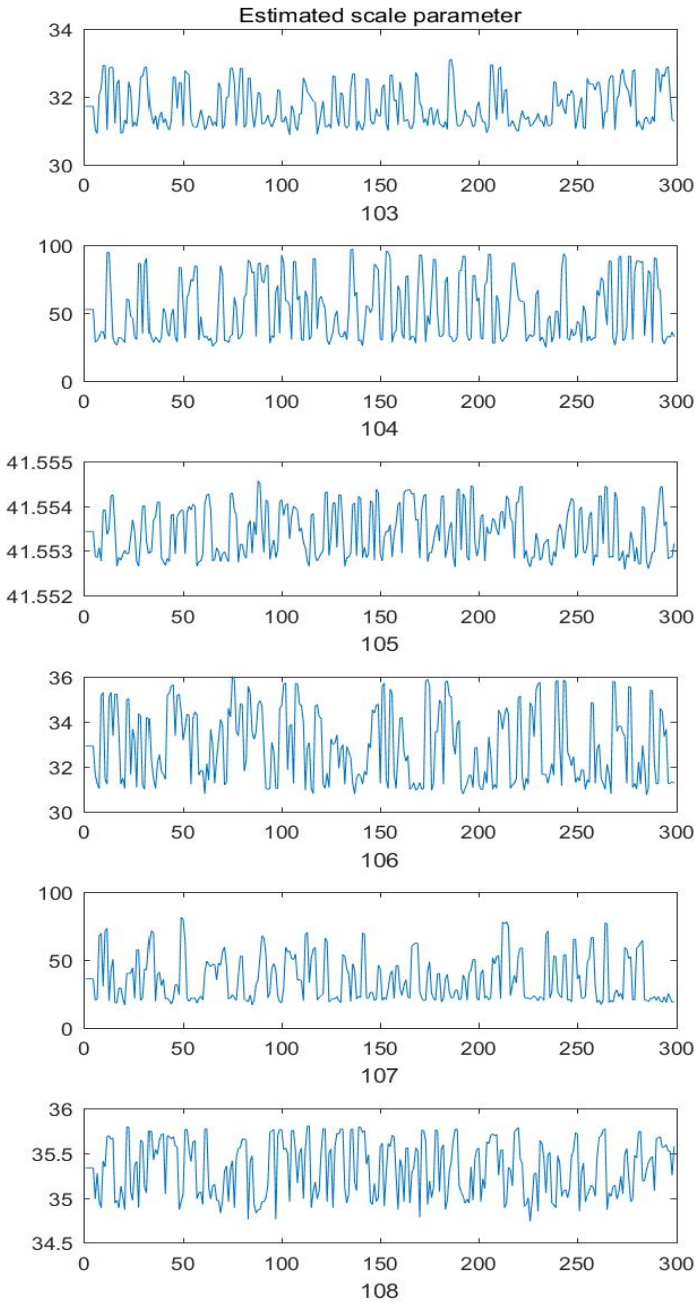
Estimated scale parameter
103
104
105
106
107
108

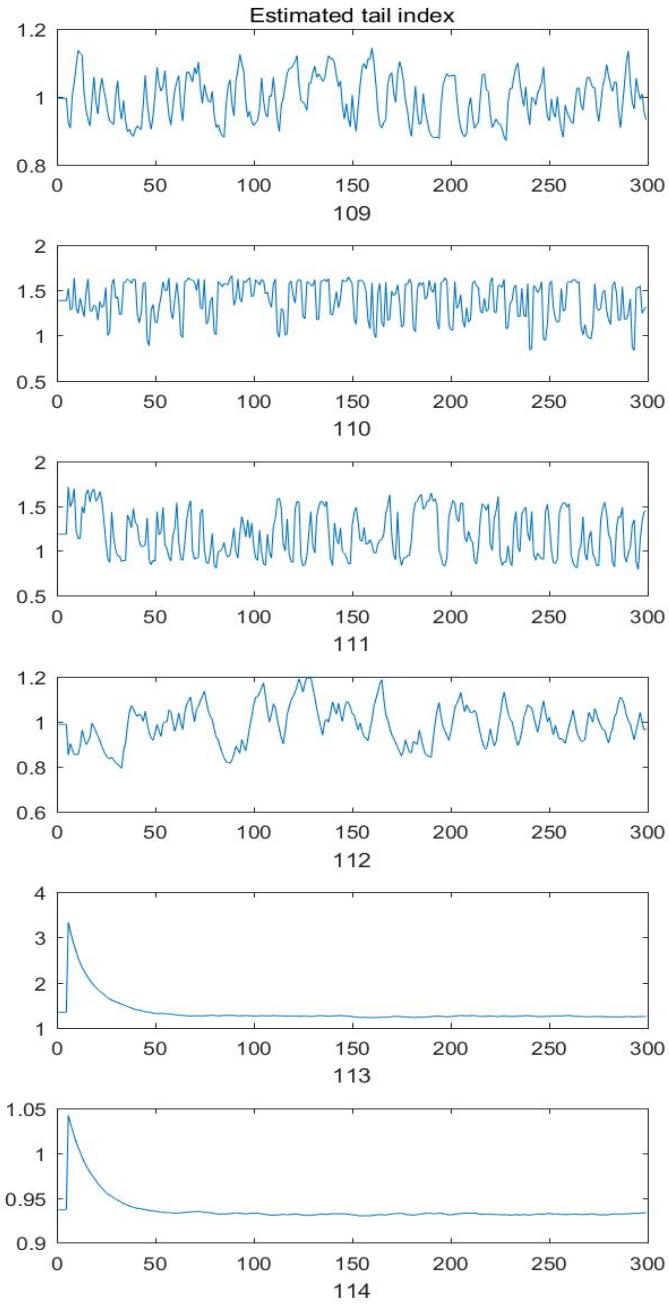
Estimated tail index
109
110
111
112
113
114

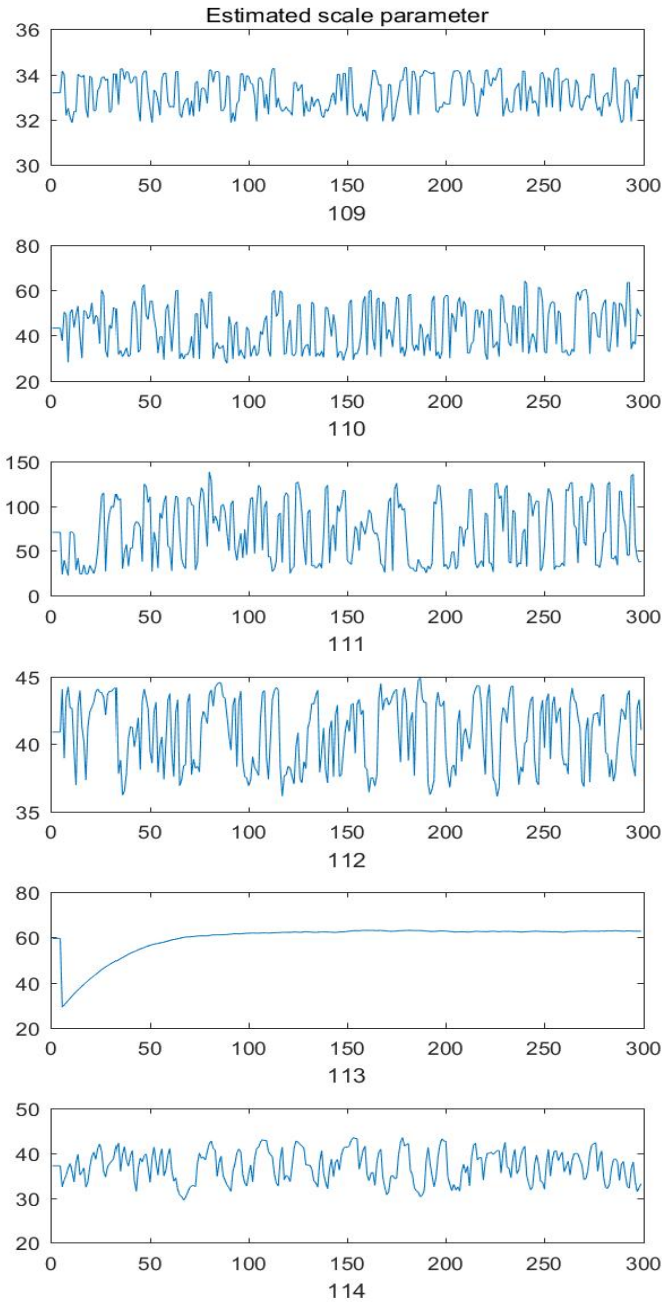
Estimated scale parameter
109
110
111
112
113
114

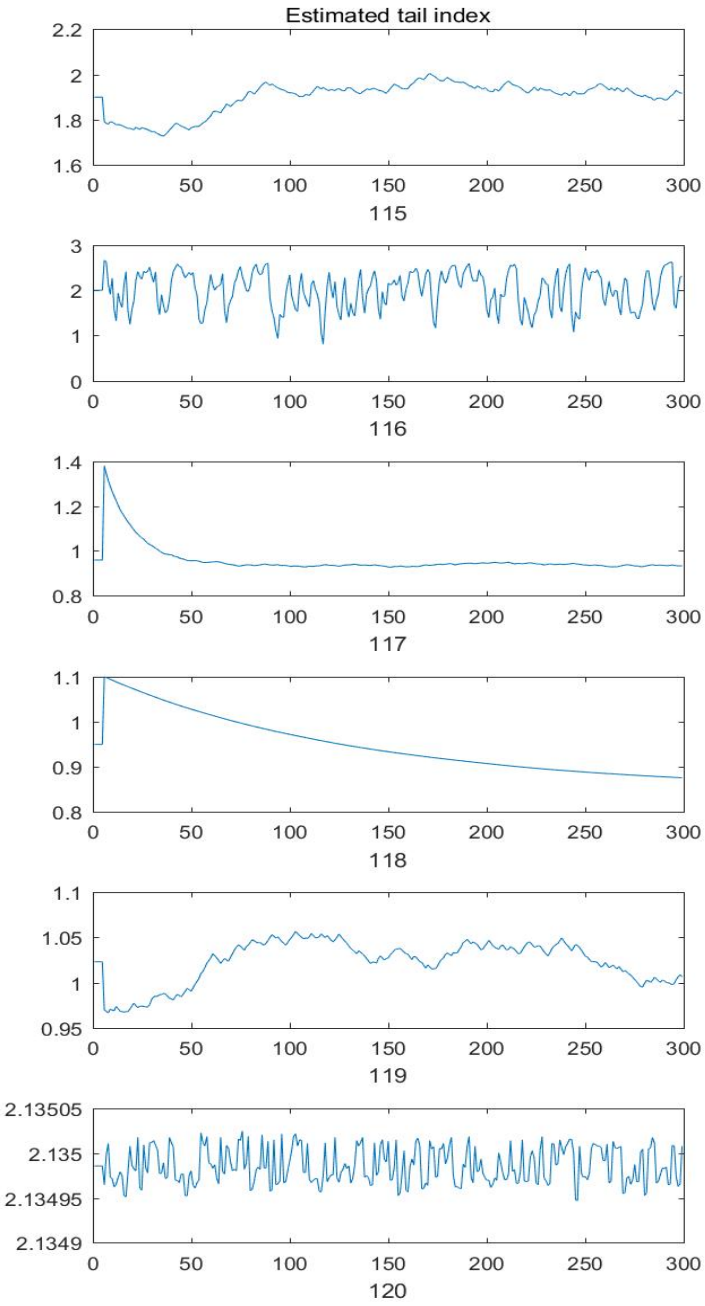
Estimated tail index
115
116
117
118
119
120

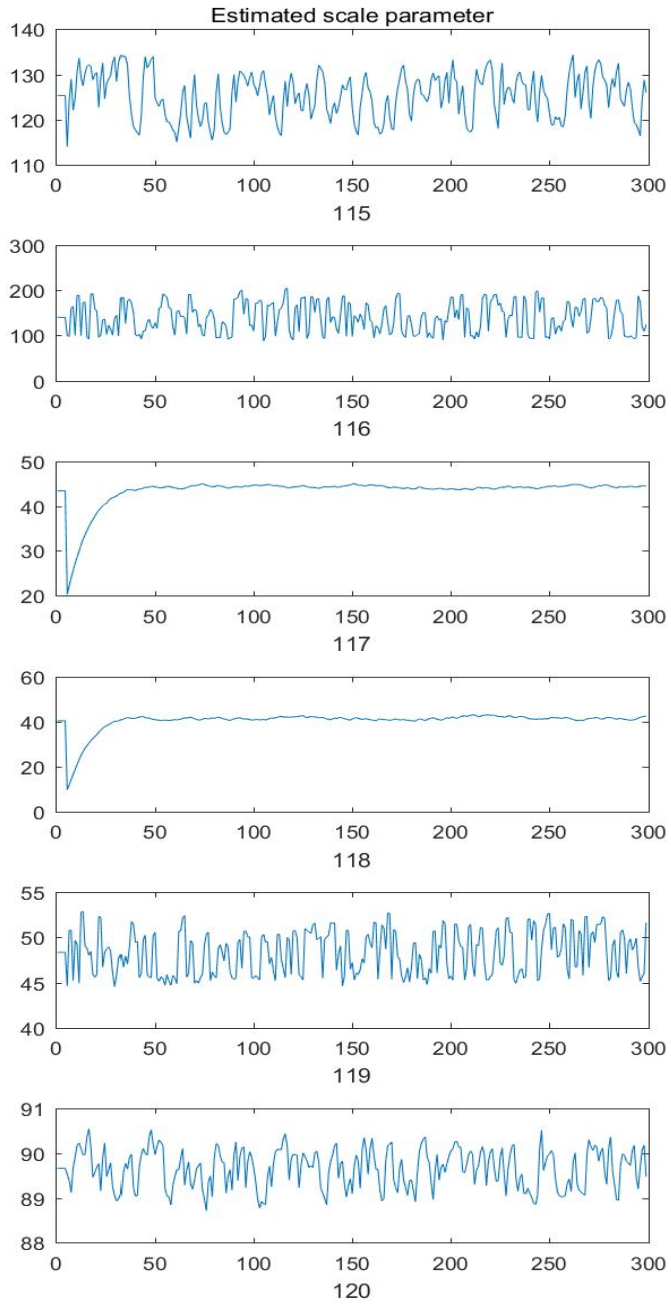
Estimated scale parameter
115
116
117
118
119
120

7.3 AcFL model with spatial correlation

Part	γ_0	γ_1	γ_2	γ_3	γ_4	γ_5	β_0	β_1	β_2	β_3	β_4	β_5	μ
1	-3.914	0	29.023	15.782	6.632	21.873	5.404	0	1.523	0.022	0	0	102.532
2	-2.796	0	25.232	19.408	0.227	0.017	12.593	0	63.423	88.077	20.255	60.333	102.034
3	-3.385	0	30.676	28.69	0.274	0.018	7.838	0	13.536	0.682	5.172	6.862	60.513
4	-1.514	0.399	13.073	23.733	0	0	13.232	0	75.231	91.396	14.007	31.293	79.182
5	-3.199	0	34.379	117.856	0	0	5.584	0	3.074	0.057	0.387	0.021	79.76
6	-3.384	0.044	33.001	126.519	0.686	0.02	7.599	0	18.597	1.286	0	0	72.851
7	-2.813	0.218	29.197	58.597	0	0	9.742	0	56.529	274.267	0	0	36.397
8	-2.8	0.281	32.76	749.106	0	0	5.703	0	7.152	0.231	0	0	45.705
9	-2.377	0.153	21.249	40	1.416	8.454	7.486	0	27.045	19.118	1.109	14.261	24.941
10	-0.402	0.844	1.245	0.257	0	0	10.961	0	71.24	145.155	0	0	22.328
11	-1.657	0	1.861	0.02	8.138	14.205	11.794	0	67.807	37.946	0.09	0.016	113.933
12	-2.813	0.197	25.662	25.552	0.173	0.016	8.266	0	14.692	0.298	4.612	15.557	119.911
13	-3.33	0.025	39.176	145.599	0	0	5.97	0	3.348	0.062	0	0	59.772
14	-2.951	0.181	25.373	237.12	6.319	11.809	11.009	0	61.646	56.414	1.394	11.205	77.936
15	-3.882	0.453	43.348	241.756	0	0	14.059	0	95.236	175.668	8.431	42.759	92.242
16	-3.005	0.027	29.101	55.63	1.49	20	7.712	0	5.577	0.072	13.692	38.856	89.188
17	-2.786	0	30.075	78.592	0	0	5.345	0	1.81	0.037	0	0	55.45
18	-2.839	0.053	22.353	13.135	0.743	0.023	6.684	0	7.67	0.596	5.074	8.632	21.096
19	-1.922	0.102	17.044	24.536	0	0	6.217	0	9.224	0.441	1.836	9.883	32.784
20	-3.88	0	39.884	99.516	0	0	4.961	0	5.261	0.557	0.236	0.051	17.099
21	-4.49	0	33.82	54.766	9.884	16.985	10.734	0	64.271	73.35	0	0	101.138
22	-2.845	0.081	23.589	67.362	1.385	0.015	12.76	0	68.228	87.164	16.777	47.31	115.019
23	-3.417	0.048	35.394	59.349	0.504	0.01	12.616	0	68.111	81.109	9.313	17.564	74.951
24	-2.268	0.199	21.242	36.893	0	0	6.551	0	3.037	0.05	7.991	11.114	87.993
25	-2.278	0.492	21.581	40	0	0	8.791	0	26.759	1.565	0	0	94.435
26	-3.639	0	39.212	88.143	0	0	11.839	0	63.122	82.107	10.003	16.64	95.388
27	-2.647	0.112	22.473	39.987	0.625	0.017	7.322	0	2.713	0.052	18.502	29.209	62.366
28	-2.867	0.246	22.488	98.328	5.417	20	7.068	0	16.156	1.292	0	0	44.153
29	-2.486	0.256	32.822	292.286	0	0	8.062	0	40.147	712.637	0	0	-4.999
30	-1.524	0	4.966	0.298	0.641	0.047	9.091	0	48.811	117.517	2.661	1.088	22.253
31	-0.639	0.282	1.116	0.028	1.017	1.885	9.567	0	29.195	3.276	7.23	19.973	83.077
32	-3.345	0	26.47	52.013	1.157	0.013	7.955	0	19.886	0.764	0	0	99.494
33	-0.54	0.023	2.334	0.025	0	0	10.859	0	48.896	23.956	0.29	0.007	53.349
34	-2.197	0.097	24.053	65.603	0	0	12.372	0	59.881	69.024	15.657	59.961	71.869
35	-2.095	0	22.444	62.352	0	0	9.784	0	58.018	170.888	0	0	107.068

Part	γ_0	γ_1	γ_2	γ_3	γ_4	γ_5	β_0	β_1	β_2	β_3	β_4	β_5	μ
36	-2.615	0.562	32.683	382.173	0.755	6.419	11.208	0	67.693	291.739	0.537	0.016	68.043
37	-2.741	0	21.972	16.052	0.138	0.017	6.191	0	6.247	0.105	0	0	73.145
38	-0.546	0.217	1.407	0.045	0	0	9.72	0	46.87	38.561	0.753	0.04	50.204
39	-1.776	0.123	16.982	15.563	0.247	0.034	8.704	0	37.013	93.534	3.175	34.261	10.923
40	-2.668	0.561	29.622	389.467	0	0	11.835	0	87.667	443.918	0	0	27.725
41	-2.942	0	31.833	73.951	0	0	5.877	0	4.875	0.139	1.038	8.968	84.731
42	-2.696	0.348	19.919	20	0.68	0.023	6.532	0	7.679	0.081	0	0	113.65
43	-2.003	0.141	21.969	80.753	0	0	7.271	0	14.343	0.559	0	0	102.69
44	-1.262	0.18	6.826	0.105	0	0	12.109	0	53.882	50.633	13.541	45.522	72.549
45	-3.275	0.074	31.8	9.025	0.12	0.013	12.438	0	59.915	72.122	10.871	21.867	41.841
46	-4.181	0.023	53.387	293.565	0	0	11.236	0	57.661	173.319	12.259	86.944	77.119
47	-2.261	0.27	24.683	221.08	0.36	5.241	10.909	0	63.917	60.063	0	0	89.65
48	-2.684	0.142	24.234	20.143	0	0	10.124	0	58.475	107.549	0	0	68.16
49	-2.925	0.154	30.802	154.33	0	0	6.028	0	4.437	0.106	3.196	5.822	42.104
50	-2.962	0.132	28.79	124.601	0.66	0.04	6.79	0	12.58	0.843	0.381	0.04	27.229
51	-3.38	0.13	40.594	446.2	0	0	5.559	0	1.997	0.026	0	0	87.687
52	-2.979	0.324	27.12	104.372	4.013	20	11.318	0	69.289	93.232	0	0	95.983
53	-3.394	0.464	31.187	50.393	1.397	2.826	12.344	0	81.907	94.451	0	0	119.627
54	-2.813	0	16.139	0.878	0.812	0.011	8.516	0	29.728	9.033	0.134	0.011	106.417
55	-2.063	0.137	21.48	40	0.1	8.659	8.361	0	20.255	1.033	1.524	8.136	95.374
56	-3.072	0.026	31.447	70.857	2.758	5.349	10.19	0	60.59	260.796	0	0	85.612
57	-2.076	0.35	23.901	327.21	0	0	10.489	0	56.358	38.422	0	0	85.646
58	-2.01	0.34	20.783	38.111	0	0	8.468	0	28.04	16.144	0.426	0.019	40.548
59	-2.685	0.125	20	7.922	0.189	0.023	7.367	0	18.848	2.078	0.083	0.023	42.441
60	-3.091	0.194	31.522	190.306	0	0	5.798	0	8.864	0.472	0	0	36.386
61	-2.44	0.179	21.725	19.099	0	0	6.698	0	6.782	0.089	0.211	0.016	93.442
62	-3.149	0	28.295	31.385	0.447	0.015	7.427	0	8.743	0.103	6.169	19.922	131.028
63	-2.908	0	29.934	39.76	0.233	0.016	5.659	0	1.92	0.024	0	0	104.69
64	-0.447	0.124	1.338	0.028	0	0	11.14	0	62.495	75.583	0.763	0.017	98.806
65	-2.997	0	26.584	18.979	0.573	0.013	8.777	0	29.519	5.655	0.492	15.381	75.778
66	-4.104	0.27	49.4	231.074	0.169	15.743	11.134	0	68.201	174.217	0	0	78.722
67	-2.041	0.106	15.753	20	0.527	0.027	8.343	0	23.259	1.216	0	0	76.286
68	-2.057	0	17.725	36.889	0	0	6.761	0	15.505	1.35	0	0	62.799
69	-3.014	0.23	34.429	280.318	0	0	9.425	0	55.611	254.384	0	0	34.83
70	-2.901	0	34.645	231.797	0	0	5.896	0	4.094	0.1	0.159	0.036	39.722
71	-2.396	0	20.987	31.112	0.903	0.042	8.924	0	41.076	37.094	0	0	97.946
72	-2.017	0	4.589	0.087	6.858	1.787	9.944	0	26.849	2.453	9.557	4.64	109.315
73	-2.003	0.443	11.285	1.189	0.131	0.013	9.386	0	47.69	49.665	0	0	89.831
74	-3.643	0.396	32.397	315.082	7.554	15.189	11.345	0	58.838	52.021	1.44	0.014	72.897
75	-2.368	0.458	28.218	400.678	0	0	16.231	0	96.874	452.263	37.042	95.274	73.78
76	-4.499	0	52.942	227.357	0.769	13.486	10.705	0	63.814	169.772	0	0	61.114
77	-2.424	0.524	18.559	30.024	0.576	0.015	9.943	0	39.67	15.801	5.664	1.264	66.345
78	-0.813	0.381	2.867	0.172	0	0	9.965	0	46.046	19.918	0.649	0.021	57.282
79	-2.211	0.374	19.266	38.853	0	0	9.28	0	44.968	23.454	0	0	49.53

Part	γ_0	γ_1	γ_2	γ_3	γ_4	γ_5	β_0	β_1	β_2	β_3	β_4	β_5	μ
80	-3.121	0.306	30.915	68.469	0.595	0.139	10.978	0	76.757	782.803	0	0	33.021
81	-3.318	0.211	31.928	52.677	3.014	18.538	6.011	0	2.857	0.038	0	0	81.125
82	-3.296	0	32.157	68.339	3.378	16.458	8.056	0	6.786	0.094	12.118	10.9	101.29
83	-1.995	0.343	15.631	12.15	0.09	0.015	5.419	0	2.281	0.031	0.038	0.03	79.534
84	-2.637	0	22.221	34.039	1.544	3.686	9.551	0	42.218	19.2	0.589	0.022	61.223
85	-3.684	0.338	35.951	310.547	4.181	13.061	12.427	0	68.583	281.554	19.02	21.697	58.464
86	-1.696	0.301	12.838	25.994	0.241	0.021	12.319	0	36.958	3.887	24.574	12.482	72.486
87	-1.59	0.413	9.781	2.884	0	0	6.133	0	6.305	0.101	0	0	67.053
88	-3.723	0.095	21.294	52.268	11.773	12.565	11.354	0	68.299	51.636	0	0	60.629
89	-2.09	0.409	13.819	3.528	0	0	10.484	0	52.986	40.626	0.655	0.019	43.965
90	-2.305	0.398	20.131	32.842	0	0	9.995	0	52.161	69.995	1.265	0.058	43.485
91	-3.491	0.138	37.729	96.231	0	0	10.347	0	57.93	69.497	0	0	79.255
92	-4.477	0.074	57.361	303.366	0	0	10.635	0	59.95	136.655	0	0	54.966
93	-4.254	0.052	47.605	269.161	0.668	0.015	6.301	0	5.52	0.135	0	0	38.04
94	-2.621	0.232	29.538	297.559	0	0	6.2	0	7.59	0.2	0	0	51.609
95	-2.803	0.499	29.245	330.742	1.493	14.325	10.545	0	53.987	39.636	3.453	24.02	57.019
96	-2.744	0.7	32.483	927.59	0	0	14.998	0	115.183	508.235	12.7	159.026	67.559
97	-0.608	0.073	0.81	0.04	0	0	10.386	0	67.122	127.481	0	0	65.088
98	-0.609	0.112	0.898	0.042	0.36	0.022	8.647	0	26.105	2.293	1.47	5.781	53.32
99	-2.859	0.319	28.198	308.378	2.038	12.903	9.561	0	49.729	38.168	0	0	47.354
100	-2.913	0.1	33.059	249.664	0	0	7.132	0	18.293	2.827	0	0	35.151
101	-0.469	0.527	1.002	0.035	0	0	10.372	0	65.851	297.861	0	0	64.772
102	-2.835	0.178	26.016	31.191	0	0	10.487	0	56.713	86.024	4.871	19.341	64.928
103	-3.285	0.331	35.616	237.719	0	0	11.218	0	57.268	57.25	10.438	41.699	51.732
104	-2.284	0.378	24.757	316.188	0	0	7.155	0	14.589	0.602	0	0	50.904
105	-0.438	0.341	0.997	0.051	0	0	7.355	0	4.622	0.107	15.123	18.095	52.999
106	-2.25	0.521	5.327	6.62	12.324	12.309	12.987	0	85.921	110.864	1.003	0.02	62.186
107	-3.057	0	29.391	68.73	0	0	7.082	0	12.045	0.428	3.287	13.517	53.422
108	-1.87	0.205	11.031	2.155	0	0	9.125	0	42.935	28.234	0.449	0.068	52.212
109	-0.644	0.473	1.921	0.123	0	0	10.862	0	56.393	57.913	6.587	22.177	45.315
110	-2.067	0.116	20.547	64.816	0.162	0.033	7.911	0	37.549	110.701	0.288	26.663	28.545
111	-1.9	0.29	16.408	12.244	0	0	8.109	0	18.018	1.028	0.416	0.061	41.609
112	-1.061	0.372	0.79	0.045	4.955	2.083	10.062	0	49.567	32.715	0.302	0.026	44.74
113	-1.295	0.382	13.219	44.893	0	0	10.551	0	58.425	67.007	0	0	38.966
114	-2.126	0.156	18.882	56.334	0.983	19.998	9.532	0	47.396	36.369	0.257	0.034	48.291
115	-2.421	0.168	23.273	52.981	1.069	0.032	9.654	0	31.34	63.816	11.71	14.455	-4.993
116	-2.155	0.413	27.149	239.141	0	0	9.092	0	31.84	44.277	5.653	42.095	-4.998
117	-2.407	0.204	21.248	54.764	1.373	13.254	9.116	0	40.592	19.935	0	0	47.642
118	-2.126	0.347	23.692	309.377	0	0	11.209	0	59.296	280.723	14.364	22.018	45.506
119	-0.945	0.458	6.496	3.537	0	0	12.147	0	48.235	30.217	17.672	7.715	44.568
120	-1.322	0.323	19.575	303.676	0	0	8.472	0	43.163	822.966	0.347	0.044	-5.000

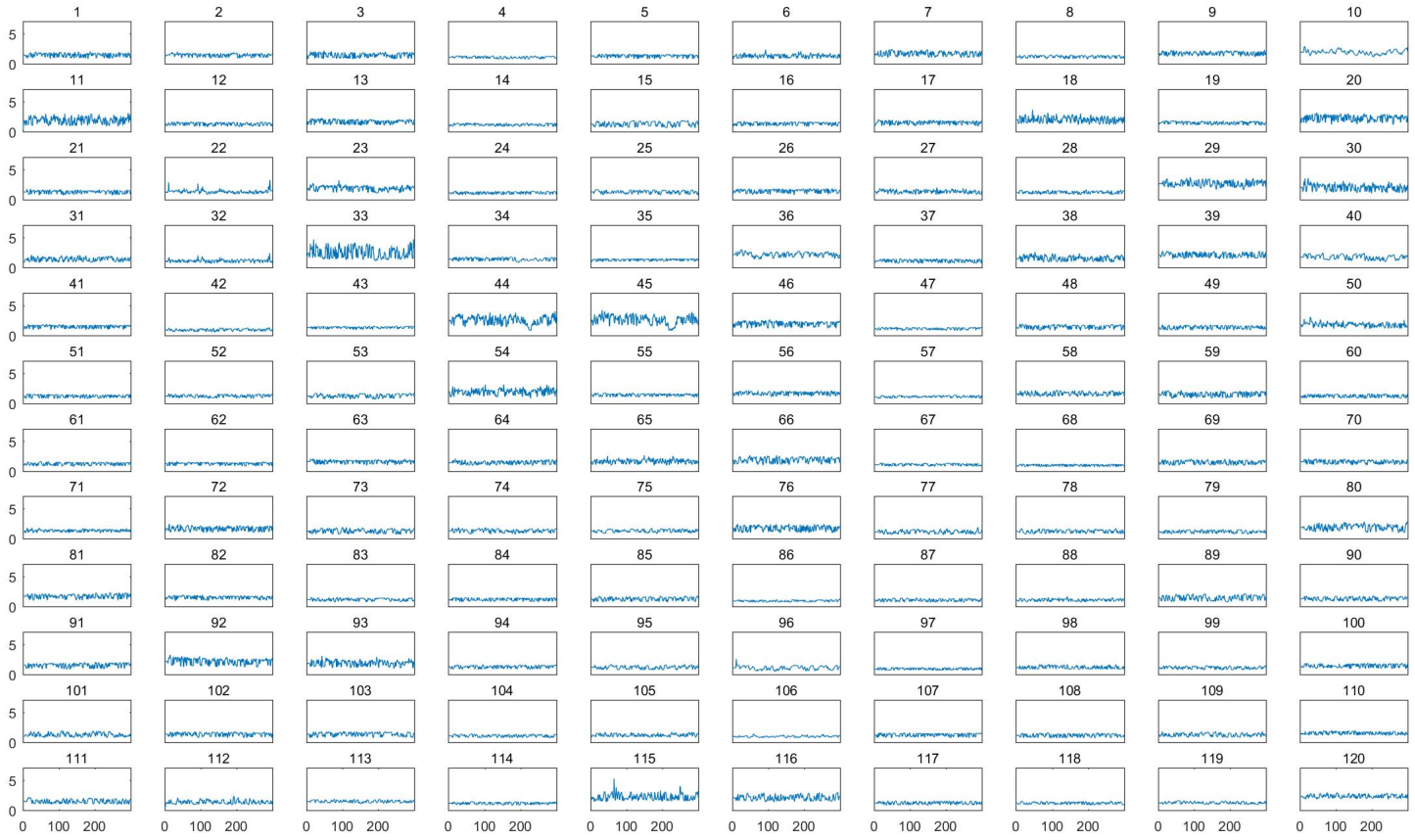
Estimated tail index plots for 120 subareas
1 2 3 4 5 6 7 8 9 10
11 12 13 14 15 16 17 18 19 20
21 22 23 24 25 26 27 28 29 30
31 32 33 34 35 36 37 38 39 40
41 42 43 44 45 46 47 48 49 50
51 52 53 54 55 56 57 58 59 60
61 62 63 64 65 66 67 68 69 70
71 72 73 74 75 76 77 78 79 80
81 82 83 84 85 86 87 88 89 90
91 92 93 94 95 96 97 98 99 100
101 102 103 104 105 106 107 108 109 110
111 112 113 114 115 116 117 118 119 120
0
5
0 100 200

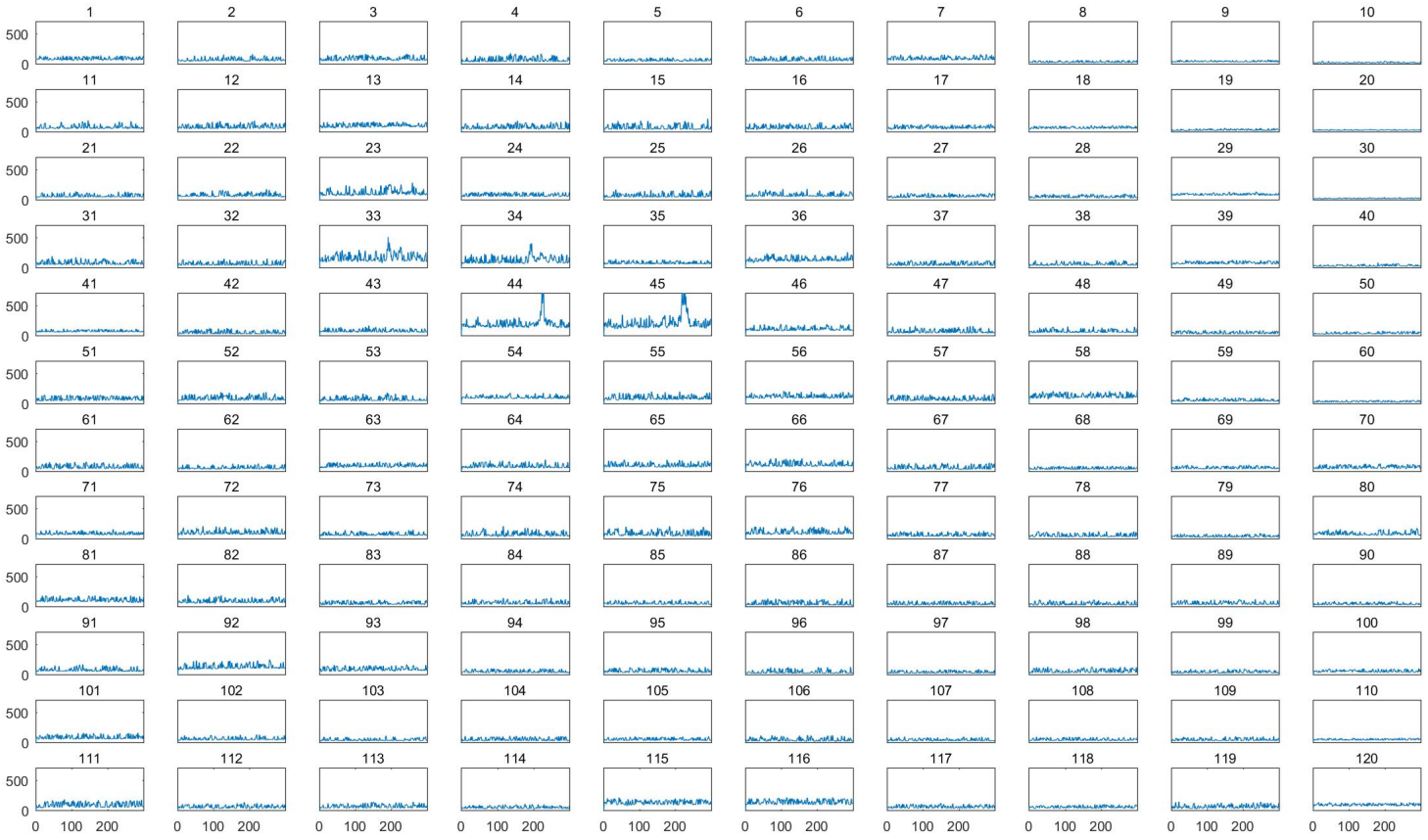
Estimated scale parameter plots for 120 subareas
1 2 3 4 5 6 7 8 9 10
11 12 13 14 15 16 17 18 19 20
21 22 23 24 25 26 27 28 29 30
31 32 33 34 35 36 37 38 39 40
41 42 43 44 45 46 47 48 49 50
51 52 53 54 55 56 57 58 59 60
61 62 63 64 65 66 67 68 69 70
71 72 73 74 75 76 77 78 79 80
81 82 83 84 85 86 87 88 89 90
91 92 93 94 95 96 97 98 99 100
101 102 103 104 105 106 107 108 109 110
111 112 113 114 115 116 117 118 119 120
500
0
0 100 200

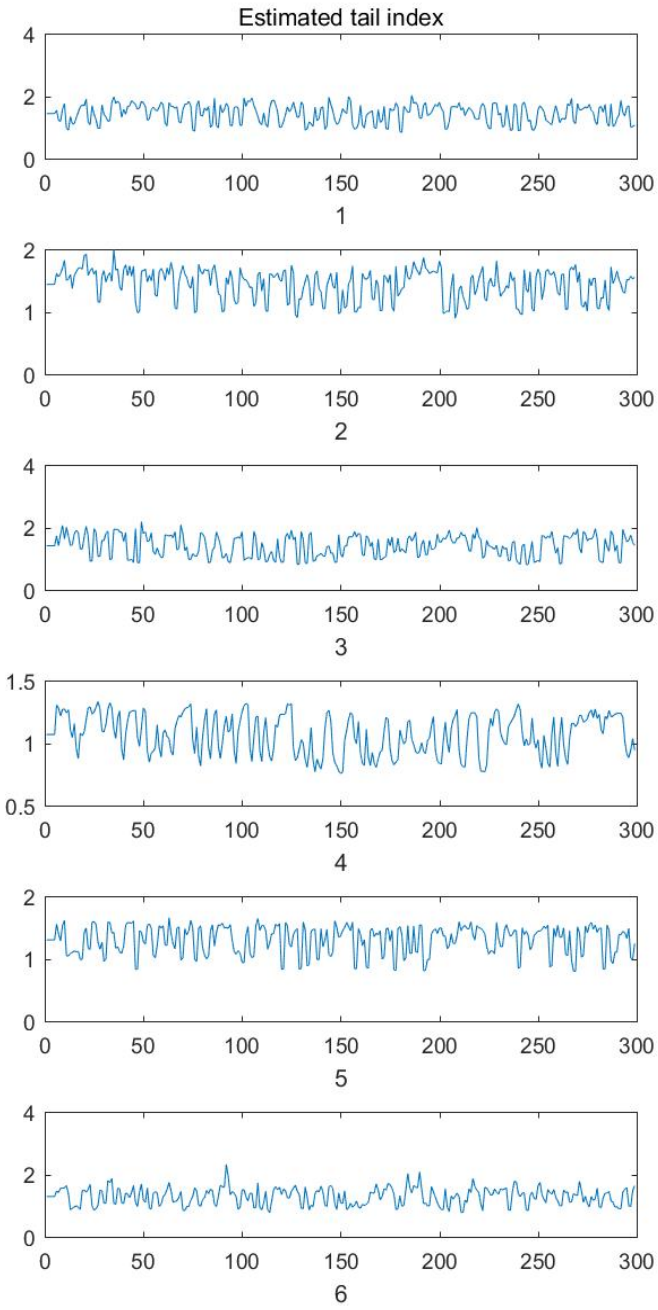
Estimated tail index
1
2
3
4
5
6

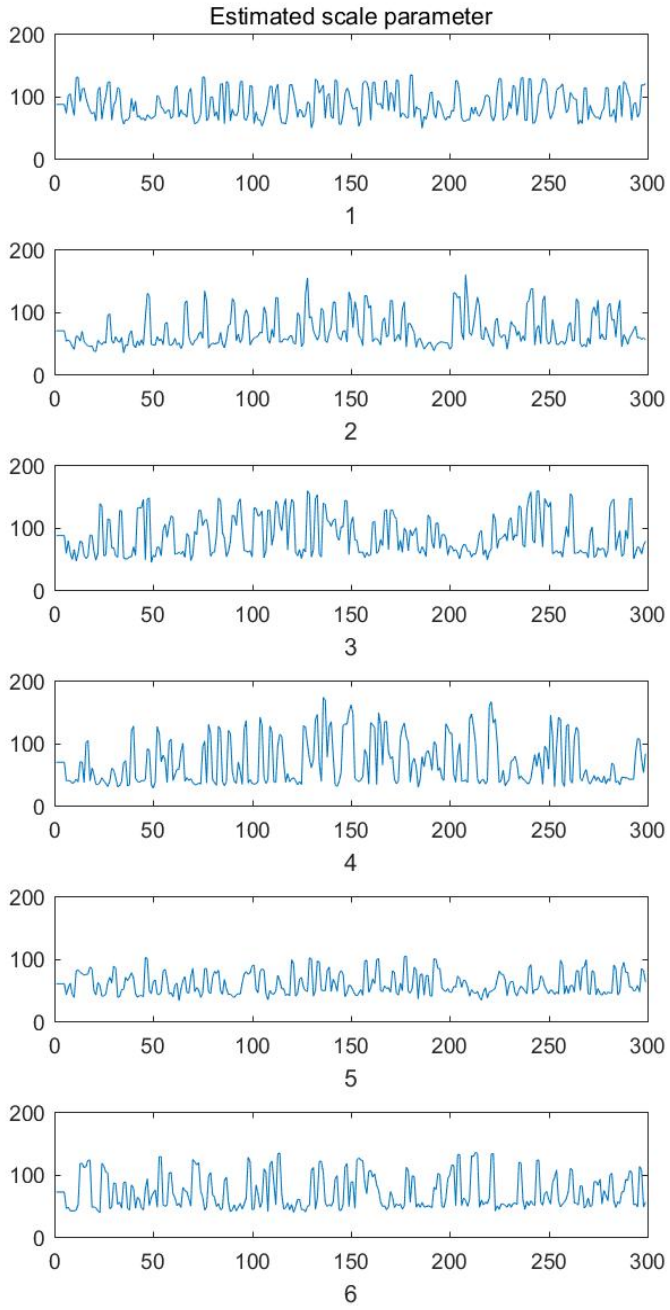
Estimated scale parameter
1
2
3
4
5
6

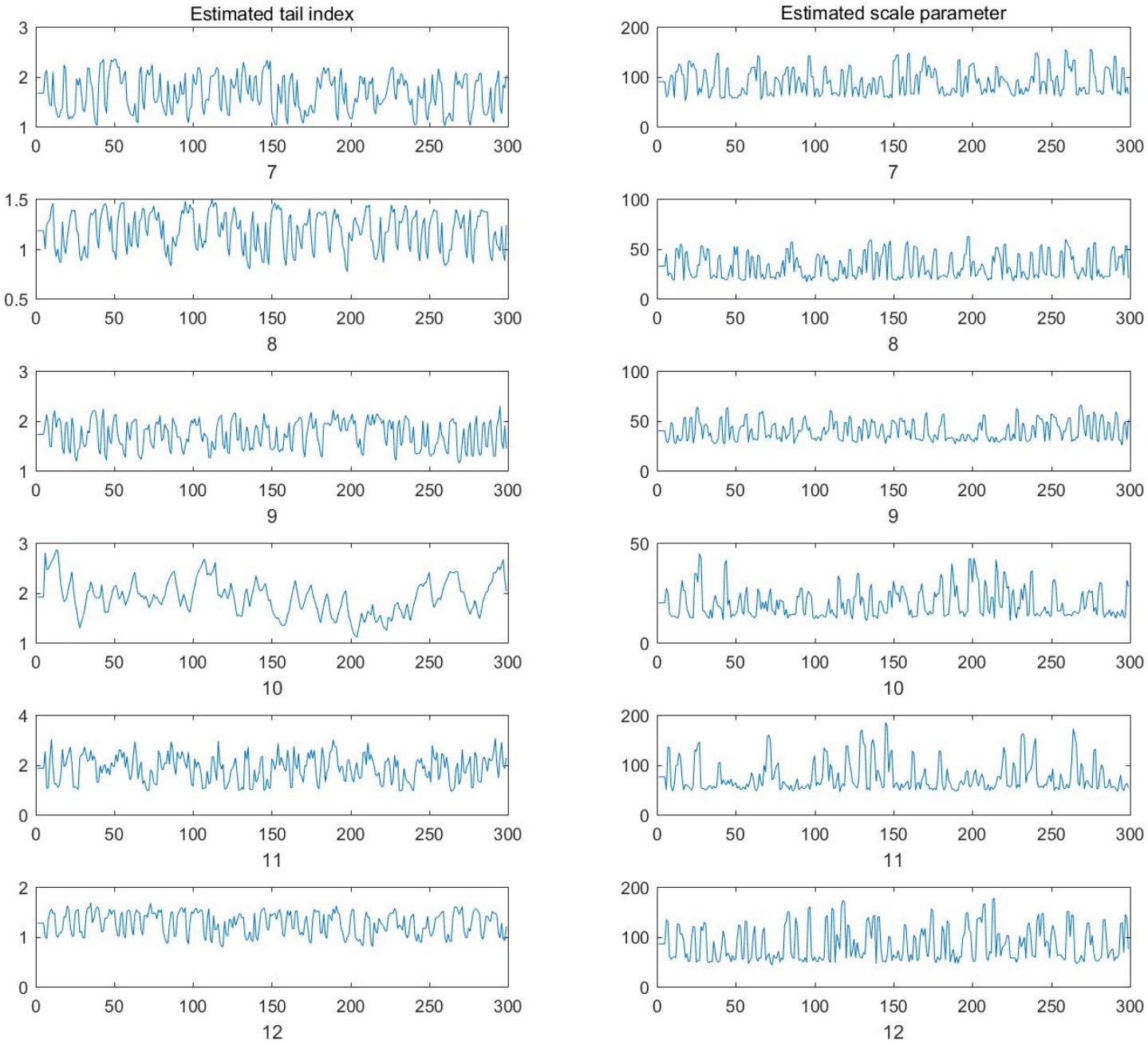
Estimated tail index
Estimated scale parameter
7
8
9
10
11
12

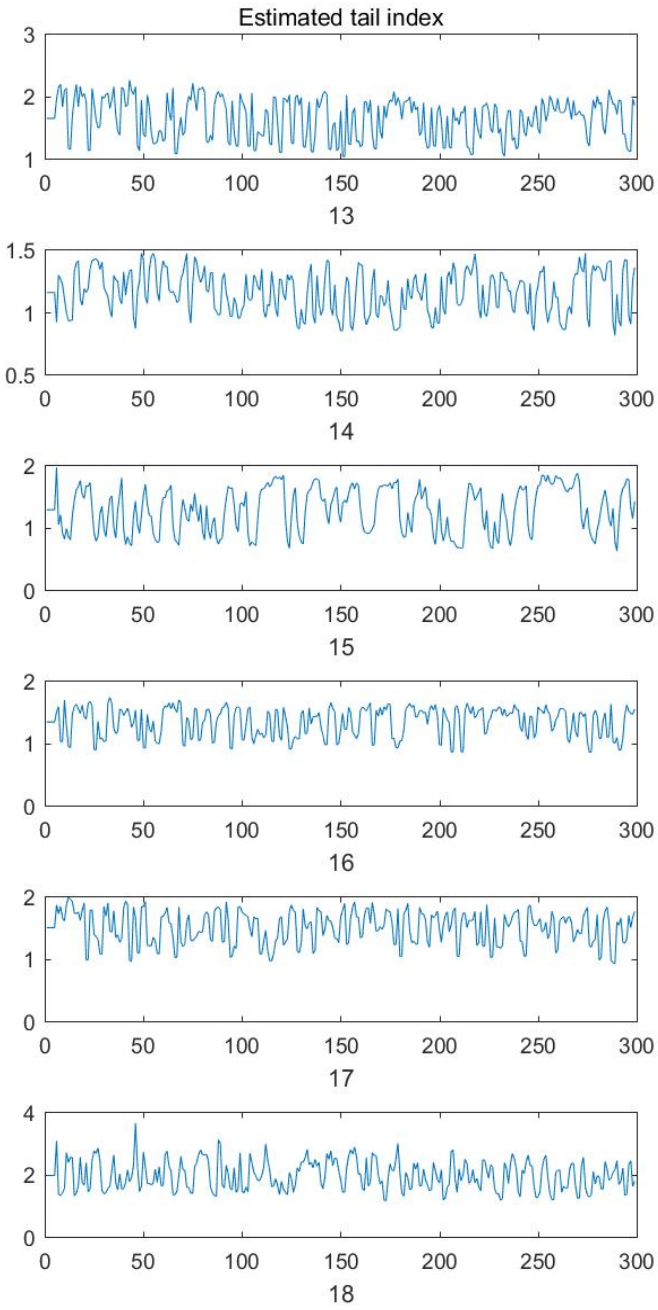
Estimated tail index
13
14
15
16
17
18

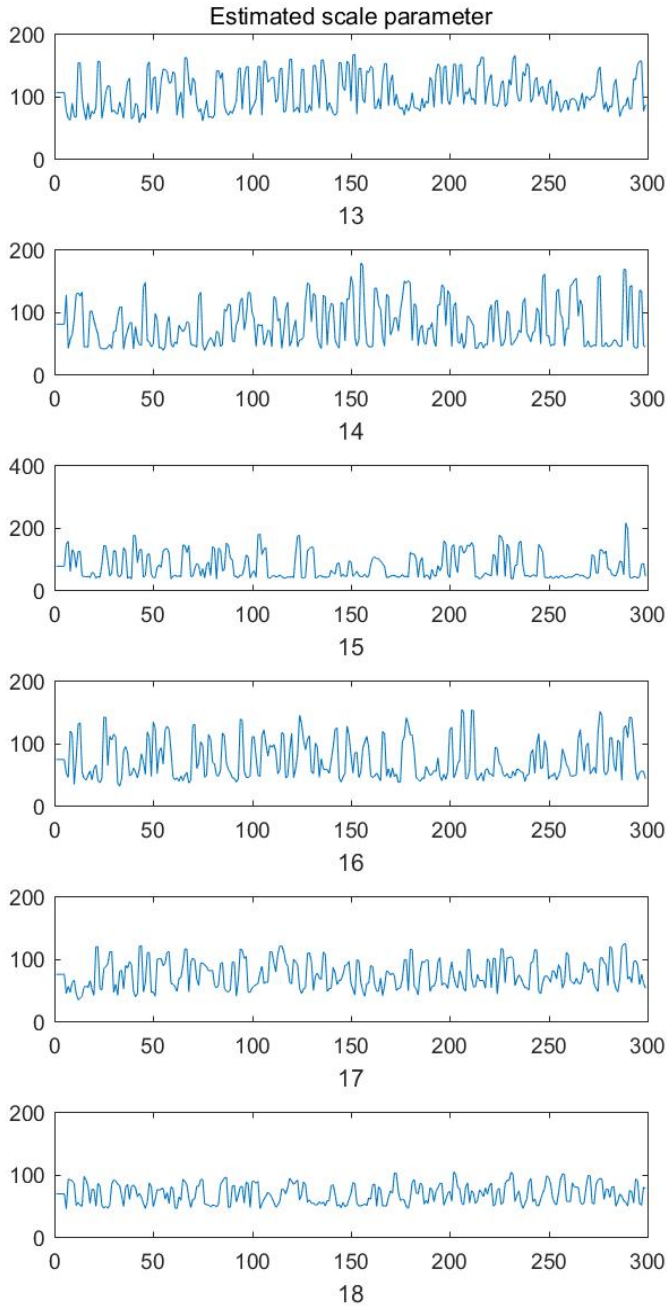
Estimated scale parameter
13
14
15
16
17
18

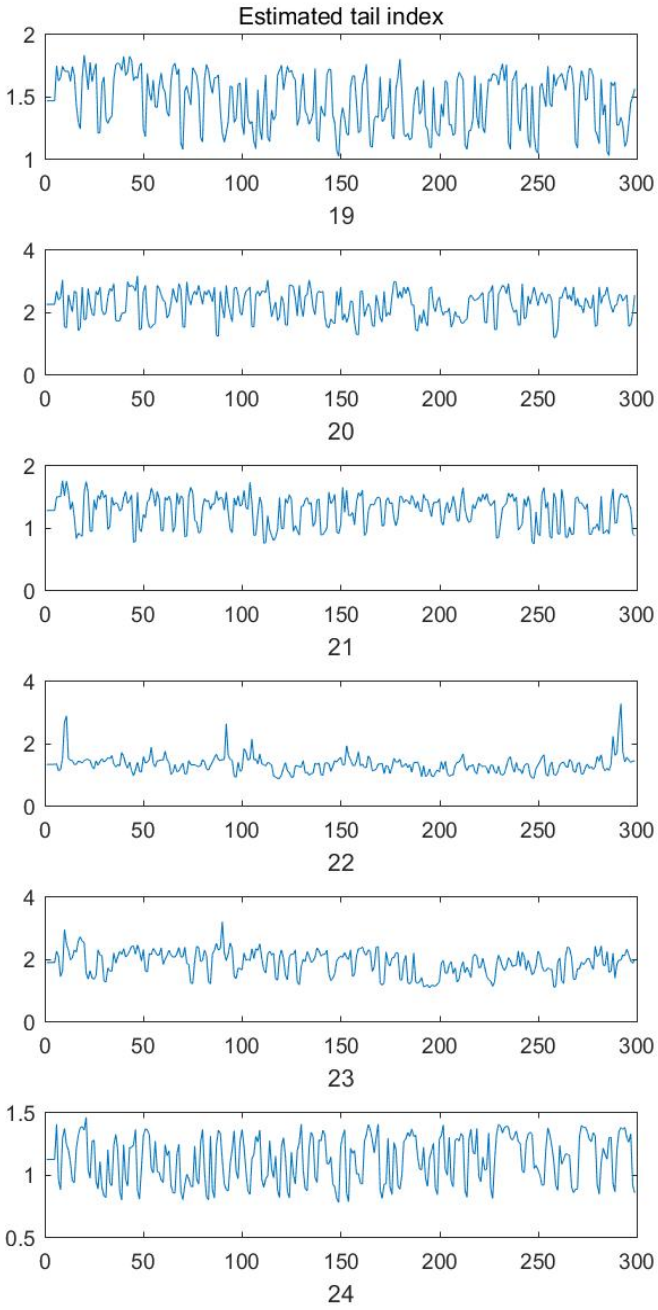
Estimated tail index
19
20
21
22
23
24

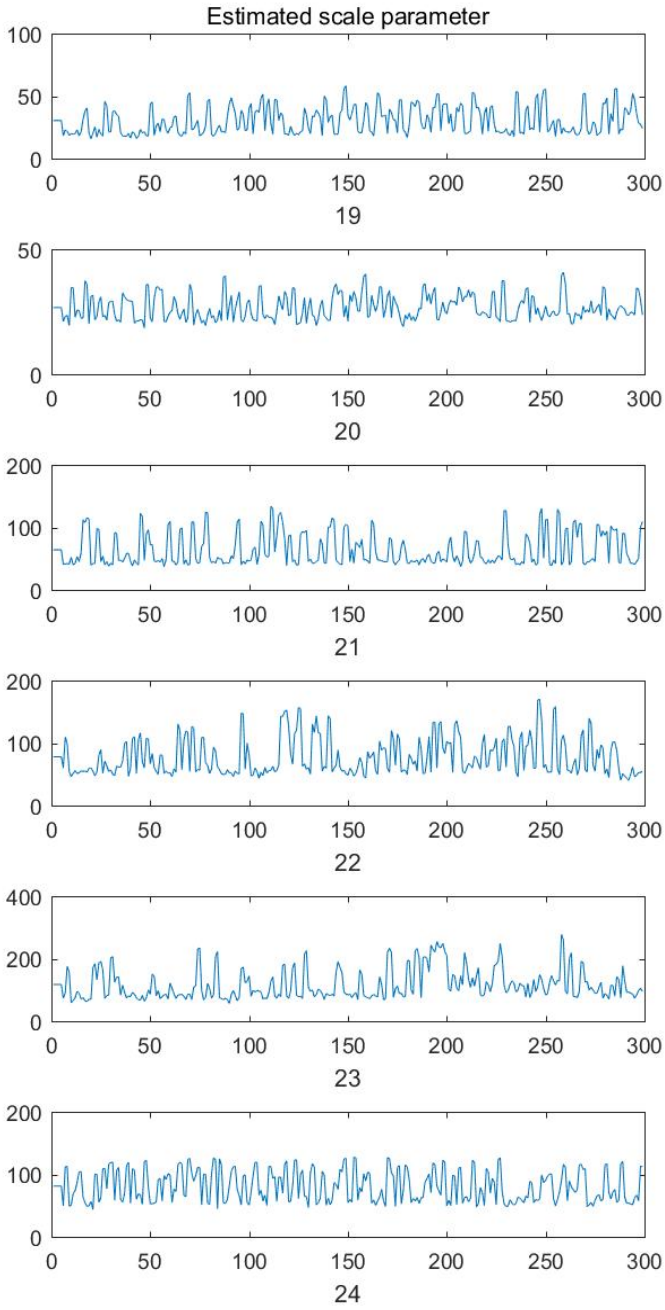
Estimated scale parameter
19
20
21
22
23
24

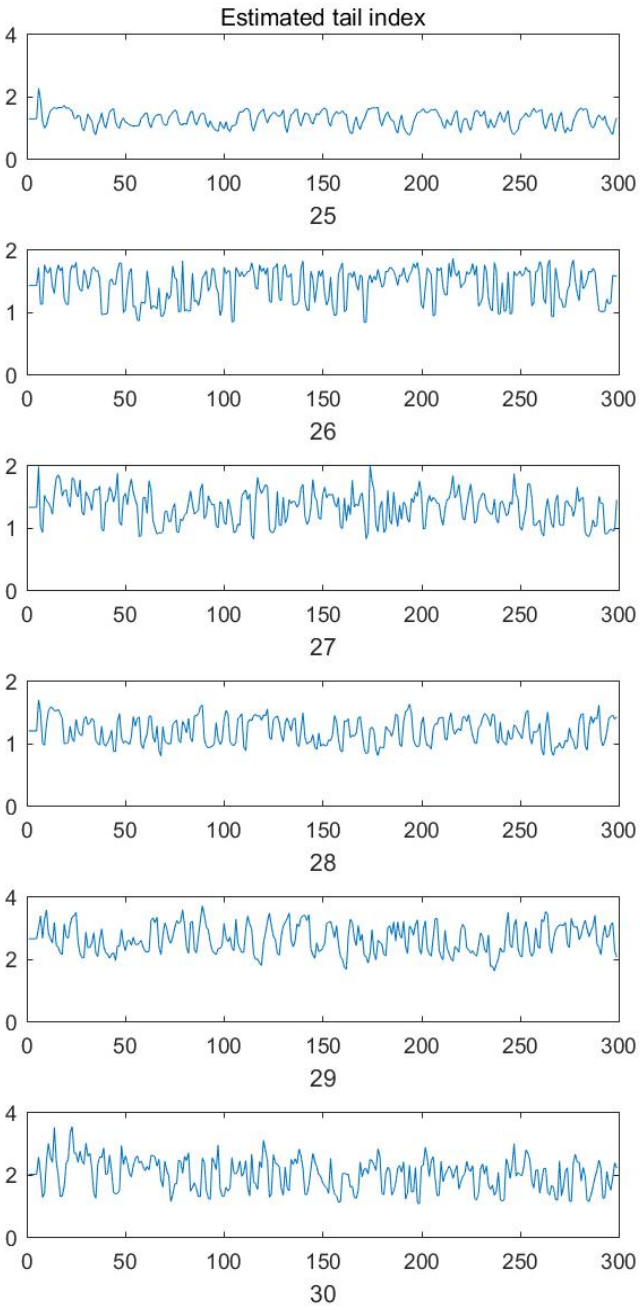
Estimated tail index
25
26
27
28
29
30

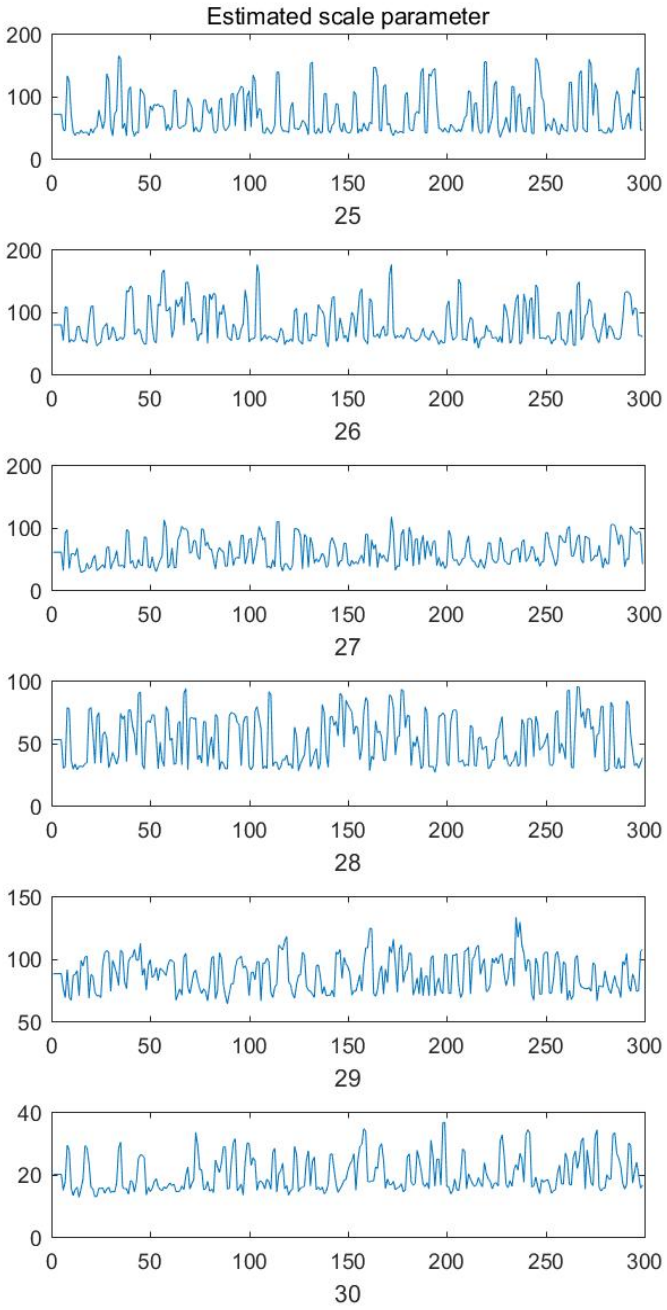
Estimated scale parameter
25
26
27
28
29
30

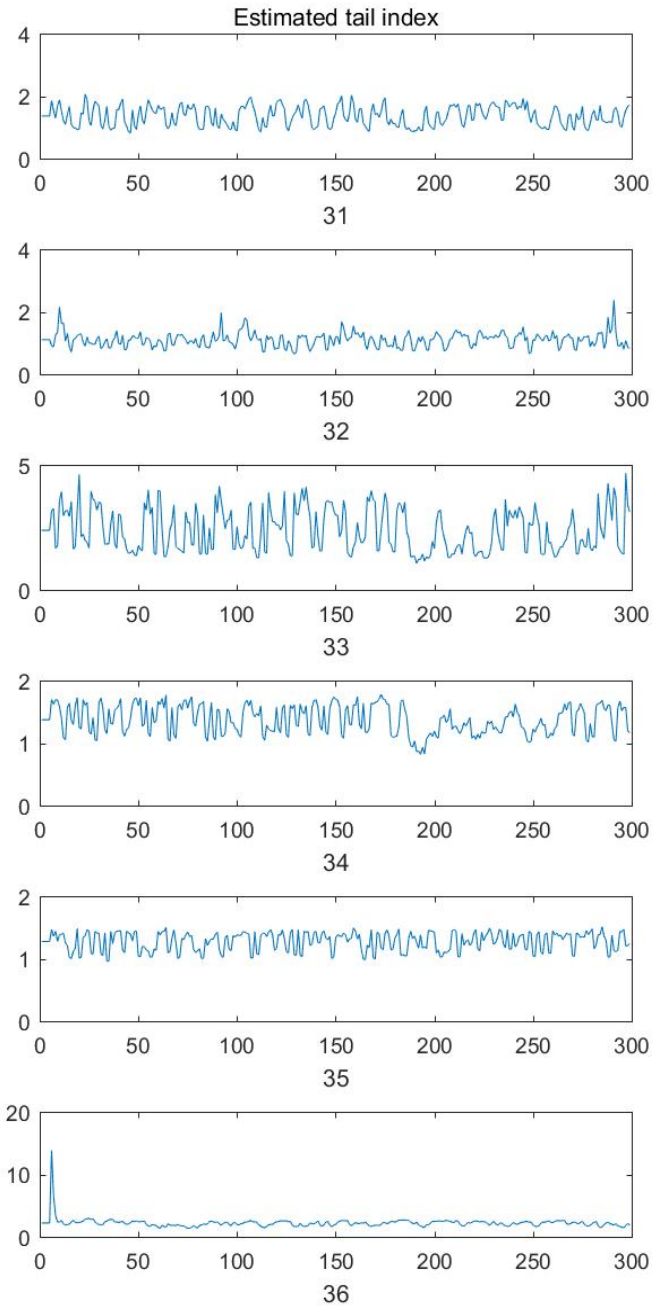
Estimated tail index
31
32
33
34
35
36

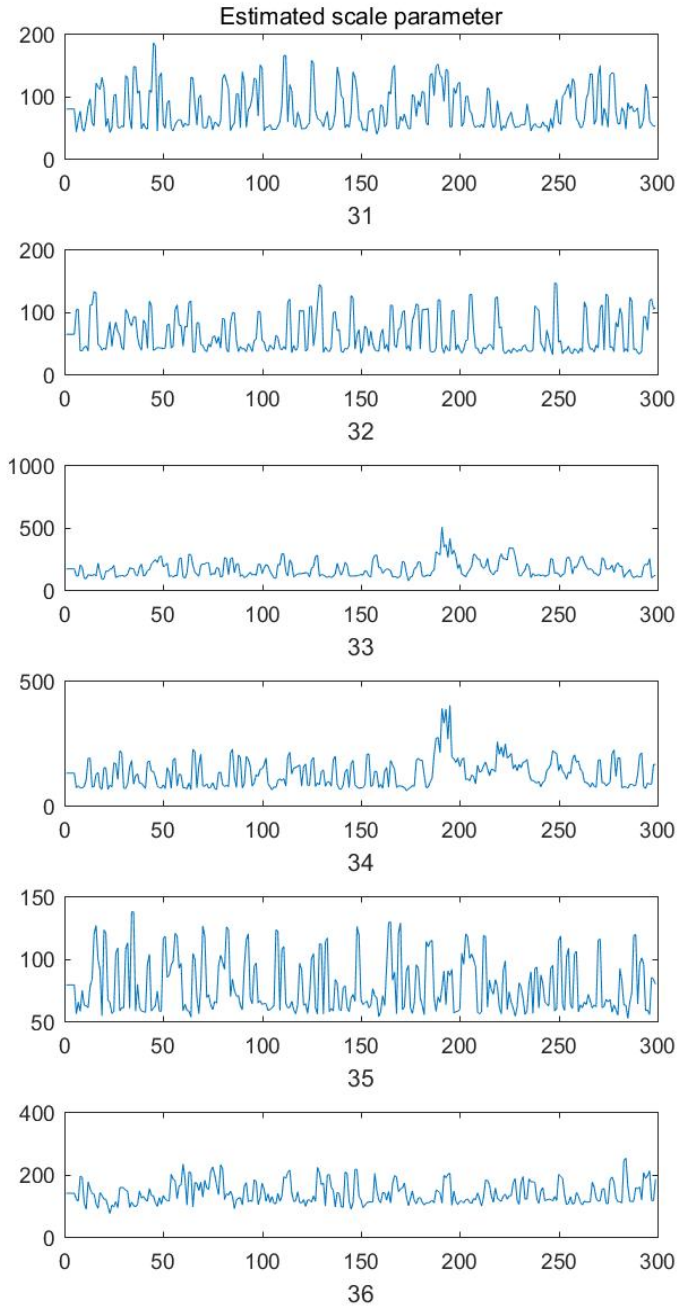
Estimated scale parameter
31
32
33
34
35
36

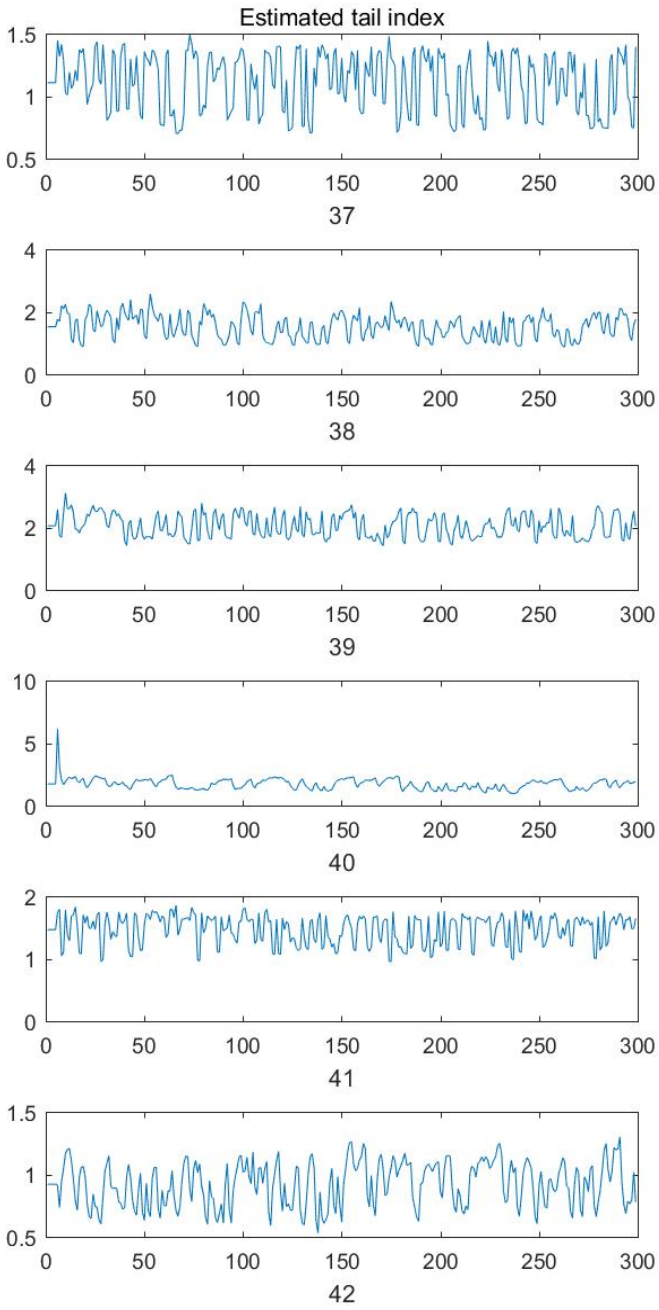
Estimated tail index
37
38
39
40
41
42

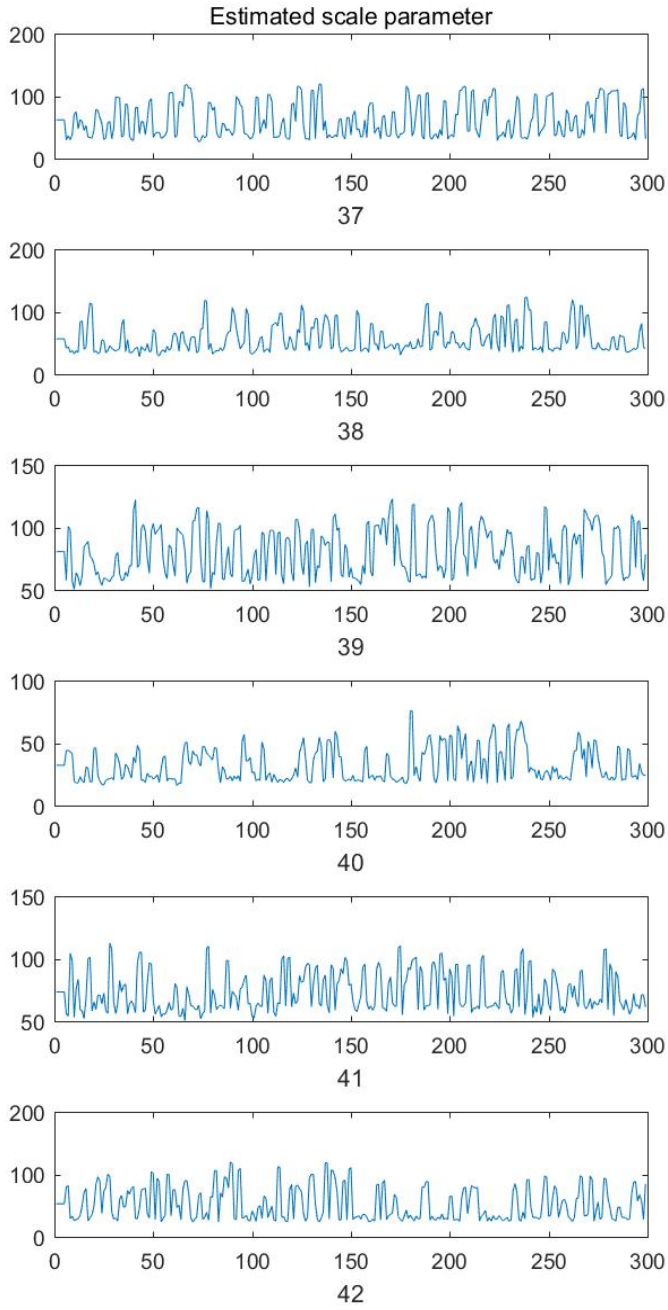
Estimated scale parameter
37
38
39
40
41
42

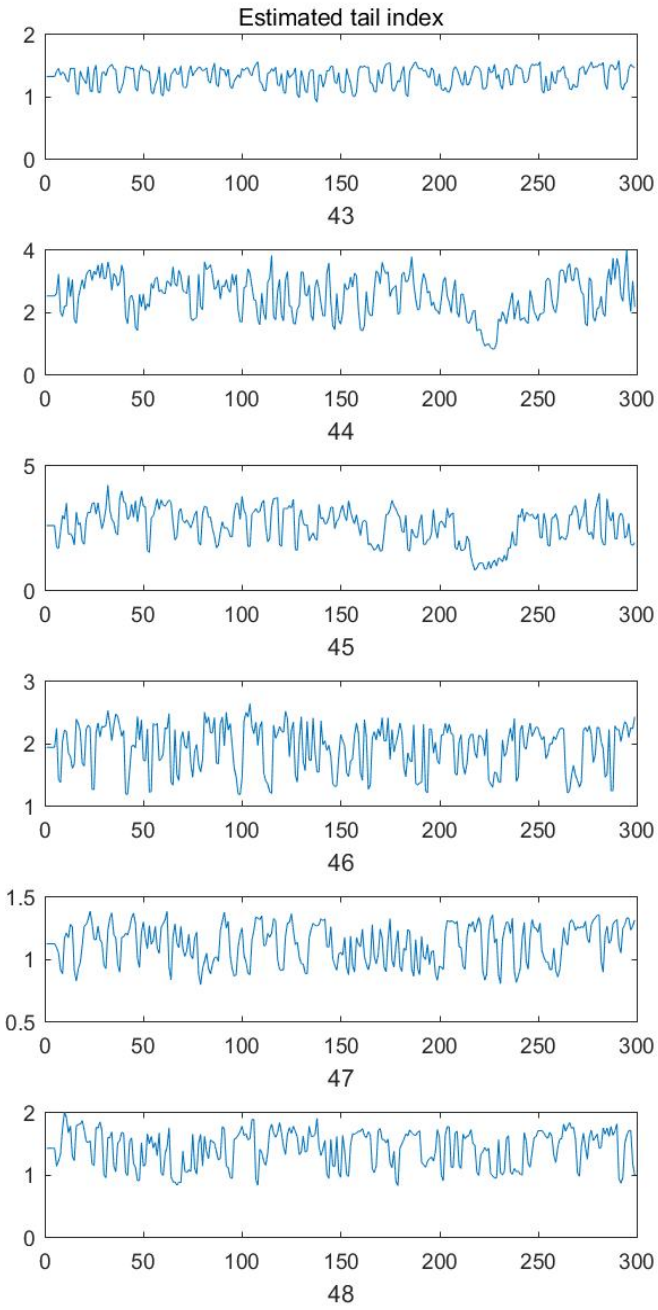
Estimated tail index
43
44
45
46
47
48

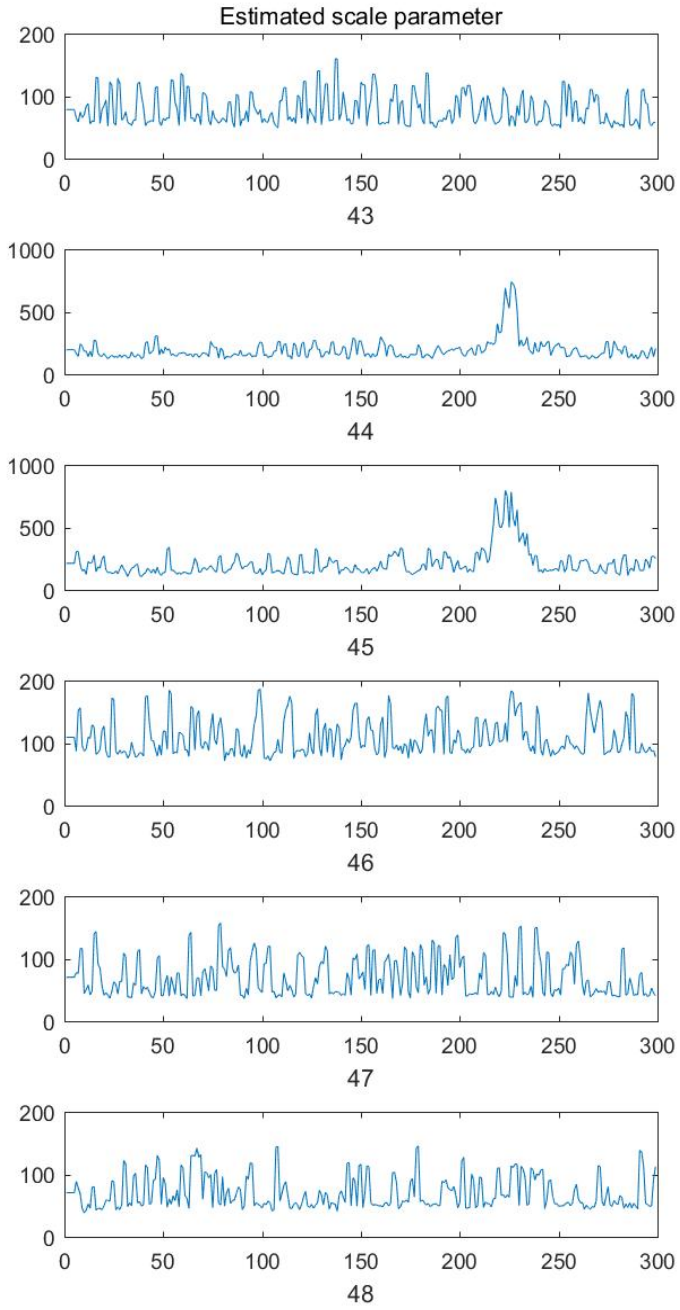
Estimated scale parameter
43
44
45
46
47
48

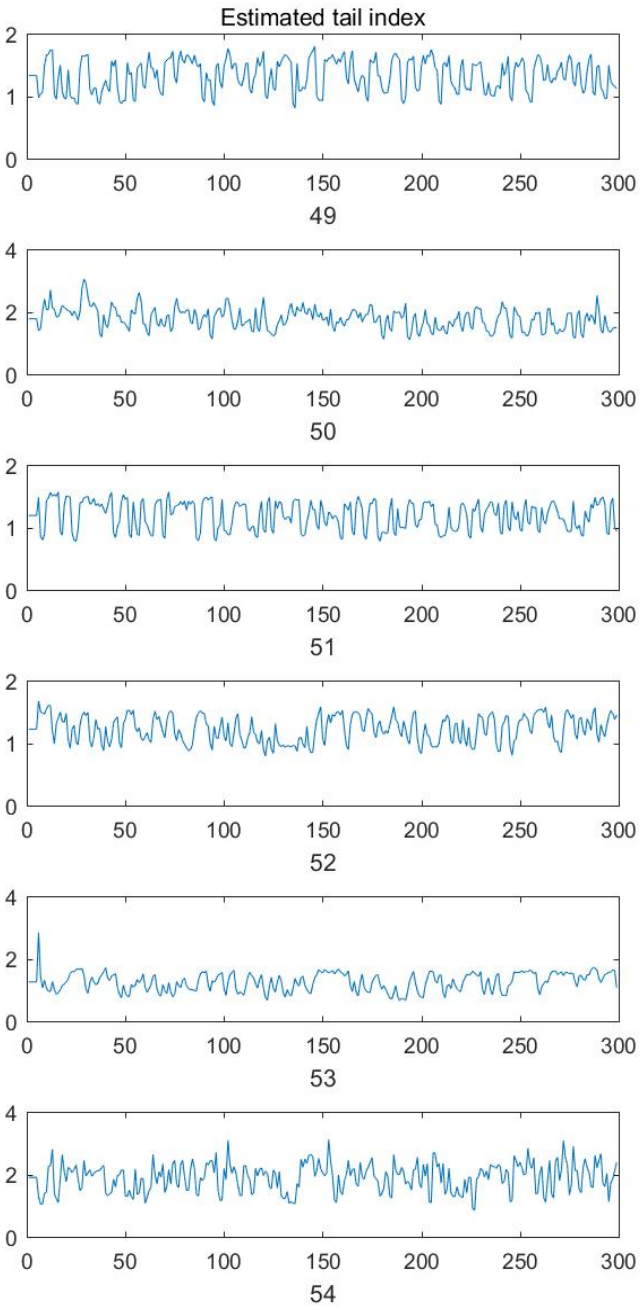
Estimated tail index
49
50
51
52
53
54

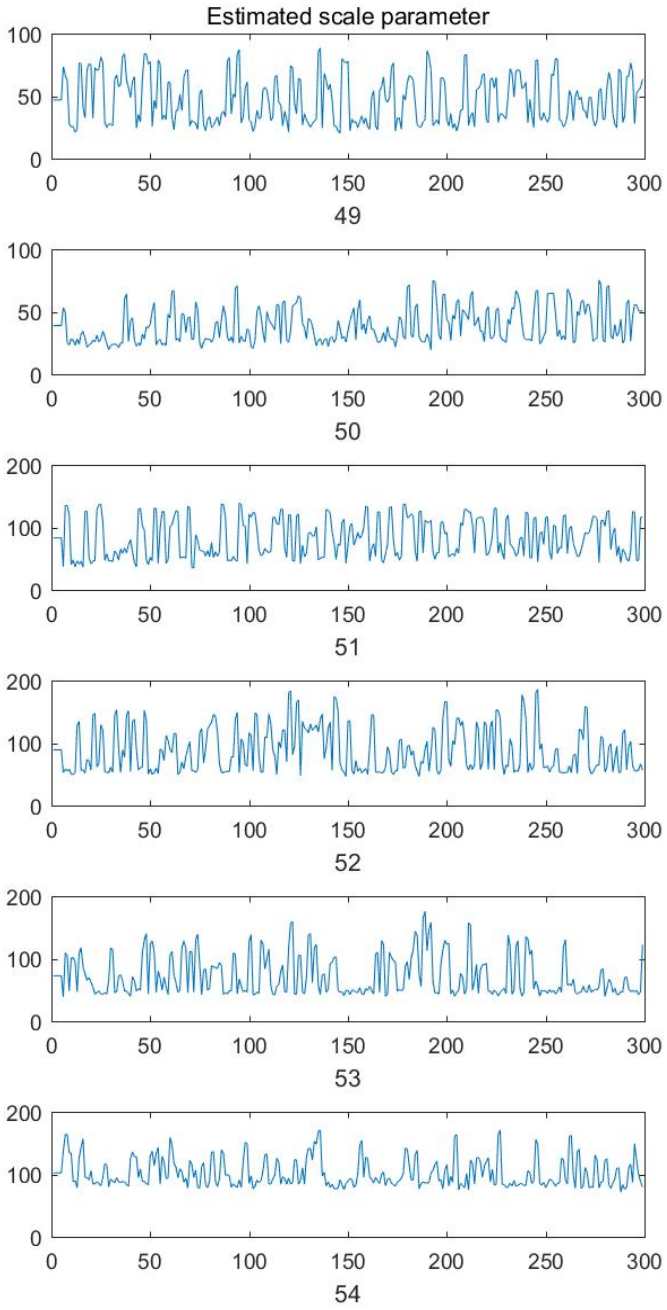
Estimated scale parameter
49
50
51
52
53
54

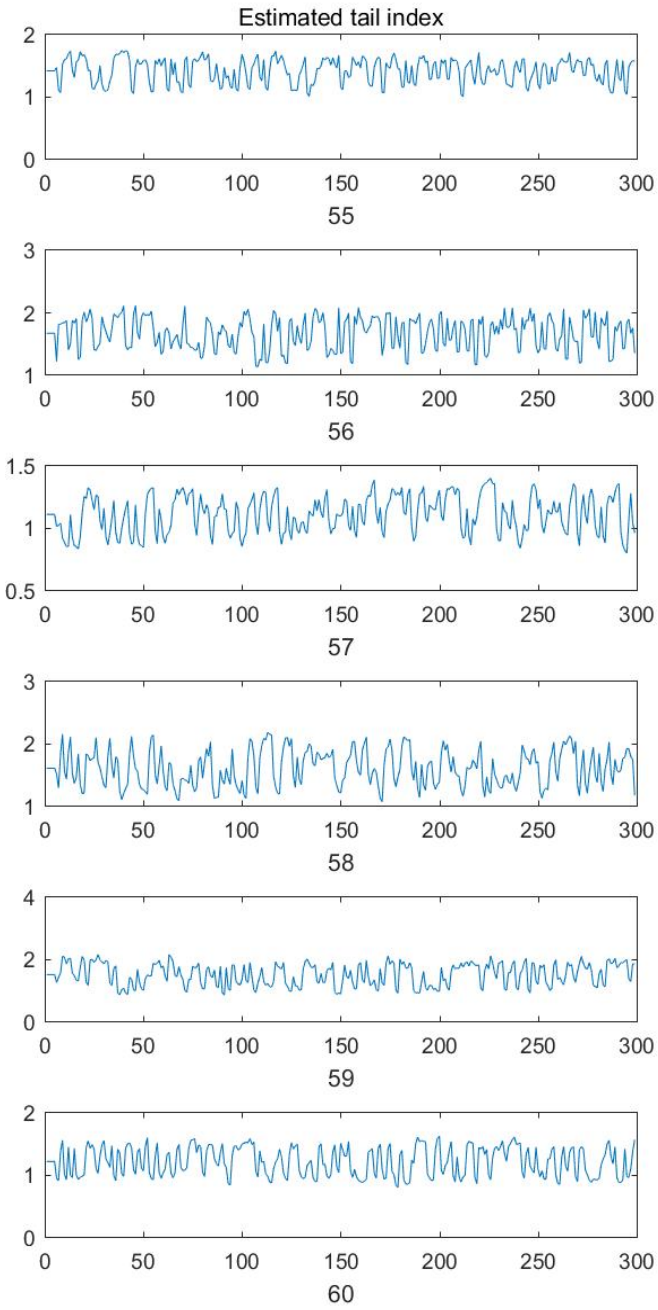
Estimated tail index
55
56
57
58
59
60

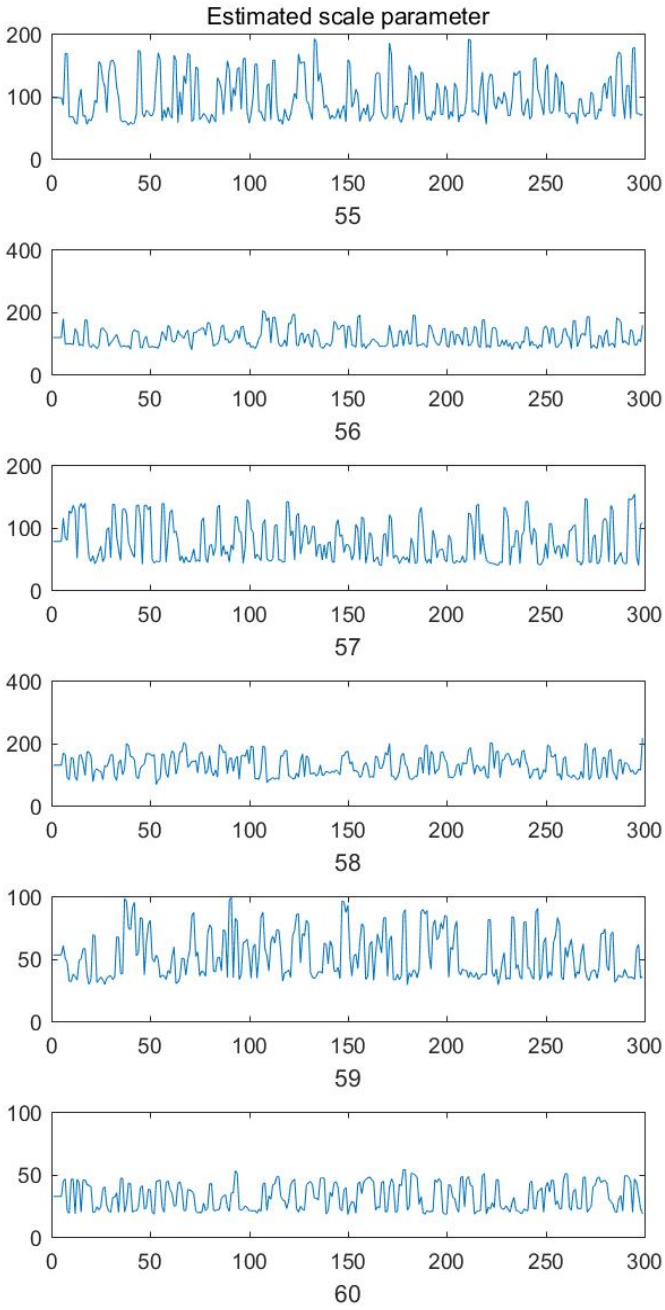
Estimated scale parameter
55
56
57
58
59
60

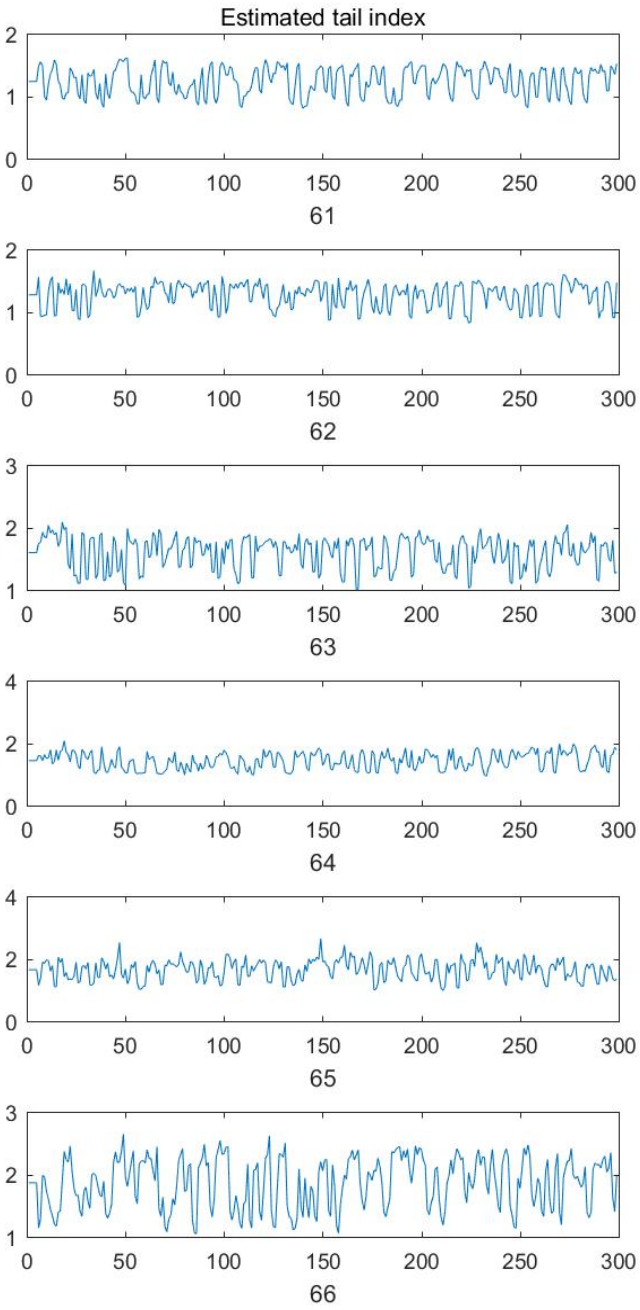
Estimated tail index
61
62
63
64
65
66

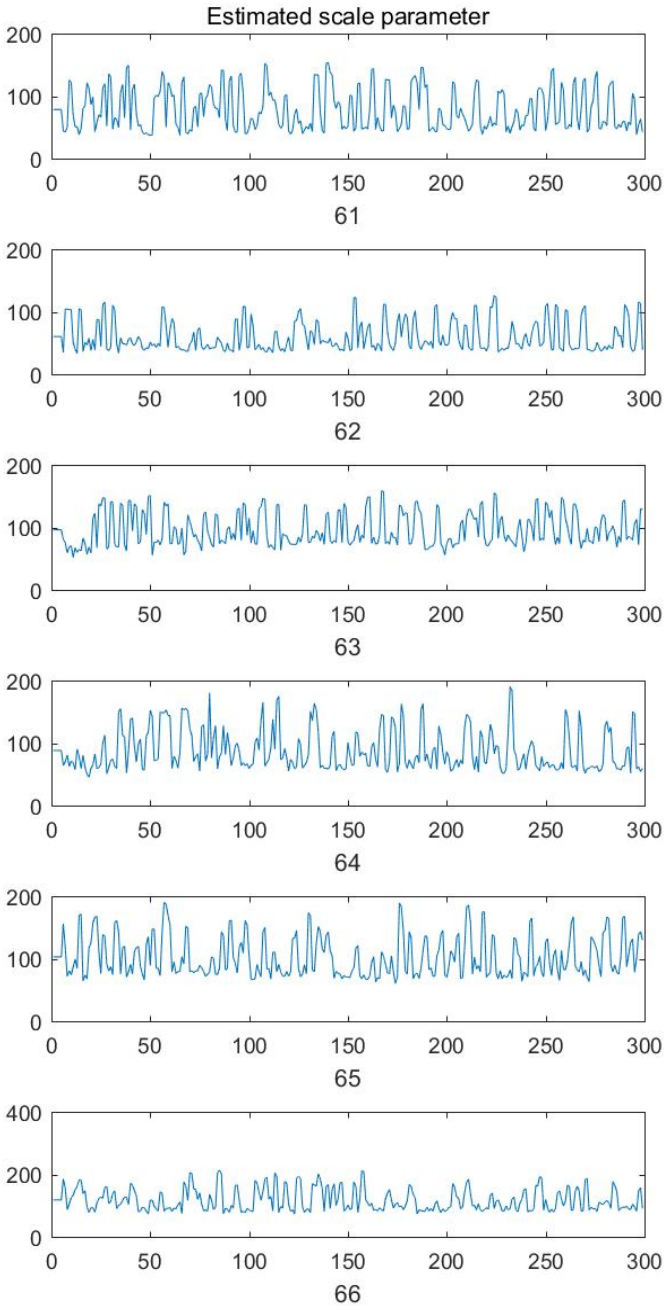
Estimated scale parameter
61
62
63
64
65
66

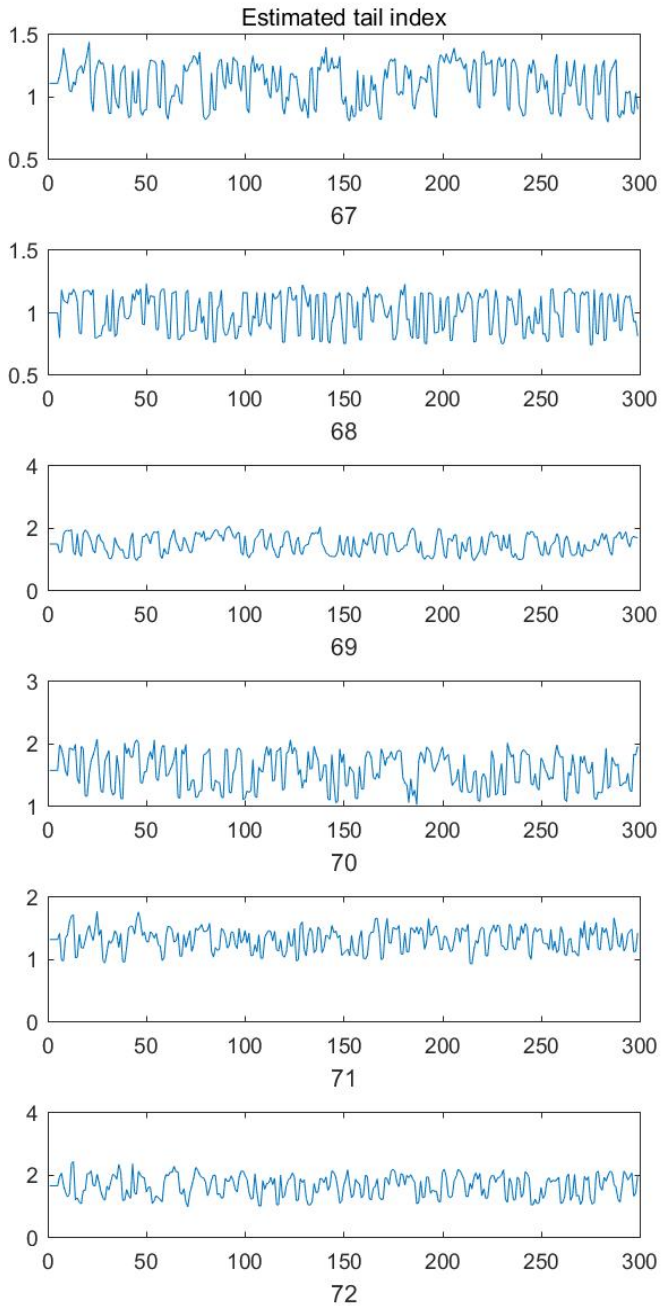
Estimated tail index
67
68
69
70
71
72

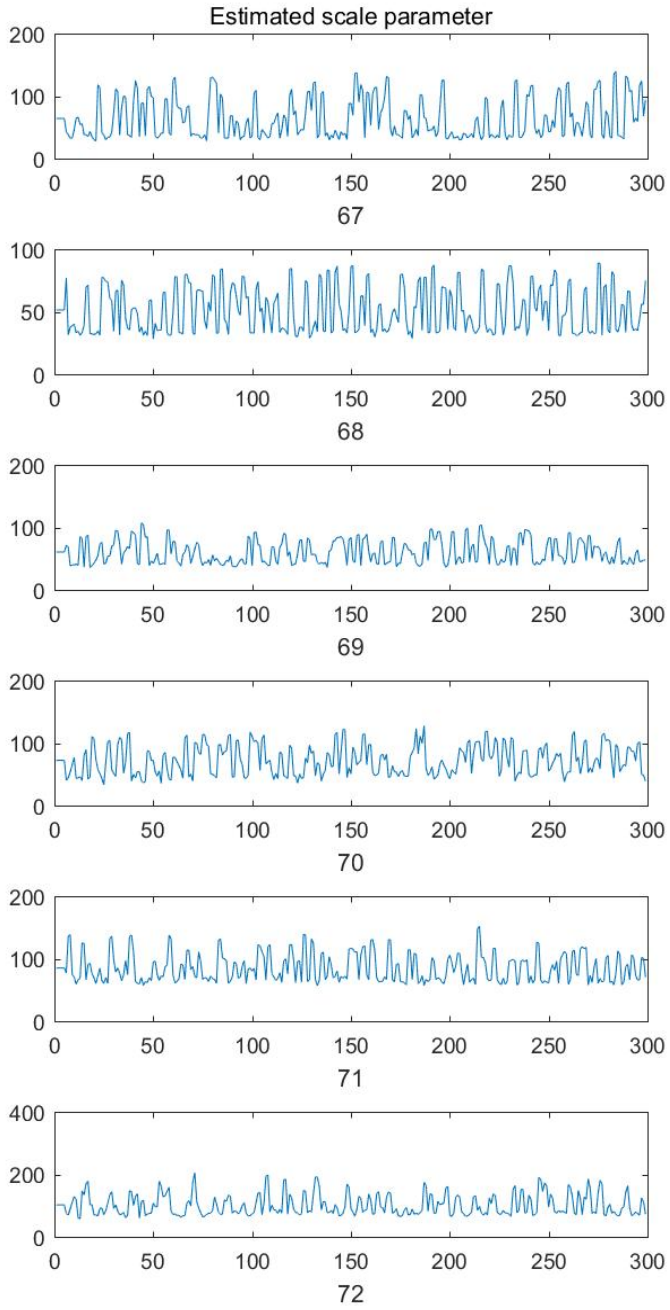
Estimated scale parameter
67
68
69
70
71
72

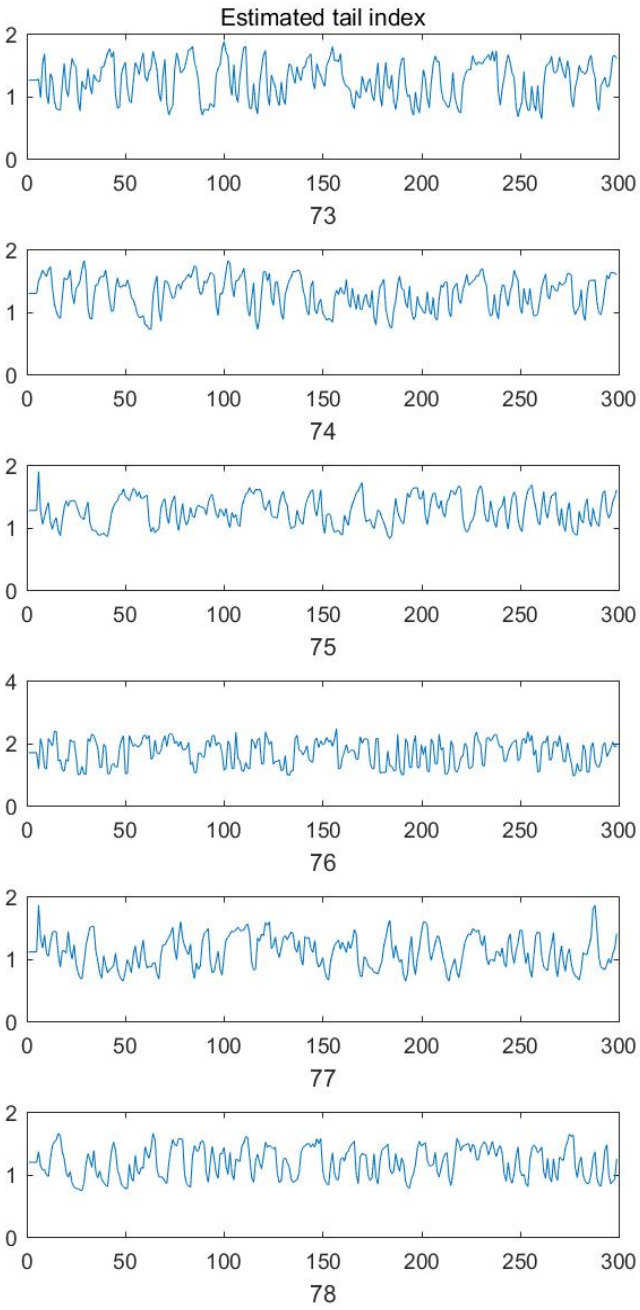
Estimated tail index
73
74
75
76
77
78

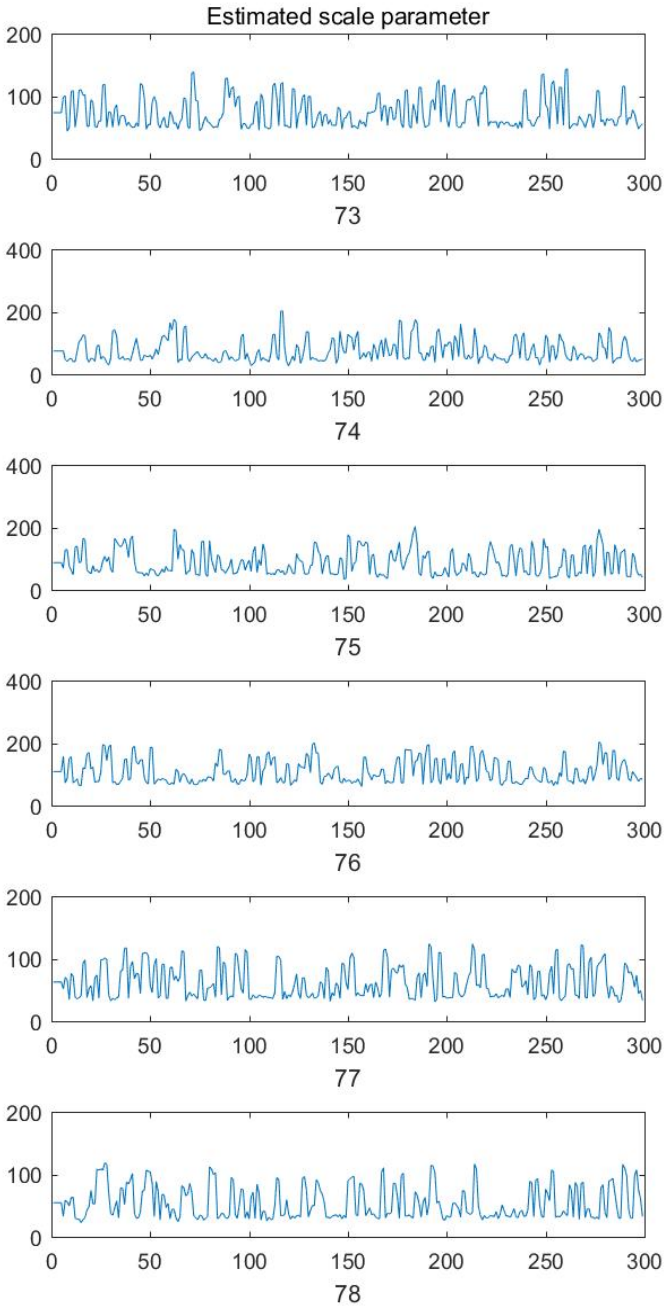
Estimated scale parameter
73
74
75
76
77
78

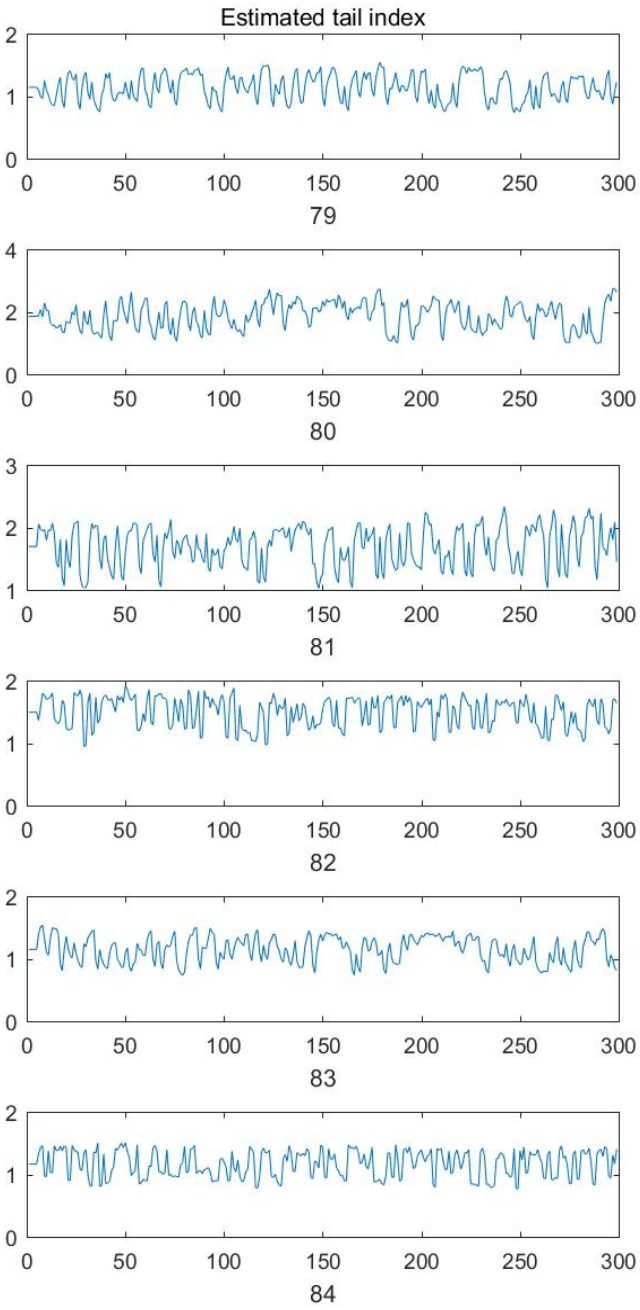
Estimated tail index
79
80
81
82
83
84

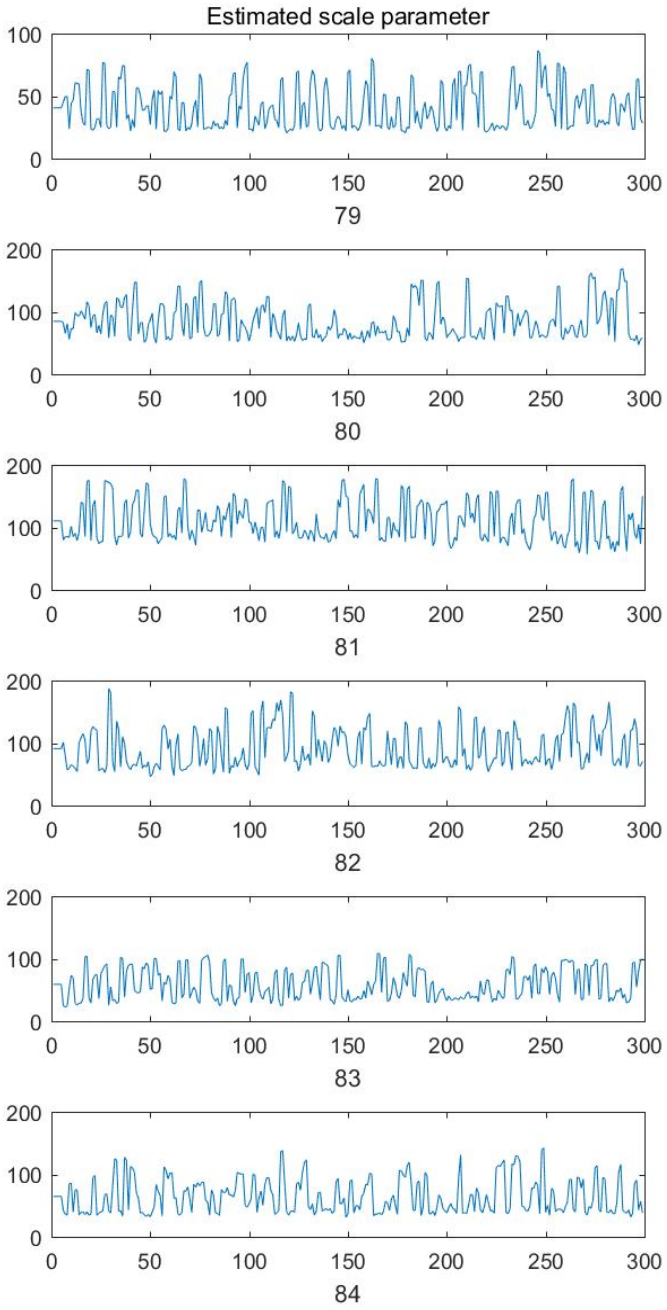
Estimated scale parameter
79
80
81
82
83
84

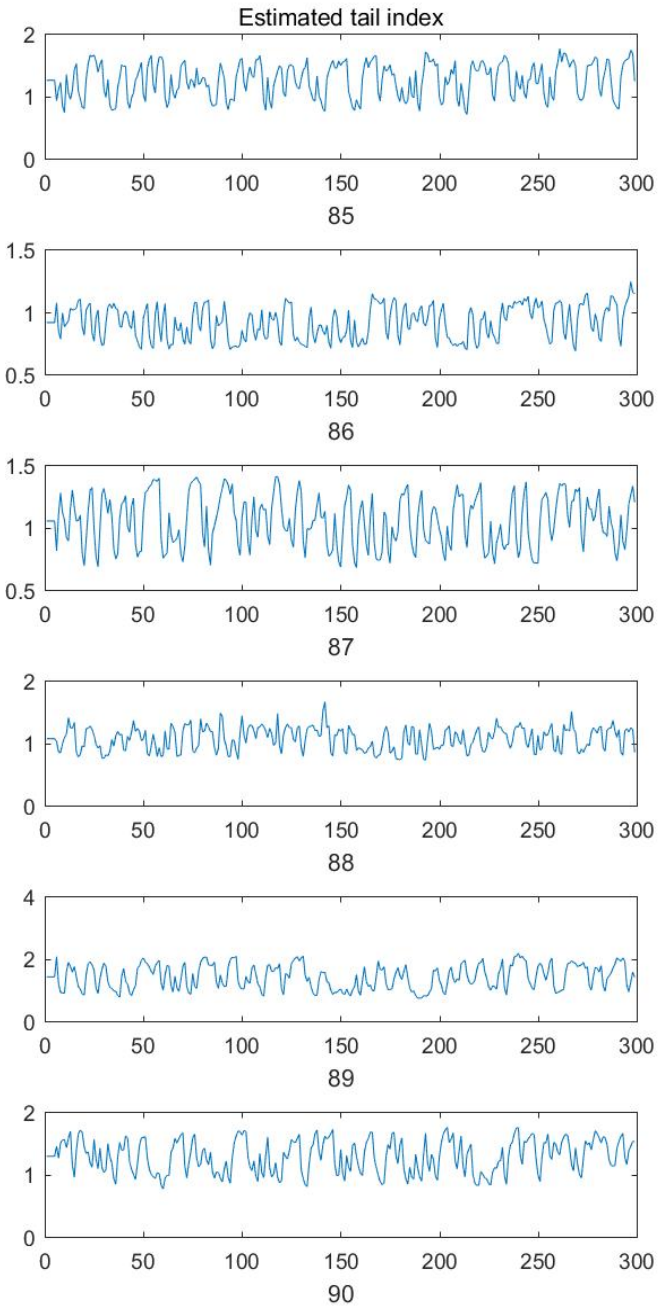
Estimated tail index
85
86
87
88
89
90

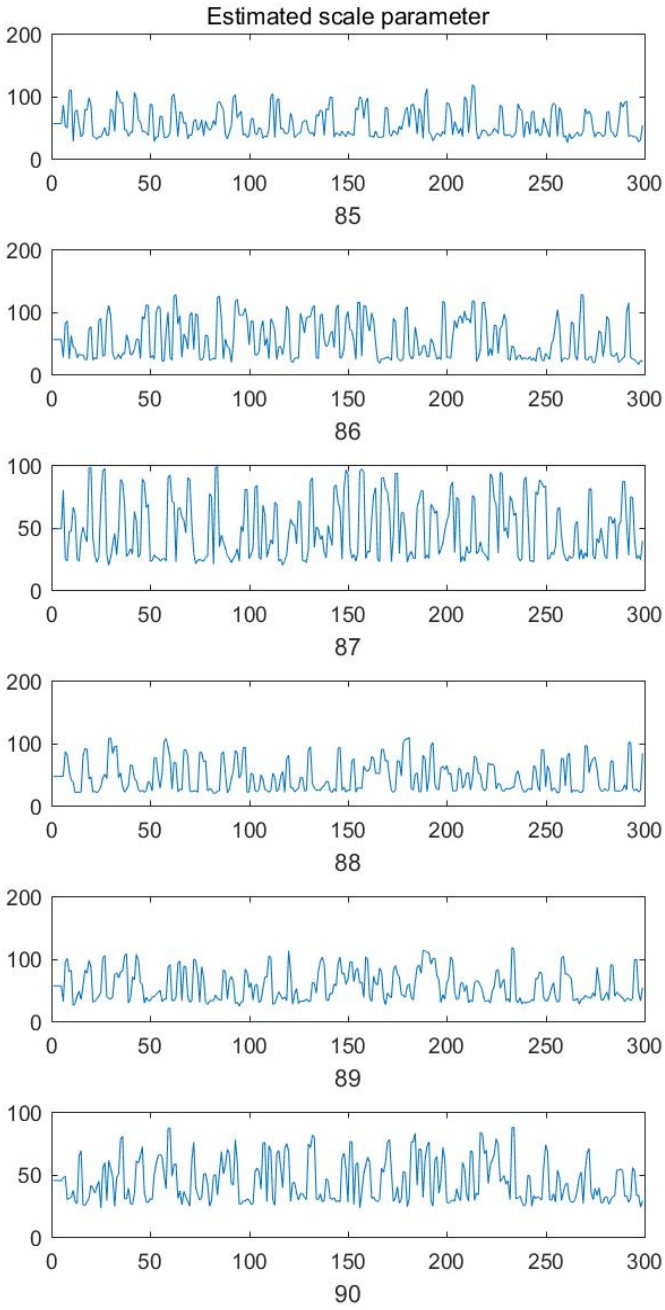
Estimated scale parameter
85
86
87
88
89
90

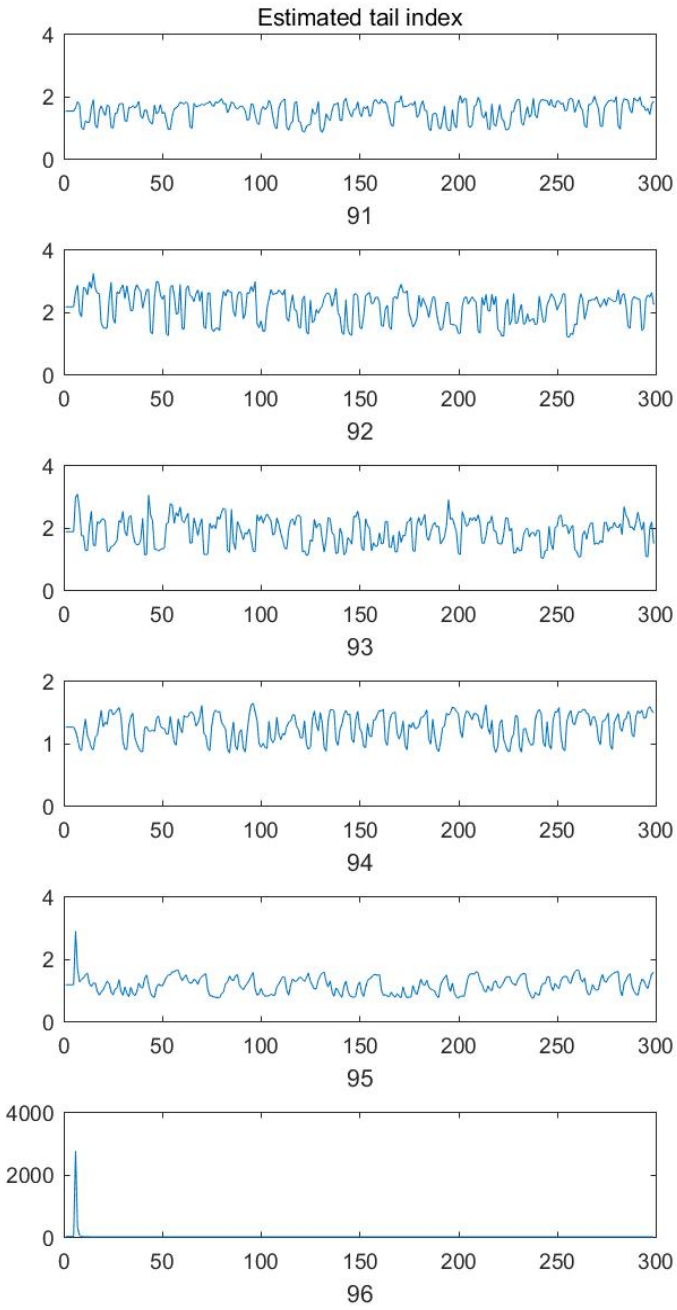
Estimated tail index
91
92
93
94
95
96

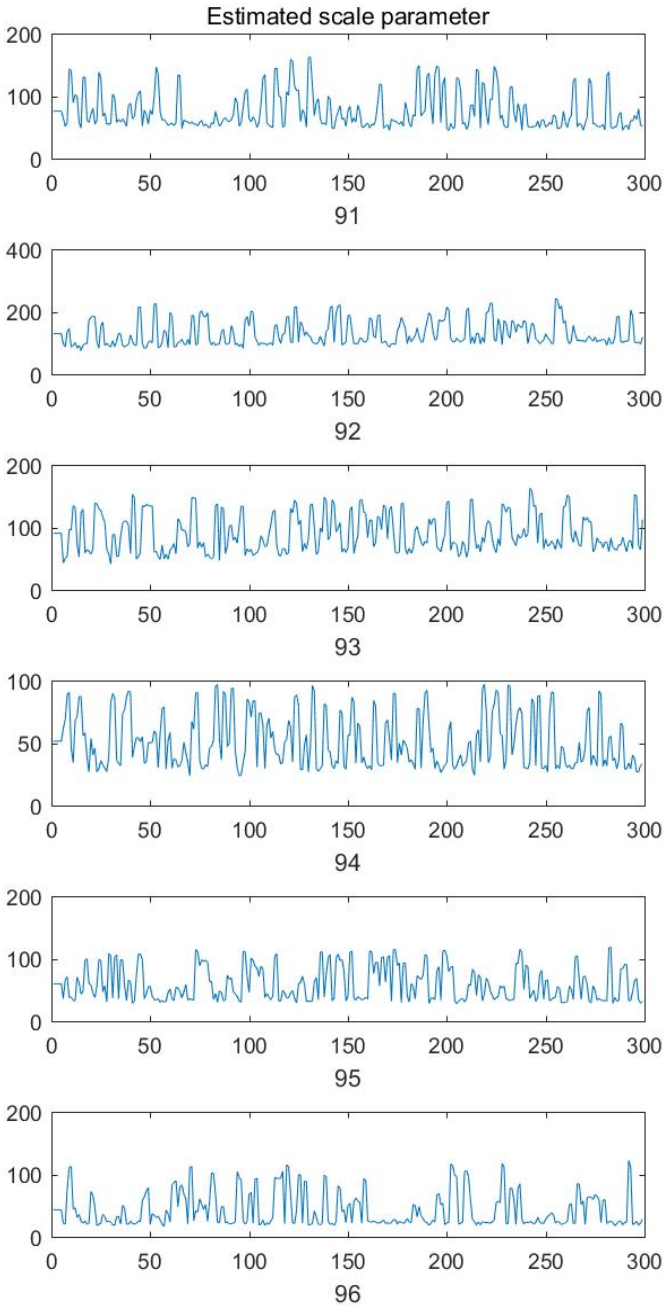
Estimated scale parameter
91
92
93
94
95
96

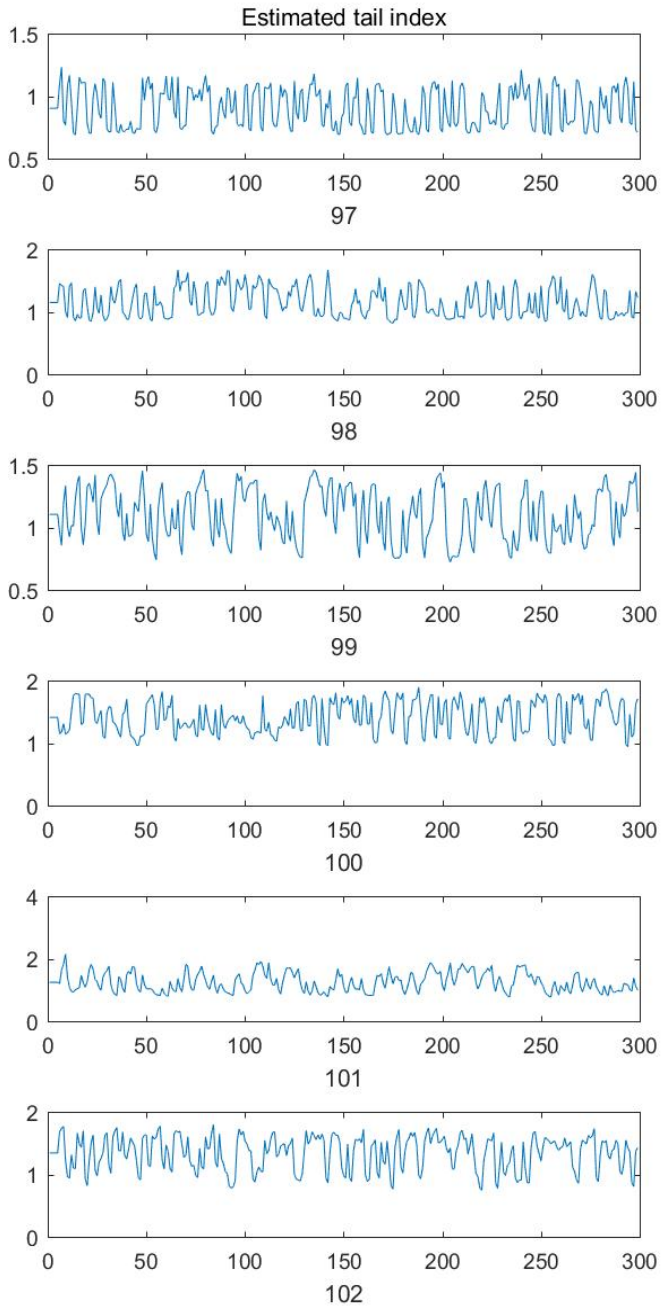
Estimated tail index
97
98
99
100
101
102

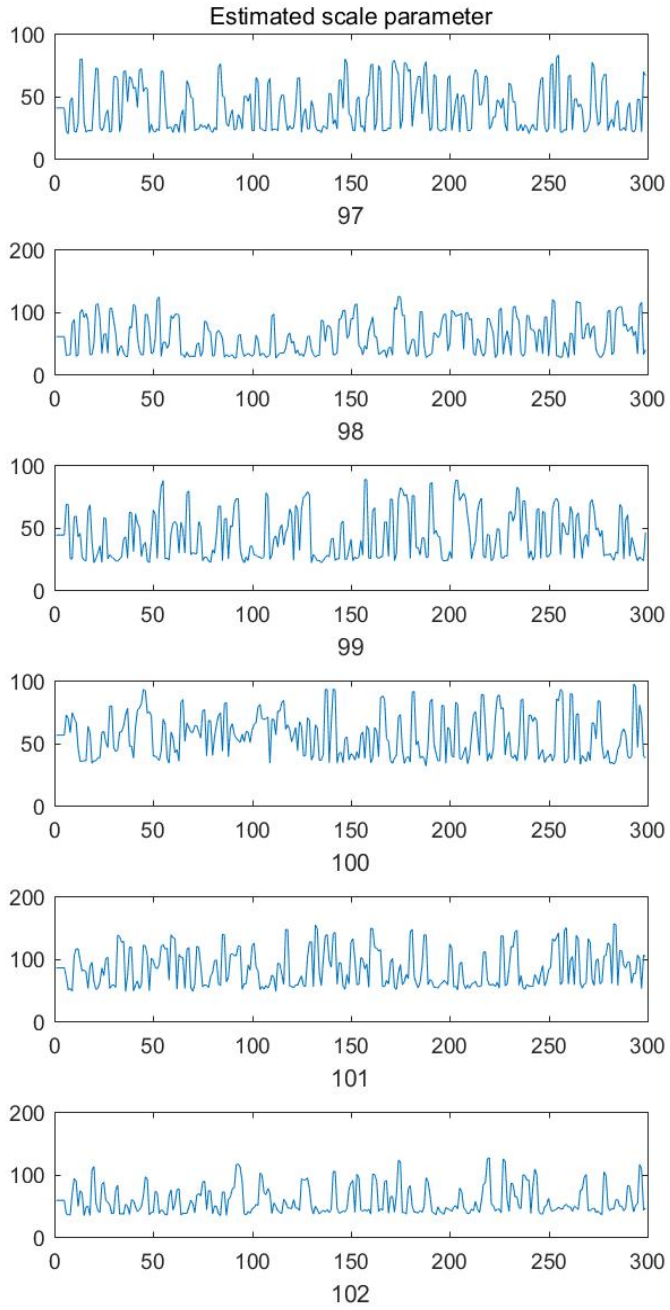
Estimated scale parameter
97
98
99
100
101
102

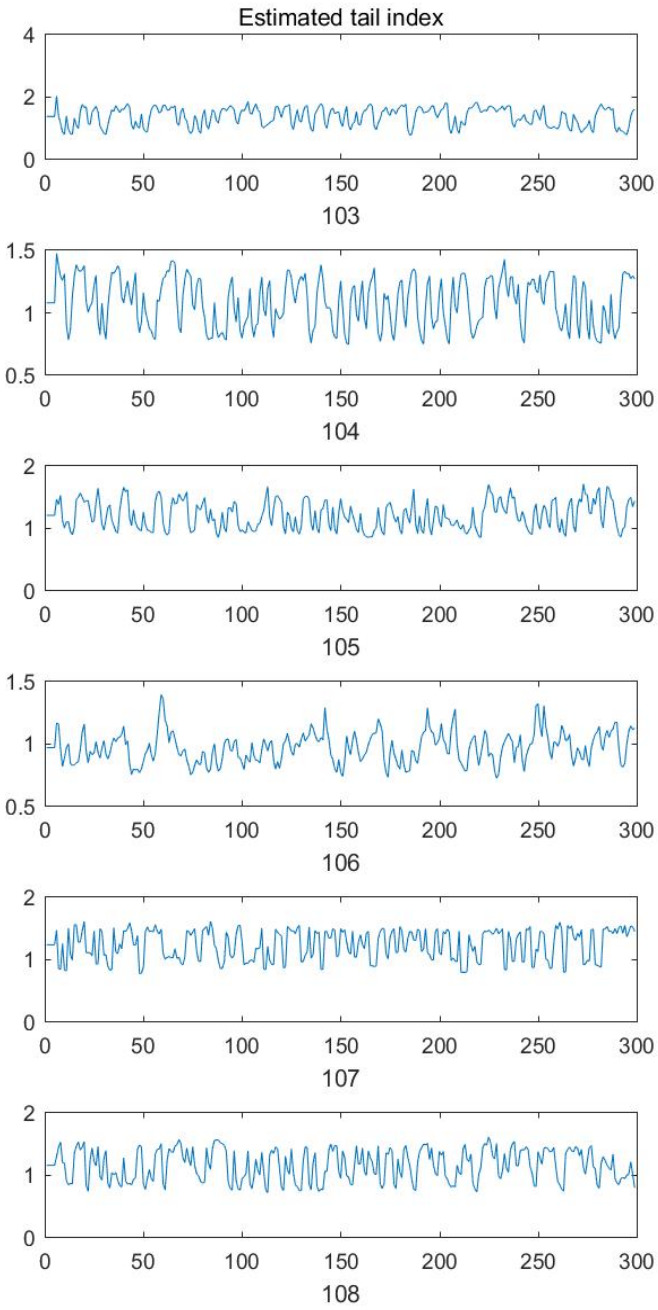
Estimated tail index
103
104
105
106
107
108

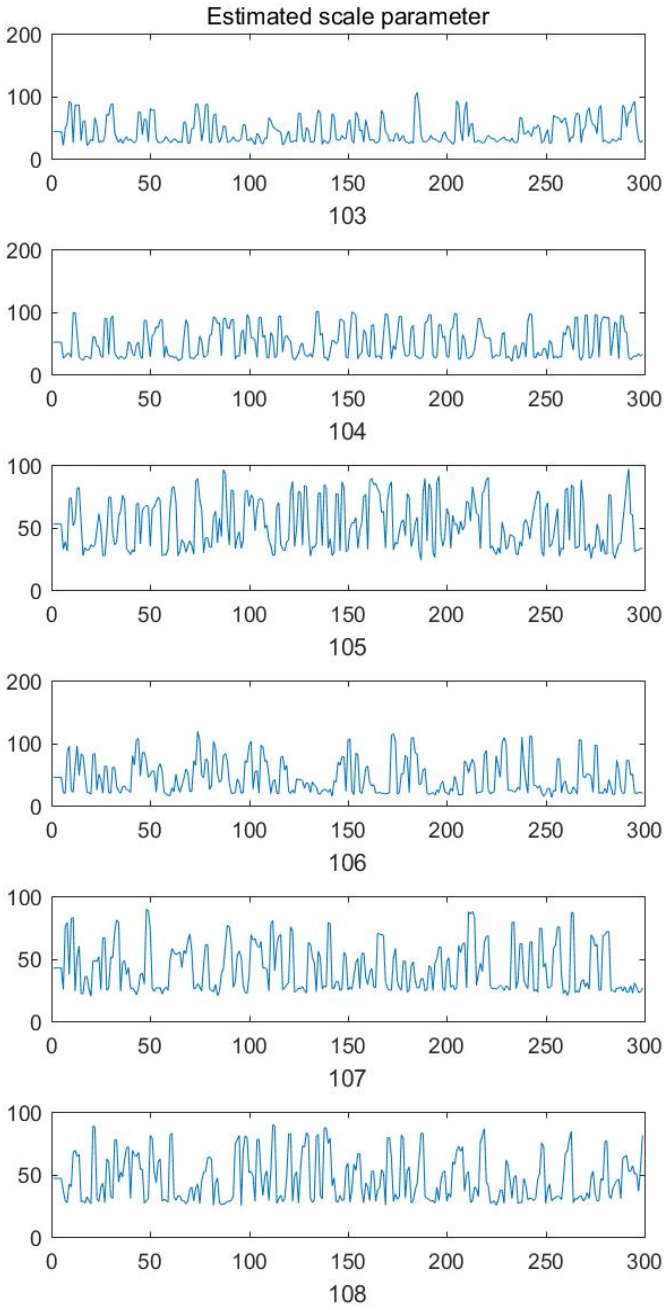
Estimated scale parameter
103
104
105
106
107
108

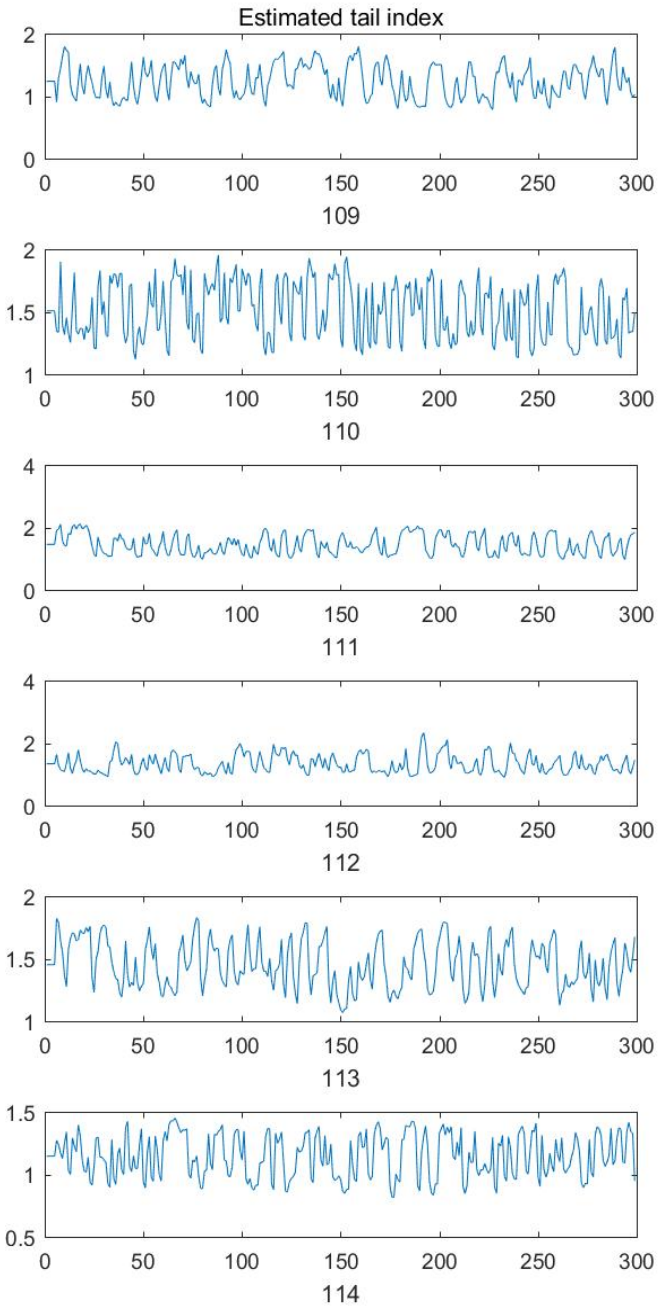
Estimated tail index
109
110
111
112
113
114

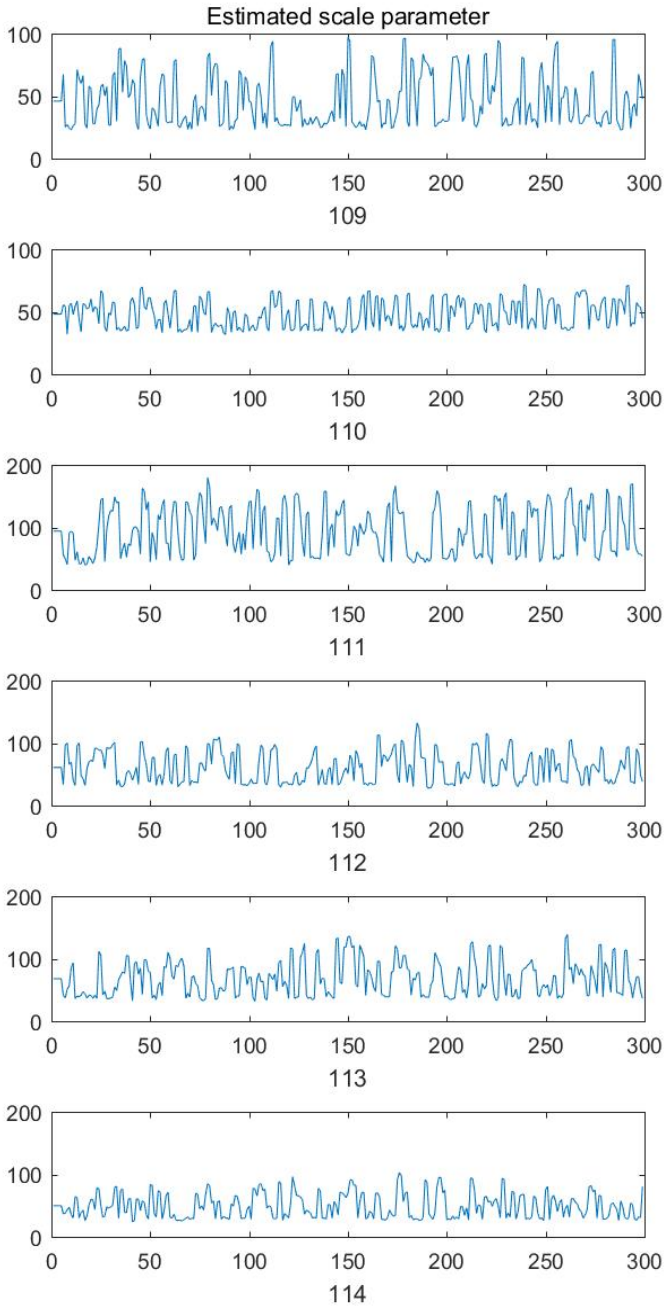
Estimated scale parameter
109
110
111
112
113
114

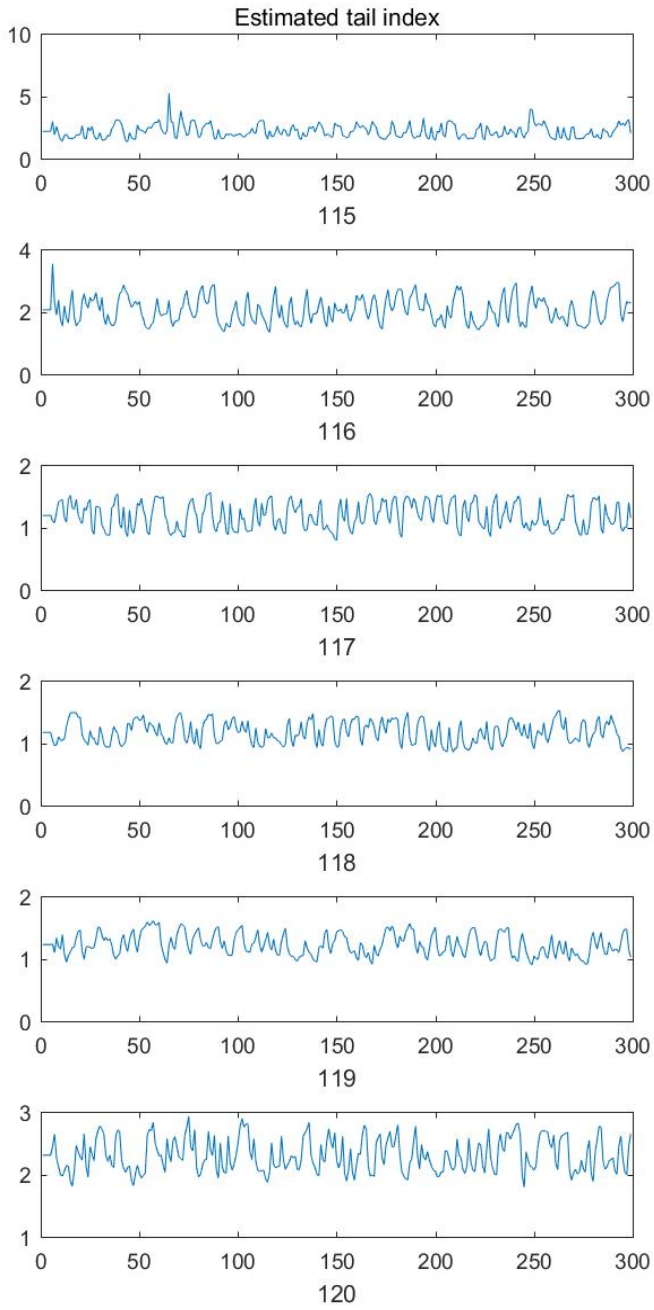
Estimated tail index
115
116
117
118
119
120

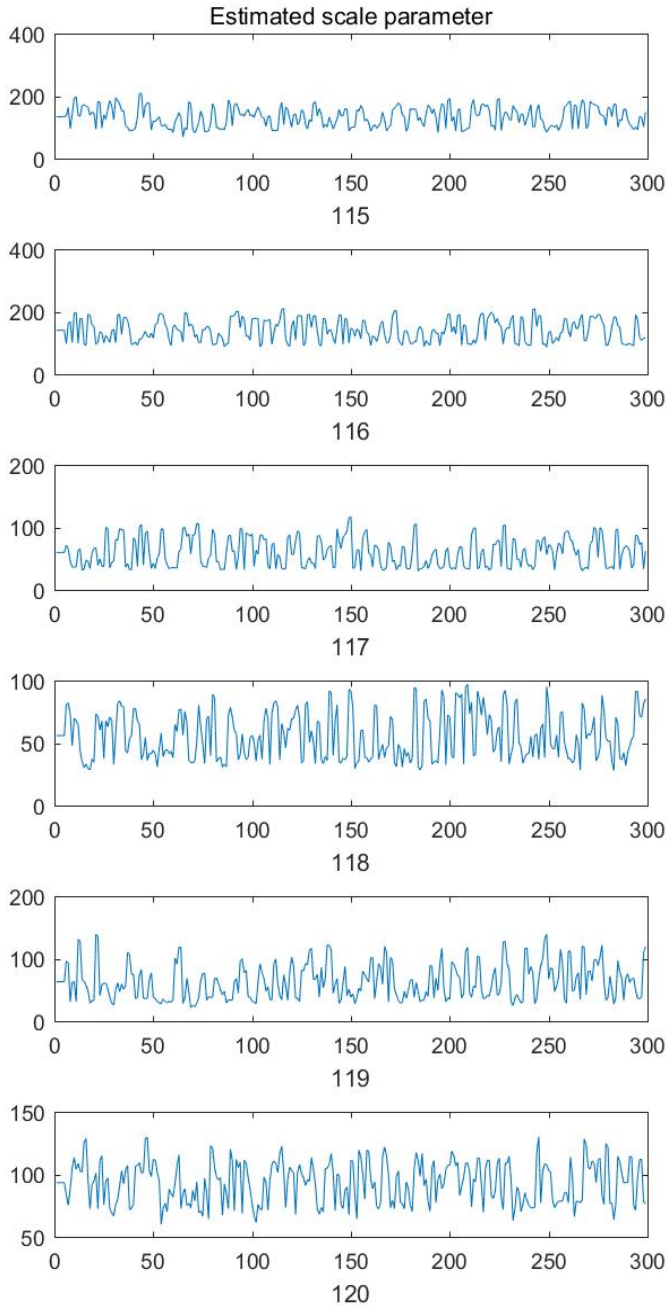
Estimated scale parameter
115
116
117
118
119
120

Bibliography

[1] Ahmed, O. W., Qahwaji, R., Colak, T., Higgins, P. A., Gallagher, P. T.,and Bloomfield, D. S. (2013). Solar flare prediction using advanced feature extraction, machine learning, and feature selection. *Solar Physics*, 283(1), 157-175.

[2] Augusto, C. R. A., Fauth, A. C., Navia, C. E., Shigeouka, H.,and Tsui, K. H. (2011), Connection Among Spacecrafts and Ground Level Observations of Small Solar Transient Events, *Experimental Astronomy*, 34, 177–197.

[3] Bali, T. and Weinbaum, D. (2007). A conditional extreme value volatility estimator based on high-frequency returns. *Journal of Economic Dynamics and Control*, 31(2):361-397.

[4] Billingsley, P. (1961). The Lindeberg-Levy theorem for martingales. Proc. Amer. Math. Soc., 12:788-792.

[5] Bobra, M. G.,and Couvidat, S. (2015). Solar flare prediction using SDO/HMI vector magnetic field data with a machine-learning algorithm. *The Astrophysical Journal*, 798(2), 135.

[6] Bollerslev, T. (1986). Generalized autoregressive conditional heteroskedasticity. *Journal of Econometrics*, 31:307-327.

[7] Boucheron, L. E., Al-Ghraibah, A.,and McAteer, R. J. (2015). Prediction of solar flare size and time-to-flare using support vector machine regression. *The Astrophysical Journal*, 812(1), 51.

[8] Buishand, T. A., L. de Haan, and C. Zhou. 2008. On spatial extremes: With application to a rainfall problem. *Annals of Applied Statistics*, 2:624–42.

[9] Chan, K. and Tong, H. (1994). A note on noisy chaos. *Journal of Royal Statistical Society - Series B*, 56(2):301-311.

[10] Chavez-Demoulin, V., Embrechts, P., and Sardy, S. (2014). Extreme-quantile tracking for financial time series. *Journal of Econometrics*, 188(1):44-52.

[11] Chiapino, M., Clémençon, S., Feuillard, V., and Sabourin, A. (2019). A multivariate extreme value theory approach to anomaly clustering and visualization. *Computational Statistics*, 1-22.

[12] Colak, T., and R. Qahwaji (2009), Automated Solar Activity Prediction: A hybrid computer platform using machine learning and solar imaging for automated prediction of solar flares, *Space Weather*, 7, S06001, doi:10.1029/2008SW000401.

[13] Cooley, D., Nychka, D., and Naveau, P. (2007). Bayesian Spatial Modeling of Extreme Precipitation Return Levels. *Journal of the American Statistical Association*, 102, 824–840.

[14] Dahan, E., and Mendelson, H. (2001). An Extreme-Value Model of Concept Testing. *Management Science*, 47, 102–116.

[15] Davis, R. A., and Resnick, S. I. (1989). Basic properties and prediction of max-ARMA processes. *Advances in applied probability*, 21(4), 781-803.

[16] Davis, R. A., and Resnick, S. I. (1993). Prediction of stationary max-stable processes. *The Annals of Applied Probability*, 497-525.

[17] de Fondeville, R., and Davison, A. C. (2018). High-dimensional peaks-over-threshold inference. *Biometrika*, 105(3), 575-592.

[18] de Haan, L. (1984). A spectral representation for max-stable processes. *The Annals of Probability*, 12:1194–1204.

[19] de Haan, L., and Ferreira,A. (2006), ExtremeValue Theory: An Introduction, New York: Springer.

[20] Deheuvels, P. (1983). Point processes and multivariate extreme values. *Journal of multivariate analysis*, 13(2), 257-272.

[21] Deng, L. and Zhang, Z. (2018). Assessing the features of extreme smog in china and the differentiated treatment strategy. *Proceedings of the Royal Society A.*, 474:20170511.

[22] Deng, L. and Zhang, Z. (2020). The haze extreme comovements in beijing-tianjin-hebei region and its extreme dependence pattern recognitions. *Science Progress*, page In press.

[23] Engle, R. and Russell, J. (1998). Autoregressive conditional duration: a new model for irregularly spaced transaction data. *Econometrica*, 66:1127-1162.

[24] Falconer, D., Barghouty, A. F., Khazanov, I., and Moore, R. (2011). A tool for empirical forecasting of major flares, coronal mass ejections, and solar particle events from a proxy of active-region free magnetic energy. Space Weather, 9(4), 1-12.

[25] Ferreira, A., and de Haan, L. (2014). The Generalized Pareto process; With a View Towards Application and Simulation. *Bernoulli*, 20, 1717–1737.

[26] Fonseca, C., H. Ferreira, L. Pereira, and A.P.Martins. 2014. Stability and contagion-measures for spatial extreme value analyses. *Kybernetika* 50:914–28.

[27] Francq, C. and Zakoian, J. (2004). Maximum likelihood estimation of pure GARCH and ARMAGARCH processes. *Bernoulli*, 10(4):605-637.

[28] Georgoulis, M. K., and Rust, D. M. (2007). Quantitative forecasting of major solar flares. *The Astrophysical Journal Letters*, 661(1), L109.

[29] Hall, P., Peng, L., and Yao, Q. (2002). Moving-maximum models for extrema of time series. *Journal of Statistical Planning and Inference*, 103(1-2), 51-63.

[30] Hansen, B. (1994). Autoregressive conditional density estimation. *International Economic Review*,35(3):705-730.

[31] Huang, X., Zhang, L., Wang, H.,and Li, L. (2013). Improving the performance of solar flare prediction using active longitudes information. *Astronomy and Astrophysics*, 549, A127.

[32] Huser, R., and Wadsworth, J. L. (2019). Modeling spatial processes with unknown extremal dependence class. *Journal of the American Statistical Association*, 114(525), 434-444.

[33] Jalbert, J., Favre, A. C., Bélisle, C., and Angers, J. F. (2017). A Spatio-Temporal Model for Extreme Precipitation Simulated by a Climate Model, With an Application for Assessing Changes in Return Levels and IDF Curves Over North America. *Journal of the Royal Statistical Society*, Series C, 66, 941–962.

[34] Kabluchko, Z., Schlather, M., and de Haan, L. (2009). Stationary Max-Stable Fields Associated to Negative Definite Functions. *Annals of Probability*, 37, 2042–2065.

[35] Kelly, B. (2014). The dynamic power law model. *Extremes*, 17(4):557-583.

[36] Kelly, B. and Jiang, H. (2014). Tail risk and asset prices. *The Review of Financial Studies*, 27(10):2841-2871.

[37] Kharin, V., and Zwiers, F. (2005). Estimating Extremes in Transient Climate Change Simulations. *Journal of Climate*, 18, 1156–1173.

[38] Kusano, K., Bamba, Y., Yamamoto, T. T., Iida, Y., Toriumi, S., and Asai, A. (2012). Magnetic field structures triggering solar flares and coronal mass ejections. The Astrophysical Journal, 760(1), 31.

[39] Laurini, F. and Tawn, J. A. (2009). Regular variation and extremal dependence of garch residuals with application to market risk measures. *Econometric Reviews*, 28:146-169.

[40] Lee, J. Y., Moon, Y. J., Kim, K. S., Park, Y. D., and Fletcher, A. B. (2007). Prediction of daily maximum x-ray flux using multilinear regression and autoregressive time-series methods. Journal of The Korean Astronomical Society, 40(4), 99-106.

[41] Leka, K. D., and Barnes, G. (2003). Photospheric magnetic field properties of flaring versus flare-quiet active regions. II. Discriminant analysis. The Astrophysical Journal, 595(2), 1296.

[42] Li, R., Cui, Y., He, H.,and Wang, H. (2008). Application of support vector machine combined with K-nearest neighbors in solar flare and solar proton events forecasting. *Advances in Space Research*, 42(9), 1469-1474.

[43] Liu, K., Mei, Y.,and Shi, J. (2015). An adaptive sampling strategy for online high-dimensional process monitoring. *Technometrics*, 57(3), 305-319.

[44] Lou Thompson, M., Reynolds, J., Cox, L., Guttorp, P., and Sampson, P. (2001). A Review of Statistical Methods for the Meteorological Adjustment of Tropospheric Ozone. *Atmospheric Environment*, 35, 617–630.

[45] Makelainen, T., Schmidt, K., and Styan, G. (1981). On the existence and uniqueness of the maximum likelihood estimate of a vector-valued parameter in

xed-size samples. *Annals of Statistics*, 9:758-767.

[46] Mao, G. and Zhang, Z. (2018). Stochastic tail index model for high frequency

nancial data with bayesian analysis. *Journal of Econometrics*, 205:470-487.

[47] Morris, S. A., Reich, B. J., Thibaud, E., and Cooley, D. (2017). A Space-Time Skew-tModel for Threshold Exceedances. *Biometrics*, 73, 749–778.

[48] Mossin, J. (1966). Equilibrium in a capital asset market. *Econometrica*, 34(4):768-783.

[49] NASA. (2009). Solar Dynamics Observatory: Our Eye on the Sun. A Guide to the Mission and Purpose of Nasa's Solar Dynamics Observatory

[50] Naveau, P., Zhang, Z., and Zhu, B. (2011). An extension of max autoregressive models. *Statistics and Its Interface*, 4(2), 253-266.

[51] Nishizuka, N., Sugiura, K., Kubo, Y., Den, M., Watari, S., and Ishii, M. (2017). Solar flare prediction model with three machine-learning algorithms using ultraviolet brightening and vector magnetograms. The Astrophysical Journal, 835(2), 156.

[52] Nishizuka, N., Sugiura, K., Kubo, Y., Den, M.,and Ishii, M. (2018). Deep flare net (DeFN) model for solar flare prediction. The *Astrophysical Journal*, 858(2), 113.

[53] Padoan, S. A., Ribatet, M., and Sisson, S. A. (2010). Likelihood-based inference for max-stable processes. *Journal of the American Statistical Association*, 105(489), 263-277.

[54] Papaioannou, A., Anastasiadis, A., Sandberg, I., Georgoulis, M. K., Tsiropoula, G., Tziotziou, K., ... and Hilgers, A. (2015). A novel forecasting system for solar particle events and flares (FORSPEF). In Journal of Physics: Conference Series (Vol. 632, No. 1, p. 012075). IOP Publishing.

[55] Qahwaji, R., and Colak, T. (2007). Automatic short-term solar flare prediction using machine learning and sunspot associations. Solar Physics, 241(1), 195-211.

[56] Raboonik, A., Safari, H., Alipour, N.,and Wheatland, M. S. (2016). Prediction of solar flares using unique signatures of magnetic field images. *The Astrophysical Journal*, 834(1), 11.

[57] Reich, B. J., and Shaby, B. A. (2012). A Hierarchical Max-Stable Spatial Model for Extreme Precipitation. *Annals of Applied Statistics*, 6, 1430–1451.

[58] Reich, B. J. and Shaby, B. A. (2019). A spatial markov model for climate extremes. *Journal of Computational and Graphical Statistics*, 28(1):117-126.

[59] Rong, B., Rui, X., Wang, G., and Yang, F. (2011). Dynamic modeling and H_∞ independent modal space vibration control of laminate plates. Science China Physics, Mechanics and Astronomy, 54(9), 1638.

[60] Sang, H., and Gelfand, A. E. (2009). Hierarchical Modeling for Extreme Values Observed Over Space and Time. *Environmental and Ecological Statistics*, 16(3), 407-426.

[61] Schlather, M. (2002). Models for Stationary Max-Stable Random Fields. *Extremes*, 5, 33–44

[62] Smith, R. (1985). Maximum likelihood estimation in a class of nonregular cases. *Biometrika*, 72(1):67-90.

[63] Smith, R. L., and Weissman, I. (1996). Characterization and estimation of the multivariate extremal index. *Manuscript, UNC*.

[64] Smith, R. L., and Goodman, D. (2000). Bayesian risk analysis. Chapter 17 of Extremes and Integrated Risk Management, edited by P. Embrechts.

[65] Steward, G. A., Lobzin, V. V., Wilkinson, P. J., Cairns, I. H., and Robinson, P. A. (2011). Automatic recognition of complex magnetic regions on the Sun in GONG magnetogram images and prediction of flares: Techniques for the flare warning program Flarecast. Space Weather, 9(11), 1-13.

[66] Tang, R., Shao, J., and Zhang, Z. (2013). Sparse moving maxima models for tail dependence in multivariate

nancial time series. *Journal of Statistical Planning and Inference*, 143(5):882-895.

[67] Thibaud, E., and Opitz, T. (2015). Efficient Inference and Simulation for Elliptical Pareto Processes. *Biometrika*, 102, 855–870.

[68] Wang, A., Xian, X., Tsung, F.,and Liu, K., (2018) A spatial-adaptive sampling procedure for online monitoring of big data streams, *Journal of Quality Technology*, 50:4, 329-343, DOI: 10.1080/00224065.2018.1507560

[69] Welsch, B. T., Li, Y., Schuck, P. W., and Fisher, G. H. (2009). What is the relationship between photospheric flow fields and solar flares?. The Astrophysical Journal, 705(1), 821.

[70] Winter, L. M., and Balasubramaniam, K. S. (2014). Estimate of Solar Maximum Using the 1-8 Å Geostationary Operational Environmental Satellites X-Ray Measurements. *The Astrophysical Journal Letters*, 793(2), L45.

[71] Winter, L. M., and Balasubramaniam, K. (2015). Using the maximum X-ray flux ratio and X-ray background to predict solar flare class. Space Weather, 13(5), 286-297.

[72] Xie, Y., Huang, J.,and Willett, R. (2012). Change-point detection for high-dimensional time series with missing data. *IEEE Journal of Selected Topics in Signal Processing*, 7(1), 12-27.

[73] Yu, D., Huang, X., Wang, H., and Cui, Y. (2009). Short-term solar flare prediction using a sequential supervised learning method. Solar Physics, 255(1), 91-105.

[74] Yu, D., Huang, X., Hu, Q., Zhou, R., Wang, H., and Cui, Y. (2010). Short-term solar flare prediction using multiresolution predictors. The Astrophysical Journal, 709(1), 321.

[75] Zhang, X., and Bernd, S. (2016). Tail risk in government bond markets and ECB unconventional policies. Working paper, March.

[76] Zhang, Z. and Smith, R. L. (2010). On the estimation and application of max-stable processes. *Journal of Statistical Planning and Inference*, 140(5):1135-1153.

[77] Zhang, Z. and Zhu, B. (2016). Copula structured m4 processes with application to high-frequency financial data. *Journal of Econometrics*, 194(2):231-241.

[78] Zhao, Z. (2020). Dynamic Bivariate Peak over Threshold Model for Joint Tail Risk Dynamics of Financial Markets. *Journal of Business and Economic Statistics*, 10.1080/07350015.2020.1737083.

[79] Zhao, Z., Zhang, Z.,and Chen, R. (2018), Modeling maxima with autoregressive conditional Fréchet model. *Journal of Econometrics*. 207(2), 325-351.